POLYMER COMPOSITES

Volume 6/No. 4/October 1985

Composites '84

National Research Council of Canada
Industrial Materials Research Institute

CONTENTS

193 L.A. UTRACKI/Guest Editor

195 A. GARTON and J.H. DALY/Characterization of the Aramid: Epoxy and Carbon: Epoxy Interphases

201 C. RICHARD, K. HING, and H.P. SCHREIBER/Interaction Balances and Properties of Filled Polymers

209 T.G.M. VAN DE VEN/The Flow of Suspensions

215 C.-Y. MA, J.L. WHITE, P.C. WEISSERT, and K. MIN/Flow Patterns in Calcium Carbonate and Titanium Dioxide Filled Polyethylene in the Entrance Region of a Capillary Die

222 I. MANAS-ZLOCZOWER, A. NIR, and Z. TADMOR/Dispersive Mixing in Roll-Mills

232 B. FISA/Mechanical Degradation of Glass Fibers During Compounding with Polypropylene

242 M.R. PIGGOTT, P.S. CHUA, and D. ANDISON/The Interface Between Glass and Carbon Fibers and Thermosetting Polymers

249 T. VU-KHANH, B. SANSCHAGRIN, and B. FISA/Fracture of Mica-Reinforced Polypropylene: Mica Concentration Effect

261 A.D. BESHAY, B.V. KOKTA, and C. DANEAULT/Use of Wood Fibers in Thermoplastic Composites II: Polyethylene

272 B. SCHLUND and M. LAMBLA/Modification of the Dynamic Damping Behavior of Epoxy/Glass Fiber Composites Via Fiber Coating with Functional Latices

282 T. KATSURA, M.R. KAMAL, and L.A. UTRACKI/Some Properties of Polypropylene Filled with Metal Fibers

296 M.T. KORTSCHOT and R.T. WOODHAMS/Electromagnetic Interference Shielding with Nickel-Coated Mica Composites

305 Subject and Title Index

306 Author Index

PUBLISHED BY THE SOCIETY OF PLASTICS ENGINEERS, INC.

POLYMER COMPOSITES

Published by the Society of Plastics Engineers

EDITOR—ROGER S. PORTER

% Polymer Science and Engineering
University of Massachusetts
Amherst, Mass. 01003

ASSOCIATE EDITOR—RICHARD E. BALL

% Western New England College
Springfield, Mass. 01119

GUEST EDITOR—L. A. UTRACKI

% Industrial Materials Research Institute
National Research Council of Canada
75, Boul de Mortagne
Boucherville, Quebec
Canada J4B 6YA

ADVISORY BOARD

LAWRENCE J. BROUTMAN
Illinois Institute of Technology

ANTHONY T. DI BENEDETTO
University of Connecticut

NIKOLAY ENIKOLOPYAN
USSR Academy of Sciences

DAVID H. KAELBLE
Arroyo Computer Center

JOHN L. KARDOS
Washington University

FREDERICK J. MCGARRY
Massachusetts Institute of Technology

L. NICOLAIS
University of Naples

R. BYRON PIPES
University of Delaware

N. S. SCHNEIDER
Army Materials and Mechanics Research Center

PUBLICATIONS COMMITTEE

D. W. RILEY, Chairman
Extrusion Engineers

R. P. BRADDICKS, JR.
Plastics Consultant

LEONARD H. DREXLER
AT&T Consumer Products

R. D. FORGER
Society of Plastics Engineers

J. L. HULL
Hull Corporation

WILLIAM C. KUHLKE
Shell Chemical Co.

V. E. MALPASS
Ferro Corporation

M. A. MENDELSOHN
Westinghouse Electric Corp.

R. S. PORTER
University of Massachusetts

A. A. SCHOENGOOD
Society of Plastics Engineers

G. R. THOM
Regal Plastics Company

A. M. VARNER
Moldflow USA, Inc.

A. E. WHITNEY, JR.
Plastics Consultant

Copyright by the Society of Plastics Engineers, Inc., 1985. POSTMASTER: Send address changes to POLYMER COMPOSITES, 14 Fairfield Dr., Brookfield Center, CT 06805. Telephone (203) 775-0471, TELEX 643-712. Reproduction in whole or in part without written permission is strictly prohibited.

Polymer Composites (ISSN 0272-8397) is published at Waverly Press, Easton, MD 21601. Address changes, undeliverable copies and orders for subscriptions should be sent to Circulation Manager, Society of Plastics Engineers, 14 Fairfield Dr., Brookfield Center, CT 06805. Published quarterly. Second class postage paid at Brookfield Center, Conn. and additional entry offices. Accepted at special postal rate provided in P.M. Sec. 132.122.

Neither the Society of Plastics Engineers, Inc., nor **Polymer Composites** is responsible for the views expressed by individual contributors either in articles published in **Polymer Composites** or in technical papers presented at meetings of the Society.

Subscription rates for 1985: SPE members, 1 year—$24. Nonmembers, 1 year—$60. Delivery outside North America, add $8 per year

SOCIETY OF PLASTICS ENGINEERS, INC.
Business and Executive Offices, 14 Fairfield Dr., Brookfield Center, Conn. 06805

ROBERT D. FORGER
Publisher

MICHAEL R. CAPPELLETTI
Circulation Manager

JEANNE M. CROTTY
Production Manager

PAM ARSENAULT
Copy Editor

OFFICERS OF THE SOCIETY

RICHARD G. JOHNSON
President

GREG R. THOM
President-elect

JOHN R. KRETZSCHMAR
First Vice President

BRUCE A. PETERSEN
Second Vice President

JACQUES DE CRAENE
Vice President for International Affairs

VIVIAN E. MALPASS
Secretary

LEONARD H. DREXLER
Treasurer

ROBERT D. FORGER
Executive Director

POLYMER COMPOSITES is indexed by:—Chemical Abstracts—Engineering Index, Inc.

Composites '84
National Research Council of Canada
Industrial Materials Research Institute

The symposium "Composites-'84" of November 20, 1984, was the fourth one in a series on "Polymer Composites" and the twelfth organized and sponsored by the Industrial Materials Research Institute of the National Research Council of Canada. The remaining eight belong to the two other series on "Mathematical Modeling of Plastics Processing and Properties", and on "Polymer Blends". Proceedings of the symposia are published in the technical journals of the Society of Plastics Engineers: POLYMER ENGINEERING AND SCIENCE or POLYMER COMPOSITES. The meetings take place at the Institute, located in Boucherville, Quebec, Canada.

The dreaded "Orwell's year" is almost over. Comparing reality with prophecies, we can feel a grim satisfaction that the "advances" of social engineering have not been as rapid as Orwell expected. In fact, those persons who are "in plastics" should feel rather cheerful. In 1978, the volume of plastics production began to exceed that of raw steel. By 1983, this difference had already reached 29 percent! The growth rate of the plastics industry is a healthy 6 percent per annum. Furthermore, anyone working on polymer alloys, blends, or composites must be blissfully happy. According to the latest figures from C. H. Klein and Co., the 1983 USA consumption of polymers for blending and for making composites constituted 10 and 12 percent of the total value of the manufactured resins. Taking into account the projected growth rates, by 1988 these numbers will increase to 13 and 16 percent, i.e., the value of resins which will go into the production of polymer alloys, blends and composites will be nearly one third of the total. Another source projects slightly different figures but gives an equally optimistic forecast—by 1990 polymer composites will consitute about 30 percent of the total plastics production volume.

Working in a multilingual environment at the Institute, we have more problems defining the meaning of commonly used words than those who operate within the boundaries of a single language. This also forces us to be sensitive to ambiguities in use of technical terms. To set the record straight, the term "polymer composites" refers to the class of plastics containing any type of solid material. Depending on the type of solids, we distinguish three groups: (i) filled plastics, with small non-reinforcing particles, (ii) composites—with reinforcing, mostly anisometric particles, and (iii) the long and continuous fiber composites. Terms such as "compound," "blend," "mixture," etc.... do not, per se, refer to the solid-filled polymers.

During "Composites-'84," twelve papers were presented in the same order as published in this issue. As our young "tradition" dictates, we cover as wide an area within polymer composites as possible, starting with a thermodynamic aspect and going through rheology, characterization, and onto processing. The first two papers by Garton and Daly, and by Richard, Hing, and Schreiber provide description of new methods of interface characterization; Garton and Daly use internal reflection infrared spectroscopy, the other authors use inverse gas chromatography. Since the latter group is also working on plasma modification, the paper provides important information on the type of interactions determining the composites' behavior. Theo van de Ven's review on rheology of suspensions in Newtonian media delineates a boundary of our knowledge of these model systems. The next paper (from the newly formed Akron Polymer Engineering Center) by Ma, White, Weissert and Min demonstrates the effect of filler addition on suppression of the die entry vortices, melt fracture, and the extrudate swell. Manas-Zloczower, Nir, and Tadmor present a new model of filler dispersion on a two-roll-mill. Fisa discusses the attrition of glass fibers during processing; the attrition was found to be independent of the method of fiber addition. The two following papers by Piggott, Chua, and Andison and by

Vu-Khanh, Sanschagrin, and Fisa refer to fundamental aspects of testing the composites. Piggott, *et al.*, report on direct measurements of the frictional forces between fiber and matrix, while Vu-Khanh *et al.*, discuss the mechanism of fracture for mica composites. The paper by Beshay, Kokta and Denault is the first part in a series of communications on the method of grafting wood fibers and behavior of these materials as fillers in thermoplastic composites. If the calculated costs and reported performance are confirmed by industrial tests, this may be a long awaited breakthrough in technology. Schlund and Lambla describe a new method of glass fiber coating. The impregnating bath is made of amino-silane with a sequentially polymerized latex. The method is flexible, imparting desired properties to the composite by judicious selection of monomers and sequences of latex polymerization. The two final papers by Katsura, Kamal, and Utracki and by Kortschot and Woodhams discuss new methods of generation of electrically conductive composites. In the first paper, the mild-steel fibers, and in the second, nickel coated mica flakes were used as fillers. In both cases, on addition of 10 volume percent of filler the resistivity of the material (polypropylene or linear low density polyethylene) decreases from the neat polymer value of 3×10^{16} to about 10 (ohm.cm).

Organizing these symposia is a task which only those who have experienced it can appreciate. It takes many months of preparation, begging, threatening, agonizing, and waiting. But all this is forgotten when the event is successful. The joy comes from seeing well-balanced presentations, from hearing about new discoveries, and from participating in lively discussions. I wish to express my thanks, and my gratitude to the authors, to the chairmen of the morning and afternoon sessions, Professors M. R. Kamal and J. L. White, respectively, and to the participants. In my obviously impartial opinion, this was an excellent meeting as evidenced by the texts and discussions published in this issue.

L. A. Utracki
Guest Editor

Characterization of the Aramid:Epoxy and Carbon:Epoxy Interphases

ANDREW GARTON *and* JOHN H. DALY

Division of Chemistry
National Research Council of Canada
Ottawa, Ontario, Canada KIA OR6

The matrix/reinforcement interphase in aramid fiber/epoxy and carbon fiber/epoxy composites were modeled by coating an internal reflection spectroscopy (IRS) element with a thin layer of an aramid or of carbonized poly(acrylonitrile) (PAN). The coated element was then used as a substrate on which the curing of an epoxy resin took place. Infrared (IR) spectroscopy was used to demonstrate that the simulated reinforcement surfaces modified the crosslinking chemistry in the first 200–400 nm of epoxy matrix adjacent to the surfaces, producing an interphase of matrix material with properties different from those of the bulk of the epoxy matrix. This hypothesis was confirmed by the fabrication and testing of a series of unidirectional aramid fiber/epoxy and carbon fiber/epoxy composites.

INTRODUCTION

Aramid fiber/epoxy and carbon fiber/epoxy composites are attractive for many structural applications because they successfully exploit the high specific strength and stiffness of the reinforcing fibers, while retaining the processibility and chemical resistance characteristic of epoxy-based composites. As with all composites, the interphase between the fibrous reinforcement and the plastic matrix is crucial to the performance of aramid/epoxy and carbon/epoxy composites (1). This paper describes the results of spectroscopic analysis of the interphase between an epoxy matrix and either an aramid surface or a carbonized poly(acrylonitrile) (PAN) surface. The chemical differences detected by spectroscopy are then compared to physical property differences in aramid fiber/epoxy and carbon fiber/epoxy composites.

MATERIALS

The epoxy resin was a commercial diglycidyl-type resin (Epon 828, Shell). The curing agents were nadic methyl anhydride (NMA, Fisher, vacuum distilled, 93 parts per hundred of resin) with benzyldimethylamine catalyst (BDMA, Ciba-Geigy, vacuum distilled, 1 part) or diaminodiphenylmethane (DDM, Ciba-Geigy, 30 parts, uncatalyzed). The resin, curing agent, and catalyst were mixed and degassed in the conventional fashion (2). Commercial aramid fibers (Kevlar 49, Dupont, 1140 denier) and carbon fiber (Thornel T-500 12 K, Union Carbide) reinforcements were used in the preparation of unidirectional composities.

PROCEDURES FOR FABRICATION AND TESTING OF COMPOSITES

The reinforcing fibers were wound onto a steel former using a modified lathe. The fibers were then subjected to various drying histories (see later) and impregnated with the resin/curative mixture in a vacuum oven (3, 4). The samples were cured under pressure between two steel plates in an air oven. The cure cycle for the NMA system was 4 hours at 100°C + 8 hours at 160°C and for the DDM system was 3 hours at 100°C + 3 hours at 150°C.

The cured composite samples were cut with a high speed band saw [blade reversed for aramid fiber composites (5)]. Samples for dynamic mechanical analysis (DMA) were subjected to forced torsion, perpendicular to the fiber direction, in a Rheometrics Mechanical Spectrometer (RMS-605). A constant strain amplitude of 0.1 percent was used and the shear storage modulus (G'), loss modulus (G'') and loss tangent (tan δ) were recorded as a function of temperature and frequency. Apparent interlaminar shear strengths were measured according to ASTM D2344-76, with the fiber direction parallel to the long axis of the test specimen. Several samples were also fractured in flexure parallel to the fiber direction and the fracture surfaces were examined by optical microscopy.

DESCRIPTION OF SPECTROSCOPIC TECHNIQUE

Briefly, IRS allows infrared (IR) spectroscopic analysis of the thin surface layer of a sample in contact with the IRS element. The "depth of pen-

etration" (d_p) of the IR radiation into the sample surface depends on a variety of optical parameters, such as angle of incidence, IR wavelength and the refractive indices of the sample and of the IRS element (6). For the conditions chosen here (germanium IRS element, 60° incidence, mid-IR wavelengths), d_p is 300 to 500 nm depending on the wavelength. More complete details of the IRS technique are available elsewhere (3, 4, 6).

In the work described here, the IRS element was coated with a thin layer (≤100 nm) of a material which is chosen to simulate the surface of a reinforcement. The standing wave at the element surface is therefore able to penetrate through this thin surface layer and examine the first 200 to 400 nm of epoxy matrix adjacent to the surface coating.

IRS spectra were obtained at 4 cm^{-1} resolution using a Nicolet 7199 FT-IR spectrometer, equipped with a Wilks model 10 IRS attachment.

An aramid surface coating was applied by dipping the element into a 0.5 weight-percent solution of an aramid fiber (Kevlar 49, DuPont) in concentrated sulfuric acid. The dip-coated element was immersed in an aqueous coagulation bath for 30 minutes to remove the acid, and excess coagulated aramid was removed, by wiping, from all but the desired sampling area (a 20 by 40 mm area on one side of the IRS element). The coated element was then dried in vacuum at 150°C. As an initial attempt to chemically simulate a carbon fiber surface, a germanium element was dip-coated with about 100 nm of PAN from dimethylsulphoxide solution. The PAN coating was then partially carbonized by heating in air at 175°C for 48 hours and in vacuum or in argon to temperatures up to 650°C. Experiments are continuing, using progressively higher carbonization temperatures, to better simulate the chemical nature of a carbon fiber surface. The epoxy resin/curative mixture was placed over the coated surfaces (or a dry, freshly polished, germanium element as a control) as a ca. 100 μm thick layer, and covered with a clean dry Pyrex microscope slide.

For the NMA-cured system, the consumption of anhydride curing agent was followed by the decrease in the 1780 cm^{-1} absorption, and the production of ester crosslinks was monitored by the increase in the 1740 cm^{-1} absorption. Absorptions were ratioed to the magnitude of the initial anhydride absorption at 1780 cm^{-1} in each experiment, so as to obtain concentration indices (4). For the DDM-cured system, the consumption of epoxide was monitored by the decrease in the characteristic epoxide absorption at 915 cm^{-1} (4).

RESULTS OF SPECTROSCOPIC ANALYSIS

Figure 1 shows the IRS spectra of a thin aramid coating and a thin carbonized PAN coating. Note that these spectra are moderately intense and complex, which will complicate spectroscopic analysis when the spectra are superimposed on the spectrum of the epoxy matrix, e.g., when an aramid coated IRS element is used to follow the crosslinking kinetics of the epoxy resin. However, it should

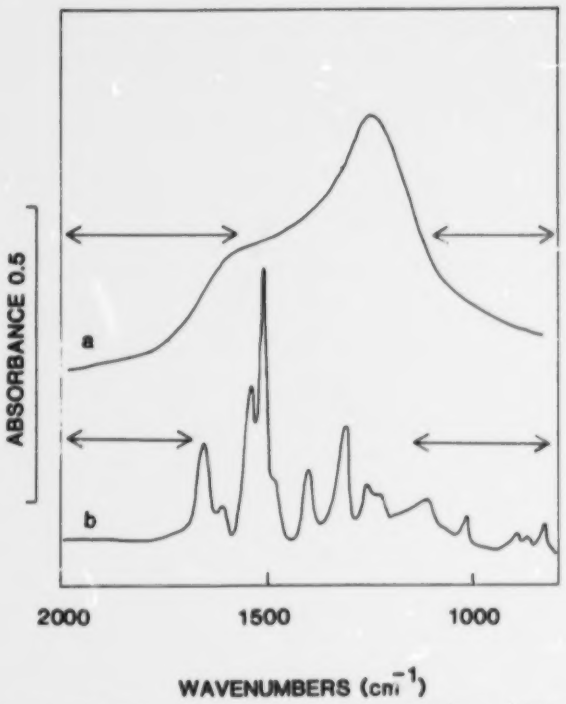

Fig. 1. IRS spectra of thin surface coatings, (a)-carbonized PAN, (b)-aramid [poly(p-phenyleneterephthalamide)]. Regions marked by arrows have sufficiently low IR absorption to be classed spectral "windows."

be noted that there are "windows" in the spectra of the coatings, i.e., frequency ranges where the coatings absorb only weakly. If these windows coincide with informative absorptions in the matrix overlayer, the absorptions of the coating will not interfere greatly with the interpretation of spectral changes in the matrix.

IRS spectra of the NMA-epoxy system, before and after curing, are shown in *Fig. 2*. The crosslinking process is accompanied by a loss of anhydride groups (decrease of 1780 cm^{-1} absorption) and a gain of ester groups (increase of 1740 cm^{-1} absorption). The consumption of epoxide groups is difficult to monitor because the characteristic epoxide absorption at 915 cm^{-1} overlaps with absorptions due to the anhydride curing agent. For the DDM-cured system, the consumption of epoxide groups can be monitored at 915 cm^{-1}, but consumption of the amine curing agent cannot be followed reliably with the aramid-coated element because of overlap of the characteristic amine absorptions with the spectra of the surface coating.

Figure 3 shows the effect of the aramid coating on the consumption of anhydride curing agent and formation of ester products in the NMA-epoxy system, during a cure cycle of 3 hours at 100°C and 3 hours at 150°C. When the aramid coating was vacuum dried immediately before application of the epoxy resin, the reaction kinetics were only slightly different from those of the control (a dry, freshly polished, germanium surface). However, when the aramid coated element was conditioned in a humid environment (95 percent RH, 23°C), for one hour,

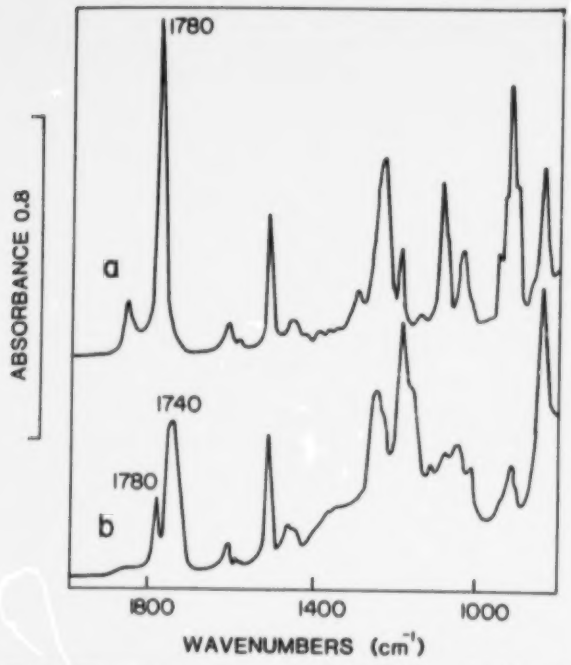

Fig. 2. IRS spectra of epoxy resin/NMA/BDMA on a freshly polished germanium element (germanium absorptions subtracted), (a)-initial, (b)-after 3 hours at 100°C + 3 hours at 150°C.

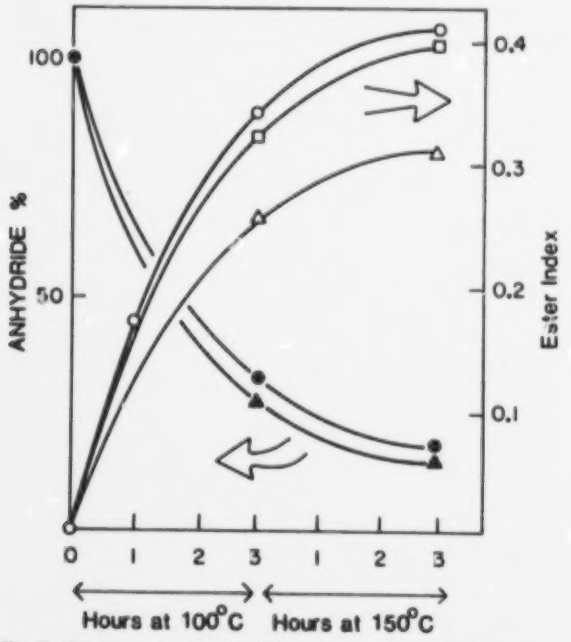

Fig. 3. Consumption of anhydride and production of ester groups during the cure of epoxy resin/NMA/BDMA in 200 to 300 nm surface layer by IRS; ○●-control-freshly polished germanium, □-adjacent to "vacuum dried" aramid coating, △▲-adjacent to "humid aged" aramid coating.

before application of the epoxy resin, the rate of consumption of anhydride was increased, and the final yield of ester products was decreased by about 25 percent.

For the DDM-epoxy system, the aramid coating had no discernable effect on the consumption of epoxy groups in roughly the first 400 nm of resin adjacent to the surface (*Table 1*). It should be noted, however, that only a relatively mild cure schedule was used here (1 hour at 100°C and 1 hour at 150°C). At higher temperatures, it is possible that the amide functionality of the aramid may play a more significant role in the crosslinking chemistry.

Figure 4 shows that a humid aged carbonized PAN surface also modifies the crosslinking kinetics in the first 200 to 300 nm of matrix adjacent to the surface. The rate of consumption of anhydride is increased and the final level of ester products and residual curing agent is decreased, as compared to the control.

PHYSICAL PROPERTIES OF COMPOSITES

As expected, the damping of forced torsional oscillation in unidirectional aramid/epoxy composites is strongly temperature dependent (*Fig. 5*). The magnitude of tan δ is a measure of the fraction of the torsional energy dissipated as heat during the oscillation. A peak is observed in tan δ close to the onset of molecular mobility in the interphase and in the bulk matrix.

The unreinforced NMA-cured epoxy has a peak

Table 1. Residual Expoxide in DDM-Cured Epoxy Resin After 1 hour at 100°C + 1 hour at 150°C

Sample	Residual Epoxide
Control	10% (Average of 3)
Aramid Coated	9% (Average of 3)

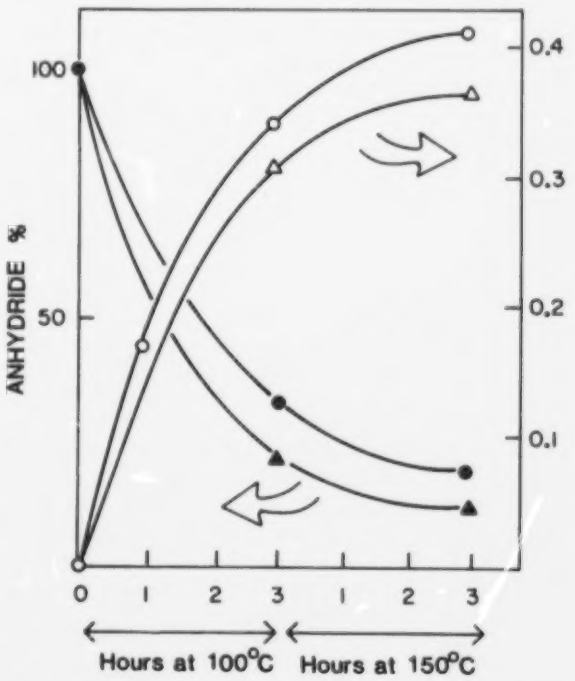

Fig. 4. Consumption of anhydride and production of ester groups during the cure of epoxy resin/NMA/BDMA in 200 to 300 nm surface layers by IRS. ○●-control-freshly polished germanium, △▲-adjacent to humid-aged carbonized PAN coating.

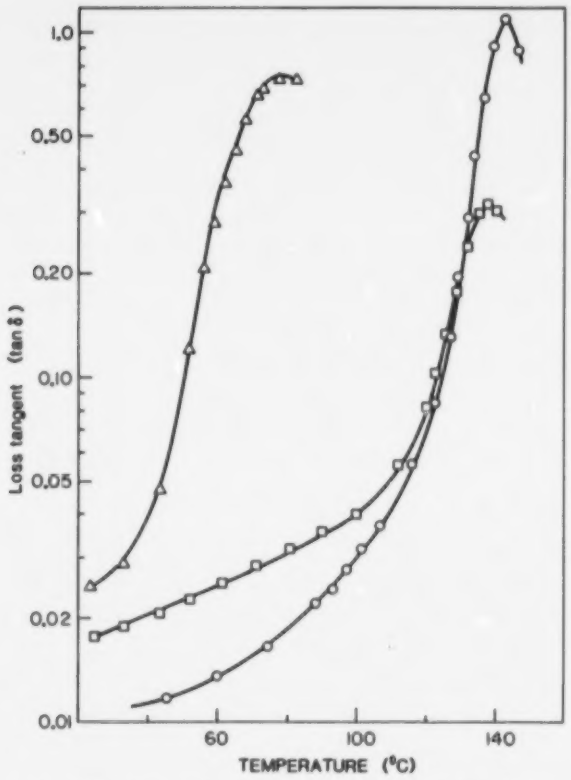

Fig. 5. DMA of aramid:epoxy composites; O-unreinforced epoxy resin/NMA/BDMA, □-reinforced with "vacuum dried" aramid fiber, △-reinforced with "conditioned" aramid fiber.

in tan δ at about 140°C. The peak in tan δ can be moved to an appreciably lower temperature when an aramid reinforcement is present (at 50 to 60 volume-percent), particularly if no great care has been taken to dry the reinforcement (*Fig. 5*). The term "conditioned" in *Fig. 5* refers to fiber which had been stored at 65 percent RH and 23°C for several months before use. Such a sample has a moisture content of about 3 percent (7), although this value will be reduced somewhat by the thermal treatment involved in the initial stages of the composite fabrication process (30 min in air at 70°C, then brief exposure to vacuum at 70°C as the resin is poured onto the fiber assembly). The term "vacuum dried" in *Fig. 5* refers to samples which were dried in vacuum at 100°C overnight, exposed briefly to the laboratory atmosphere while the resin was placed in the vacuum oven, then revacuumed before impregnation with the resin. Such a fiber will have a low moisture content. Drying histories intermediate between these two extremes produced tan δ peak temperatures between the two values shown in *Fig. 5* (4).

It was further demonstrated that the effect of the moisture was to modify the crosslinking chemistry, and not simply to plasticize the epoxy matrix, by subjecting the composite made with "conditioned" aramid fibers to a thorough drying procedure (150°C in vacuum for 18 hours). The temperature of the tan δ maximum was increased by only about 5°C by this drying procedure, confirming an irreversible change in the crosslinking chemistry had taken place in the crosslinked epoxy matrix during the initial cure.

Table 1 showed that the aramid surface had little effect on the crosslinking chemistry of the DDM-cured epoxy resin. *Figure 6* contains the corresponding DMA data, which show that the physical properties of the composite are similarly unaffected.

Carbon fiber/epoxy composites are also affected by the humidity history of the reinforcement, although the magnitude of the effect is not as pronounced as with the aramid reinforcement. In *Fig. 7*, the "conditioned" fiber was exposed to 95 percent RH and 23°C for 18 hours before being impregnated with resin in the conventional fashion. The "semi-dry" sample was placed in an air oven at 90°C for 1 hour before impregnation. The "vacuum dried" sample had a drying history identical to that of the corresponding aramid fiber. Increasing the humidity history of the carbon fiber reinforcement resulted in a significant lowering of the temperature of the tan δ maximum.

Interlaminar shear strengths of aramid NMA-cured epoxy composites also proved sensitive to the himidity history of the aramid fiber, as suggested in the commercial product literature (5). A composite made with "semi-dry" aramid had a significantly lower short beam shear strength than its "vaccuum dried" equivalent (*Table 2*). The "con-

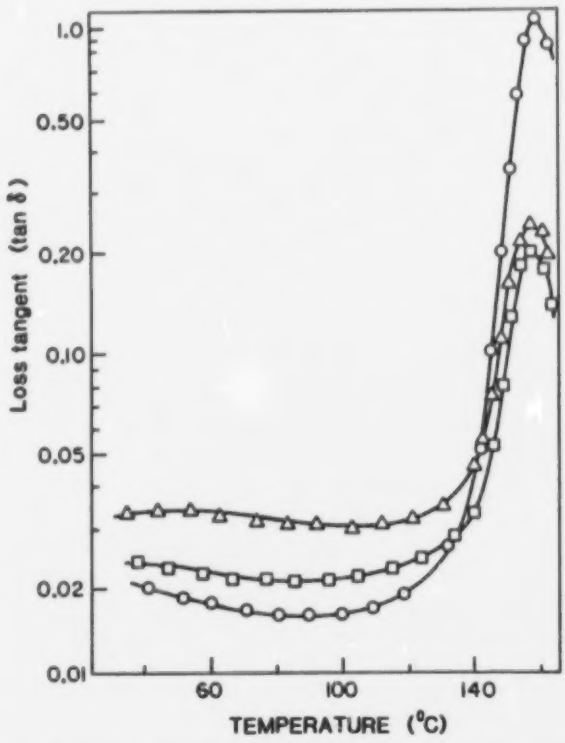

Fig. 6. DMA of aramid:epoxy composites; O-unreinforced epoxy resin/DDM, □-reinforced with "vacuum dried" aramid fibers, △-reinforced with "conditioned" aramid fibers.

Table 2. Interlaminar Shear Strengths of Aramid:Epoxy and Carbon Fiber Epoxy Composites.

Sample	Strength MPa	Standard Deviation MPa
Vacuum dried aramid/NMA-cured epoxy	63.8	2.0
"Semi-dry" aramid/NMA-cured epoxy	59.0	2.0
"Conditioned" aramid/NMA-cured epoxy	v. low	—
Vacuum dried carbon fiber/NMA cured epoxy	108.0	2.9
Conditioned carbon fiber/NMA-cured epoxy	109.3	2.8

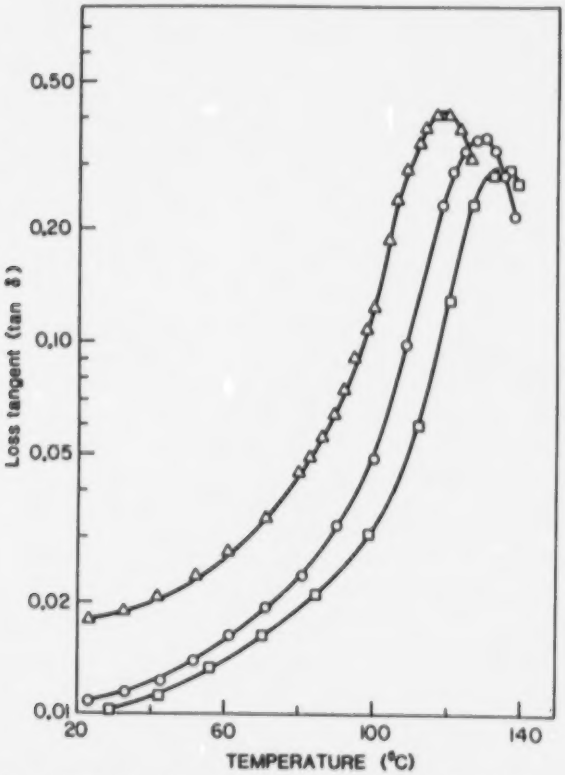

Fig. 7. DMA of carbon:epoxy composites; reinforced with "conditioned" carbon fibers, reinforced with "semi-dry" carbon fibers, and reinforced with "vacuum dried" carbon fibers.

ditioned" aramid fiber produced a composite which was so fragile that it could not be cut satisfactorily to produce the small test specimens necessary for ASTM D2344-76. The interlaminar shear strength of the carbon fiber NMA-cured epoxy composites was less sensitive to the himidity history of the fiber. The "conditioned" fiber produced a composite with short beam shear strengths similar to its semi-dry equivalent (*Table 2*).

The fracture surfaces of composites made with "conditioned" aramid fibers (*Fig. 8b*) illustrate the poor adhesion between the matrix and the reinforcement. The "vacuum dried" aramid (*Fig. 8a*) produced a composite with a significantly greater degree of fiber-matrix adhesion, as evidenced by the greater integrity of the fracture surface.

CONCLUSIONS

The crosslinking chemistry of anhydride-cured epoxies is significantly affected by an aramid surface or by a carbonized PAN surface. The agent

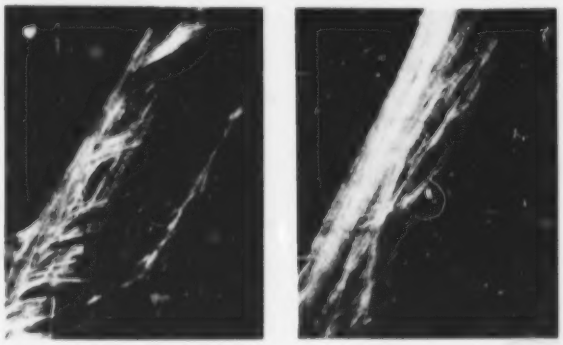

Fig. 8. Optical micrographs of fracture surfaces produced by flexure of composites perpendicular to the fiber direction. Matrix was epoxy resin/NMA/BDMA; (a)-composite prepared with "vacuum dried" aramid fiber, (b)-composite prepared with "conditioned" aramid fiber.

responsible for much of the surface effect is water, adsorbed or absorbed by the simulated reinforcement surface. The possible chemical pathways for such an effect are described in detail elsewhere (3, 4).

The modification of the crosslinking chemistry produces an interphase of matrix material with properties different from those of the bulk of the matrix. This results in a marked change in the physical properties of the composites.

Work is continuing on the PAN coatings carbonized at higher temperatures, so as to more realistically model the chemical processes of carbon fiber production. The effect of surface treatments and sizings on carbon fibers is also being investigated both by selectively removing the sizing from commercial fibers and by modification of the carbonized PAN coatings by etching, or the application of an epoxy resin overlay (8).

REFERENCES

1. E. P. Plueddemann, Ed, "Composite Materials, Vol. 6, Interfaces in Polymer Matrix Composites", Academic Press, New York (1974).
2. H. Lee and K. Neville, "Handbook of Epoxy Resins," McGraw-Hill, New York (1967).
3. A. Garton, *J. Polym. Sci., Polym. Chem. Ed.*, **22**, 1495 (1984).
4. A. Garton and J. H. Daly, *J. Polym. Sci., Polym. Chem. Ed.*, **23**, 1031 (1985).
5. "Kevlar 49 Data Manual," E. I. Dupont de Nemours and Co. Inc., Wilmington, Delaware (1978).
6. N. J. Harrick, "Internal Reflection Spectroscopy," Wiley, New York (1967).
7. L. Penn and F. Larsen, *J. Appl. Polym. Sci.*, **23**, 59 (1979).
8. L. T. Drzal, M. J. Rich, and M. F. Koenig, *J. Adhesion*, **16**, 133 (1983).

PANEL DISCUSSION

R. T. Woodhams: Henry has shown that conditioning of the fiber can affect mechanical properties of the composites. For instance, drying increases the shear modulus of the composites. Is that reaction reversible? As an example, if you make a composite from dry fibers and then condition it in a humid environment allowing it to reach equilibrium, are you not going to end up with the same properties you would have starting with wet fibers?

A. Garton: No. Actually we did the opposite experiment. When a sample is made from conditioned, wet fibers and then thoroughly dried in a vacuum oven, we do not get back to the starting point. The water changes the cure chemistry and does not just plasticize the matrix, which would be reversible as you point out.

T. G. M. van de Ven: If you are interested in the adhesion forces between fibers and matrix one of the things to do would be to estimate the interfacial free energies of the fiber surfaces. Have you looked in this direction to characterize the adhesion forces?

A. Garton: No, we did not. We were particularly concerned with the fiber-matrix interphase *after* the composite is cured. I agree that the surface energetics of the fiber are important, but we wanted to study that surface after it has become bonded to the plastic matrix, when we cannot use such techniques.

L. A. Utracki: Mike Piggott has a patent on coating the continuous fibers with a sort of stress releasing agent, a substance which lowers the adhesion between the fiber and a matrix. This technique allows dissipation of local stresses which may cause break in the fiber starting the catastrophic failure of the continuous fiber composite, and thus improving, e.g., the tensile strength at break. Did you measure the mechanical properties, especially in tension, of your composites as a function of fiber drying or conditioning?

A. Garton: Tensile properties frequently are limited by the size of the largest defect in the sample. We felt that these composites were not sufficiently defect-free to provide reliable tensile data.

Interaction Balances and Properties of Filled Polymers

C. RICHARD, KUNTHARET HING, *and* H. P. SCHREIBER

Department of Chemical Engineering
Ecole Polytechnique de Montreal
Montreal, Quebec, Canada

The dispersion behavior of calcium carbonate ($CaCO_3$), of mica and of sized sand fractions in poly(vinyl chloride) (PVC) and polypropylene (PP) has been evaluated using fillers with various surface treatments. Mechanical properties of the compounds were also studied in order to question the role of interfacial forces in the context of dispersion and property parameters. Surface characteristics of polymers and fillers were obtained from inverse gas chromatography data. It has been shown that in the acidic PVC matrix, rapid dispersion of fillers is favored when strong acid-base interactions exist at polymer filler contacts. Similarly, mechanical properties at large extension are improved by acid-base interactions. In contrast, for polypropylene (PP), a van der Waals force material, fillers without pronounced acid or base surface characteristics tend to disperse more rapidly and produce mechanically stronger compounds. The importance of filler surface properties and thus, apparently, of acid-base interfacial forces varies directly with increasing particle size of the dispersed phase.

INTRODUCTION

The use of fillers, fibers, and other solids to develop specific properties in plastics has grown enormously in practical importance. A considerable amount of research has been devoted to understanding the principles of property development in composite systems. There is tacit agreement in this regard on the important role of the compatibility between matrix polymer and additive, but frequently this factor is not considered in detail when formulating composites or when rationalizing specific performance features. There are many examples of this ambivalence to the role played by component interactions in composites. Halpin-Tsai theory (1), dealing with properties in fiber-reinforced composites, simply assumes that there is good adhesion at the matrix-additive interface. Nielsen notes (2) that semi-theoretical treatments of mechanical properties, as expressed by the Kerner equation, for example, take into account the geometry of the additive and the viscoelastic character of the polymer, but make no specific statement on the state of the interfaces.

Similarly, according to Hashin and Shtrickman (2), Lewis and Nielsen (3), etc. modulus calculations fail to account quantitatively for the contribution made by the conditions at interfaces. Two main reasons appear to account for this situation: first, in some cases, properties at low deformation, including shear or elastic moduli, which are often prime performance criteria in composites, are in fact only weakly dependent on the degree of interaction at interfaces (4, 5). Second, it has been difficult to devise useful experimental measurements of component interaction.

The latter difficulty presumably also accounts for the relative neglect of interaction phenomena when dealing with properties which, in multi-component polymer systems, are manifestly dependent on these effects. Ultimate elongation and stress properties are notable with failure often due to adhesive break-down at the matrix-additive interface, rather than to cohesive failure in one of the system's components. Models for the ultimate tensile properties of filled polymers, however, frequently are based on dispersions of particles with defined geometry but without adhesion at the polymer-additive interface (6). Further development is needed concerning relationships linking component interactions and the properties of multi-component polymers.

The present work aims to contribute to the need noted above. It does so by applying component interaction parameters, obtained from inverse gas chromatography (IGC) experiments, to an examination of mixing behavior and of mechanical properties in filled PVC and PP compounds.

The IGC Route to Interaction Parameters

The principles of IGC have been the subject of several recent articles (7–9). They combine polymer solution theory with partition principles of gas

chromatography to permit calculations of free energy, or "thermodynamic interaction" parameters for solid (polymer) vapor pairs. The technique has been extended to the evaluation of interaction parameters for stationary phases combining two solids, e.g., polymer-plasticizer or polymer-polymer (9, 10). Recent work in our laboratories has further broadened the usefulness of IGC (11, 12). Using vapor probes which have been characterized as Lewis acids and bases (13, 14), it is possible to assign an acid-base interaction number to the solids used in a polymer composite, thereby offering a numerical index of the specific contact interaction between matrix and additive. The index, Ω, is defined by:

$$\Omega = (V_g^0)_a/(V_g^0)_b \qquad (1)$$

where the V_g^0 are specific retention volumes by the solid of the chosen acid and basic vapors, respectively. The Ω parameter is readily accessible experimentally over a wide temperature range. Inherent in it, however, is the limitation that equal Ω may be obtained from pairs of V_g^0 ranging from very small to very large numbers. Therefore we propose a second interaction parameter given as:

$$\Sigma = (V_g^0)_a + (V_g^0)_b \qquad (2)$$

the Σ number representing a specific interaction site frequency in a given component. In combination through Ω and Σ numbers, the IGC technique, therefore, appears to offer a convenient experimental route to the desired interaction characteristics in filled polymer compounds.

EXPERIMENTAL

Materials

The matrix polymers in this work were PP and a mildly plasticized PVC. The polymers are well contrasted in their interaction capabilities, PP being a dispersion force material, while previously we had shown PVC to be an acidic solid (11). The PP was a commercial polymer with a melt flow index of 1.6 and $M_v \sim 3.1 \times 10^5$, as determined from intrinsic viscosity measurements in trichlorobenzene at 140°C. The PVC, a K.67 commercial resin, was used in compounded form with di-iso-octyl phthalate (DIOP) plasticizer and a tribasic thermal stabilizer in a formulation PVC/DIOP/stabilizer = 100/12/3 (parts per hundred of PVC).

The fillers involved were $CaCO_3$, mica and, in a limited number of cases, Ottawa sand. The $CaCO_3$ was an uncoated, commercial product with a B.E.T. surface area of 5.5 $m^2 \cdot g^{-1}$ and an average particle size of 1.5 μm. The mica was of phlogopite mineralization; the platelets had average lengths of about 100 μm. Sand, an unconventional additive to polymers, was used because it could be readily separated into narrowly distributed fractions with different average particle sizes. This was useful since it has been suggested (15) that the influence of interfacial conditions on the properties of composites was strongly dependent on the dimension of the minor phase additive. The Ottawa sand specimens were used as received and in plasma-treated surface modified form (see below). Both versions were wet-screened to produce fractions with these average particle diameters: S1 = 22 μm, S2 = 55 μm, and S3 = 108 μm.

All solids were used in the form received and following surface modifications designed to produce basic, neutral, and acidic characteristics. Surface modification was carried out by treating the solids in cold, microwave plasmas using vapors selected to produce the desired surface effects. The principles of surface modification by microwave plasma treatments have been described in detail elsewhere (11, 15–17). Here, plasma treatments were carried out in a tubular quartz reactor at monomer pressures in the range 0.5 to 1.5 torr. Microwave (2.45GH) power in the range 100 to 200 W was fed to the reactor which housed the solid substrates at $T \sim 100$°C. Plasma treatments were of variable duration (30 to 180 sec.), depending on the reactivity of the gases and vapors employed.

Compounding

Compounding was performed with a Brabender Plasticorder. Filled PVC samples were prepared at 170°C, while PP was compounded at 195°C. Filler content was 20, 30, and 40 weight percent, but the majority of data involved in this work is for compounds with 30 weight percent filler. The Brabender was always filled to set, constant volume (45 cm^3), and operated at 50 rpm to generate torque-time curves which were followed until a steady-state torque value had been maintained for at least 2 min. Since ease of dispersion is a valid characterization index for such polymer compounds, the torque versus time curve was integrated to the time needed for a steady-state torque reading. This integral is identified as *A*, and is porportional to the energy requirement for filler dispersion. However, the *A* parameter does not describe the fineness of dispersion attained in a given mixing operation. Following compounding, these materials were compression molded (170°C for PVC and 195°C for PP), and used for property determinations as described below.

Mechanical Properties

Mechanical properties of the various filled PVC and PP stocks were measured from stress-strain responses, obtained with an Instron tester at a jaw separation speed of 2.0 $cm \cdot min^{-1}$. A minimum of five determinations were made for each compound. Averaged values of tensile modulus and of ultimate properties were used in making performance comparisons.

RESULTS AND DISCUSSION

IGC Characteristics

The interaction parameters Ω and Σ for the materials used in this study are given in *Table 1*. Data are at 30°C; there is evidence (11, 12) that acid-base characteristics are somewhat temperature de-

Table 1. IGC Characteristics of Materials Used in Study

Note: Ω is ratio of V_g^0 for t-butanol (acid) and THF (basic) probe
Σ is sum of these V_g^0. All IGC data at 30°C.

Material:	PP		PVC		PVC[a]		MICA		$CaCO_3$		SAND	
	Ω	Σ	Ω	Σ	Ω	Σ	Ω	Σ	Ω	Σ	Ω	Σ
Surface Conditioning[b]												
1. None	0.97	61.1	0.37	78.0	0.68	91.6	1.16	51.3	1.30	101.2	1.08	17.8
2. Ar plasma	—	—	—	—	—	—	1.02	47.3	1.19	104.9	—	—
3. NH_3 plasma	—	—	—	—	—	—	1.49	38.8	1.70	100.5	1.94	16.3
4. PDMS plasma	—	—	—	—	—	—	0.93	41.5	1.04	77.3	—	—
5. C_2H_4 plasma	—	—	—	—	—	—	0.96	49.6	0.91	91.3	—	—
6. Butanol plasma	—	—	—	—	—	—	0.54	37.7	0.60	81.8	—	—
7. t-butylamine plasma	—	—	—	—	—	—	1.93	40.4	2.75	81.0	—	—

[a] Refers to PVC compound: PVC/DIOP/Stabilizer 100 phr/12 phr/3 phr
[b] Performed in microwave plasma at substrate T ~ 100°C

pendent so that the indices given in *Table 1* may not accurately represent the interaction behavior during compounding. They are pertinent to the use properties of the materials, however. As expected, the Ω for PP is near unity, typical of solids in which dispersion forces are dominant. Again, as in earlier work (11), PVC was found to be an acidic solid, with Ω substantially less than unity. The compounded version of PVC remains acidic, but to a lesser degree. Of the fillers as received, sand is essentially "neutral" while mica and $CaCO_3$ surfaces are progressively more basic ($\Omega > 1.0$). The interaction site frequency Σ for PVC is somewhat increased by plasticization, and is relatively small in the sand sample.

Categoric changes in Ω are produced by plasma treatments of particulates, as shown in *Table 1*. Treatments in butanol vapor generate acidic surfaces in mica and $CaCO_3$, while strongly basic surface interactions are produced by treatments in t-butylamine and ammonia. A similar shift toward basic interactions is produced by NH_3 plasma treatments of sand. The decreased Σ for plasma treated versions of $CaCO_3$ and mica indicate a reduced site frequency, possibly due to local sintering leading to slight reductions in specific surface areas. Decreases of this magnitude (~20 percent) have also been observed recently with high surface area carbon blacks (18) which had been plasma treated. For convenience, the numbers used in *Table 1* to identify surface treated fillers will be retained throughout this paper.

Dispersion Behavior

The energy needed for dispersion, *A*, clearly reflects the state of specific interactions between polymer and filler. This is documented in *Figs. 1* and 2 for PP and PVC, respectively. The data shown for 30 weight percent filler are typical of those also obtained at other filler loads. The *A* parameters are plotted against ΔΩ, this being defined as

$$\Delta\Omega = \Omega_{polymer} - \Omega_{filler}. \qquad (3)$$

The procedure generates very different relationships in the two cases. With PP (*Fig. 1*), a distinct minimun occurs when $\Delta\Omega \rightarrow 0$, that is, when filler surfaces are dominated by dispersion forces (versions 4 and 5 of mica and $CaCO_3$, see *Table 1*), or

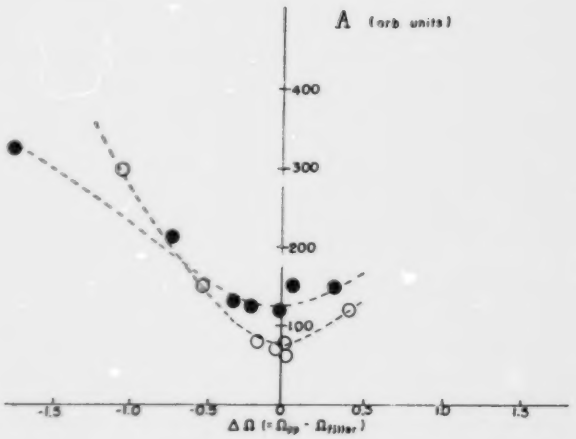

Fig. 1. Apparent relationship between dispersion energy requirement and matrix-filler interaction. PP matrix, 30 weight percent of ● $CaCO_3$ and ○ mica.

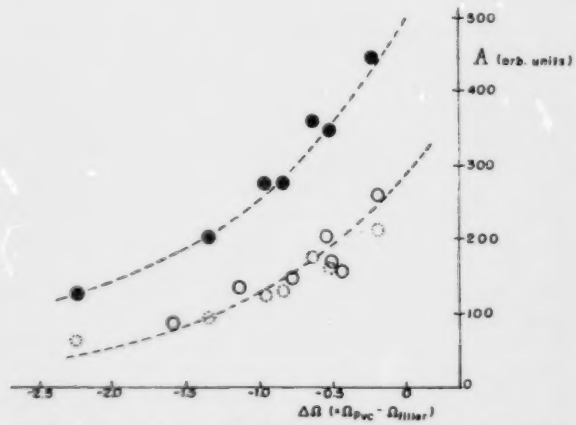

Fig. 2. Apparent relationship between dispersion energy requirement and matrix-filler interaction PVC matrix, 30 weight percent of ● $CaCO_3$, ○ mica, and ◌ represents $CaCO_3$ data recalculated to normalize on Σ values—see text and Table 1.

when acidic and basic sites are in numerical balance (e.g., mica-2, *Table 1*). The relationship in *Fig. 1* is nearly independent of the filler used. Thus, neither the differences in Ω between mica and $CaCO_3$ or the fact that in terms of Σ, $CaCO_3$ has a higher specific interaction site frequency, appear to influence the dispersion parameter.

The pattern of results for PVC, shown in *Fig. 2*, strongly infers an important influence on A of specific interactions and of site frequencies. Clearly, easy dispersion is linked with negative values of $\Delta\Omega$—that is with fillers having basic surface characteristics such as versions 3 and 7 of the solids. (In this case $\Delta\Omega$ is calculated using the Ω for pure PVC. Implied is a measure of the polymer-filler interaction unmodified by the presence of other additives). The relationships in *Fig. 2* for $CaCO_3$ and mica are strongly differentiated in the A axis, unlike those for PP as matrix. We propose that this is a reflection of differences in Σ for the two fillers. Evidently, larger numbers of interacting points between polymer and filler increase the dispersion energy requirement. This may be due to less flexible and therefore more shear-resistant polymer layers near the surfaces. The origins, in Σ, of the different coordinate positions in *Fig. 2* are supported by the results of a simple superposition procedure, indicated by dotted symbols in *Fig. 2*. The site frequency ratio between $CaCO_3$ and mica, $a = \Sigma_{CaCO3}/\Sigma_{mica}$, averaged for the seven filler versions, is 2.1. Assuming that

$$A_{CaCO3} = a\, A_{mica} \qquad (4)$$

A_{CaCO3} was recalculated using the given shift factor. The two sets of data now coincide reasonably well. More refined approaches to such a superposition may involve non-linear analogues to *Eq 4*, inclusion in the shift factor of the dispersion force site frequencies and of the probable temperature dependence of Σ.

Mechanical Properties

Tensile stiffness (initial modulus), stress, and elongation at rupture were selected as the parameters descriptive of mechanical behavior at low and high deformation, respectively. Their variation, relative to properties of the control polymer, is displayed in the bar graphs of *Figs. 3–5*. In discussing these results, the assumption is made that interfacial factors are responsible for observations. It is, of course, possible that an additional contribution to property effects arises from different degrees of dispersion attained under present standard mixing operations. However, fineness of dispersion in such an event would be regarded as yet another property parameter of filled polymers which is sensitive to interfacial forces. This point is under further study.

The behavior of initial modulus in filled PP generally supports the concept that mechanical properties at low deformation are only weakly dependent on interfacial effects. The variation from case to case somewhat exceeds the experimental reproducibility (±8 percent), but there is no clearly discernible pattern in the data. In the PVC system, however, trends are apparent; one of these is the greater reinforcing tendency produced by basic solids (#3 and 7), and a weakening effect produced by the strongly acidic, butanol-modified version of the fillers (#6). The second trend shows mica to be slightly more responsive than $CaCO_3$ to surface modifications produced by plasma treatments. The trend is also suggested by properties at high deformation. This will be considered again later in this

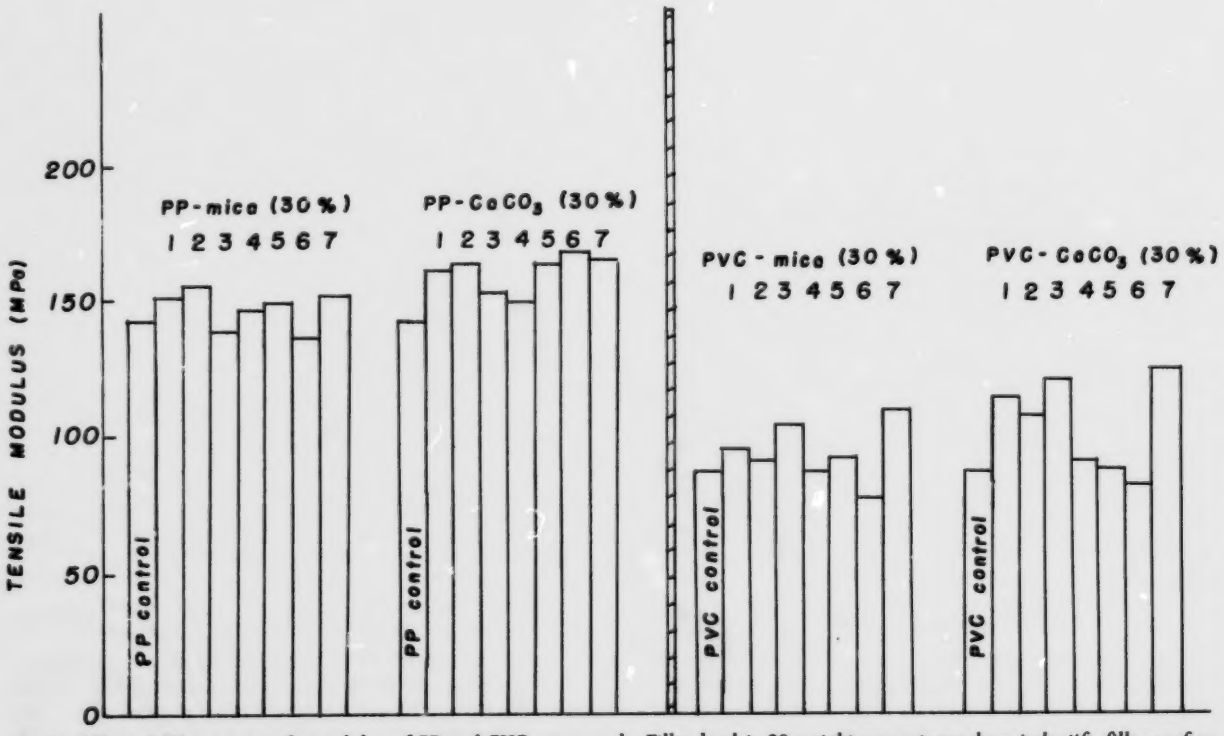

Fig. 3. Effect of fillers on tensile modulus of PP and PVC compounds. Filler load is 30 weight percent; numbers indentify filler surface treatment given in Table 1.

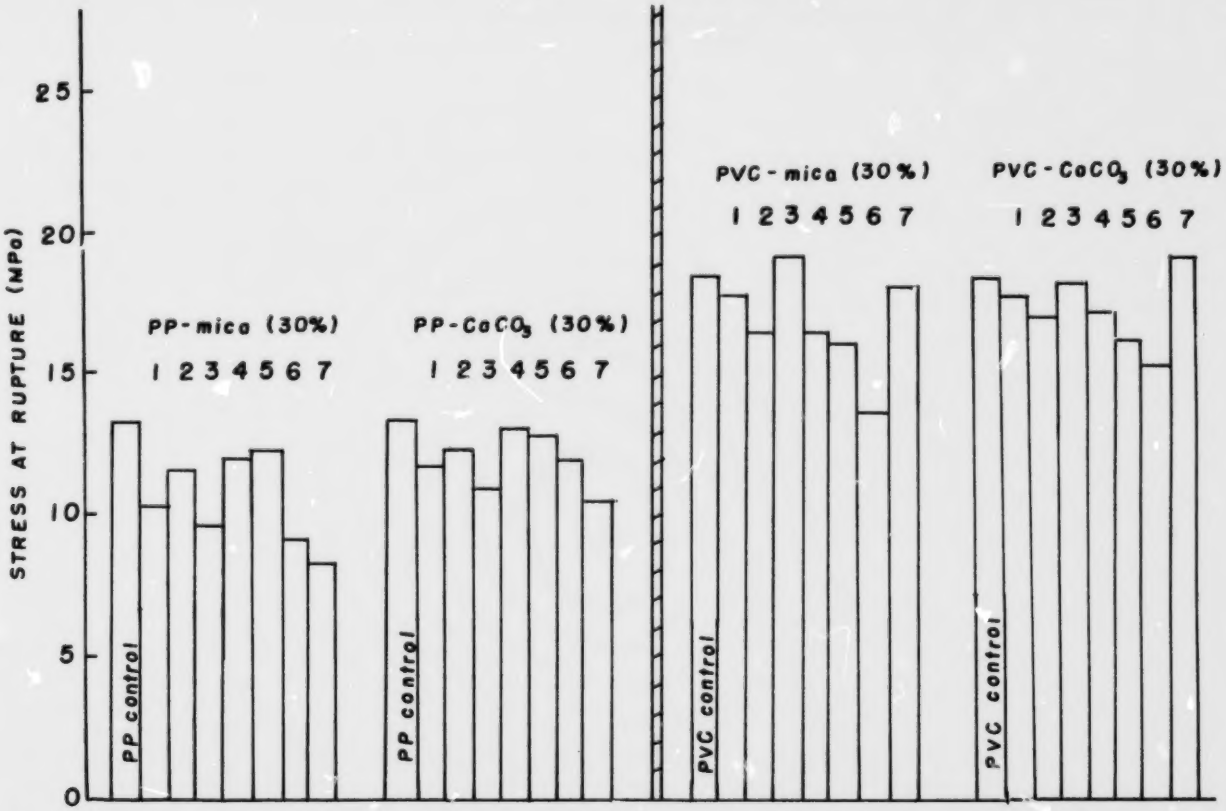

Fig. 4. Effect of fillers on stress at rupture of PP and PVC compounds; numbers identify filler surface treatments given in Table 1.

section. The reinforcing performances suggest that even properties at low deformation respond to surface interactions when these involve strong acid-base couplings between polymer and filler.

The dependence of ultimate mechanicals on interfacial phenomena is clearly shown in *Fig. 4* and 5. In PP and PVC alike, stress and elongation-at-rupture reflect the interaction balance at polymer-filler contacts. The pattern of results closely resembles that of the mixing energy parameter A (*Figs. 1* and 2). Thus, in PP, solids with dispersion-force surface properties are preferable fillers to those with pronounced acidic or basic interaction characteristics. Unlike the *A* parameter, however, $CaCO_3$ and mica are differentiated as to magnitude of effect produced, $CaCO_3$ being the more effective filler. The larger surface area of $CaCO_3$ may be responsible for this effect. In the acidic PVC matrix, the analogy between the behavior of *A* and the ultimate tensile parameters is pronounced. The elongation at break of compounds using strongly basic fillers is noticeably greater than when "neutral" or acidic surface modifications have been produced. At high deformation, sensitive response of mechanical properties to interfacial forces and thus, presumably, to adhesion between polymer and filler is therefore evident.

Again, as with the initial modulus, the variations in ultimate stress and elongation produced by plasma treatments of fillers appear to be greater for mica than for $CaCO_3$. It is possible, of course, that the higher concentration of interaction sites (Σ) in $CaCO_3$ produces inherently stronger bonding with both PP and PVC than is the case with mica. Certainly, there has been recognition (19, 20) of difficulties in using mica as a reinforcing filler for polymers, and changes in the surface chemistry of this solid might therefore be expected to produce particularly significant effects on composite properties.

The smaller particle size of $CaCO_3$ may be another reason for reduced sensitivity to surface conditioning. This would follow concepts expressed by Gent and coworkers (15), that interfacial factors in the mechanical properties of composites become more important as the dimensions of the reinforcing agent become large compared with the size of initiation sites for failure (e.g., the size of stress concentration sites leading to Griffith-type failures in materials such as reinforced polymers and rubbers).

This point was questioned more closely through use of the fractionated, and surface-modified sand samples. Only the PVC was used in this series of experiments. The variation of mechanical properties with surface condition is clearly significant, as shown in *Table 2*. At each of the loadings for which data are given, the performance of compounds with NH_3-plasma-modified sand is superior to comparable performance when unmodified sand is involved. The result reconfirms the need to consider acid-base interactions when estimating the mechanical

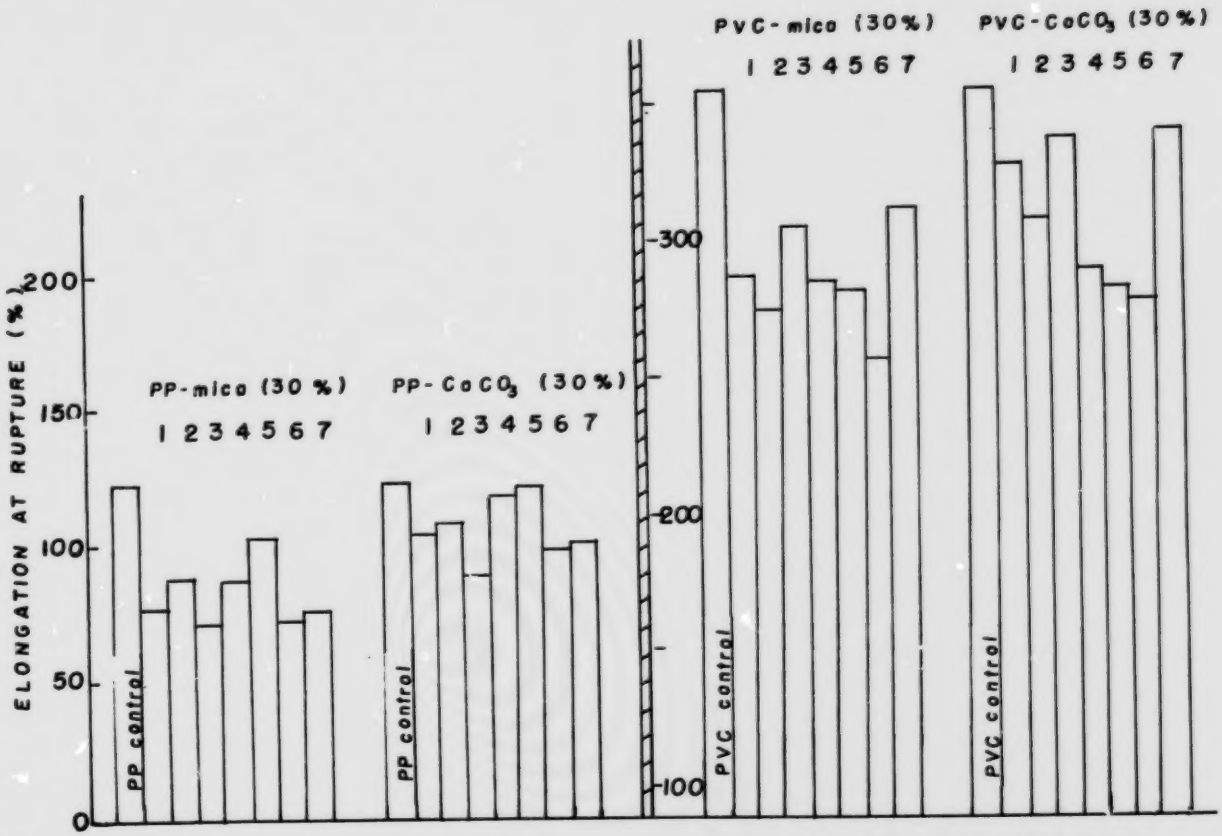

Fig. 5. Effect of fillers on ultimate elongation of PP and PVC compounds; numbers identify filler surface treatments given in Table 1.

Table 2. System PVC-Sand: Effect of Particle Size on Mechanical Properties

Property	Tensile Modulus* MPa.	Tensile Stress* MPa.	E.L. @ Break* (Percent)
Unfilled PVC	660	18.4	356
30 Percent sand:			
S_1	870	19.2	215
S_1 modified	910	19.0	245
S_2	900	17.4	208
S_2 modified	980	18.7	250
S_3	930	16.0	210
S_3 modified	1060	20.1	268
40 Percent sand:			
S_1	910	16.2	195
S_1 modified	950	15.3	220
S_2	920	15.4	182
S_2 modified	990	17.7	245
S_3	1010	15.7	185
S_3 modified	1130	18.0	260

* Average of 5 determinations; errors are ±60 MPa in modulus; ±1.1 MPa in stress, ±25 percent in ultimate elongation.

properties of filled polymers, especially at high deformation. The data also allow a calculation of the increment in mechanical properties, when going from compounds with unmodified to those with plasma-modified sand, and its possible dependence on particle size. Incremental performance data have been calculated for tensile modulus and elongation at rupture.

Figure 6 shows the results at the two sand loadings (30 and 40 weight-percent). The trend displayed in this representation is in line with the findings of Gent and coworkers (15), that is, the contribution of acid-base interactions to the enhancement of these mechanical properties increases with increasing particle size. Since critical dimensions for failure sites are likely to be in the micron or submicron range, significant increments due to surface modification are produced even in compounds using the smallest sand particles (~22 μm). As shown in *Fig. 6*, however, the variation with particle size exceeds estimated experimental error; the relationship therefore indicates the increased importance

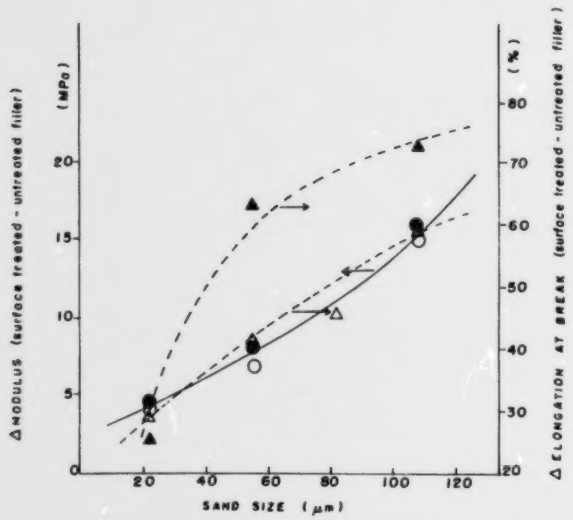

Fig. 6. Effects of surface treatment on mechanical properties of sand-filled PVC: Variation with particle size. Open symbols, 30 weight percent loading; filled symbols, 40 weight percent loading.

of interfacial forces when larger reinforcing geometries are involved in the formulation of composite structures. Finally, also noted in *Fig. 6* is the virtual independence of the elongation results on filler load level and the questionable loading dependence in modulus data. At least in the limited loading range studied therefore, (40 weight-percent maximum), the neglect of interaction forces in formulating composites would be unwarranted.

CONCLUSIONS

1) Surface interactions have been shown to be important in the dispersion of fillers in polymer matrices and in determining the mechanical properties of filled PVC and PP compounds.

2) Strong acid-base interaction promotes dispersion and improves the performance of filled compounds when the matrix polymer has pronounced acid (or base) surface properties. In non-polar (dispersion-force) polymers, preference should be given to fillers without pronounced acid or base properties.

3) The significance of surface and interfacial forces increases with filler particle size.

4) Microwave plasma treatments were shown to be effective means for surface conditioning fillers for use with PVC and PP matrices.

ACKNOWLEDGMENT

This research was supported by grants from the Natural Sciences and Engineering Research Council, Canada. Additional support from Northern Telecom Inc. is greatly appreciated. We thank Mrs. J. Klemberg Sapieha for valuable assistance in plasma treatment experiments.

REFERENCES

1. J. E. Ashton, J. C. Halpin, and P. H. Petit, "Primer on Composite Materials: Analysis," Technomic Publishing Co. Inc., Stamford (1969).
2. L. E. Nielsen, *J. Compos. Mater.*, **1**, 100 (1967).
3. T. B. Lewis and L. E. Nielsen, *J. Appl. Polym. Sci.*, **14**, 1449 (1970).
4. J. L. Kardos, *Am. Chem. Soc., Div. Polym. Chem., Polym. Prepr.* **24**, 185 (1983).
5. M. Kapuscinski and H. P. Schreiber, *Polym. Eng. Sci.*, **21**, 433 (1981).
6. M. Markis and L. Nicolais. *J. Appl. Polym. Sci.*, **15**, 469 (1971).
7. O. Olabisi, L. W. Robeson, and M. T. Shaw, "Polymer-Polymer to Miscibility," Academic Press, New York (1979).
8. J. E. Guillet, "Progress in Gas Chromatography," J. H. Purnell, Ed., Wiley-Interscience, New York (1973).
9. B. Riedl and R. E. Prud'homme, Polyblends '84, National Research Council of Canada Symposium Proceedings p. 3.1 (1984).
10. D. D. Deshpande, D. Patterson, H. P. Schreiber, and C. S. Su, *Macromolecules*, **1**, 530 (1974).
11. H. P. Schreiber, M. R. Wertheimer, and M. Lambla, *J. Appl. Polym. Sci.*, **27**, 2269 (1982).
12. H. P. Schreiber, C. Richard, and M. R. Wertheimer, "Physicochemical Aspects of Polymer Surfaces," Vol. 2, p. 739, K. Mittal. Ed., Plenum Publishing, New York (1983).
13. R. S. Drago, G. G., Vogel, and T. E. Needham, *J. Am. Chem. Soc.*, **93**, 6014 (1971).
14. P. M. Cuickor and J. M. Prausnitz, *J. Phys. Chem.*, **76**, 598 (1972).
15. A. N. Gent, G. S. Fielding-Russell, D. L Livingston, and D. W. Nicholson, *J. Mater. Sci.*, **16**, 949 (1981).
16. H. P. Schreiber, Y. Tewari and M. R. Wertheimer, *J. Appl. Polym. Sci.*, **20**, 2663 (1976).
17. M. R. Wertheimer, J. E. Klemberg-Sapieha, and H. P. Schreiber, *Thin Solid Films*, **115**, 109 (1984).
18. A. L. Rollin, J. Bertin, M. R. Wertheimer, and H. P. Schreiber, to be published.
19. A. Garton, "Characterization of the Interface: Some Initial Results for Mica-Polypropylene Composites", IMRI Mini-Symposium, "Composites-81", Montreal, December (1981).
20. B. Sanschagrin, B. Fisa, and B. Favis, 30th Annual Technical Conference, Society of Plastic Engineers, 683, (1984).

PANEL DISCUSSION

W. E. Baker: Are these V_g^0's normalized on the basis of weight, surface area, or volume? Do you have Ω for high and low density polyethylenes?

H. P. Schreiber: Yes to both of your questions. The first question is a very good one. The V_g^0's should be normalized to constant surface area but in this case they are to constant mass. However, since we are making strictly internal comparisons this is of little importance; the plasma treatment changes the total surface area very little. As far as the second question is concerned, we have done not only HDPE and LDPE but also LLDPE, PP and so on. These data are available. The values of Ω's were found to be close to unity. Last Tuesday in this room I gave a much better talk than today showing some Ω values for polyethylenes. It turns out that these are very sensitive to even minor amounts of surface damage caused either by thermal degradation or by oxygen occlusion, unsaturation and so on. Generally speaking if one is very cautious in the preparation of IGC columns, one finds $\Omega = 1.00 \pm 0.05$. For thermally degraded samples we observed values as high as 1.15.

R. T. Woodhams: It seems that more and more evidence accumulates that in order to get a signifi-

cant improvement of mechanical properties the particles ought to be about 1 μm in diameter. This is true for both inorganic as well as organic particle composites. Until one gets down to these dimensions one cannot see the spectacular improvements in, e.g., ductility or impact toughness. I am referring in particular to works by Jo Radosta and Kris Mather from Pfizer.

H. P. Schreiber: This is true. In my talk on rutile-reinforced polyethylenes and chlorinated polyethylene I showed that one will not get significant improvement of properties until a proper balance of the acid-base interactions is reached. The particles were quite small. At low volume of rutile one did see enhancement of ductility by 10 to 15 weight percent, relative to the neat polymer matrix. Elongation at rupture went through a maximum as the volume fraction increased. This enhancement for fixed particle size seems to be critically dependent on the acid-base balance. We feel that the specific interphase interactions in composites are of great importance.

L. A. Utracki: You showed the values of Ω and Σ for sand. You also measured these parameters for glass fibers. Are they similar?

H. P. Schreiber: They are similar in Ω but not in Σ; Σ's for glass fibers are even lower. I do not understand what is happening with glass fibers. We have been getting values of $\Sigma = 1$ or 2. It seems that from the point of IGC, octane, butylamine, THF, butanol ..., simply do not interact with glass. This essentially says that there are no interaction sites of any kind.

L. A. Utracki: Are you talking of treated glass fibers, as they invariably are by the manufacturer, or pure glass fibers?

H. P. Schreiber: Well, I do not know. This is E-glass. We also have samples of this with amino-silane coatings. It turns out, curiously enough, that I really do not know what happens with amino-silane. It increases Σ by a factor of about 10 without changing Ω values. It seems that amino-silane changes the ability of E-glass to interact, but it does not make it either acidic or basic.

M. Schwartz: Have the values of Ω and Σ for LLDPE been published?

H. P. Schreiber: Published values are for HDPE and LDPE but not LLDPE. But these are not very interesting Michael, they are all very similar. What is curious is that in a sequence of LDPE from different manufacturers, presumably due to different frequency of branch points, etc., there are apparent changes in Σ but not in Ω, i.e., in a sequence $\Omega = 0.97$ to 1.03 but $\Sigma = 40$ to 90. We do not know what to make of this. In principle this should correlate with reactive conditions, branch frequency, or branch length, or something of this type.

L. A. Utracki: Henry, it seems to me that you are treating polar and non-polar polymers in a completely different fashion. You proposed to divide the A-values for PVC by the ratio of Σ's—your magic number of 2.1—but you do not treat PP results in a parallel manner. Why?

H. P. Schreiber: You already have an answer. The reason why we divided A-values of PVC by 2.1 was precisely because the data for $CaCO_3$ and mica were separated by that factor as obtained from the Σ-values for these two fillers. That led to the idea that indeed where you have two sets of fillers, each of them describing a range of acid-base interactions with the matrix polymer, and yet differentiated on the Y-axis, then maybe the next factor which influences the position of these curves is the frequency of reactive sites in the filler. In the case of the PP matrix, a difference in acid-base interactive sites in $CaCO_3$ and mica does not matter; on the other hand we would argue that the important factor in the case of PP is the ratio of V_g^0–octane values. If it happened that V_g^0–octane for C_aCO_3 were very different from that of mica, then there would be a large difference in the density of interacting sites of the van der Waals type and the curves ought to be separated. Now, the V_g^0–octane for the two fillers are actually quite similar, and so the similarity of curves is not surprising and no "shift factor" is needed.

L. A. Utracki: This is a very interesting outcome of the discussion. What you are telling us is that in effect you have two types of interactions which must be considered separately: the acid-base type which people like Fawkes, Drago and others are advocating, and on top of these you seem to feel that one should consider the old van der Waals interactions, presumably dominant in non-polar polymers of polyolefin type.

H. P. Schreiber: Yes, I think that you are right. The kind of data we are generating indicate that it is quite important to consider both interaction types when the matrix is polyolefinic.

The Flow of Suspensions

T. G. M. VAN DE VEN

Pulp and Paper Research Institute of Canada
and
Department of Chemistry
McGill University
Montreal, Quebec, Canada, H3A 2A7

Most rheological and rheo-optical properties of suspensions such as viscosity and light-scattering intensities can be expressed in terms of the average orientation and/or the average concentration distribution of the suspended particles. In general one can distinguish several distinct regimes: (i) infinitely dilute, (ii) dilute, (iii) semi-dilute or moderately concentrated, and (iv) concentrated suspensions. Cases (i) and (ii) are regimes in which particle interactions are either absent or only two-body interactions are important. These cases can, in general, be well described theoretically. Regime (iii) is characterized by n-body ($n \geqq 2$) interactions and is the least understood. Regime (iv) can often be described in terms of a cell model in which the motion of a reference particle, or the fluid motion around it, is described.

INTRODUCTION

Understanding the behavior of colloidal dispersions is important in many respects, and consequently much work has been devoted to this problem. Depending on the nature of the interaction between the suspended particles, such a system can be either stable or unstable, i.e., the possibility exists that collisions among particles lead to aggregation. The stability of suspensions is one of the most important aspects and, at least for model systems, is reasonably well understood, both in quiescent and in flowing systems. A second important aspect is the flow behavior of suspensions. Again it is useful to differentiate between unstable and stable suspensions. In unstable systems particles coagulate into flocs and usually after some time a dynamic equilibrium is established between floc formation and break-up. Satisfactory theories exist for the description of such systems (1–3).

Here we shall be concerned with the flow behavior of stable systems. This review is by no means complete, but it attempts give a short outline of the major ideas and results in this area.

We can distinguish several distinct regimes: (i) infinitely dilute suspensions, (ii) dilute suspensions in which two-body interactions are important, (iii) semi-dilute or moderately concentrated, and (iv) high concentrations.

In particular, we will emphasize the differences and analogies between suspensions of spheres and suspensions of rod or disk-shaped particles.

INFINITELY DILUTE AND DILUTE SUSPENSIONS

The properties of flowing suspensions depend on the motions and interactions of the suspended particles. In general the particles undergo rather complicated rotational and translational motions and collisions. For the full description of a system one must know both the number and the orientation distribution of the particles at every instant. For arbitrarily shaped particles a coupling exists between these two distributions (4), but for particles with sufficient symmetry, such as ellipsoids, rods, disks, ribbon-shaped particles, etc., such coupling is absent. In such cases the number distribution is described by the translational convective diffusion equation:

$$\frac{\partial n}{\partial t} = \nabla\cdot(\underline{D}_t\cdot\nabla n) - \nabla\cdot(\underline{u}n). \qquad (1)$$

Here n is the number distribution of particles, t the time, $\underline{D}_t$ the translational diffusion tensor, and $\underline{u}$ the translational velocity due to the shear field (or any other external fields). Similarly the orientation distribution p is described by the rotary convective diffusion equation:

$$\frac{\partial p}{\partial t} = \nabla\cdot(\underline{D}_r\cdot\nabla p) - \nabla\cdot(\underline{\omega}p), \qquad (2)$$

where $\underline{D}_r$ is the rotary diffusion tensor and $\underline{\omega}$ the angular velocity of the particles caused by shear

(and/or other external fields). All properties of suspensions can be expressed in terms of n and p.

As an example, let us consider the viscosity of a suspension consisting of rod or disk-shaped particles. In this case *Eq 2* simplifies to

$$\frac{\partial p}{\partial t} = D_r \nabla^2 p - \nabla \cdot (\underline{\omega} p) \tag{3}$$

where D_r is the rotary diffusion coefficient of the particle. It follows immediately from *Eq 3* that the viscosity of the system will depend on the type of flow which it is subjected. The type of flow determines the angular velocity $\underline{\omega}$ which in turn determines the orientation distribution p of the particles.

Let us consider a dilute suspension subjected to a simple shear flow, the suspending medium being Newtonian. In this case the angular velocity vector $\underline{\omega}$ has two components, $d\theta/dt$ and $\sin\theta d\phi/dt$, given by (5):

$$\frac{d\theta}{dt} = \frac{1}{4} BG \sin 2\theta \sin 2\phi \tag{4a}$$

$$\frac{d\phi}{dt} = \frac{1}{2} G(1 + B\cos 2\phi), \tag{4b}$$

where θ and ϕ describe the orientation of a particle (see *Fig. 1*), G is the rate of shear and B is a shape factor. For spheroidal particles, B is related to the axis ratio r by

$$B = \frac{r^2 - 1}{r^2 + 1}. \tag{5}$$

For other axisymmetric particles one can define an equivalent axis ratio r_e, which replaces r in *Eq 5*. From *Eqs 4b* and *5* it can be seen that an individual particle rotates periodically about the X_1-axis, with a period of rotation given by

$$T = \frac{2\pi}{G} (r_e + r_e^{-1}). \tag{6}$$

Several solutions of *Eq 3* with $\underline{\omega}$ given by *Eq 4*

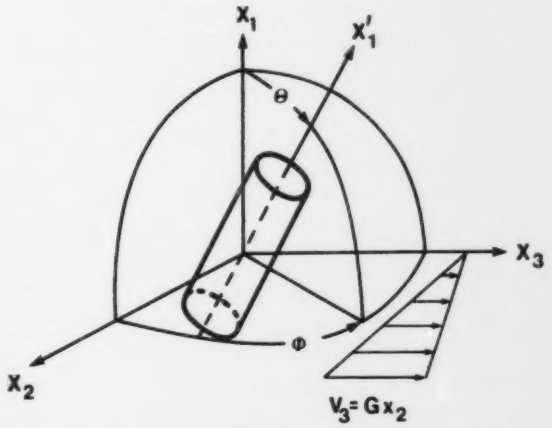

Fig. 1. Coordinate system describing the rotation of the axis of revolution X'_1 of an axisymmetric particle in a simple shear flow given by $V_3 = Gx_2$. X_i are space fixed Cartesian coordinates. The spherical polar angles specify the orientation of X'_1.

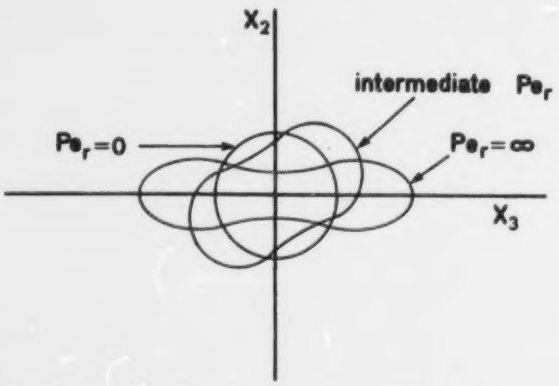

Fig. 2. Schematics of steady state solutions of the rotary convection diffusion equation (projection on X_2X_3-plane). The distribution changes gradually from random ($Pe_r = 0$) till the case where the probability of finding particles aligned with the flow is maximum ($Pe_r = \infty$).

can be found in the literature, especially for Péclet numbers $Pe_r = G/D_r \ll 1$ (dominant Brownian motion) (6, 7), and $Pe_r \gg 1$ (flow dominated) (8, 9). Steady state orientation distributions ($\partial p/\partial t = 0$) of projections on the X_2X_3-plane are shown schematically in *Fig. 2*. It can be seen that when $Pe_r = 0$ all orientations are equally probable, i.e., p = constant, while for $Pe_r = \infty$, orientations with $\phi = 90°$ are more probable than orientations of $\phi = 0°$. In this case p is given by

$$p_\infty = \frac{2}{TG(1 + B\cos 2\phi)}, \tag{7}$$

a relation which follows directly from *Eq 4b*. Thus p is directly related to $d\phi/dt$; the lower the angular velocity at a given orientation, the more likely to find a particle at that orientation. For intermediate Péclet numbers, the distribution is skewed with a maximum occurring in the range $\phi = 45°$ to $90°$.

Motions similar to those described by *Eqs 4–7* occur in other linear two-dimensional flows, although in certain flows particle rotation is absent, (e.g., in extensional flow), which substantially facilitates the description of such systems. Knowledge of the orientation distribution p allows one to calculate the vicosity of flowing suspensions.

The viscosity of a suspension can be expressed as:

$$\eta = \eta_0(1 + k_1 c + k_2 c^2 + \cdots), \tag{8}$$

where η_0 is the viscosity of the suspending medium and c the volume fraction of particles. The coefficients k_n depend on particle shape, orientation, the presence of diffuse ionic double layers (in case of electrically charged particles), and the type of flow. The coefficient k_1 depends on properties of individual single particles, k_2 depends on two-body interactions and in general k_n on n-body interactions. The calculation of these coefficients presents formidable difficulties, especially for $n \geq 2$.

The coefficient k_1, often referred to as intrinsic viscosity, $[\eta]$, can for axisymmetric particles be expressed as (10, 11):

$$[\eta] = C_1 \langle \sin^4\theta \sin^2 2\phi \rangle + C_2 + C_3 \langle \sin^2\theta \rangle + \frac{C_4}{Pe_r} \langle \sin^2\theta \sin 2\phi \rangle \quad (9)$$

The constants C_i depend on the shape of the particle and the quantities in angular brackets are orientational averages. They can be found by averaging over all orientations. E.g.:

$$\langle \sin^2\theta \rangle = \int_0^{\pi} \int_0^{2\pi} \sin^2\theta \, p(\theta, \phi; t) \sin\theta \, d\theta \, d\phi, \quad (10)$$

where p is the solution of the rotary convective diffusion equation (*Eq 3*). Because p depends on time, it can be seen that the orientational averages occurring in *Eq 9* and hence $k_1 = [\eta]$ will vary with time. When $D_r = 0$ (no rotary Brownian motion), *Eq 3* has an infinite number of solutions, all except one of periodicity $T/2$ (for particles with fore-aft symmetry). Hence for a monodisperse system all properties will vary periodically with period $T/2$. Such oscillatory behavior has never been observed in real systems because, for a variety of reasons, the oscillations are attenuated. Causes for the attenuation are (i) polydispersity in particle shape which causes a spread in the distribution of periods of rotation, (ii) rotary Brownian motion which causes a change in the orientation distribution function, (iii) particle interactions which affect the periodicity of particle rotation, (iv) non-uniformity in flow, and (v) deviations from axisymmetry. In real systems a combination of these factors is operating.

From these arguments it follows that in general a suspension of spheroidal particles when sheared will pass through a transient regime characterized by damped oscillations before reaching a steady state orientation distribution. An example of this behavior is given in *Fig. 3*, which shows experimental results for η versus time for a suspension of rods with $r_e = 5.2 \pm 0.9$, together with theoretical predictions calculated from *Eq 9* [after Ivanov, *et al.* (12)]. In these calculations, only damping due to polydispersity in shape is taken into account, which for that system is the main cause of damping.

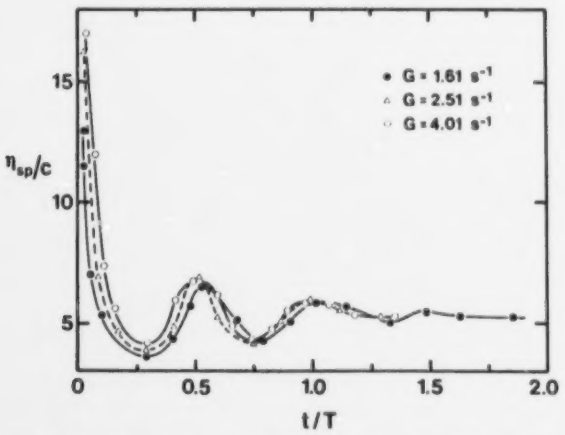

Fig. 3. Example of a damped oscillation in the viscosity of suspensions of rods. $r_e = 5.2 \pm 0.9$. Initial orientation $\theta = 90°$, $\phi = 0°$. The dashed line is calculated from Eq 9, taking polydispersity into account (after Ivanov et al (12)). The solid lines are smooth fits through the experimental data.

Obviously such oscillations only occur in systems of nonspherical particles. For spherical particles it can be shown from *Eqs 3* and *9* that $[\eta] = 2.5$, in agreement with the classical result of Einstein (13). For spheres $[\eta]$ becomes independent of the type of flow, in contrast to suspensions of anisometric particles.

Besides particle shape and type of flow, $[\eta]$ also depends on electrical double layers that often surround colloidal particles, especially in aqueous or other polar media. The presence of the double layer as well as its deformation in flow contribute to the energy dissipation in the system. This contribution was first calculated by Smoluchowski (14) and improved upon in Refs. 15 and 16. For spherical particles, the result can be written as

$$[\eta] = 2.5 + \frac{f(\kappa a)}{\sigma \eta_0 a^2} \left(\frac{e\zeta}{kT} \right)^2. \quad (11)$$

Here σ is the specific conductance of the electrolyte solution, a the sphere radius, e the electronic charge, ζ the ζ-potential of the particle, and $f(\kappa a)$ a known function of κa, κ^{-1} being the characteristic length of the double layer. The contribution of the double layer to the intrinsic viscosity is known as the primary electroviscous effect. For non-spherical particles a similar contribution exists, but neither theory nor experimental observations are available.

The coefficient k_2 is often expressed as $k_2 = k'[\eta]$, where k' is referred to as the Huggins' coefficient. Theoretical results are available for suspensions of spheres. The value of k_2 depends on the type of flow. The reason for the flow dependence can be readily seen. The value of k_2 depends upon the distribution of particles around a reference particle, which is described by *Eq 1*. The solution of this equation depends on the particle velocity u in the flow field. For neutral spheres, according to various theories (17), k_2 is in the range 6 to 10. For non-spherical particles no results are available. Again the presence of double layers surrounding the particle affects k_2. For interacting particles the double layers overlap and the corresponding change in the ion-distribution around particles contributes to k_2. This contribution is referred to as the secondary electroviscous effect. Again only for spheres has this contribution been calculated (18, 19).

Some experimental results cast light on the interaction of non-spherical particles in flow. As mentioned above, particle interactions cause damping in the transient oscillations in viscosity and other properties. When Brownian motion is absent and the damping is primarily caused by polydispersity in shape and particle interactions, the characteristic damping time τ can be expressed as

$$\frac{1}{\tau} = \frac{1}{\tau_\sigma} + \frac{1}{\tau_{int}}, \quad (12)$$

where τ_s is the relaxation time due to polydispersity and τ_{int} is (10),

$$\tau_{int} \cong \frac{\pi \ln r_e}{4Gr^2c}, \tag{13}$$

the order of magnitude of which agrees with experimental data (12).

Another relevant experimental observation is that the average period of rotation varies with volume fraction. The reason is that during a collision between two particles, the period of rotation is strongly affected. Experiments suggest that on the average, changes in the period T during a head-on collision are of the same order of magnitude as T itself (20).

We have mainly concentrated on the viscosity of suspensions. This is related to the component P_{23} of the stress tensor P_{ij} by $\eta = P_{23}/G$. Other components of the stress tensor exhibit similar behavior. For example, the normal stress differences $P_{11} - P_{22}$ and $P_{11} - P_{33}$ also exhibit transient behavior with steady state limits. Hence, although dilute suspensions are not viscoelastic, they do exhibit normal stress differences. Suspensions of which the suspending medium is viscoelastic are, of course, viscoelastic themselves; however, they also exhibit transient behavior because of the rotational motion of the suspended particles. For axisymmetric particles the motion differs from that given by *Eq 4*; there is a slow drift in the orbit constant and phase angle (21) which will cause damping even in the ideal case of suspensions of identical particles.

More than two-body interactions become progressively more difficult to describe. It seems that little progress will be made in this direction in the near future.

SEMI-DILUTE AND MODERATELY CONCENTRATED SUSPENSIONS

Many studies have been performed in order to better understand the volume fraction dependence of the viscosity of suspensions of spheres and other shaped particles. In general, at low concentrations η is given by *Eq 8* and smoothly approaches infinity as the volume fraction c approaches the volume fraction of close packing c_p. For spheres, probably the best result, based on an effective medium theory, is that of Krieger and Dougherty (22):

$$\eta_r = \left(1 - \frac{c}{c_p}\right)^{-2.5c_p}, \tag{14}$$

where η_r is the relative viscosity ($\eta_r = \eta/\eta_0$). In general c_p depends on particle packing, which will be altered when a suspension is subjected to shear. Thus, in the limit of zero shear, c_p has usually a different value than in the limit of high shear. As a result, suspensions of spheres are shear thinning, with well-defined low and high shear limits. In some cases shear thickening is observed at high shear rates, probably due to a disordering effect caused by the presence of small aggregates (23, 24). In the case of neutral spheres it can be concluded from dimensional arguments that (25)

$$\eta_r = f(Pe_t, c), \tag{15}$$

where Pe_t is the translational Péclet number: $Pe_t = Ga^2/D$. Several empirical relations of type (15) have been proposed.

When the spheres are electrically changed, besides Pe_t and c, η_r also depends on various dimensionless numbers which characterize the double layer interactions. When double layer effects are large, the difference between the low and high shear viscosity limits can be quite large, up to several orders of magnitude (26), giving rise to apparent yield stress behavior. Qualitatively one can think of such systems as having an effective volume fraction c_{eff} which is larger than c because of the presence of the electrical double layer which increases the effective radius of the particle.

In suspensions of non-spherical particles, besides Pe_t and c, η_r also depends on particle shape. Qualitatively the behavior is again similar; the viscosity increases with volume fraction. Comparisons with suspensions of different shaped particles and with the theory of Doi and Edwards (27), have been made by Utracki (28) and are shown in *Fig. 4*. Systems and anisometric particles are also shear thinning, going smoothly from a zero to a high shear limit (33).

In all cases the shear thinning is caused by changing the packing order in the suspension. For neutral spheres at low shear rates the packing is random, while at high shear rates the spheres settle in layers which slide over each other.

CONCENTRATED SUSPENSIONS

There is substantial evidence that at high shear rates layers of particles slide over each other prior to reaching the high shear limit, i.e., such systems are still shear thinning (23). In such cases the shear thinning can be explained by the recent results of Tomita and van de Ven (34); in such systems the structure is still changing when varying the shear rate. By applying the right angle Bragg diffraction technique in flowing dispersions (*Fig. 5*), it was found that the distance between sliding layers in-

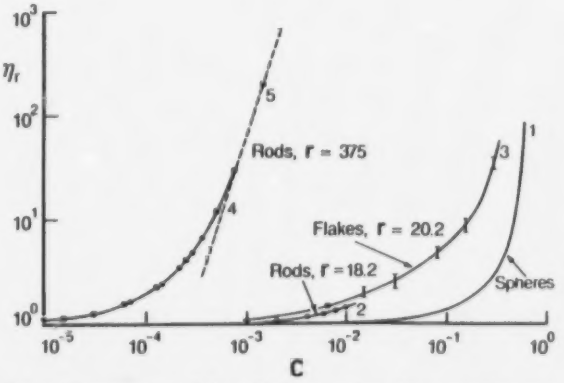

Fig. 4. Comparison of the relative viscosity of a suspension consisting of various shaped particles. 1. spheres (29); 2. glass fibers in sucrose solution (30); 3. mica flakes in polyethylene (31); 4. xanthan in salted water (32); and 5. theoretical prediction for rods (27) [$\eta_r \propto c^3$ (after Utracki (28))].

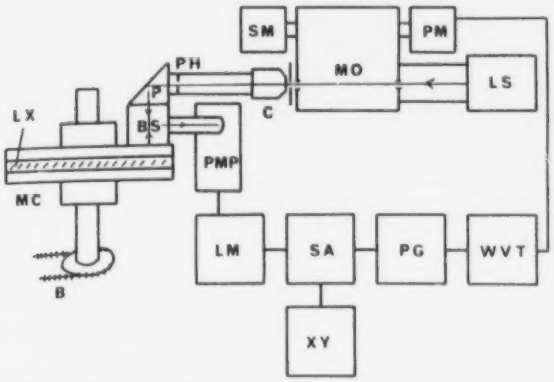

Fig. 5. Experimental set-up for right-angle Bragg diffraction. A latex sample LX is placed between two plates of a micro-Couette MC and is subjected to a simple shear by rotating the lower plate by means of belt B. The remaining parts are used to measure the intensity of the back reflected light as a function of wavelength. LS, light source; MO, monochromator; PH, pinhole; P, prism; BS, beam splitter; PMP, photomultiplier; LM, light meter; SA, signal averager; PG, pulse generator; WVT, wave-voltage transformer; SM, scanning motor; PM, potentiometer; XY, X-Y recorder; after Tomita and van de Ven (34).

creases with increasing shear rate. In this way the impact of collisions between spheres in neighboring layers is diminished; hence the viscosity is lowered. Increasing the distance between layers results in a higher concentration of spheres within each layer. This increase in concentration has been verified by grating diffraction (34, 35). *Figure 6* shows experimental results of the spacing in sheared suspensions of monodisperse polystyrene latex particles of radius 249 nm, obtained from both Bragg and grating diffraction experiments. It can be seen that the spacing can increase by as much as 10 percent. A semi-quantitative explanation has been given (34) by considering the balance of colloidal and hydrodynamic forces in the system.

Similar changes can be expected in other suspensions as well. In suspensions consisting of mixtures of monodisperse systems, particle segregation occurs (36). For systems of non-spherical particles one can assume that similar ordering and sliding will occur, in some sense, similar to the flow of liquid crystals, although little experimental evidence is available.

The behavior of stable colloidal systems is, in some sense, much simpler than that of neutral particles. For sufficient high concentrations and/or low electrolyte concentrations in the absence of shear, stable systems are already ordered, usually in hexagonally close-packed arrangements. Suspensions of neutral spheres are initially random and, when subjected to a simple shear flow, they will perturb the linear velocity profile. The same applies to the parabolic profile in Poiseuille flow. In such cases a plug flow develops (37) where all the shear is in a thin layer near the wall, while the bulk of the suspension is at near zero shear in the center region. One must then be extremely careful in interpreting rheological data; the results obtained may pertain to the region near the wall and may not be characteristic for the bulk. This behavior is not restricted to suspension of spheres, but to other suspensions as well, such as wood pulp suspensions (38) and suspensions of red blood cells (39).

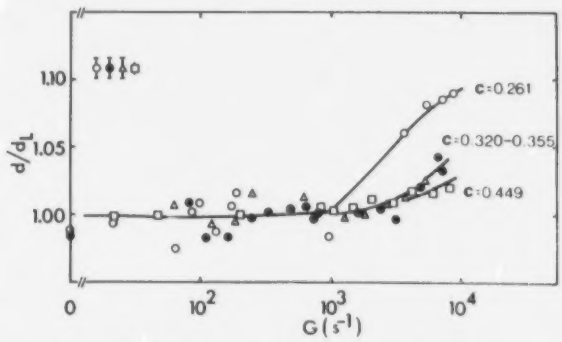

Fig. 6. Changes in distance d between sliding layers (divided by the zero-shear limit d_L) as a function of shear rate for suspension of latex spheres of radius 249 nm, at various volume fractions c. Open symbols are obtained by Bragg diffraction, closed symbols from grating diffraction (34).

CONCLUDING REMARKS

We have given a short overview of the important factors that play a role in the flow of suspensions. The general behavior is reasonably well understood, but much more theoretical work is needed to understand the details. In particular, the effects of particle shape and the behavior of suspensions containing mixtures of several particles need further study.

REFERENCES

1. B. A. Firth and R. J. Hunter, *J. Colloid Interf. Sci.*, **57**, 266 (1976).
2. T. G. M. van de Ven and R. J. Hunter, *Rheol. Acta*, **16**, 534 (1977).
3. R. J. Hunter and J. Fraine, *J. Colloid Interf. Sci.*, **76**, 107, (1980).
4. H. Brenner, *Int. J. Multiphase Flow*, **1**, 195 (1974).
5. G. B. Jeffery, *Proc. R. Soc. London*, **A102**, 161 (1922).
6. T. G. M. van de Ven and S. G. Mason, *J. Colloid Interf. Sci.*, **57**, 517 (1976).
7. C. Cohen and L. G. Leal, *J. Chem. Phys.*, **68**, 5348 (1978).
8. E. J. Hinch and L. G. Leal, *J. Fluid Mech.*, **57**, 753 (1973).
9. T. G. M. van de Ven, K. Takamura, and S. G. Mason, *J. Colloid Interf. Sci.*, **82**, 373 (1981).
10. A. Okagawa, R. G. Cox, and S. G. Mason, *J. Colloid Interf. Sci.* **45**, 303 (1973).
11. M. Zuzovsky, Z. Priel, and S. G. Mason, *J. Rheol.* **24**, 705 (1980).
12. Y. Ivanov, T. G. M. van de Ven, and S. G. Mason, *J. Rheol.*, **26**, 213 (1982).
13. A. Einstein, *Ann. Phys.*, **17**, 549 (1950).
14. M. Smoluchowski, *Kolloid Zschr.*, **18**, 190 (1916).
15. W. Krasney-Ergen, *Kolloid Zschr.*, **74**, 172 (1936).
16. F. Booth, *Proc. R. Soc. London*, **A203**, 533 (1950).
17. G. K. Batchelor and J. T. Green, *J. Fluid Mech.*, **56**, 401 (1972).
18. F. S. Chan, J. Blachford, and D. A. I. Goring, *J. Colloid Interf. Sci.*, **22**, 378 (1966).
19. W. B. Russel, *J. Fluid Mech.*, **85**, 209 (1978).
20. D. S. Jayasuriya and T. G. M. van de Ven (in preparation).
21. E. Bertram, H. L. Goldsmith, and S. G. Mason, *Rheol. Acta*, **14**, 776 (1975).
22. I. M. Krieger and T. J. Dougherty, *Trans. Soc. Rheol.* **3**, 137 (1959).

23. R. L. Hoffman, *J. Colloid Interf. Sci.*, **46**, 491 (1974).
24. I. M. Krieger and G. N. Choi, "Advances in Rheology", Vol. 2, p. 641, Fluids, Univ. Nac. Aut. de Mexico (1984).
25. I. M. Krieger, *Adv. Colloid Interf. Sci.*, **7**, 101 (1963).
26. J. W. Goodwin, in "Colloidal Dispersions", Ch. 8, ed., J. W. Goodwin, Royal Soc. of Chemistry, Burlington House, London (1982).
27. M. Doi and S. F. Edwards, *J. Chem. Soc., Faraday Trans. II*, **74**, 560, 918 (1978).
28. L. A. Utracki, *Rubber Chem. Technol.*, **57**, 507 (1984).
29. D. G. Thomas, *J. Colloid Sci.*, **20**, 267 (1965).
30. A. Attanasio, U. Bernini, P. Galloppo, and G. Sergé, *Trans. Soc. Rheol.*, **16**, 147 (1972).
31. F. Fisa and L. A. Utracki, *Polym. Compos.*, **5**, 36 (1984).
32. C. E. Chauvateau, *J. Rheol.*, **26**, 111 (1982).
33. C. E. Chaffey and R. S. Porter, *J. Rheol.*, **201**, 249 (1984).
34. M. Tomita and T. G. M. van de Ven, *J. Colloid Interf. Sci.*, **49**, 374 (1984).
35. M. Tomita, K. Takano, and T. G. M. van de Ven, *J. Colloid Interf. Sci.*, **92**, 367 (1982).
36. H. Goto and H. Kuno, *J. Rheol.*, **28**, 197 (1984).
37. A. Karnis, H. L. Goldsmith, and S. G. Mason, *J. Colloid Interf. Sci.*, **22**, 531 (1966).
38. O. L. Forgacs, A. A. Robertson, and S. G. Mason, *Pulp & Paper Mag. Can.*, **59**, 117 (1958).
39. H. L. Goldsmith and S. G. Mason, 5th European Conference on Microcirculation, Gottenburg 1968, Bibli. Anat. No. 10, p. 1 (Karger 1969).

PANEL DISCUSSION

L. A. Utracki: I invited Theo van de Ven to give us a brief outline of what is known in suspension rheology, how much the theoretical treatment and the experiments on suspensions in Newtonian media are able to explain. Flow and processability of composites may be treated as a next step of complication—composites are suspensions of frequently unstable, viscoelastic liquids under non-equilibrium conditions. In science we try to assign the most probable explanation from a variety of possible ones. To be a good scientist is to be successful in such a selection. The knowledge of similar or simpler systems is the second best thing. If we know how the suspensions behave, we may be able to better explain flow of the composites. In particular, the orientation and flow of anisometric filler particles must be based on the information developed by suspension rheologists.

J. L. White: One thing you did not mention is the Reynolds theory of dilatancy and the experiments of Hoffman at the Monsanto Co. He slowly sheared concentrated suspensions observing the diffraction patterns. Then he would go above the critical shear rate region where the ordered structure would break-up, and there would be a sharp increase in viscosity at the same time. That observation paralleled the earlier Reynold's and Freundlich's results.

T. G. M. van de Ven: Yes, there is some information in the literature indicating that at very high shear rates there may be some shear thickening. This indeed is what Hoffman found. His explanation was that in suspensions of concentrated spheres you also have non-spherical aggregates. On shearing, the spheres rotate due to vorticity. The non-spherical particles severely affect the sliding layers of rotating spheres. At a certain value of the shear rate you get a disordering effect due to the presence of non-spherical aggregates. It is not certain if the dilatancy can occur in a true suspension of spherical bodies. Experiments on suspensions of large spheres without aggregates have not so far resulted in any observation of viscosity increase with shear rate.

M. R. Kamal: I know that your talk was directed toward the shear type of flows. I wonder if you can make any statement in relation to elongational flow.

T. G. M. van de Ven: The extensional flows are much simpler as here the particles assume a steady-state orientation, and they do not rotate. It is much simpler to compute the behavior in elongational fields. All the transient effects will not be oscillatory but rather a smooth transition from one state to another. I do not know what will happen in a very concentrated suspension. In elongation one cannot visualize the flow by the sliding layers mechanism, but rather by divergence or convergence. In other words, another mechanism must be responsible for minimizing energy dissipation.

L. Piche: In the average-medium model for spherical particles it does not appear that the distribution of the dimension of the particles has a lot of influence. Intuitively this would not be true for non-spherical bodies. Since you are using the average-medium theory how can this polydispersity be introduced? It is rather a difficult concept to introduce into self-consistent models.

T. G. M. van de Ven: I agree. At least at the present state of development one cannot introduce it in this fashion. You can do it in an exact manner by the expansion solution for coefficients k_1 and k_2. These depend on the size and shape distribution of the particles. As soon as you go to the effective medium theory you lose some of the exactness. The theory is not rigorous and you have to give something up. The thing which is usually thrown out is indeed what you mentioned. You get one approximation for all kinds of flows. There may be ways of introducing the polydispersity, but then you would have to differentiate all types of shapes and flow fields. So far this has not been done.

Flow Patterns in Calcium Carbonate and Titanium Dioxide Filled Polyethylene in the Entrance Region of a Capillary Die

CHIN-YUAN MA, JAMES L. WHITE, FREDERICK C. WEISSERT, *and* KYONSUKU MIN

Polymer Engineering Center
The University of Akron
Akron, Ohio 44325

Experiments to determine the influence of calcium carbonate and titanium dioxide on flow patterns in die entrance regions are reported. The addition of loadings of calcium carbonate and tatanium dioxide of 5 volume percent and more is found to suppress the development of vortices in low density polyethylene at the entrance of a 180° entrance angle die. Vortex suppression was found in more complex entrance regions as well. Similar behavior has been found for carbon black compounds.

INTRODUCTION

There have been extensive investigations of flow patterns in the entrance region of a die for thermoplastics for more than a generation (1–5). These studies have depicted vortices in the entry of dies for low density polyethylene and polystyrene. Little attention has been given to compounds of particle filled polymer melts until recently. The present authors (6) have recently reported an investigation of flow patterns in compounds of low density polyethylene with compounded carbon black. They found that the addition of more than 5 volume percent carbon black eliminated the vortices in 180° entrance angle dies. Flow patterns in dies of varying entry designs were investigated.

In this paper, we extend our investigations to compounds of calcium carbonate and titanium dioxide in low density polyethylene and contrast the results to our earlier studies of carbon black filled polyethylene.

EXPERIMENTAL

Materials

The base polymer used was a commercial low density polyethylene (LDPE) (Chemplex 3404). The particles which were studied are calcium carbonate (Pfizer Multiflex MM USP) and titanium dioxide (SCM Zopaque RG). The compounds investigated involve volume loadings which are summarized in *Table 1*.

Die Designs

The experiments were carried out in an Instron Capillary Rheometer. A range of die designs were used. These are summarized in *Fig. 1*. These include 180° entrance angle dies, converging and diverging entrance dies, dies with an off centered hole, and dies with two capillaries.

Procedure

The general experimental procedure used involves compression molding the compound in the reservoir of an Instron Capillary Rheometer. Holes were drilled diagonally through the diameter of the rods, and extruded filaments of compounds of opposite color were inserted in the rods. Carbon black filaments of roughly the same shear viscosity were inserted in rods of compounds of calcium carbonate/polyethylene and titanium dioxide/polyethylene. The rods were then reinserted in the rheometer barrel, melted, and extruded for a period. The temperature used was 150°C. The apparatus was then cooled under pressure by extruding at the lowest rate. The rod was removed from the rheometer and longitudinally cross-sectioned. This procedure is essentially that of Ballenger and White (7) as generalized by Ma, *et al.* (6) (see *Fig. 2*).

Purging experiments were also carried out. We variously purged each of the compounds out of the lower part of the reservoir with a second material. The calcium carbonate and titanium dioxide compounds were purged with carbon black compound of nearly the same viscosity and the carbon black filled polymer by equal viscosity white compounds. The rods were then cooled under pressure, solidified, removed, and longitudinally cross-sectioned.

RESULTS

Longitudinal cross-sections of rods removed from the region above a capillary die with various en-

Table 1. Compounds investigated

Particulate	Supplier	Grade	Mean particle size (μm)	Volume Fraction	Designation
Calcium carbonate	Pfizer	Multiflex MM USP	0.07	0.01	*A*
				0.05	*B*
				0.10	*C*
				0.20	*D*
Titanium dioxide	SCM	Zopaque RG	0.18–0.22	0.01	*E*
				0.05	*F*
				0.10	*G*
				0.19	*H*
				0.30	*I*

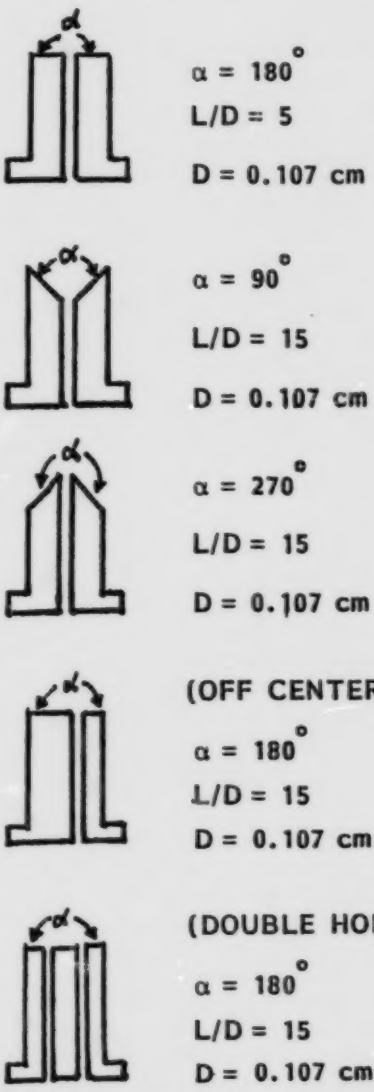

Fig. 1. Capillary die design used in this study.

trance angles are shown in *Fig. 3*. These indicate vortices with 180° entrance angle and diverging dies but not in converging entrance regions. Complex vortices of different sizes are observed around an off-set or eccentrically placed capillary hole in a die. Vortices also exist in the corner of the die with two holes with 180° entrance angle.

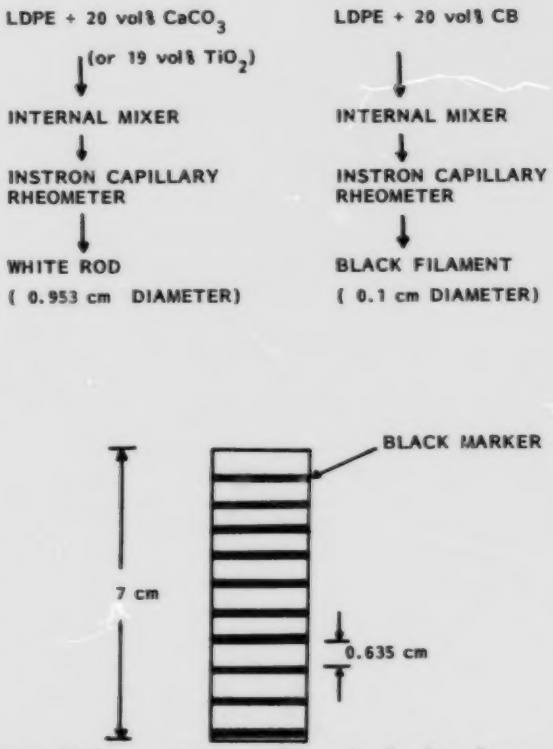

Fig. 2. Marking procedures used on rods placed in rheometer barrel.

We exhibit a 20 volume percent calcium carbonate compound (*D*) with a 180° entrance angle in *Fig. 4*. No vortices are observed, only streamline flow into the die entry. The streamlines found for the filled polymers are more or less independent of extrusion rate. Similar observations for a 19 volume percent titanium dioxide compound (*H*) are shown in *Fig. 5*.

Purging experiments have also been carried out for the 180° entrance angle die. Typical experimental results are shown in the longitudinal cross-section of *Figs. 6–9* for compounds *D* and *H*. All the material in the lower part of the reservoir, except in the deepest corner, is purged.

Longitudinal cross-sections for calcium carbonate compounds of varying loadings in 180° entrance angle dies are shown in *Fig. 10*. It shows that vortices are only found in the 1 and 5 volume percent samples. The vortex size decreases as the filler

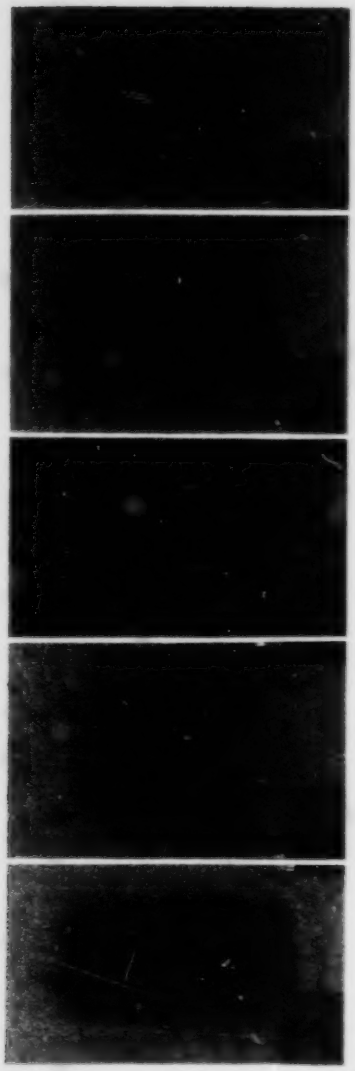

Fig. 3. Flow patterns in longitudinal cross-sections at the entrance of dies for low density polyethylene at T = 150°C $\dot{\gamma}_{app} = 76s^{-1}$. The dies used are: (a) 180° entrance angle, (b) 270° entrance angle, (c) 90° entrance angle, (d) off center, 180° entrance angle, (e) double holes, 180° entance angle, $\dot{\gamma}_{app} = 40s^{-1}$.

loading level increases. Similar observations for titanium dioxide compounds are shown in *Fig. 11*.

The streamlines for the compounds *D* and *H* are shown in *Fig. 12* for a converging entrance die. Both exhibit an absence of vortices. Flow into a greater than 180° entrance angle die is shown in *Fig. 13*. Both show a simple direct streamline flow following the barrel and die periphery. The diverging die behavior may indicate regions of long residence time.

Longitudinal sections for "off-centered hole" 180° die entrances are summarized in *Fig. 14*. Both compounds *D* and *H* show a direct streamline flow. *Fig. 15* shows longitudinal sections for dies with two holes with 180° entrance angles. Again no vortices are observed for the compounds.

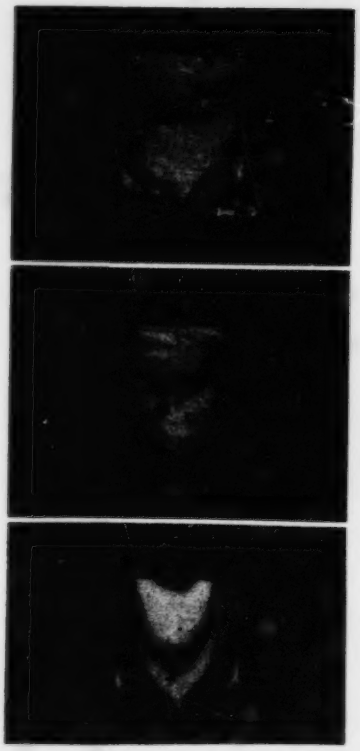

Fig. 4. Flow patterns in longitudinal cross-sections at a 180° angle entrance for a 20 volume percent calcium carbonate compound (D) at 150° C at varying extrusion rates: (a) $7.6s^{-1}$, (b) $76s^{-1}$, (c) $760s^{-1}$.

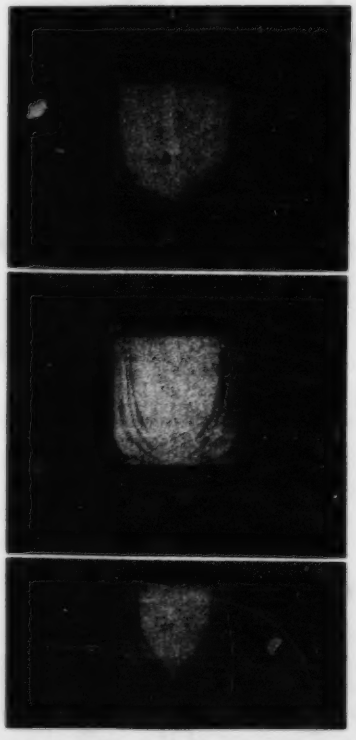

Fig. 5. Flow patterns in longitudinal cross-sections at a 180° angle entrance for a 19 volume percent titanium dioxide compound (H) 150°C at varying extrusion rates: (a) $7.6s^{-1}$, (b) $76s^{-1}$, (c) $760s^{-1}$.

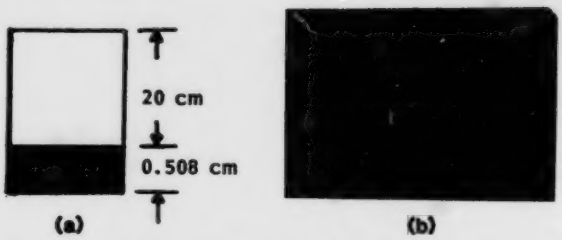

Fig. 6. Longitudinal cross-sections of material (top = compound D, bottom = 20 vol % CB) in reservoir for purging experiments with 180 entrance angle at T = 150°C, $\dot{\gamma}_{app} = 76s^{-1}$.

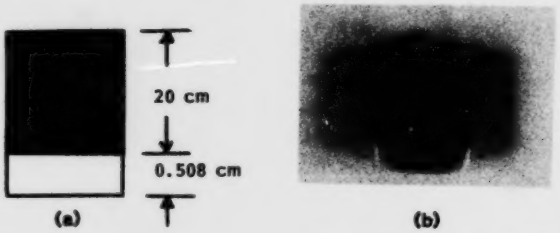

Fig. 7. Longitudinal cross-sections of material (top = 20 vol percent CB, bottom = compound D) in reservoir for purging experiments with 180° entrance angle at T = 150°C, $\dot{\gamma}_{app} = 76s^{-1}$.

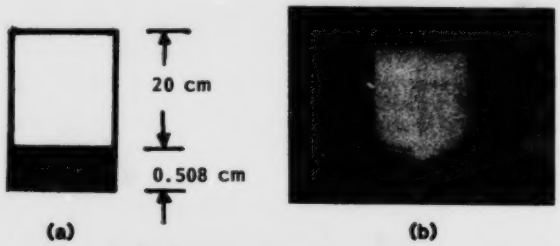

Fig. 8. Longitudinal cross-sections of material (top = compound H, bottom = 20 vol percent CB) in reservoir for purging experiments with 180° entrance angle at T = 150°C, $\dot{\gamma}_{app} = 76s^{-1}$.

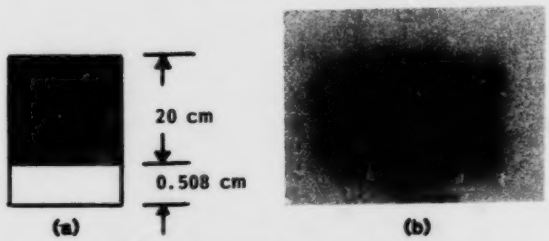

Fig. 9. Longitudinal cross-sections of material (top = 20 vol percent CB, bottom = compound H) in reservoir for purging experiments with 180° entrance angle at T = 150°C. (a) initial condition, (b) after 30 minutes purging, $\dot{\gamma}_{app} = 76s^{-1}$.

DISCUSSION

Our results are essentially the same as those cited in our earlier investigation (6) using carbon black-LDPE compounds. Vortices in 180° entrance angle geometries were suppressed by the addition of more than 5 percent of the particulates. Vortices are similarly suppressed in diverging entrance dies and dies with offset or multiple hole entries.

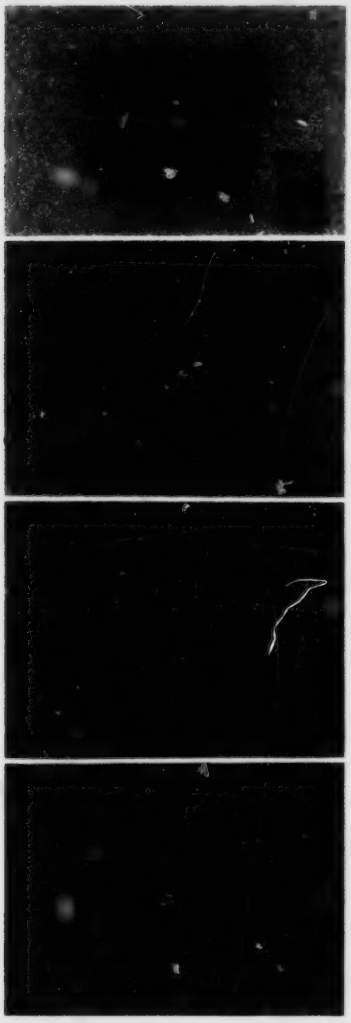

Fig. 10. Longitudinal cross-sections showing the influence of calcium carbonate loading on entrance flow for (a) compound A, (b) compound B, (c) compound C, (d) compound D, at 150°C, $\dot{\gamma}_{app} = 76s^{-1}$.

The disappearance of these vortices is certainly associated with the changes in rheological properties with addition of small particulates. The main effect of filler addition is shown in *Fig. 16*, where we plot shear viscosity versus shear stress for the LDPE and compounds *D*, *H*, and *I*. High loadings of small particulates lead to yield values. Similar findings for titanium dioxide and calcium carbonate compounds have been reported earlier in the literature (8–10). The same effect was found for the LDPE-carbon black compounds in our earlier work (6). In this earlier paper (6) we speculated that the disappearance of vortices may be associated with the change of the elongational viscosity from an increasing to a decreasing function of stretch rate. A full numerical simulation would be a better approach; however, existing constitutive equations for such systems (11, 12) have not been adequately tested.

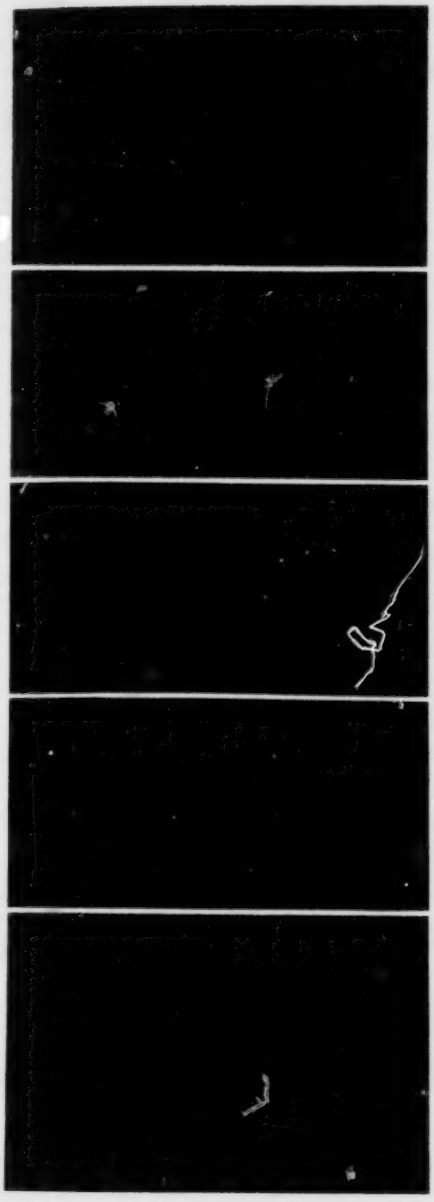

Fig. 11. Longitudinal cross-sections showing the influence of titanium dioxide loading on entrance flow for (a) compound E, (b) compound F, (c) compound G, (d) compound H, (e) compound I, at 150°C, $\dot{\gamma}_{app} = 76s^{-1}$.

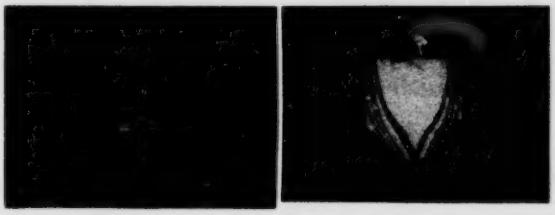

Fig. 12. Longitudinal cross-sections showing streamlines for converging flows for (a) compound D, (b) compound H.

Fig. 13. Longitudinal cross-sections showing streamlines for diverging flows for (a) compound D, (b) compound H.

Fig. 14. Longitudinal cross-sections showing streamlines for "off-center hole" with 180° die entrance angle for (a) compound D, (b) compound H.

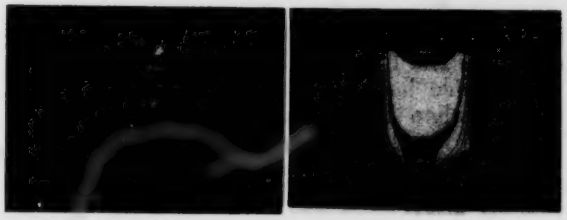

Fig. 15. Longitudinal cross-sections showing streamlines for "two holes" with 180° die entrance angle for (a) compound D, (b) compound H.

ACKNOWLEDGMENTS

We would like to thank Professor A. I. Isayev for his helpful comments. This paper is part of the Polymer Engineering Center's Rubber Process Engineering Agenda (RUPEA) program. The financial support of the Goodyear Tire and Rubber Company, Firestone Tire and Rubber Company, BFGoodrich Company, GenCorp, Gates Rubber Company, Bridgestone Research Company and the Armstrong Rubber Company is appreciated.

REFERENCES

1. J. P. Tordella, *Trans. Soc. Rheology*, **1**, 203 (1957).
2. E. B. Bagley and A. M. Birks, *J. Appl. Phys.*, **30**, 556 (1960).
3. E. B. Bagley and H. P. Schreiber, *Trans. Soc. Rheology*, **5**, 341 (1961).
4. T. F. Ballenger and J. L. White, *J. Appl. Polym. Sci.*, **15**, 1949 (1971).
5. J. L. White and A. Kondo, *J. Non-Newt. Fluid Mech.*, **3**, 41 (1977).
6. C. Y. Ma, J. L. White, F. C. Weissert, and K. Min, *J. Non-Newt. Fluid Mech.* **17**, 275 (1985).
7. T. F. Ballenger and J. L. White, *Chem. Eng. Sci.*, **25**, 1191 (1970).
8. N. Minagawa and J. L. White, *J. Appl. Polym. Sci.*, **20**, 501 (1976).
9. H. Tanaka and J. L. White, *Polym. Eng. Sci.*, **20**, 949 (1980).
10. Y. Suetsugu and J. L. White, *J. Appl. Polym. Sci.*, **28**, 1481 (1983).

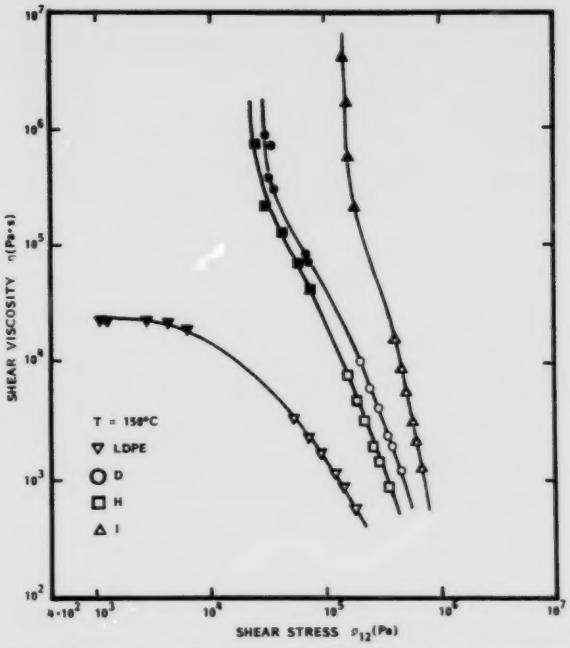

Fig. 16. Shear viscosity-shear stress data for LDPE, compounds D, H, and I at 150°C. Solid symbols are measured by a constant shear rate sandwich viscometer. Open symbols are measured by a capillary rheometer.

11. J. L. White and M. Tanaka, *J. Non-Newt. Fluid Mech.*, **8**, 1 (1981).
12. Y. Suetsugu and J. L. White, *J. Non-Newt. Fluid Mech.*, **14**, 121 (1984).

PANEL DISCUSSION

H. P. Schreiber: As you pointed out, in the ancient times we had been doing flow visualization of polyethylenes and I recall that one of the reasons was to see what happens to the flow lines and melt fracture when filler is added. These two responded equally dramatically. Do you have any insight as to what the filler is doing in terms of modification of the network structure, which in turn may produce these shifts in the visual effects.

J. L. White: I have looked upon what they do to the entry pattern in a phenomenological sense. The filler introduces yield stresses to the system what fundamentally changes the fluid mechanics. Concerning melt fracture, it is well established that filler considerably reduces extrudate swell and produces much smoother extrudate, i.e., forces the melt fracture to a higher shear stress region.

H. P. Schreiber: Yes, it seems that the filler affects the elastic response of the material. This may indicate that very significant modification has occurred as far as a transition from network to domain structure is concerned. The question is if this transition accounts for modification of the entry region as well as the melt fracture.

J. L. White: In highly filled systems it would seem to me that the primary factor is the particle-particle interaction rather than the chain entanglement interaction. In the swell problem, when the material leaves a die the stresses in the wall regions drop off very rapidly from high values to below the yield stress. If one looks upon swell as a simple elastic recovery process then the modulus which is involved in that ought to be almost equal to the modulus of quiescent material which contains the interacting filler network. This modulus is considerably higher than the modulus of the matrix. This may account for a reduction of the extrudate swell.

H. P. Schreiber: In our work on rutile filled polyolefins we demonstrated that the surface conditioning of the filler plays a considerable role on the rheological and mechanical property. Do you know if the pattern you have been showing is general, if it is applicable to these variously treated rutiles? Or would you expect that the pattern depends on the conditioning of the particle surface?

J. L. White: I know that coating the small particles such as TiO_2, $CaCO_3$ or others and reduces the particle-particle interaction and can greatly reduce the viscosity level (see e.g. Ref. 10 in the paper, and the works cited therein). We have not looked at every variable. We tested three different filler systems: TiO_2, $CaCO_3$, and carbon black (CB). It would be useful to continue the work. The $CaCO_3$ is probably a more versatile one. All TiO_2 in the world is made in one particle size, sometimes coated, sometimes not.

H. P. Schreiber: This is precisely the point. We had a series of TiO_2 of the same particle size but differently coated. These may be interesting to use in your context.

J. L. White: I rather thought that it may be more interesting to study $CaCO_3$ which are commercially available in sizes from 0.07 to 17 μm. These grades can also be surface treated as is TiO_2.

T. G. M. van de Ven: I was very intrigued by your vortices. They remind me of the vortices which are observed in blood flow in the region of sudden expansion or construction of an artery or an obstacle in a vein. The small particles, the platelets or blood cells, leave these vortices. This means that under a steady state condition these regions are empty of platelets. However, large particles, such as a rouleau of platelets, do not leave the vortex. In short, all the big particles end up in the vortices and the platelets in the blood stream. Do you observe a similar fractionation in your systems? You talked about the volume fraction but what about the effect of particle size?

J. L. White: All the particles we looked at were small, in the range where the particle-particle interaction is dominant. All this work involved rather high volume loadings. For instance you do not see full suppression of vortices below 10 volume per-

cent. It would be useful to look at a wider range of particle sizes. We should look at glass spheres or glass fibers which are in the range of 10 μm and above where you are out of this inter-particle interaction regime of dominance to the hydrodynamics as the dominant. There, the situation can be very different.

T. G. M. van de Ven: Do you know if you have different concentration of particles in the vortex region than in the bulk?

J. L. White: We could measure it easily, but we did not. We could simply slice up the solidified plug and measure the density as a function of the special coordinates.

L. A. Utracki: From what you said it seems that you are considering the yield stress to be the sole responsible factor for both the vortex suppression and reduction of the extrudate swell. Putting aside the arguments if and which other factors should also be considered, one may ask what level of yield stress is required for each of these suppressions to take place. Furthermore, one may ask if there is a correlation between the flow conditions, e.g., shear stress, geometry, ..., and the magnitude of shear stress required for suppression.

J. L. White: Yes, but I am not certain if I will be able to do it for next year's meeting or not. However, let me comment on this. Neil Cogswell made the suggestion in the 1970's that those polymer melts which exhibit vortices have elongational viscosity functions which show strong increases on stretching. Those polymer melts which do not have vortices have constant or decreasing elongation viscosity function with the rate of stretching. On one hand, you have LDPE and polystyrene and on the other, commercial PP and HDPE as those which do not exhibit the vortices.

M. R. Kamal: People like Vlachopoulos, Crochet, and others have been able to make the calculations whereby they were able to show these circulation flows at the entry region. What is it one must include in the equations when solving them for filled systems so that these circulations are suppressed.

J. L. White: The only consitutive equations describing filled systems are those developed by my graduate students and myself. These are published in *J. Non-Newtonian Fluid Mechanics* between 1979 and 1984 (see e.g. Refs. 11 and 12 in the paper). Those equations could be applied to the calculations you mentioned, and hopefully they would predict in a numerical simulation what is observed. But if you follow the literature on flow patterns in the entrance region as developed, say by Crochet, what you find out is that among the numerous non-linear viscoelastic constitutive equations (there are probably a thousand of them) he can select different ones which are very similar in shear flow but make different predictions on entry vortices. It is not apparent what differentiates the two groups of these highly tested constitutive equations. The danger in starting to carry out the numerical simulation with our constitutive equations at this point is that they have not been that severely tested in a wide enough range of flows. We have done steady state shear and uniaxial extension and transient shear flow. One has to do much more than that.

Dispersive Mixing in Roll-Mills

I. MANAS-ZLOCZOWER,* A. NIR, *and* Z. TADMOR

Department of Chemical Engineering
Technion-Israel Institute of Technology
Haifa 32000, Israel

A theoretical model of the dispersive mixing process in roll-mills is proposed. The model is based on the assumption that intensive mixing is dominated by agglomerate rupture in the narrow nip high shear flow field between the rolls. The dynamics of agglomerate size distribution and its dependencies on a number of variables and parameters are presented.

INTRODUCTION

The mixing of solid additives into a polymeric matrix generally involves rupture of agglomerates formed by the solid phase, a subsequent separation of closely packed particles (energy intensive operations referred to as **dispersive** or **intensive** mixing), and distribution of the separated fragments throughout the molten polymer (by and large an extensive mixing process). Depending upon the polymer-additive system and mixer machine design, each of these steps may be rate determining.

Still in wide use for compounding rubber and plastics are roll-mills, invented in 1835 by Edwin Chaffee. The simple and versatile design of roll-mills makes them very convenient, especially for experimental compounding.

Most of the literature concerning roll-mills deals with their hydrodynamic analysis (1–17). Certain phenomena associated with roll-milling elastomers, i.e., the adhesion of the masticated mass as a clinging "blanket" to one roll or the other, were explained by Tokita and White and (18, 19) in terms of rheological properties of the material. Scale-up procedures using various criteria (20, 21) were also reported. However, there seems to be no published information concerning dispersion rating and agglomerate size distribution for mixing on roll-mills, nor any attempt to predict and explain the mixing process from fundamental considerations.

Following the lines and assumptions formulated in a previous article concerning dispersive mixing in internal mixers (22), in this paper we propose a mathematical model of the intensive mixing process in roll-mills.

OUTLINE OF THE THEORETICAL MODEL

The theoretical model proposed here is based on the assumption that intensive mixing is dominated by agglomerated rupture in the narrow nip high shear flow field between the rolls.

Agglomerates are assumed to be clusters of particles held together by cohesive forces of predictable magnitude. The flow field in which the agglomerates are freely suspended, exerts hydrodynamic forces on their external surfaces, which in turn generates internal stresses within the clusters. When hydrodynamic separating forces exceed cohesive forces, rupture occurs (23).

Agglomerate break-up is modeled as a repetitive process. An initial large agglomerate ruptures first into two equal sized fragments. Next, each fragment is considered as a new agglomerate of smaller size, which has a chance to be ruptured again in a subsequent path. For the sake of simplicity, it is assumed that all fragments are similar in shape regardless of size. The process continues until the "ultimate" particle size, which can no longer be broken by hydrodynamic forces, is reached.

Considering a large number of spherical particles, randomly packed into an isotropic and homogeneous agglomerate, Rumpf (24) showed that in such a system, a theoretical tensile strength σ can be calculated in terms of the strength of the individual bonds at points of contact. He obtained the following expression:

$$\sigma = \frac{9}{8}\left(\frac{1-\epsilon}{\epsilon}\right)\frac{F}{d^2}, \tag{1}$$

where ϵ is the volume void fraction, d is the diameter of spherical particles forming the agglomerate, and F is the attractive cohesive force of a single bond. Making use of the Bradley and Hamaker (25) theory for the interaction potential between two spheres, the expression for F can be approximated by

$$F = \frac{A}{12z^2}\frac{d_1 d_2}{(d_1 + d_2)} \tag{2}$$

where A is the Hamaker constant for the interaction of the two bodies, z is the physical adsorption separation distance (typically 0.4 nm for adhering spheres) and d_1 and d_2 are the diameters of the two spheres, respectively.

Following Hamaker (25), the value of A for the

* Present address: Department of Chemical Engineering, Case Western Reserve University, Cleveland, OH 44106.

interaction of two bodies in a medium other than vacuum is given by:

$$A = (\sqrt{A_{ii}} - \sqrt{A_{jj}})^2 \tag{3}$$

where A_{ii} and A_{jj} are, respectively, the constant for the bodies interacting in vacuum and the constant for the medium. For indentical spheres, *Eq 2* can be rewritten:

$$F = C_0 d \tag{4}$$

with

$$C_0 = \frac{(\sqrt{A_{ii}} - \sqrt{A_{jj}})^2}{24z^2} \tag{5}$$

Substituting *Eq 4* into *Eq 1*, the cohesive force F_c of the agglomerate is given by

$$F_c = \frac{9}{8}\left(\frac{1-\epsilon}{\epsilon}\right)\frac{C_0}{d} S \tag{6}$$

where S is the cross-sectional contact area at the ruptured plane. The hydrodynamic separating force for an axisymmetric particle freely suspended in a homogeneous shear flow field of an incompressible Newtonian liquid is given by (26):

$$F_h = \chi \pi \mu \dot{\gamma} c^2 \sin^2\theta \sin\phi \cos\phi \tag{7}$$

where χ is a constant which depends on the particle shape, μ is the viscosity of the liquid, $\dot{\gamma}$ is the local shear rate, c is a dimension characterizing the size of the particle, and θ and ϕ are instantaneous orientation Euler angles. For the case of a doublet of two touching spheres of radius c, Nir and Acrivos (26) evaluated $\chi = 12.23$.

It is assumed in this model that agglomerates are elongated bodies of revolution, with fore-and-aft symmetry and therefore, the only possible relative motion in the shear flow field is a rotation. There is no possibility for a particle to cross streamlines from one shear zone to another. Zia, Cox and Mason (27) derived the angular velocities of rotation for a spheroid with large to small axes ratio, r_e

$$\frac{d\theta}{dt} = b\,\dot{\gamma} \sin\theta \cos\theta \sin\phi \cos\phi \tag{8}$$

$$\frac{d\phi}{dt} = \dot{\gamma}\,\frac{r_e^2 \cos^2\phi + \sin^2\phi}{r_e^2 + 1} \tag{9}$$

with

$$b = \frac{r_e^2 - 1}{r_e^2 + 1}. \tag{10}$$

Equations 8 and *9* can be integrated to give the orientation angles $\theta(t)$ and $\phi(t)$ in terms of the initial orientations θ_0 and ϕ_0 at the entrance to the nip region. The above kinematics is valid for arbitraily shaped bodies of revolution with fore-and-aft symmetry (28) with r_e denoting an effective axis ratio.

It is worth noting here that the effective axis ratio for a body of an arbitrary revolution is not necessarily equal to the actual dimensional one. A doublet of two touching equal spheres has (26) $r_e = 1.982$ rather than 2.

An agglomerate will rupture when the hydrodynamic separating force exceeds the cohesive one (i.e., $\frac{F_h}{F_c} \geq 1$). The force ratio is obtained by dividing *Eq 7* with *Eq 6* which gives

$$\frac{F_h}{F_c} = (\mu\dot{\gamma}) Z^* \sin^2\theta \sin\theta \cos\phi \tag{11}$$

with

$$Z^* = \frac{8}{9}\,\chi\,\frac{\epsilon}{1-\epsilon}\,\frac{d}{C_0}. \tag{12}$$

The most important conclusion from *Eq 11* is that agglomerate rupture is independent of agglomerate size; it is proportional to the local shear stress ($\mu\dot{\gamma}$) in the liquid, and it is a sensitive function of the instantaneous agglomerate orientation (θ, ϕ).

The dependence of rupture on the nature of the agglomerate, its shape, and its strength is introduced via Z^*. The smaller the Z^*, the more difficult it is to break the agglomerate. *Equation 12* indicates that the higher the cohesion force (C_0), the smaller the particles forming the agglomerate (d); and the lower the porosity, the smaller the value of Z^*, and hence the more difficult it is to rupture the agglomerate.

Roll-mill mixers consist of two rolls which generally rotate at different speeds (*Fig. 1*). This, together with roll temperature settings, enable the formation of a band on one of the surfaces. Certain materials have an "affinity" for one of the rolls. Tokita and White (18, 19) describe this and other phenomena associated with roll milling elastomers in terms of rheological properties of the material. At a certain upstream location $x = X_2$, the melt

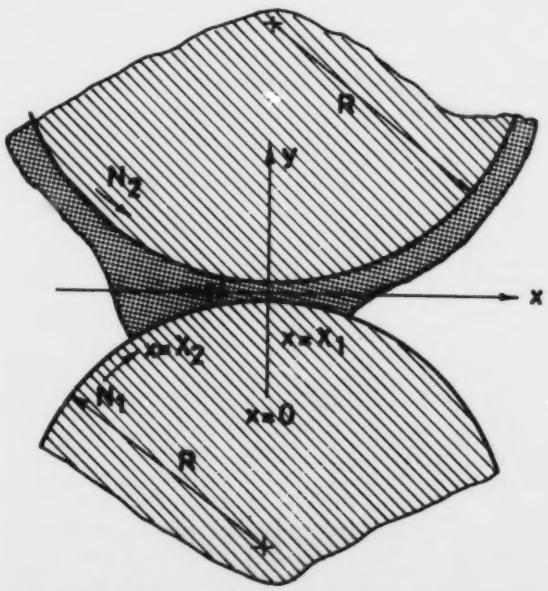

Fig. 1. Schematic representation of the two-roll geometry.

contacts both rolls. Further downstream at the location $x = X_1$ the polymer detaches itself from one of the rolls. The location of the points X_1 and X_2, for given geometry and operating conditions, depends on the total volume of processed polymer only.

In this model, we assume that dispersive mixing occurs exclusively in the nip zone of the two rolls geometry, between the locations X_1 and X_2, where the high shear flow field enables agglomerate rupture. Outside this area, the molten polymeric matrix containing the agglomerates forms a band, undergoing a plug type flow on one of the rolls.

Since the mixture undergoes a plug type flow on one of the rolls, at any given time all fluid elements or agglomerates have experienced the same number of passes in the nip region.

As the mixing process starts, agglomerates enter the high shear nip region with a random orientation. The local shear rate and the instantaneous orientation of the agglomerate change as it freely rotates along the streamline of the flow field. Thus, the magnitude of the separating force is a function of initial agglomerate orientation at the entrance to the high shear zone and of its relative position in the flow field.

As mentioned before, one of the fundamental assumptions of this model is that particles do *not* cross streamlines. Since there is a shear rate distribution in the flow field between the roll surfaces, the fraction of ruptured agglomerates leaving the gap during each pass is different for different streamlines. Moreover, this fraction is a function of agglomerate orientation at the entrance to the gap. In this model we assume that once broken, the fragments become randomly oriented in the flow field. Agglomerates which were not broken enter the nip in the following pass with the same orientation they had when they left the high shear zone on the previous pass, since no rotation prevails in the plug flow outside the gap. Thus, in calculating the fraction of broken agglomerates leaving the gap after each pass, we have to account for the prescribed (not random) orientation distribution of those agglomerates which escaped unbroken during previous passes. By following particles in multiple passes and accounting also for the residence time distribution function (predictable from the flow pattern), agglomerate size distribution and dispersion can be obtained.

Initially, the molten polymeric matrix contains a grossly uniform distribution of agglomerates of a given size distribution and random orientations. As mixing proceeds, different size and orientation distributions of agglomerates develop on each streamline of the flow field. During the operation, cutting of the blanket and rolling are carried out, thereby facilitating composition and orientation randomization throughout the whole system. Thus, the frequency of cutting the blanket is another operational parameter which has to be considered in developing the theoretical model. It is assumed that cutting and rolling also bring about agglomerate orientation randomization.

HYDRODYNAMIC ANALYSIS OF ROLL-MILLS

A detailed review of the hydrodynamic analysis of the flow between two rolls is given elsewhere (29).

Following Takserman-Krozer (15), we use bipolar coordinates to describe the fluid flow between the rotating cylinders.

Figure 1 depicts the flow configuration schematically. Two identical rolls of radii R rotate in opposite directions with different frequency of rotation. The peripheral velocities of the two roll surfaces are V_1 and V_2, and their minimum separation at the nip is H. The following assumptions are made: the flow is steady, laminar, and isothermal; the fluid is incompressible and Newtonian; there is no slip at the walls; the axial length of the cylinders is very large compared with their respective radii, and the flow can therefore be considered as two-dimensional; and the clearance-to-radius ratio is very small throughout the flow region.

The bipolar coordinates α and β are defined in *Fig. 2*, where

$$\alpha = \ln \frac{r_2}{r_1} \quad (-\infty < \alpha < \infty) \tag{13}$$

$$\beta = \langle) A_1 P A_2 \quad (0 \leq \beta \leq 2\pi) \tag{14}$$

For very narrow gap clearances the flow is confined to the region $-\alpha_0 \leq \alpha \leq \alpha_0$ where $\alpha_0 \ll 1$. Solving for the equations of continuity and motion, under the aforementioned simplifications and using asymptotic expansions for $\alpha_0 \ll 1$, the following expression for the flow streamfunction Ψ is obtained

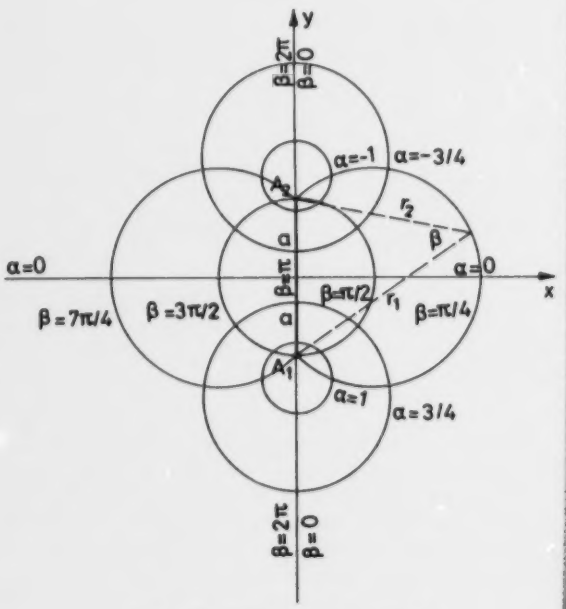

Fig. 2. Bipolar coordinates α and β.

$$\Psi = \frac{V_1 + V_2}{4\alpha_0^2}(h - h_1)(\alpha^3 + \alpha_0^3)$$

$$-\frac{3(V_1 + V_2)}{4}(h - h_1)(\alpha + \alpha_0) + V_1 h(\alpha + \alpha_0) \qquad (15)$$

$$+\frac{(V_1 - V_2)h}{2\alpha_0}\left[\frac{\alpha^2 - \alpha_0^2}{2} - \alpha_0(\alpha + \alpha_0)\right]$$

where h is the metric tensor of the bipolar coordinates, approximated by $h \simeq (RH)^{1/2}(1 - \cos\beta)^{-1}$, h_1 is the value of h calculated at the exit coordinate $\beta = \beta_1$ and the circles $\alpha = \alpha_0$ and $\alpha = -\alpha_0$ represent the roll contours. The value of Ψ varies from $\Psi = 0$ at $\alpha = -\alpha_0$ to $\Psi = q$ (volumetric flow rate per unit width) at $\alpha = \alpha_0$. Flow streamlines in the nip zone of the roll-mills are presented in *Fig. 3*. Shear rate distributions along various streamlines in the gap region between the rolls are given by

$$\dot{\gamma} \cong \frac{1}{h^2}\frac{\partial^2\Psi}{\partial\alpha^2}$$

$$\cong \frac{1}{2h\alpha_0}\left[\frac{3(V_1 + V_2)(h - h_1)}{\alpha_0 h}\alpha + (V_1 - V_2)\right] \qquad (16)$$

and are depicted in *Fig. 4*.

It is worth noting here that the axial locations where the rolls "bite" the polymer and where the polymer detaches from one of the surfaces are uniquely related to each other via the functional relationship, obtained from the condition of zero pressure at both locations

$$2(1 + 2\cos\beta_1)(\beta_1 - \beta_2)$$

$$-4(1 + \cos\beta_1)(\sin\beta_1 - \sin\beta_2) \qquad (17)$$

$$+\sin 2\beta_1 - \sin 2\beta_0 = 0.$$

Here β_1 and β_2 are the exit and entrance coordinates, respectively.

From *Eq 17* it is clear that when $\beta_2 = \pi$, i.e., when the location X_2 is situated at the minimum gap separation, $\beta_1 = \pi$. In this case, $X_1 = X_2 = 0$, the polymer "blanket" thickness equals the minimum gap separation and the pressure is zero everywhere. The unlimited increase of β_2, i.e., the removing of the entrance section from the nip will cause a decrease of β_1, i.e., a removing of the exit section down to an asymptotical value $\beta_1 = 2.25$. On the other hand, using *Eq 15*, a relationship between the flow rate, q, or the total volume of polymer per unit width on the roll-mill, v, and the exit coordinate, β_1, assuming constant "blanket" width, is given by

$$v = \frac{1}{1 - \cos\beta_1}\, v_{min}. \qquad (18)$$

Here v_{min} is the minimum amount (per unit width) of polymer obtainable for a "blanket" thickness equal to the minimum gap separation. Since β_1 varies from π to 2.25, the ratio of v/v_{min} will vary from 1 to 1.228. When the ratio v/v_{min} exceeds the maximum value of 1.228 a circulatory flow develops in the entrance region.

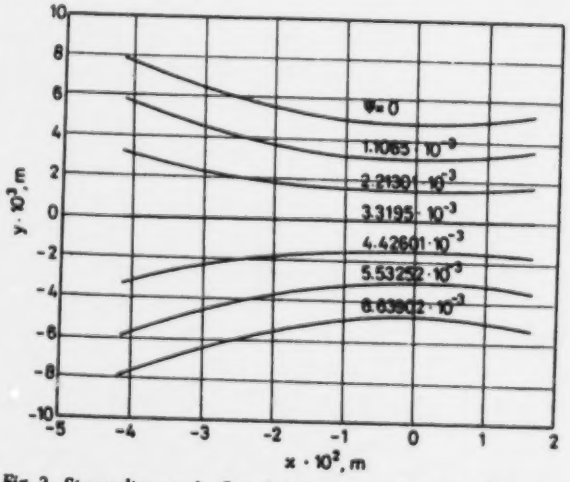

Fig. 3. Streamlines in the flow field between rolls for the following geometry and operating conditions: $H = 9.525 \times 10^{-3}$ m, $R = 2.794 \times 10^{-1}$ m, $V_1 = 6.35 \times 10^{-1}$ m/s, $V_1/V_2 = 1.01$, $v/v_{min} = 1.1$.

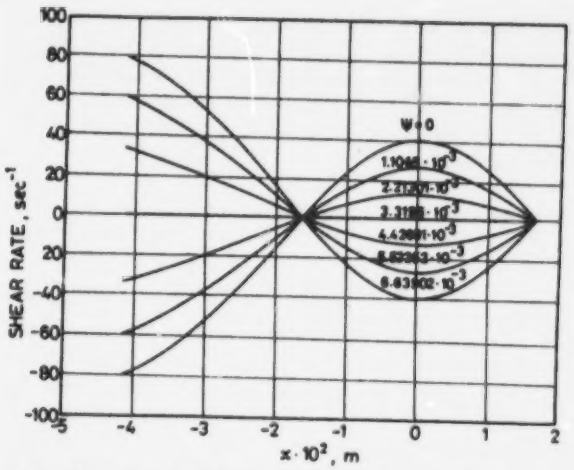

Fig. 4. Shear rate distributions along various streamlines in the flow field between the rolls, for conditions given in Fig. 3.

FRACTION OF BROKEN AGGLOMERATES DURING ONE PASS THROUGH THE NIP

As outlined before, the fraction of broken agglomerates during one pass through the nip is a sensitive function of the relative position (specific streamline) in the flow field, as well as of particle orientation distribution at the entrance to the gap. The last one is prescribed by the agglomerates' history, namely the number of previous successive passes during which they escaped unbroken.

Consider a fluid element containing many agglomerates which escaped unbroken during i successive passes, entering the narrow gap between the rolls on a streamline Ψ for the $(i + 1)$ pass. At the entrance to the gap they have a given orientation distribution. If the orientation of the axis of an individual particle is specified by a unit vector, $\vec{c}$, then the population of vectors, $\vec{c}$, points in all directions specified by the given orientation distribution. Denote by $\Omega_{\Psi,1+1}$, the surface area of the portion of a sphere covered by the specific orienta-

tion distribution. The probability of finding vectors pointing in the direction θ_0 to $\theta_0 + d\theta_0$ and ϕ_0 to $\phi_0 + d\phi_0$ within $\Omega_{\Psi,i+1}$ is given by the ratio of the segment of a sphere bounded by these angles to the total surface area $\Omega_{\Psi,i+1}$ of the given orientation distribution:

$$f(\theta_0, \phi_0)d\theta_0 d\phi_0 = \frac{1}{\Omega_{\Psi,i+1}} \sin\theta_0 \, d\theta_0 d\phi_0, \qquad \theta_0, \phi_0 \in \Omega_{\Psi,1+1}. \tag{19}$$

Denote $W_{\Psi,i+1}$ the fraction of agglomerates that are broken in the gap in this pass. Then:

$$W_{\Psi,i+1} = \int_{\theta_0^*} \int_{\phi_0^*} f(\theta_0, \phi_0)d\theta_0 d\phi_0 \qquad \theta_0^*, \phi_0^* \in \Omega_{\Psi,i+1} \tag{20}$$

where θ_0^* and ϕ_0^* are the intervals over the surface of initial orientations $\Omega_{\Psi,i+1}$, in which the condition $\frac{F_h}{F_c} \geq 1$ is met along the path. The angle ranges θ_0^* and ϕ_0^* can be computed using *Eqs 8*, 9 and *11*.

The surface of initial orientations at each entrance to the gap is a function of relative position in the flow field (specific streamline) and of the number of previous successive unsuccessful passes through the high shear zone. As the mixing process starts, or after cutting the polymer "blanket", agglomerates are assumed randomly oriented. In addition, as specified before, once broken, fragments acquire any possible orientation. For these randomly oriented agglomerates, the surface of initial orientations is given by the whole surface area of a unit radius sphere:

$$\Omega_{\Psi,0} = 4\pi \quad \text{for all} \quad \Psi. \tag{21}$$

On each streamline, agglomerates which experienced i successive unsuccessful passes through the gap enter the high shear zone for the $(i+1)^{th}$ pass with an orientation distribution $\Omega_{\Psi,i+1}$ inherited from the previous $\Omega_{\Psi,i}$ surface which correspond to the i^{th} pass:

$$\Omega_{\Psi,i+1} = (1 - W_{\Psi,i})\Omega_{\Psi,i}. \tag{22}$$

By an iterative computation procedure, it can be shown that:

$$\Omega_{\Psi,i+1} = (4\pi) \prod_{j=0}^{i} (1 - W_{\Psi,j}) \qquad i = 0, 1, 2, \cdots K-1 \tag{23}$$

where K represents the maximum number of passes between two successive cuttings of the polymer "blanket."

Using *Eq 23* with *Eq 20*, the values of the fraction of broken agglomerates during one pass through the gap, as a function of the number of previous successive unsuccessful passes on each streamline of the flow field, can be computed.

AGGLOMERATE SIZE DISTRIBUTION

The rupture of the agglomerates is modelled as a repetitive process, whereby a large agglomerate of initial size D_0 (denoting the large axis of the equivalent spheroid) is broken into two small agglomerates of size D_1, which further rupture into smaller agglomerates of size D_2 and so on. Assuming that each fragment acquires the shape of the parent agglomerate and that the total volume of particles remains unchanged, the size of an agglomerate after i ruptures is related to the size of the initial agglomerate D_0 via

$$D_i = \frac{D_0}{2^{i/3}}. \tag{24}$$

Each pass through the nip between the two rolls may bring about rupture of some agglomerates. It is assumed that each agglomerate can be broken only once during each pass through the high shear zone, since the residence time there is typically shorter than particle rotation period. Hence, after k passes there is an agglomerate size distribution D_i with i varying from 0 to k. If, for a certain pass m, the corresponding D_m reaches the "ultimate" particle size, from this moment on agglomerate size will vary from D_0 to D_m.

In order to facilitate composition and orientation randomization throughout the system, cutting and rolling of the polymer "blanket" are carried out at intervals of time. In this model we assume that this operation is executed after each K passes through the high shear zone. In the interval of time corresponding to the K successive passes between the rolls, agglomerate size and orientation distributions are different on each streamline. Moreover, each agglomerate size has its own corresponding orientation distribution.

Denote by $u_{i,k,\Psi,l}$ the volume (or number) fraction of agglomerates of size D_i, in a volume element that has experienced k passes through the high shear zone, on a streamline Ψ, and has an orientation distribution prescribed by $(l-1)$ successive unsuccessful passes through the gap. This fraction is given by:

$$u_{i,k,\Psi,l} = (1 - W_{\Psi,l-1})u_{i,k-1,\Psi,l-1} \qquad \text{for} \quad l = 2, 3, \cdots L \tag{25}$$

or

$$u_{1,k,\Psi,l} = \sum_{n=1}^{L} W_{\Psi,n} \, u_{i-1,k-1,\Psi,n} \tag{26}$$

for $l = 1$ (random oriented particles)

with

$$jK \leq k \leq (j+1)K \qquad j = 0, 1, 2 \cdots \tag{27}$$

$$L = k - i + 1 \quad \text{if} \quad i \geq (jK + 1) \tag{28}$$

$$L = k - jK \quad \text{if} \quad i < (jK + 1). \tag{29}$$

The total volume fraction $U_{i,k,\Psi}$ of agglomerates of size D_i after k number of passes, on a streamline Ψ is given by

$$U_{i,k,\Psi} = \sum_{l=1}^{L} u_{i,k,\Psi,l} \qquad (30)$$

$$i = 1, 2, \cdots k-1 \quad \text{for} \quad m > k$$

$$i = 1, 2, \cdots m-1 \quad \text{for} \quad m < k$$

and

$$U_{0,k,\Psi} = u_{0,k,\Psi,L} \quad \text{with} \quad L = k - jK \qquad (31)$$

$$U_{m,k,\Psi} = u_{m,k,\Psi,1} + U_{m,k-1,\Psi}. \qquad (32)$$

The number of passes, k, is related to the mixing time, t, via

$$k = \frac{V_i}{2\pi R} t \qquad i = 1 \text{ or } 2 \qquad (33)$$

where R is the radius of the equal sized rolls and the use of the peripheral velocity of one roll or another (V_1 or V_2) is dictated by the "affinity" of the material for one of the rolls.

Agglomerate size distribution in the batch, $Y_{i,k}$ (fraction of agglomerates of size D_i after k passes through the nip) is calculated, accounting also for the residence time distribution function:

$$Y_{i,k} = \frac{\int_0^q U_{i,k,\Psi}\, d\Psi}{q} \qquad (34)$$

where q is the volumetric flow rate per unit width predictable from the flow pattern.

As mentioned before, cutting the "blanket" after each K passes brings about composition and orientation randomization throughout the system. This is expressed by:

$$u_{i,jK,\Psi,1} = Y_{i,jK} \qquad i = 0, 1, 2, \cdots m \qquad (35)$$

$$j = 0, 1, 2 \cdots$$

and

$$u_{i,jK,\Psi,l} = 0 \quad \text{for} \quad l > 1. \qquad (36)$$

In common practice, mixing quality is measured as the fraction of agglomerates in the mixture, exceeding a certain critical size, D_{cr}, (e.g., 9 μm for carbon black in rubber). Defining λ_k as the volume fraction of "undispersed" agglomerates after k passes through the gap, i_k is given by:

$$\lambda_k = \sum_{i=0}^{n} Y_{i,k} \qquad (37)$$

where n is set by the following inequality (22):

$$\frac{D_0}{2(n+1)/3} < D_{cr} < \frac{D_0}{2n/3}. \qquad (38)$$

PRELIMINARY SIMULATION STUDIES

The theoretical model can be used for simulating the effect of geometrical design variables and operating conditions on mixing performance.

One important parameter in mixing on roll-mills is the total amount of polymer to be processed. *Figure 5* shows the effect of the volume of polymer (per unit width of the rolls) on dispersion, at three mixing times. For a given machine geometry, there is a lower limit of this parameter, at which no dispersive mixing takes place. Increasing the amount of material brings about an expansion of the high shear zone of the polymer, causing an increasing number of agglomerates to rotate and be exposed to sufficiently large separating forces. However, as soon as the amount of polymer exceeds a certain limit, a circulatory flow develops in the entrance region and no further improvement of mixing is expected.

A critical design variable of the two-roll geometry is the minimum gap separation. As mentioned above, for a given amount of polymer to be processed on the roll-mills, the clearance can vary between certain limits. A too-small gap size causes a circulatory flow in the entrance region, whereas a too-large one does not allow the material to undergo shear. Between these limits, increasing gap size results in reducing shear stress and consequently fewer agglomerates are broken. This effect is illustrated in *Fig. 6* for three different mixing times.

Another important parameter in mixing on roll-mills is the friction ratio V_1/V_2, e.g., the ratio of the peripheral velocities of the two roll surfaces (*Fig. 7*). Increasing this ratio by reducing the velocity of the slower roll, V_2, improves mixing. The higher the friction ratio, the larger the shear stress, and as a result, the fraction of undispersed agglomerates diminishes.

The effect of roll speed on mixing at a constant friction ratio is shown in *Fig. 8*. By increasing roll speed under the simulated conditions, both the number of passes at a given mixing time and shear stress increase; hence, the fraction of undispersed agglomerates is sharply reduced. However, since isothermal flow conditions were assumed, the effect

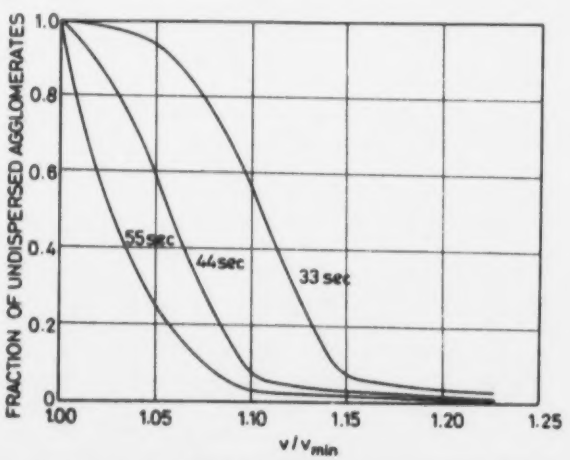

Fig. 5. Simulated fraction of undispersed agglomerates as a function of the total amount of polymer to be processed, for mixing carbon black into rubber on roll-mills. The following geometry and operating conditions are assumed: $H = 9.525 \times 10^{-3}$ m, $R = 2.794 \times 10^{-1}$ m, $V_1 = 6.35 \times 10^{-1}$ m/s, $V_1/V_2 = 1.25$, cutting the blanket each 10 passes; Newtonian viscosity $\mu = 10^3$ N.s/m^2.

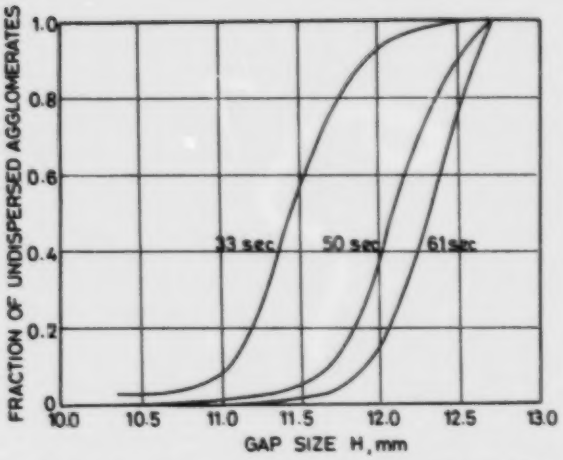

Fig. 6. Simulated fraction of undispersed agglomerates as a function of minimum gap separation, assuming conditions as in Fig. 5.

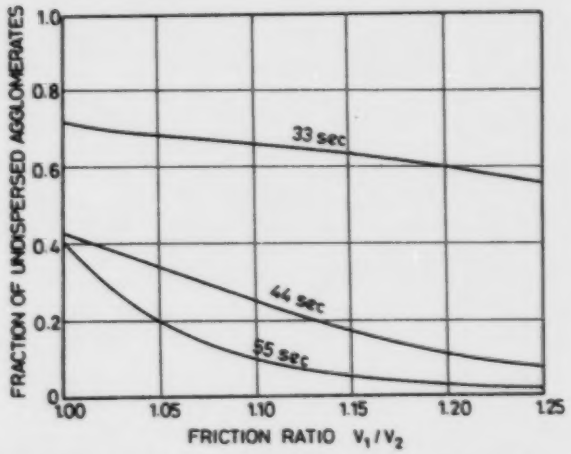

Fig. 7. Simulated fraction of undispersed agglomerates as a function of the velocity ratio of the two rolls. Conditions as in Fig. 5 with $v/v_{min} = 1.1$.

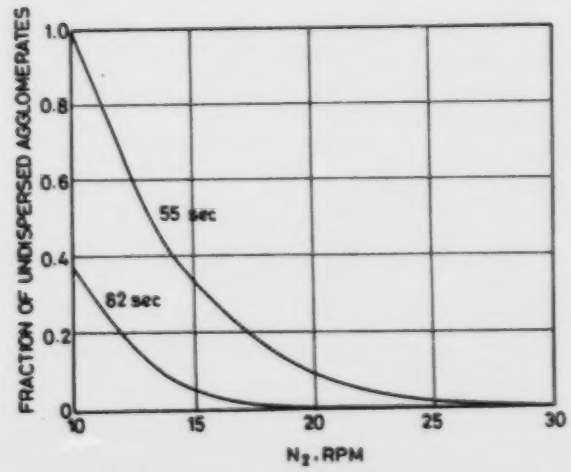

Fig. 8. Simulated fraction of undispersed agglomerates as a function of roll speed. Conditions as in Fig. 5 with $v/v_{min} = 1.1$ and $V_1/V_2 = 1.1$.

is overestimated.

Finally, Fig. 9 depicts the effect, on the fraction of undispersed agglomerates, of cutting the polymer "blanket" at different intervals of time when mixing carbon black into rubber. Under the simulated conditions, cutting the "blanket" at smaller intervals of time seems to have a minute effect on the fraction of undispersed agglomerates; however, compositional uniformity throughout the system is considerably improved.

DISCUSSION

In this paper we proposed a mathematical model of the dispersive mixing process on roll-mills, which concentrates on the dynamics of agglomerate size distribution and its dependence on a number of variables and parameters. From a formal point of view, the mathematical model presented here consists of the following three main sub-models, each having different mathematical characteristics: (a) the overall flow pattern in the mixer; (b) the hydrodynamic behavior of freely suspended agglomerates in the high shear zone; and (c) the structural model of the additive agglomerate (typically carbon black). Each of these sub-models is discussed next.

The overall flow pattern in roll-mills is modelled as a steady recycling stream over the high shear zone, and a plug type flow on one of the rolls outside the gap region. This is a strictly deterministic subunit. The idealized hydrodynamic analysis of the roll-mill is limited to a Newtonian fluid under isothermal flow conditions. In solving realistic velocity and temperature profiles in the gap, non-Newtonian and non-isothermal effects must also be taken into account. In such a case, numerical methods must be used.

The model lacks any solution details about the entrance region to the high shear zone where additional agglomerate rupture may occur. By neglecting this aspect, the model underestimates mixing efficiency.

On the other hand, the assumption that polymer

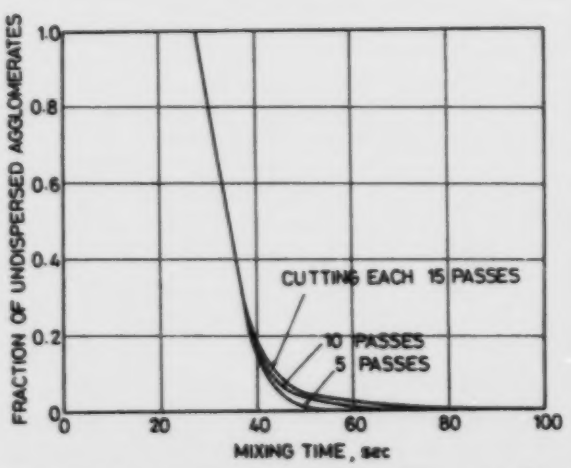

Fig. 9. Simulated fraction of undispersed agglomerates as a function of mixing time, cutting the polymer blanket at different intervals of time. Conditions as in Fig. 5 with $v/v_{min} = 1.1$.

composite is uniformly distributed on the rolls has to be cautiously evaluated.

Cutting and rolling the polymer "blanket" at certain intervals of time provides the only extensive mixing component to the whole mixing process. It is reasonable to assume that, for a given mixing quality, model predictions will underestimate mixing time. The two detrimental effects may possibly balance each other.

The hydrodynamic behavior of a freely suspended agglomerate on a given streamline in the high shear zone is uniquely determined by its orientation at the entrance to the gap. However, the assumption of a random orientation distribution at the entrance to the gap as the mixing process starts or after cutting the polymer "blanket" introduces some stochastic elements into the mode. In addition, agglomerate rupture in the high shear zone causes further particle orientation randomization.

A key assumption in the hydrodynamically driven agglomerate rupture process is a well-behaved splitting process, whereby the parent agglomerate gives rise to two identical fragments similar in shape to the parent agglomerate. The real process may, of course, involve a much more complex fragmentation mechanism.

Hydrodynamic forces on agglomerates are calculated assuming locally homogeneous isothermal flow of Newtonian fluids. The broad range of possible non-Newtonian viscoelastic effects, including lateral migration and agglomeration effects, has yet to be evaluated especially with regard to the basic assumption that particles do not cross streamlines.

Finally, the tensile strength of the agglomerate was determined by the cohesive forces between individual aggregates. The latter were assumed to have spherical shape. Since aggregates themselves are clusters of much smaller particles fused together, their interaction may be far more complex than that assumed in the model. The penetration of rubber into the agglomerate was accounted for only in terms of the numerical computation of the Hamaker constant, but in reality it may have a much more profound effect on agglomerate strength.

At this stage, the lack of any reported information concerning dispersion rating and agglomerate size distribution for mixing on roll-mills makes a comparison between the theoretical predictions and experimental results impossible.

REFERENCES

1. G. Ardichvili, *Kautschuk Gummi*, **14**, 23 (1938).
2. D. D. Eley, *J. Polym. Sci.*, **1**, 529 (1946).
3. R. E. Gaskell, *J. Appl. Mech.*, **17**, 334 (1950).
4. J. T. Bergen and G. W. Scott Jr., *J. Appl. Mech.*, **18**, 101 (1951).
5. C. Kiparissides and J. Vlachopoulos, *Polym. Eng. Sci.*, **16**, 712 (1976).
6. J. M. McKelvey, "Polymer Processing", Wiley-Interscience, New York (1962).
7. I. Brazinsky, H. F. Cosway, C. F. Valle Jr., R. Jones, R. Clark, and V. Story, *J. Appl. Polym. Sci.*, **14**, 2771 (1970).
8. J. T. Bergen, in "Processing of Thermoplastic Materials," E. C. Bernhardt, ed, Van Nostrand Reinhold, New York (1959).
9. W. W. Alston and K. N. Astill, *J. Appl. Polym. Sci.*, **17**, 3157 (1973).
10. P. R. Paslay, *J. Appl. Mech.*, **24**, 602 (1957).
11. J. S. Chong, *J. Appl. Polym. Sci.*, **12**, 191 (1968).
12. J. L. White, *Rubber Chem. Technol.*, **42**, 257 (1969).
13. W. Unkruer, Doctoral Dissertation, Technischen Hochschule, Aachen (1970).
14. M. Finston, *J. Appl. Mech.*, **18**, 12 (1951).
15. R. Takserman-Krozer, G. Schenkel, and G. Ehrmann, *Rheol. Acta*, **14**, 1066 (1975).
16. N. G. Bekin, V. V. Litvinov, and V. Yu. Petrusanskii, *Int. Polym. Sci. Technol.*, **3**, T55 (1976).
17. C. Kiparissides and J. Vlachopoulos, *Polym. Eng. Sci.*, **18**, 210 (1978).
18. N. Tokita and J. L. White, *J. Appl. Polym. Sci.*, **10**, 1011 (1966).
19. J. L. White and N. Tokita, *J. Appl. Polym. Sci.*, **12**, 1589 (1968).
20. J. M. Funt, "Mixing of Rubbers," RAPRA Publications, Shawbury, U.K., (1977).
21. M. G. Wagner, *Rubber Chem. Technol.*, **42**, 1479 (1969).
22. I. Manas-Zloczower, A. Nir, and Z. Tadmor, *Rubber Chem. Technol.*, **55**, 1250 (1982).
23. W. R. Bolen and R. E. Colwell, *SPE J.*, **14**, 24 (1958).
24. H. Rumpf, "The Strength of Granules and Agglomerates," Ch. 15, in: "Agglomeration," W. A. Knepper, ed., John Wiley Interscience, New York (1962).
25. H. C. Hamaker, *Physica*, **4**, 1058 (1937).
26. A. Nir and A. Acrivos, *J. Fluid Mech.*, **59**, 209 (1973).
27. I. Y. Z. Zia, R. G. Cox, and S. G. Mason, *Proc. R. Soc. A.*, **300**, 421 (1967).
28. F. P. Bretherton, *J. Fluid Mech.*, **14**, 284 (1962).
29. I. Manas-Zloczower, A. Nir, and Z. Tadmor, *Rubber Chem. Technol.*, **57**, 583 (1984).

PANEL DISCUSSION

T. G. M. van de Ven: Your model has many similarities with that of Hunter and Forth, which they called elastic flock model, in which they described the breakup and coagulation of flocks of particles in salt solutions. In essence, your model for hydrodynamic force balancing against the inter-particle forces is what they have done in nearly the same fashion. It may be useful to look at that work. One of the parameters which comes out from their work is the porosity of the flock. This is very much shear-rate dependent. If you go to higher shear rates you make much denser flocks. In your case, when you have a full range of rates of shear, you must be getting particles with a wide distribution of porosities. The second point is that in most systems you do not come up with flocks which no longer break up, but you get to a situation where you have a dynamic equilibrium between flock break up and flock formation, i.e., you do not have a well-defined minimum size, but an average dynamic value dependent on the shearing condition.

I. Manas-Zloczower: Our model for calculating the tensile strength of the agglomerate is based on Rumpf 's theory. Porosity is taken into account in the calculations as a constant parameter, and this is one of the many simplifying assumptions of the model. With respect to your other point that you do not end up with a well-defined minimum size of the agglomerate in the polymer matrix, my comment is that the present model is more related to a situation in which you step mixing far in advance before reaching the ultimate particle size. Therefore, for this situation the point of ultimate disper-

sion is of no great significance. However, it is true that an ultimate particle size exists. For rubber-carbon black systems, for which this model is mostly adequate, Medalia pointed out that aggregates represent the final state of subdivision.

H. P. Schreiber: One system was rutile polyethylene or chlorinated polyethylene. We used the minimum size agglomerates "by eye" dispersion measure. We plotted the size of the agglomerates as a function of the acid-base interaction difference between the rutile and the matrix, obtaining a very nice correlation, suggesting that the interaction forces holding the agglomerate together are an important factor in rating the effectiveness of a given instrument as a dispersing tool. My question is: what sort of data would you want to get to test your equation? In particular, what sort of information do you need to describe the agglomerate strength, size, etc.?

I. Manas-Zloczower: The most controversial part of the model deals with the structure of the agglomerate and the nature of the cohesive forces. With respect to the filler-matrix interactions, it was incorporated into the model only for calculating the Hamaker constant for the cohesive forces; in other words, I corrected the value of the Hamaker constant for the pure additive by considering the polymer matrix. Unfortunately, there are not too many reported data for the Hamaker constant for a large variety of additives and polymers.

H. P. Schreiber: I am not trying to push this inversed gas chromatography, but by that technique we seem to be able to correlate with the cohesive strength of the agglomerate itself. Of course we cannot calculate the Hamaker constant, but we can rate fillers. You should be able, on the basis of these easy-to-measure data, to predict the residual degree of agglomeration in a given type of mixing device. I will be very happy to show you my data.

I. Manas-Zloczower: I would be very interested to see that.

L. A. Utracki: The people here are mainly interested in dispersing anisometric particles, like mica or short glass fibers, in a polymeric matrix. There are very few representatives from the rubber industry. Could you please summarize for us how we could apply your model, what information could we get from it as far as compounding the composites on a roll-mill is concerned. It is very unfortunate that so far you were unable to confront your model with the experimental results. It is hard to believe that in 80 years of compounding rubbers with carbon blacks, nobody has produced data to test your theoretical calculations even in a qualitative manner. I am far from being as enthusiastic about the inverse gas chromatography as Henry, but maybe, as he suggests, his data are worth looking into.

My other concern is the degree of simplification incorporated into the model; assuming the Newtonian liquid is a strong assumption but even more disturbing is the neglect of the presence of the recirculating region at the entry to nip. The stationary orbits of circulating particles and orientation of the aggregates will be, in practice, very severely affected by the recirculation. It very well may be that neither the orbits nor the orientations are important as far as the final dispersion is concerned, but because of these concerns, the model must be verified with the experimental data.

Finally, I want to add my support to the comments made by Theo van de Ven. All processes of dispersion should be considered as dynamic equilibria of two kinetic processes—one of dispersion, the other of aggregation. The kinetic constant may be quite different and in some cases the reaggregation may be too slow to influence your results, but in principle this approach should be used.

I. Manas-Zloczower: The present model can be used to obtain guidelines for predicting the influence of mixer geometry and operating conditions on mixing efficiency when mixing any filler into a polymeric matrix. When I referred to axisymmetric particles I was considering their hydrodynamic behavior. The model is based on the kinematics of a small body of revolution derived by Bretherton and extended by Zia, Cox, and Mason. The hydrodynamic separating force was calculated based on a relation given by Nir and Acrivos. Some of your fillers may exhibit the same hydrodynamic behavior. Even if they do not, as far as obtaining first guidelines for mixing efficiency for given mixer geometry and operating conditions, the model is useful. To obtain accurate results for non-axisymmetric particles, the model should be modified by considering other relations for describing particles' hydrodynamic behavior. I was also surprised that I was not able to find any quantitative information in the literature for mixing on a roll-mill. I am referring to agglomerate size distribution or fraction of undispersed agglomerates as a function of mixing time.

As for the reaggregation aspect, the present model was derived in principal for describing carbon black dispersion in rubber. For these particles, as well as for $CaCO_3$ or TiO_2, the dynamic behavior regarding the ultimate particle size is not significant. Besides, for describing mixing quality, big agglomerates exceeding a critical size are more important than the ultimate stages of particle dispersion. However, for fillers which exhibit strong reaggregation behavior, the model predictions should be re-evaluated.

M. R. Kamal: Am I to understand that your solution for the flow field was based on the rheological properties of the matrix?

I. Manas-Zloczower: Yes. I assumed a Newtonian fluid for the matrix. The viscosity of the polymeric matrix for a rubber-carbon black system was evaluated from published data for the viscosity as a function of composition.

M. R. Kamal: I am surprised that you stuck to these drastic assumptions of isothermal Newtonian systems, while there are quite a few solutions, some not very new for the non-isothermal non-Newtonian calendering type of mixing. What concerns me also is the fact that in the system you have converging and diverging flows, but you did not consider the elongational properties or the elastic behavior.

I. Manas-Zloczower: For a first model, a simplified analytical solution for describing the flow field is of more advantage than a numerical one. The analytical solution was derived following Takserman-Krozer, using bipolar coordinates and assuming laminar and isothermal flow of a Newtonian fluid. I know the numerical solutions of Kiparissides and Valchopoulos, and certainly it can be incorporated into the model. With regard to the elastic behavior of certain systems, more work is needed to incorporate these aspects into the model.

R. T. Woodhams: We are interested in your interpretation, in particular, as to the level of shear stress in the nip, because mica particles are agglomerates and the individual crystal planes are held together by relatively weak forces. At a critical shear stress these individual planes began to shear apart, so you can break the mica very rapidly and efficiently in this marvelous machine called Gelimat. I was interested in knowing what sort of maximum shear stress you calculated for the nip.

I. Manas-Zloczower: I showed a slide for the shear distributions along the streamlines. The maximum shear rate is 80 s^{-1}, so in this particular case (viscosity 10^5 N.s/m^2) the maximum shear stress is 8 MPa.

J. L. White: Clearly this model can be applied to other systems beyond carbon black; but when it gets down to making the actual calculations about the forces needed to break up the agglomerates, in the case of carbon black you may do quite well with these Hamaker constants. But when you start talking about talc, $CaCO_3$ or silicates with their complex crystal structures; then how will you calculate the contact forces which would exist in the agglomerate that the hydrodynamic forces would have to overcome?

I. Manas-Zloczower: Probably you are right that for those additives I have to study in more detail the exact nature of the cohesive forces.

J. L. White: They are much larger. If you follow the rheological studies of these composites, the yield values at equivalent particle size and equivalent volume loading, $CaCO_3$ or TiO_2 have much larger yield values than the carbon black compounds, which is clearly due to much greater contact forces in these agglomerates.

I. Manas-Zloczower: The model predicts very short times for dispersing carbon black into rubber. This will probably no longer hold true for dispersing other additives. I would also like to comment that in this model, cutting and rolling the polymer blanket provides the only extensive mixing component to the process. This might not be accurate. As Dr. Utracki mentioned, there is a recirculating region at the entrance to the nip. This might also enhance composition uniformity.

Mechanical Degradation of Glass Fibers During Compounding with Polypropylene

B. FISA

Industrial Materials Research Institute
National Research Council of Canada
75 De Mortagne Blvd.
Boucherville, Quebec Canada J4B 6Y4

The objective was to study the fiber length degradation during compounding of glass fiber with polypropylene. The effect of parameters such as viscosity, total work, concentration on fiber length and dispersion was studied using an automatic particle size analyzer. The length degradation is most severe during the very first stage of the process, i.e., when fiber bundles are being filamentized. The mode of glass fiber incorporation into the melt (fiber addition to the molten resin versus to polypropylene powder prior to compounding) was found to have no effect on the final fiber length. Matrix resin viscosity affects the fiber length significantly. Concentration dependencies of fiber length for different times of compounding suggest that the degradation results from both fiber-fiber and fiber-melt interactions.

INTRODUCTION

Fillers used in thermoplastic resins can be divided into two categories. First, there are relatively inexpensive finely-divided particulate solids which are used primarily as extenders, i.e., to reduce the cost and at the same time to generate a moderate improvement of some properties. The use of calcium carbonate in poly(vinyl chloride) and of talc in polyolefins can be given as examples. The second class of fillers includes solids consisting of highly anisometric particles—fibers, flakes, etc. in which mechanical properties of the filler, such as strength and stiffness as well as its shape (particle size, aspect ratio), are of prime importance for efficient reinforcement. It is well-known that mechanical properties of thermoplastic resins, reinforced with these anisometric fillers, fall far short of the values predicted by theory. This is due to a combination of factors; some are related to poor adhesion at the filler-matrix interface, others to less than optimum orientation of filler particles in the matrix or to their degradation (attrition) during processing. With the increasing usage of these reinforced resins, the advent of new high performance/high cost engineering thermoplastics require that the reinforcing effect be maximized.

This work deals with the mechanical degradation of glass fibers during compounding with polypropylene. The reduction of the length of glass staple fibers by more than one order of magnitude, as a consequence of their incorporation into a resin, is well documented. For example, in the study by Bader and Bowyer (1) of glass fiber reinforced nylon 66, only about 20 percent of fibers exceeded the critical length ($L_c \sim 270\ \mu m$, $d = 12\ \mu m$), and none achieved the desired $5L_c$ required for efficient reinforcement. This indicates that significant gains in strength could be realized by an increase in fiber length. There are several studies on the mechanical degradation of glass fibers. Von Turkovich and Erwin (2, 3) studied single screw extrusion compounding of several glass reinforced resins and found that the amount of attrition was essentially independent of all parameters studied including the fiber concentration. The length degradation was found to occur primarily during the resin melting. In the melting zone, the glass fibers exhibited a bimodal length distribution. Lunt and Shortall (4, 5), using a larger extruder, concluded that the degradation occurs primarily at the melt film-solid bed interface, and that it could be controlled to some limited extent by processing variables. These authors suggest that incorporation of glass fiber to an already molten resin, as opposed to processing of glass fiber-resin dry blends, might give better results. Other papers dealing with this subject (6–12) also illustrate the severity of fiber length degradation during processing. The specific objective of this work was to study the compounding of glass fiber-polypropylene blends and to relate the fiber attrition to processing parameters such as work of mixing, polymer viscosity, and fiber volume fraction, to determine whether the fiber addition to a molten resin gives longer fibers than the compounding of fiber polymer dry blend. The equipment selected

for this study was a laboratory roller blade mixer which allows good control and monitoring of the compounding process.

EXPERIMENTAL

Materials

Polypropylene

Three resins of different molecular weight were used. All were in the powder or "as polymerized" form. Their properties are summarized in *Table 1*. The average particle size of the resin powder is about 300 μm. Prior to compounding 0.1 percent of Irganox 1024 and 0.1 percent of Irganox 1010, two antioxydants supplied by Ciba-Geigy, were dry blended into the polymer.

Glass Fibers

Glass fiber strands (Fiberglass Canada, type 885) chopped to a 3 mm length were used in this study. The fiber length distribution of the sample as determined by the particle size analysis described below is shown in *Fig. 1*. The average diameter of the fibers used in this work as determined microscopically on a sample of 50 fibers was 13.8 ± 2.0 μm.

Table 1. Characteristics of Polypropylene Resins*

Name	Melt Index, g/ .0 min. (ASTM D 1238)	Intrinsic Viscosity (Decahydronaphthalene, 135°C)
Profax** 6301	12	1.7
Profax 6501	4	2.25
Profax 6701	0.8	3.1

* Data provided by the supplier.
** Trademark of Hercules Inc.

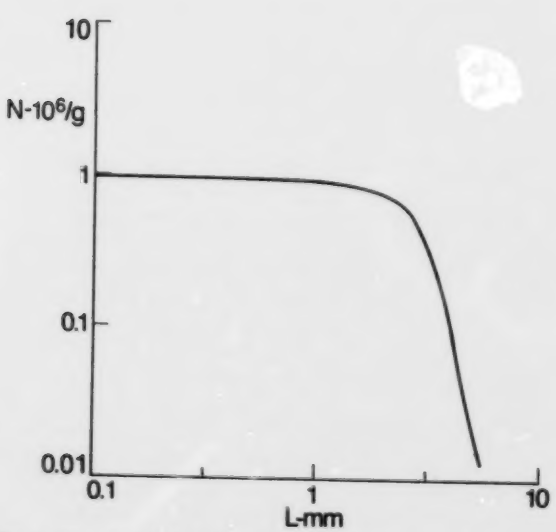

Fig. 1. Fiber length distribution curve of unprocessed fiber. N is the cumulative number of fibers longer than L per 1 g.

Compounding

Equipment

The compounding was carried out on the Plasticorder torque rheometer, Model EPL-V5501, fitted with the roller blade batch mixer from C. W. Brabender Inc. The roller blade mixer is commonly used with materials requiring strong shear forces.

Compounding Procedure

For each run, the weight of ingredients was calculated to keep the batch volume constant at 50 ml at the compounding temperature. The values of 0.75 g/cm^3 and 2.55 g/cm^3 were used as densities of polypropylene and glass respectively.

Two modes of addition of glass fiber to polypropylene were used:

— *Addition to molten resin.* Glass fiber was added gradually to the molten resin with the mixer running. For concentrations up to and including weight 5 percent, it took less than 15 seconds to incorporate all the fiber; the 10 percent blend took about 30 seconds while 40 and 60 percent blends required 45 seconds. One minute was needed for blends containing 70 percent fiber. The mixing times mentioned in the text do not include the time of incorporation. The work of mixing, W, was calculated using the formula:

$$W = 2\pi BA$$

where B is the mixer speed in rpm, and A is the value of the area under the torque-time curve as supplied by the torque integrator. The values of W used throughout this work include the mixing work performed on the blend between the time of first fiber addition and the end of the experiment.

— *Blending of glass fiber with polypropylene powder prior to compounding.* The glass-polypropylene dry blends were loaded into a hot running mixer. As the blend started to melt, the torque increased, passed through a maximum, and stabilized within about 60 seconds. The work of mixing related to this procedure includes all the work between the addition of glass fiber-polypropylene powder and the end of the run.

Recovery of Glass Fibers from Processed Blends

Between 100 and 500 mg of polypropylene/mica blend were placed in a small ceramic crucible which was introduced into a cold furnace. The temperature was gradually increased by approximately 100°C/hour until it reached 450°C where it was kept for 3 hours. The glass fiber recovered from the crucible was then ready for analysis. Blank experiments in which undegraded glass fiber was blended with polypropylene powder were performed to verify that the pyrolysis does not affect the fiber length distribution.

Fiber Length Distribution

Equipment

The fiber length distribution was determined with the HIAC-PA720 particle size analyzer manufactured by Pacific Scientific Co., Montclair, Calif. This instrument uses the so-called light blockage principle (13). A suspension of particles to be analyzed is pumped through a sensor where each particle momentarily blocks an amount of light from reaching a photodetector. The sensor is designed in such a way that the amount of light blocked is proportional to the greatest projected area of the particle. The pulses produced by the particles are sorted into 23 sizes and counted. An E-2500 sensor, having a nominal range capacity of 45 to 2500 μm (for spherical particles), was used in this work. However since the projected area of a fiber of a given length is much smaller than the one produced by a spherical particle of the same diameter, all 23 size threshold voltages were adjusted downwards from 9–5000 mV to 7–132 mV. This means that for fibers of an average diameter of 14 μm the instrument covers the length range of approximately 100 to 3500 μm.

Calibration

The instrument was calibrated using standards specially prepared for this purpose. About 20 continuous strands of the same glass fiber as the one used in the compounding experiments were inserted into a 25-mm diameter test tube. The test tube was then filled with a catalyzed unsaturated polyester resin. Once the resin hardened the tube was broken, and the resulting composite was then cut into slices of different thicknesses on an ordinary lathe. The resin was burned away and the fibers recovered. Microscopic examination revealed reasonably uniform fiber length for each standard. The number average length of each standard was determined by measuring 50 fibers in a light microscope.

Figure 2 shows the distribution curves of some of the standards used as a function of the channel voltage. The number average voltage V_n, for each standard was calculated

$$V_n = \frac{\sum V_i N_i}{\sum N_i} \qquad (1)$$

where V_i is the average voltage of the channel i, and N_i is the number of fibers counted. The calibration curve (*Fig. 3*) obeys the equation

$$L_n = 4.06 \cdot 10^{-3} V_n^{1.492} \quad (R^2 = 0.999) \qquad (2)$$

where L_n is the fiber length of the standard in millimeters, and V_n is in millivolts. For further fiber length calculations, the voltage corresponding to each channel was replaced by a fiber length calculated using the calibration equation.

Experimental Procedure

About 4 mg of glass fiber were weighed on the Sartorius-Model 4433 ultra microanalytic balance set to work with a precision of 1 μg. The fibers were then suspended in about 1000 ml of demineralized and filtered water, dispersed by placing the container with the suspension for about 1 minute in an ultrasonic bath and passed through the E-2500 sensor. The amount of suspension used was determined by weighing. Depending on the average fiber length, between 4000 and 15,000 fibers were counted during each test.

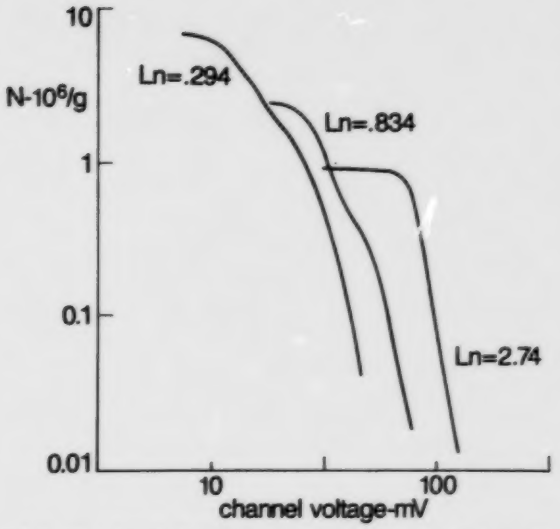

Fig. 2. Fiber length distribution curves of three standards used to calibrate the particle size analyzer as functions of channel voltages, V.

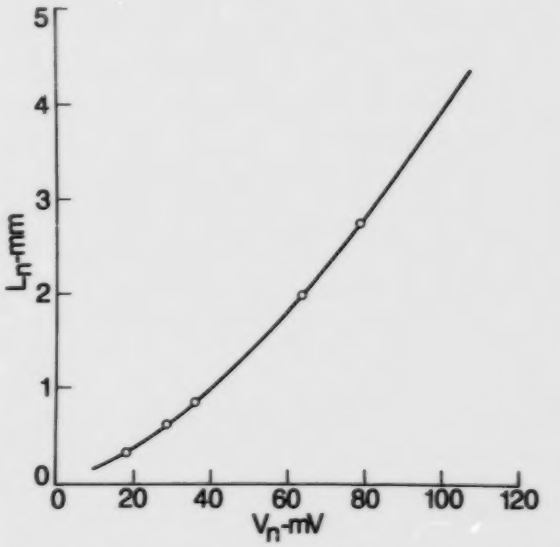

Fig. 3. Calibration curve of the HIAC particle size analyzer. V_n and L_n are defined in the text.

Calculation of Average Fiber Length

The weight average length, L_w, is used throughout this work.

$$L_w = \frac{\sum N_i L_i^2}{\sum N_i L_i} \qquad (3)$$

where N_i and L_i are the number of fibers and the fiber length associated with the fraction i(i = 1, 2, 3 . . . . 23). The use of number average length is not convenient because of the large number of short fiber fragments in processed samples.

Reliability of the Method

The particle size analyzer signal is proportional to the maximum projected area of the fiber rather than to the fiber length. Since the fibers are of a non-uniform diameter, some broadening of fiber length distribution curves (*Fig. 1*) is produced by this method, which assumes a constant fiber diameter. For example, in the 50-fiber sample used to determine the average diameter, the measured diameters covered a range of 10.5 to 18.5 μm. However this drawback does not affect the average fiber lengths because the secondary calibration was performed with the same fibers as those tested. Repeat experiments on some samples showed the standard deviation of L_w to be between 2 and 5 percent; the samples having the 500 μm < L_w < 1500 μm displayed best reproducibility. Overall reproducibility is slightly worse than with mica flakes (14), possibly because of the lower sensitivity of the sensor to the fibers (low projected area), and possibly also because of the smaller number of particles counted during one experiment.

Fiber Dispersion

Fiber dispersion was evaluated by granulating and by extruding the compounds using the Instron capillary rheometer with a 3-mm diameter capillary (L/D = 7). The flow velocity in the capillary was 2.4 cm/min. The purpose of this procedure was to orient the fibers without additional dispersion. The extrudates were then fractured in liquid nitrogen and the fracture surfaces viewed in a scanning electron microscope.

RESULTS AND DISCUSSION

Compounding Time

The fiber length degradation as a function of work of mixing is shown in *Fig. 4* for melts containing 2 and 40 percent of glass fibers. For each blend the work of mixing was varied by simply increasing the mixing time. The range of compounding times used to generate the curves was 0 to 40 minutes. The transformation of the relatively long fiber bundles into broken fragments in the final compound must occur via two processes overlapping in time. First, the bundles are filamentized into individual fibers. These fibers are much more likely to break as a result of shear stresses in the melt. *Figure 4* suggests that a significant fiber length degradation is associated with the breaking of the bundles into individual filaments. This is particularly true for the 40 percent blend. In less than 1 minute L_w is decreased by a factor of 4. The initial period is followed by a region of rather slow decline. The behavior of the 40 percent blend (volume fraction ϕ = 0.155) shows that the fiber-melt interactions often used to interpret fiber breakage in flowing polymer melts (1) play only a minor role in the initial period where the length reduction is most pronounced. The phenomenon is probably more similar in nature to grinding of fibrous substances such as wood or asbestos mineral.

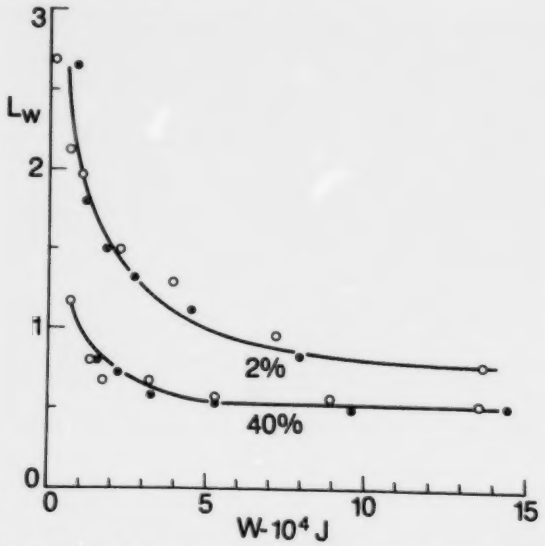

Fig. 4. Dependence of L_w on the work of mixing for blends containing 2 and 40 percent of glass fiber. W was varied by increasing the compounding time from 0 to 40 minutes. ○ - Fibers added to the molten resin, ● - compounding of fiber/resin dry blend. Profax 6501, 45 r.p.m., 200°C.

The blend containing 2 percent of glass fibers (ϕ = 0.0056) displays a different behavior. The reduction of L_w with the work of mixing is more gradual and the fibers remain substantially longer than at the 40 percent. The rate of decline of L_w gradually slows down as the fibers become shorter.

The microscopic examination of compounded samples illustrates well the relation between the filamentization of bundles and reduction in fiber length. *Figure 5A* shows the 2 percent compound just at the beginning of melting (L_w = 2.65 mm); undispersed bundles predominate with a small number of individual fibers. As the dispersion improves due to longer compounding times (*Fig. 5B* and *5C*), the average fiber length falls below 1 mm. Analogous pictures of the 40 percent blend (*Fig. 6*) reveal a more rapid fiber dispersion that at 2 percent. Since the fiber concentration is the only variable, the more rapid dispersion and length degradation has to be attributed to some type of fiber-fiber interaction.

The points used to create the curves in *Fig. 4* were obtained from two sets of experiments. In the first one, the polypropylene powder was dry blended with the glass fiber and the dry blend compounded. In the other, the glass fibers were added to an already molten resin to see whether the final fiber length would be affected. For each concentration the points fall on one curve—the mode of fiber addition does not play a measurable role in the fiber length degradation. It may be noted that an analogous study on the attrition of high aspect ratio mica flakes (14) gave identical results.

Fig. 5. Scanning electron micrographs of 2 percent glass/polypropylene compounds. A, B, C: compounding times of 0, 1 and 2 min respectively. Profax 6501, 45 rpm, 200°C, fibers added to the molten resin.

Fig. 6. Scanning electron micrographs of 40 percent glass/polypropylene compounds A, B, C: compounding times of 0, 1, and 2 min. respectively. Profax 6501, 45 rpm, 200°C, fibers added to the molten resin.

One may then question the assumption of the inherent superiority of the "filler into the molten polymer" incorporation as opposed to compounding of filler polymer dry blends.

Fiber length distribution curves of fiber samples recovered from processed blends reveal other useful information on the mechanism of the fiber fracture. *Figure 7* shows the length distribution curves of 2 percent samples compounded for 0, 1, and 2 minutes. The "zero minute" sample was prepared by stopping the mixer immediately following the addition to the melt, which took about 15 seconds. The difference between this sample and the unprocessed one is principally in the area of short

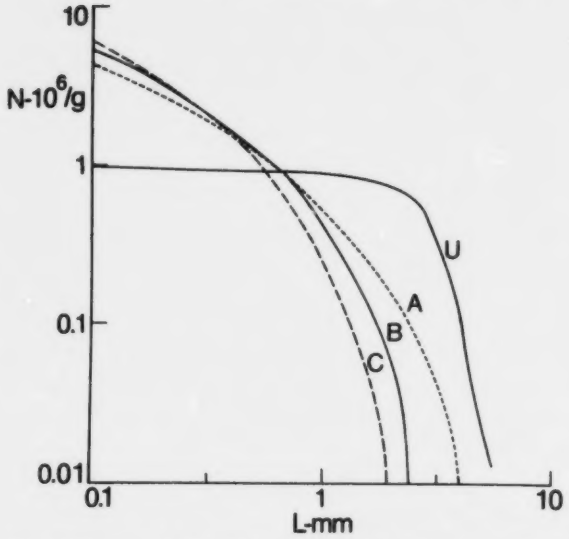

Fig. 7. Fiber length distribution curves of samples shown in Fig. 5. U-unprocessed fiber.

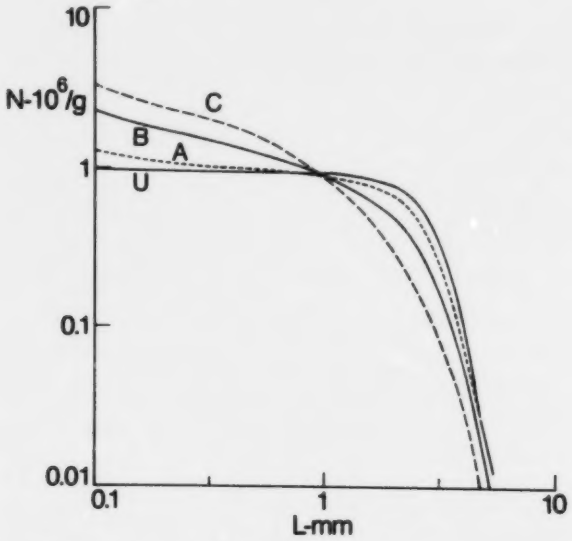

Fig. 8. Fiber length distribution curves of samples shown in Fig. 6. U-unprocessed fiber.

fibers ($L < 500$ μm). This means that the first individual filaments removed from the fiber bundles are either in the form of, or break immediately into, 300 μm and shorter fragments. During subsequent compounding (1 and 2 minute curves) the fibers break in the expected manner as evidenced by the gradual disappearance of long fibers and their transformation into relatively long fragments. At this stage the fibers probably break as a result of buckling of individual fibers. For the 40 percent sample (*Fig. 8*) similar trends are observed, although the degradation is much more rapid, resulting in a larger number of shorter fibers.

Fiber Concentration

The effect of fiber concentration in the melt on the fiber length is shown in *Fig. 9*. The L_w vs ϕ curve for mixing time of 2 minutes intercepts the Y-axis ($\phi = 0$) at a value of L_w which is of the same order of magnitude as that of the unprocessed fiber. On the other hand, after 20 minutes compounding the intercept with the Y-axis, slips to about 1 mm. Fiber fracture during processing is usually interpreted in terms of two types of interactions:

- Stresses induced on the fiber by the flowing melt without any concurrent interaction from other fibers;
- Stresses resulting from fiber-fiber interactions (collisions, spatial hindrance, friction, etc.).

The decrease of L_w with time at very low concentrations ($\phi = 0$, fiber-fiber interactions do not occur) can be considered as a measure of fiber length degradation resulting only from the fiber-melt interactions. The remaining and far more important reduction of fiber length has to be attributed to some sort of fiber-fiber interactions. These results are at variance with those of von Turkovich and Erwin (2, 3), who found no influence of fiber concentration on the final fiber length in extrusion compounded polystyrene-glass fiber composites

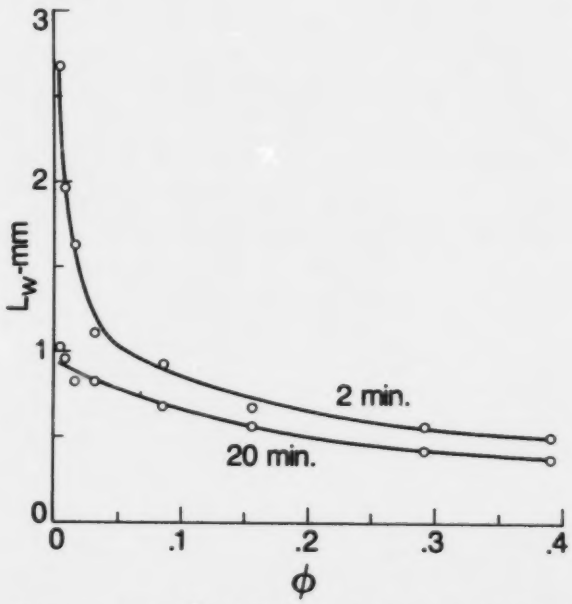

Fig. 9. L_w as a function of fiber volume fraction, ϕ, for mixing times of 2 and 20 min. Profax 6501, 45 rpm, 200°C, fibers added to the molten resin.

and concluded that fiber-fiber interactions play no role in the fiber length degradation. These authors (2, 3) obtained relatively short, final fiber lengths probably corresponding to the regions of slow decline (*Fig. 4* and *9*), where differences of the fiber length and the experimental error may have been of the same order of magnitude. It is interesting to note that similar curves (diameter, d *vs* ϕ, different mixing times) obtained with high aspect ratio mica-polypropylene melts, intercept the Y-axis at the same value of d indicating that mica flakes degrade exclusively via flake-flake interactions (14).

Polymer Viscosity

The effect of the matrix resin viscosity on the fiber length was studied by using three different resins and by varying the temperature; each resin was compounded at 180° and 200°C. Results are shown in *Fig. 10*. Again the mode of incorporation of glass fibers into the melt does not have any effect; points from both types of experiments fall on the same curves.

At the 2 percent fiber concentration, the influence of polymer viscosity on the final fiber length is particularly striking. The fiber count (as determined from the particle size analysis data) of the least degraded sample (least viscous resin compounded at 200°C) is $1.45 \cdot 10^6$/g compared to $0.95 \cdot 10^6$/g for the unprocessed fiber—only about half of the fibers broke. The most viscous blend gave a fiber count of $6.1 \cdot 10^6$/g which amounts to more than six fractures for each fiber. The 40 percent blend also shows a strong decline of L_w with the increasing resin viscosity although fiber lengths are considerably smaller.

When the compounding time is increased to 20 minutes the rate of decline of L_w with the increasing W slows down considerably for both 2 and 40 percent blends showing that fibers of lower aspect ratios are more difficult to break.

Rotor Speed

The effect of mixer rotor speed on the L_w is shown in *Fig. 11*. These curves show the now familiar decline of L_w with the work of mixing. It is interesting to note that the L_w versus W curves in *Figs. 4* and *11* are practically identical; for a given composition L_w is a function of the work of mixing only. The duration of compounding, the rotor speed, and the mode of incorporation of fibers into the melt have no influence on the final fiber length provided the work of mixing is constant.

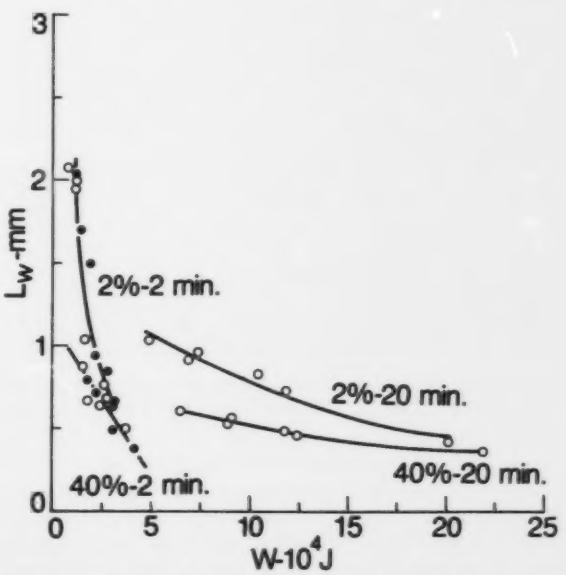

Fig. 10. L_w versus W for blends containing 2 and 40 percent glass fiber. Times of mixing were 2 and 20 min. The points on each curve were obtained by using each resin (Table 1) at temperatures of 180 and 200°C, 45 rpm ○ - Fibers added to the molten resin, ● - compounding of fiber/resin dry blend.

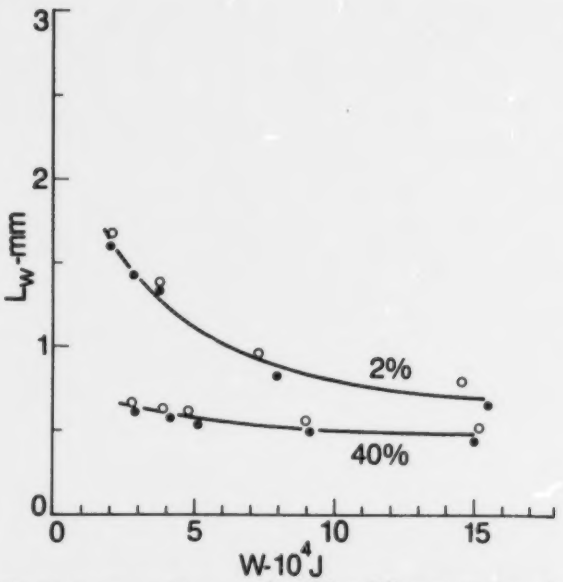

Fig. 11. L_w versus W curves obtained at different mixer speeds (15, 20, 25, 40, and 90 rpm). Compounding times 2 and 20 minutes; Profax 6501, 200°C ○ - Fibers added to the molten resin, ● - Compounding of fiber/resin dry blend.

Comparing the data from this work with the information available in the literature (1–12) gives the impression that most thermoplastic short glass fiber composites are overcompounded, i.e., the energy put into mixing exceeds what is necessary to ensure good dispersion of fibers. However this work also confirms that a significant fiber length degradation is unavoidable in conventional compounding of glass fibers.

Torque Versus Time Relationships During Compounding

The torque versus time dependencies for different glass fiber concentrations are shown in *Fig. 12*. Pure resin (0 percent) shows a very slow constant rate of decline with time. As the fiber concentration increases, the rate of decline also increases. In addition, for the 40 percent and 60 percent blends, the rate of decline increases with time. *Figure 13* shows the torque versus time curves for 40 percent glass fiber blends for all three resins used at two compounding temperatures. All experiments performed at 180°C gave reasonably stable torque. Of the 200°C experiments, only the most fluid resin would follow this pattern; the torque for the other two resins declined very sharply during the experiment. This can be attributed to a combination of effects:

- during compounding the fiber aspect ratio decreases, leading to a lower viscosity melt, hence lower torque;
- sizing is progressively removed from the fibers providing internal or external lubrication;
- chemical degradation of the resin.

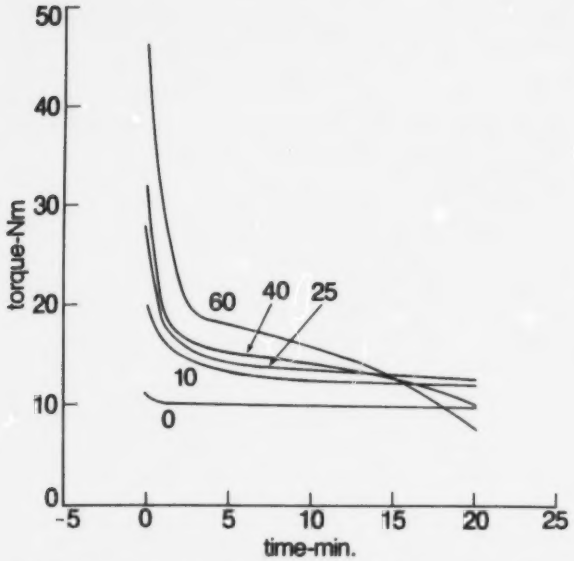

Fig. 12. Torque versus time for different glass concentrations. Profax 6501, 45 rpm, 200°C.

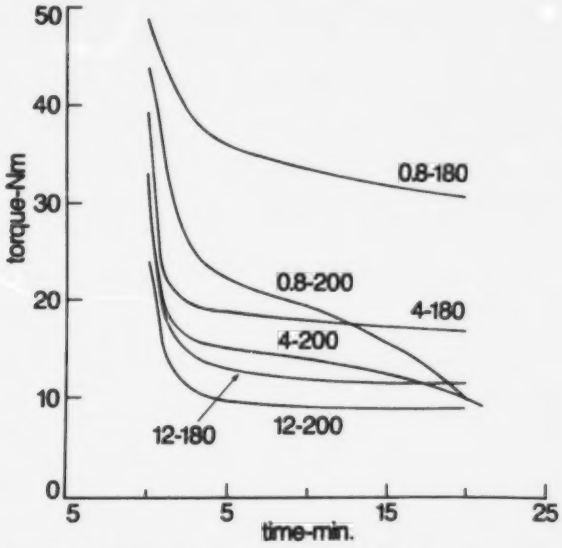

Fig. 13. Torque versus time for compounds containing 40 percent glass as a function of matrix resin viscosity, 45 rpm. The numbers refer to the matrix resin melt index and to compounding temperature.

Although the first factor undoubtedly has some influence, the absence of sharp decline observed during compounding at 180°C and in the low viscosity melts compounded at 200°C indicates that the most likely cause is the chemical degradation of the resin. The energy supplied to mix the melt is converted to heat, giving effective melt temperatures considerably higher than the nominal compounding temperatures. It is also well-known that thermocouples used to control or measure temperature in polymer processing usually measure the temperature of the metal surface rather than that of the melt in contact with it (15). Assuming that all the work of mixing supplied is converted to heat which must be transferred from the melt to the mixer, the temperature gradient between the polymer melt and the mixer is proportional to the energy input. The temperatures were recorded during the *Fig. 13* experiments and are summarized in *Table 2*. Clearly, in cases where the sharpest decline in torque was observed, the melt temperature reached levels at which polypropylene is known to undergo thermal degradation.

Table 2. Temperatures Measured During Compounding of 40% Glass Fiber Polypropylene Blends (See Fig. 13)

Resin Melt Index g/10 min.	Torque* Nm	Nominal Compounding Temperature °C	Mixer Temp.* °C
12	12	180	186
12	9.1	200	205
4	18.1	180	190
4	14.0	200	208
0.8	33.6	180	194
0.8	19.5	200	211

* After 10 min. of compounding.

SUMMARY AND CONCLUSIONS

Fiber length degradation during compounding of glass fiber with polypropylene is most severe during the very first stage of the process, i.e., when fiber bundles are being filamentized. The mode of glass fiber incorporation into the melt (fiber addition to the molten resin versus polypropylene powder prior to compounding) was found to have no effect on the final fiber length. Matrix resin viscosity affects the fiber length significantly. Concentration dependencies of fiber length for different times of compounding suggest that the degradation results from both fiber-fiber and fiber-melt interactions. The increased viscosity of the composite melt requires higher energy input to the melt during compounding. This may cause the melt temperature to increase to levels where the resin starts to degrade.

ACKNOWLEDGMENTS

The contributions of Mr. J. Dufour who developed the fiber length analysis method and of Mr. M. Thibodeau who prepared the photomicrographs are gratefully acknowledged.

REFERENCES

1. M. G. Bader and W. H. Bowyer, *Composites*, 4, 150 (1973).
2. R. von Turkovich and L. Erwin, *SPE ANTEC Tech. Papers*, 28, 439 (1982).
3. R. von Turkovich and L. Erwin, *Polym. Eng. Sci.*, 23, 743 (1983).
4. J. M. Lunt and J. B. Shortall, *Plast. Rubber Process.*, 4, 108 (1979).
5. J. M. Lunt and J. B. Shortall, *Plast. Rubber Process.*, 5, 37 (1980).
6. M. W. Darlington, B. K. Gladwell, and G. R. Smith, *Polymer*, 18, 1269 (1977).
7. L. Czarnecki and J. L. White, *J. Appl. Polym. Sci.*, 25, 1217 (1980).
8. B. A. Knutsson, J. L. White, and K. B. Abbas, *J. Appl. Polym. Sci.*, 26, 2347 (1981).
9. R. A. Schweizer, *Plast. Compound*, 4(6), 58 (1981).

10. R. A. Schweizer, *Polym. Plast. Technol. Eng.*, **18**, 81 (1981).
11. R. Burns and D. Pennington, *SPI Reinf. Plast. Compos. Inst. Annu. Conf. Proc.*, **34**, 7D (1979).
12. D. M. Bigg, SPE ANTEC Technical Papers, **30**, 668 (1984).
13. H. A. Kupfer, *Powder Metall. Int.*, **10**, 96 (1978).
14. B. Fisa, B. Sanschagrin, and B. Favis, *Polym. Compos.*, **5**, 264, (1984).
15. J. F. T. Pittman and H. Mahmoudzadeh, *Polym. Eng. Rev.*, **3**, 63 (1983).

Panel Discussion

R. T. Woodhams: Your experiments were all done in an internal mixer. Do you have any confirmation that the same process of size degradation occurs during extrusion?

B. Fisa: We have some data on degradation of mica flakes during extrusion with polypropylene in form of either powder or pellets. In this case, there does not seem to be any difference. This, in my opinion, has something to do with the dispersion of filler in the matrix. Before the polymer is molten, the filler cannot disperse so it does not break.

J. L. White: I was most interested in comparison between the results on a mica and fibers. I kept trying to visualize what was happening when you go to higher and higher loadings. We wrote a paper several years ago when we surmised that the reason that the fibers were breaking in flow was that they were undergoing Jeffrey's orbits where there were compression forces that were breaking the fibers. Presumably in mica at low and intermediate concentrations you may have more random arrangements of the flakes. But as you go to higher concentrations, you form what Freundlich used to call "tactoids," liquid crystalline-like structures. You may end up with discs rotating as they translate in the direction of flow and the compressive forces would not break a disc pressing on its axis.

B. Fisa: This is an interesting comment. As far as the mica is concerned, we actually observed an unexpected phenomenon where the reduction of diameter upon increase of concentration occurs only up to a volume fraction $\phi = 0.2$ to 0.3. Above this value, the extent of mechanical degradation was reduced. This is probably due to the fact that there are some secondary structures formed in the melt. Flakes no longer behave as individual particles.

R. E. Prud'Homme: In the light scattering experiment, it would seem to me that it is required to have the fiber in the plane which is perpendicular to the bean of light. If this requirement is not met, then if the fiber is tilted in respect to this plane, you may see only a fraction of the fiber length. How do you manage to have your fibers all well oriented?

B. Fisa: We do not attempt to get the particles oriented. Quite opposite, the flow by the sensor is turbulent, i.e., the particles rotate and the voltage difference is proportional to the highest projected area. It is not a light scattering principle which is involved but a simple shadow casting principle. We have prepared standards of given lengths and calibrated the instrument prior to measuring the attrition effects.

J. Farrell: Concerning your statement regarding the effect of melting on eventual fiber length, I have trouble comparing the melting process in a small internal mixer to actual commercial extrusion operation. Have you done any experiment on a larger scale extruder?

B. Fisa: Yes, we have done it with mica, finding the same process in the ZSK-25 as in small internal mixer.

J. Farrell: Would you expect different behavior of glass fibers due to a much higher aspect ratio?

B. Fisa: Maybe, we would have to try it.

J. Farrell: It is easy to do as far as feeding up-stream. We will be happy to supply the elements after you will wear them out.

B. Fisa: Obviously, there are other advantages and disadvantages related to feeding the glass fiber into the molten polymer. Erosion of barrel and screw may be one. Here we tried to understand the mechanism of fiber length degradation during processing.

G. Benson: There is a conflict in your statements. You said that melt viscosity was an important factor in determining the break-down. On the other hand, the method of addition of the glass as far as pre- or post-flux is not. I find it difficult to put those two statements together. Going through a melting zone causes a tremendous change in viscosity.

B. Fisa: I thought about it and came to a conclusion that probably the time to melt the polymer is relatively insignificant with respect to the total mixing time used in these experiments. I cannot offer you any better explanation. Very similar behavior was observed for both mica and glass fiber.

J. L. White: Presumably, melting does not break fibers. What happens when the material melts in the solid bed of the processing unit there is that these very long fibers are being exposed to a stress field which will move them around for the first time. And the answer as to what happens to the single screw extruder versus twin screw extruder is going to depend on the difference in the fluid mechanics of the melting mechanism. There is very substantial literature around for what happens in melting in a single screw extruder, which is slightly modified by the presence of filler. But there is nothing I have ever seen on what the melting mech-

anisms there are like in a twin screw extruder. Can Werner Pfleiderer enlighten us?

J. Farrell: You are, in effect, suggesting that the breaking mechanism will be different if the melting energy is either mechanical or electrical. The twin screw system inputs typically more energy mechanically. One of the reasons you do not see too much published information on compounding is that many people, some of which may even be in this room, would be unhappy to see some of their polymer information in one of our papers.

B. Fisa: One additional conclusion one could make on the basis of the presented data is that most commercial glass fiber filled polymers would be severely over-compounded as far as the fiber lengths are concerned.

L. A. Utracki: How does the ultimate fiber length you are reporting, L_w = 300 μm, compare to the critical fiber length?

B. Fisa: I do not have the slightest idea because this depends on the properties of the interface.

G. Benson: Did you try any double or triple passing techniques?

B. Fisa: Not for fibers, but judging by the graphs I showed, it seems that once the fibers reach their ultimate size, the rate of change is low.

The Interface Between Glass and Carbon Fibers and Thermosetting Polymers

M. R. PIGGOTT, P. S. CHUA, *and* D. ANDISON

Department of Chemical Engineering
and Applied Chemistry
University of Toronto
Toronto, Ontario, Canada M5S 1A5

The interface between the fibers and the polymer matrix controls the properties of fiber composites and has been the subject of much study. Recently, special techniques have been developed for single fiber pull-out experiments on production fibers, which make it possible to obtain data on the frictional forces which govern sliding after the interface has fractured, as well as the adhesion strength of the interface. Tests on glass in polyester and epoxy resins show that the work of fracture of the interface is much smaller than that of the resin, and that the shrinkage pressures of these matrices, when fully post-cured, are approximately the same (about 20 MPa). Coefficients of friction at the interface are 0.6 for the polyester and 1.0 to 1.6 for the epoxy. The carbon-epoxy interface yields at shear stresses as high as 60 MPa, instead of fracturing, and the coefficient of friction during sliding is about 0.4.

INTRODUCTION

The interface between the fibers and the matrix is the heart of the fiber composite. It is considered to consist of a region of finite thickness, usually referred to as the "interphase" (1). This is because the fibers are coated with adhesion promoters which are reactive, and in the case of glass fibers, are considered to develop secondary chemical bonds (Van der Waals and hydrogen bonds) with the glass, and are designed to react with the polymer matrix to give primary chemical bonds (2). In this case, the interphase is thus a polymeric material which is distinct from the polymer matrix. In the case of carbon, the fibers have a surface layer of carbon which is not as strong as the underlying fiber. This must be removed before a composite is made, since otherwise the composite will be weak (1). The removal of this layer is effected by oxidation, usually with acid. It is considered that reactive groups, (e.g., —COOH, —CHO, =CO) are present on the fiber surface after this process. In this case, chemical bonding can easily be effected with carbon, in sharp contrast to glass. Adhesion promoters are still used so that there is an interphase as there is in the case of glass. In the case of Kevlar, which is also an important reinforcing fiber, very little enlightenment is available on the adhesion promoters used, since this information is proprietary.

In the paper presented at an earlier symposium in this series, the interface was reviewed, and its importance for fiber composites was demonstrated (3). Since then, a great deal of progress has been made in characterizing the interface and its influence on composite properties, thanks to financial support from IMRI. Two aspects of this interface were examined:

1. Carbon fiber composites were made with short fibers having known critical aspect ratios, in order to test existing fiber composite theories. The results obtained strongly indicate that more theoretical work is required, and our understanding of even the most simple composite, (one containing aligned fibers all having the same length), is far from complete (4). A new theory for strength and modulus of planar random short fiber composites was moderately successful in explaining the results obtained with these composites, however (5).
2. Single fiber pull-out experiments were carried out using regular production glass fibers. It was shown that by carrying out the experiments under very carefully controlled conditions, four important interface parameters could be measured:
   (a) the work of fracture,
   (b) the shear failure stress,
   (c) the normal pressure between the polymer and the fibers, and
   (d) the coefficient of friction, μ.

This paper reviews these pull-out experiments, and presents additional results obtained recently from experiments with carbon fibers.

REQUIREMENTS FOR THE PULL OUT EXPERIMENT

The most obvious requirement for a pull out experiment is that the fiber is not too deeply embedded in the plastic, otherwise it will break instead of pulling out. Until recently, it was considered that the fiber could only be embedded to a depth equal to half its critical length, L_c, to prevent fiber fracture (6). For a fiber of strength, σ_{fu} and diameter d, subject to a constant shear stress at the interface, τ_i, resisting pull out

$$L_c = \sigma_{fu} d/4\tau_i. \tag{1}$$

Although much used in the past, this is an oversimplification since τ_i is not constant. This is because τ_i is determined by μ and the pressure across the interface. The fiber shrinks due to Poisson's effects, and when the interfacial pressure on the unstressed fiber is P_0, the pressure is reduced to P where (7)

$$P = P_0 - \nu_f \sigma_f E_m / E_f \tag{2}$$

when the matrix is not subject to external stress. Here ν_f, σ_f and E_f are respectively the approximate fiber Poisson's ratio (8), stress, and Young's modulus; E_m is the Young's modulus of the matrix. P_0 arises from the cure shrinkage of the matrix when a thermoset is used, and from purely thermal shrinkage effects in the case of thermoplastics.

If the fiber strength is sufficiently great, P can vanish, and the fibers could lose contact with the matrix. This will occur when

$$\sigma_{fu} > PE_f/\nu_f E_m. \tag{3}$$

This might be thought to imply that pull out is possible for any length so long as the fibers have a strength which is greater than, or equal to, this value.

This is not the case, however. Before pull out can occur, the adhesive bond between the fibers and the matrix must be broken. If this bond has a work of fracture, G_i, continuous bond failure is energetically possible when (9)

$$\sigma_f = \sqrt{8E_f G_i/d}. \tag{4}$$

Continuous fiber-matrix interface failure and pull out is still not possible, practically, even when this criterion is met. There are two reasons for this:

1. the longer a glass or carbon fiber is, the weaker it is (10, 11), and
2. it is impossible to ensure that an embedded fiber is perfectly straight, and extra frictional forces will result when the fiber is pulled around a curve.

Note that *Eq 4* suggests that we may expect to find that the force needed to cause bond failure is independent of embedded length, at least over a region of embedded lengths. If such a region is found, we can use it to estimate G_i.

Once bond failure has taken place, we can examine the frictional pull out. This is governed by the coefficient of friction μ, and P, P is not constant, but instead varies with σ_f, *Eq 2*, and the interfacial shear stress, τ_i, is given by

$$\tau_i = \mu P. \tag{5}$$

This shear causes the fiber stress to decline as the distance from the polymer surface, x, increases:

$$d\sigma_f dx = -2\tau_i/r \tag{6}$$

combining *Eqs 2*, 5 and 6 we can determine the force required to keep the fiber moving out of the matrix by solving the differential equation thus obtained.

An analysis of this and the bond failure step (9) gives a pull out curve such as that shown in *Fig. 1*. Notice that when we fix the embedded length (in *Fig. 1*, it is 2 mm) we find that the results are affected by the "free length" of the fiber. The "free length" is the length which is not embedded in the polymer, and not held by the grips of the machine pulling the fiber out of the polymer. It is most important that this be kept very small. If it is too large, it will not be possible to observe all the features shown in *Fig. 1*.

In the region near the origin in *Fig. 1*, the stress in the fiber is increasing, and the apparent pulled out distance is due to stretching of the free length rather than due to any actual pull out. With the free lengths shown, the elastic deformation of (a) the matrix adjacent to the fiber and (b) the fiber within the matrix, are negligible. When the stress reaches the interface failure stress (at a fiber stress of about 3 GPa, in *Fig. 1*) debonding occurs, and the stress falls. The actual value it falls to depends on the hardness of the test setup, and on the fiber free length. If too long a free length is used, or too soft a testing setup is used, a very significant length of the fiber can pull out suddenly at the instant adhesion failure occurs. The actual length pulled out depends on the free length and the softness of the setup, and in unfavorable cases this sliding does a great deal of damage at the interface, making subsequent measurements unreliable.

When a short free length and a hard test set-up

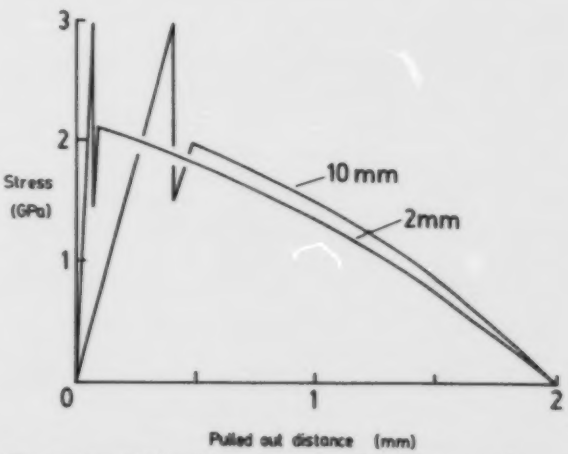

Fig. 1. Theoretical pull out curves for glass fibers on polymers with P = 30 MPa and μ = 0.2. Free length: 2 mm and 10 mm.

are used, the stress increases steeply after the sharp fall on debonding, and pull out proceeds at a stress governed by τ_i, i.e., by μ and P. In *Fig. 2* this starts when the stress again reaches 2 GPa. The slope at the instant the fiber emerges from the polymer (i.e., when the fiber stress has just fallen to zero) can be used to estimate the product μP_0. The accuracy of the evaluation depends on the free length (*Fig. 1*) and on the embedded length; it is greatest if both these are as small as possible. A correction formula for finite free length and embedded length is available (9).

If the matrix is subject to external biaxial pressures, P_a, normal to the fiber, the pull out experiment yields $\mu(P_a + P_0)$ instead of μP_0. If several different values of P_a are chosen for these experiments, a plot of $\mu(P_a + P_0)$ versus P_a will have a slope of μ and an intercept on the ordinate of μP_0. Thus μ and P_0 can be determined independently of each other.

Pull out experiments with different embedded lengths, and different applied pressures thus enable μ, P_0, and G_i to be determined. In practice, it is found that another parameter may be determined when very short embedded lengths are used. This is the shear failure stress of the interface. However, it is not always possible to obtain a value for G_i.

EXPERIMENTAL METHOD AND RESULTS

Glass Fibers

In this work, 22 μm diameter glass fibers coated with proprietary coupling agents compatible with epoxy (410-FA-2200) and polyester (475-FA-2200) were used. EPON 815 cured at room temperature with 25 percent Ancamine XT, both provided by Shell Chemicals, served as the epoxy matrix. Crystic 2-491-PA polyester resin from Ashland Chemicals, also cured at room temperature by mixing in 2 percent MEK peroxide, served as the polyester matrix. Post curing was also carried out for some of the experiments.

Figure 2 (12) shows the method used for embedding short lengths of glass fibers in polyester and epoxy resins. The thin film of polymer shown in *Fig. 2a* had three fibers embedded in it. These were then cut off above the thin film, and more polymer was added to provide a strong and stiff backing for the thin film, *Fig. 2b*. When the resin had been completely cured, the stopper was removed, and the specimens were ready to be tested. A table model Instron machine was used for pulling the fiber out. The fiber was attached to a 2 mm diameter wire (held in one grip of the machine) using cyanoacrylate glue. The free length was kept to 1 mm. The embedding method was modified slightly for use with epoxy, *Fig. 2c*. Refer to the original paper (12) for further details.

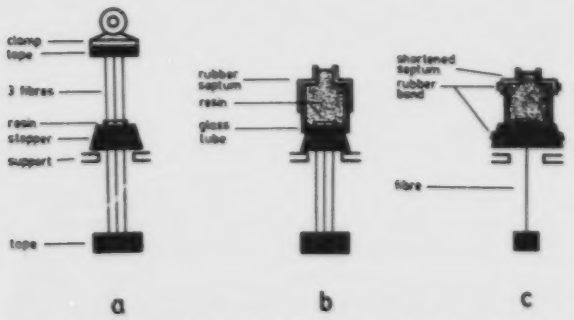

Fig. 2. Methods used for embedding a controlled, short length of fiber.

Figure 3 shows a typical pull out curve. Compared with *Fig. 1* it shows one additional feature: there are some stress excursions after adhesion failure. This is due to the normal stick-slip motion obtained with frictional sliding, promoted by changes in fiber diameter due to the Poisson's shrinkages. (The shrinkage varies as the fiber stress varies.)

The maximum force, F_a, which causes the bond failure, when plotted against embedded length, L, usually has a plateau region, at force F_p (*Fig. 4*). It also had a linearly increasing region, and an intercept, F_0. It will be observed that there is a maximum embedded length, L_{max}, for fiber pull out. For embedded lengths greater than L_{max} the fibers break, instead of pulling out. In *Fig. 4* the x's indicate fiber breakage, and the 0's represents fiber pull-out. Each point is an average of at least five results.

From F_p we can calculate G_i using *Eq 4* with σ_f equal to $4F_p/\pi d^2$. Plateau regions were observed with a 20°C and 80°C cured polyester, and a room temperature cured epoxy. When the epoxy was cured for 24 hours at 60°C, it gave no plateau region. The works of fracture thus obtained were much less (polyester 0.3 to 0.35 kJm^{-2} and epoxy 0.14 kJm^{-2}) than the Izod values of these polymers cured under the same conditions (3–5 kJm^{-2}) (12). When the fibers were coated with release agent the work of fracture of the interface was reduced, but was greater with the polyester matrix (140 Jm^{-2}) than with the epoxy (66 Jm^{-2}).

The value of τ_i estimated from the slope of the pull out curve at the instant the fiber emerged from the polymer, did not show any very significant trend with embedded length (*Fig. 5*). The average values

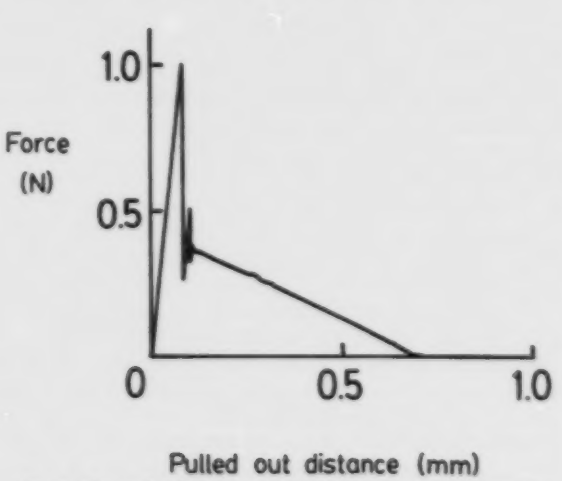

Fig. 3. Typical pull out curve obtained with glass polyester.

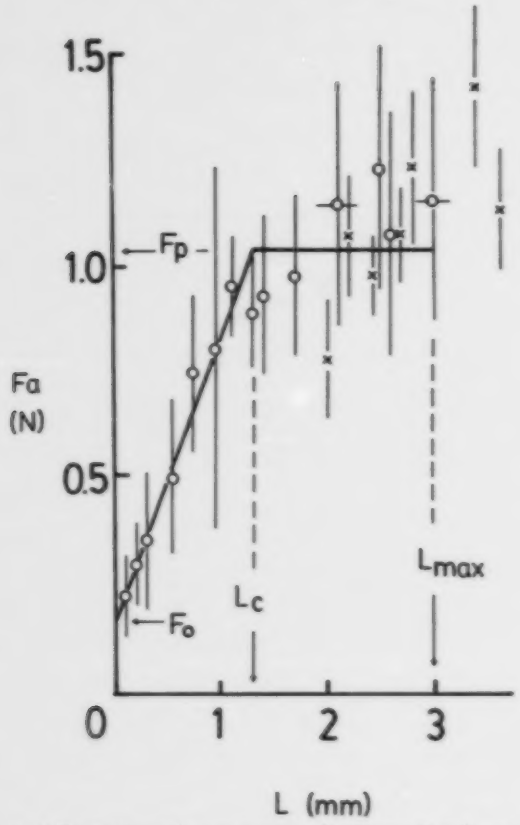

Fig. 4. Adhesion force for non post cured polyester (0-pull out, x-fiber breakage).

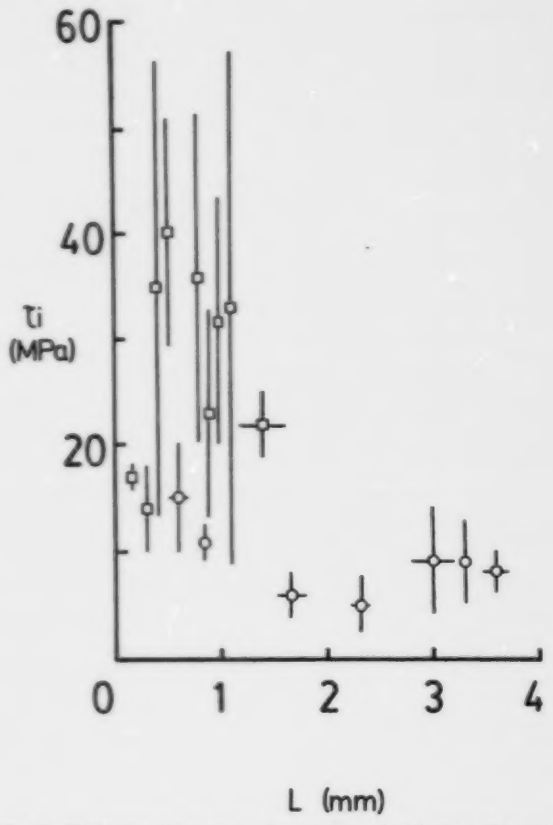

Fig. 5. Maximum shear stress for post cured polyester, (○), and epoxy (□).

obtained for this parameter were much less than the shear strengths of the matrices (estimated from the compressive strengths) in the case of the polyesters (e.g., 10 MPa compared with 46 MPa estimated from the compressive strength), but were very similar in the case of the epoxies (e.g., 34 MPa compared with 31 MPa; both examples are 80 and 60°C cured resins, but the same effects were noted when the resins were cured at room temperature only).

From the slope of the initial region of the F_a versus L plot (*Fig. 4*) we may estimate the shear strength of the interface. This was always less than the shear strength of the matrix. Its highest value was for the 80°C cured polyester (33 MPa compared with a shear strength of 46 MPa).

The maximum embedded lengths, L_{max}, were 3.0 and 3.6 mm for the 20°C and 80°C cured polyester respectively. Coating the fibers with silicone release agent increased L_{max} from 3.0 to 3.3 mm. With the epoxy resin the results were 1.3 mm, 20°C cured; 1.5 mm, 60°C cured; and 2.4 mm, silicone coated.

The short lengths of fibers used for these experiments proved to be extremely strong. Some did not fail until the stress exceeded 4 GPa. At these high stresses Poisson's shrinkages are very significant, so that P was very significantly less than P_0.

When biaxial stresses were applied to the matrix, using a ring with strain gauges attached for stress measurement, the value of τ_i did increase linearly with applied pressure (*Fig. 6*) (13). Thus, μ and P_0 could be separately evaluated.

When cured at 80°C and 60°C respectively, the polyester and epoxy gave approximately the same shrinkage pressure of about 20 MPa. Curing the polyester at 20°C resulted in a pressure of 12 MPa, while in the epoxy case the 20°C cure gave a pressure of 18 MPa. (The estimated standard deviations for the pressure measurements were 3–5 MPa; however, experiments with release agent coated fibers gave pressures within 1 MPa of the values obtained when the release agent was not present).

The coefficient of friction of the polyester was the same, 0.56 for 20°C and 80°C cure. On the other hand with the epoxy the 60°C cure increased μ from 1.08 to 1.52. The silicone release agent reduced μ to about 0.16.

Carbon Fibers

In this test, high modulus AS1 graphite fibers from Hercules Inc., sized for epoxy resin, were used. Since carbon fibers have much smaller diameters than the glass fibers (8 μm compared with 20 μm for the glass used in these experiments), much shorter embedded lengths had to be used. The free length was kept at 1 mm, since this fiber stores less

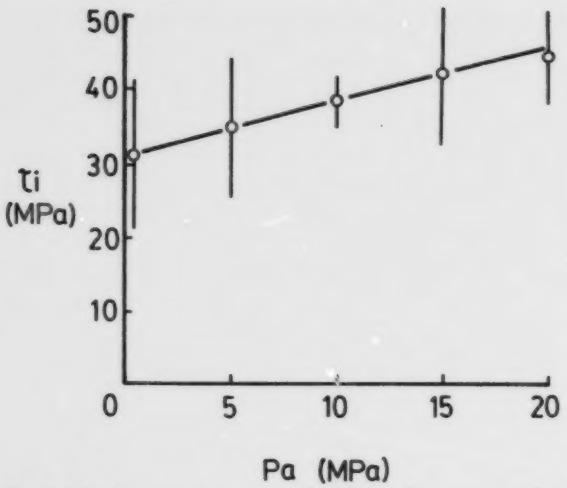

Fig. 6. Maximum stress versus applied stress for epoxy cured at 60°C for 24 hours.

energy per unit volume than glass does, due to its higher modulus.

Thin polymer films were obtained by floating the resin on mercury—a method much used in the past (14). Since the fiber could be broken more easily in flexure than in glass—due to its higher modulus, it was supported during fiber embedment on an oblong card with an oblong hole in it almost as large as the card. Otherwise the method used was similar to the method used for glass.

A typical pull out curve obtained with carbon is shown in *Fig. 7*. The large fall in stress, compared with glass (*Fig. 3*) indicates that the free length is a little too long. However, some useful results were obtained. Plots of F_a versus L did not have plateau regions when epoxy homopolymers were used. It was estimated from the maximum F_a observed that $G_i > 100$ Jm^{-2}. Maximum lengths that could be pulled were about 0.25 mm. Interfacial shear stresses at the instant the fiber emerged from the matrix were rather low, ranging from about 9 to 13 MPa—the higher value corresponding to a 135°C cure. If we use the pressures estimated for glass, these values indicate that coefficients of friction vary from 0.42 to 0.58—the higher value corresponding to the higher temperature cure.

The shear strength of the interphase, estimated from the slope of the plot of F_a versus embedded length also depended on temperature of cure. It increased from about 33 MPa for the 60°C cure to about 56 MPa for the 135°C cure.

Results Obtained with Low Shrinkage Pressure Matrices

Double ring compounds, such as spiro orthocarbonates, which undergo opening of both rings during polymerization, expand when polymerized. They may be copolymerized with epoxy resins to produce polymers having controlled shrinkage pressures, and carbon fiber composites, which have greater toughness than normal carbon epoxies (15), can be made with them.

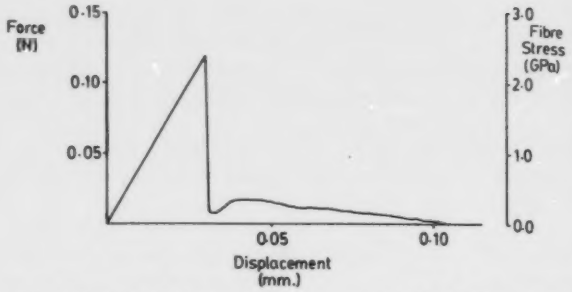

Fig. 7. Typical single fiber pull out curves obtained with carbon.

Single fiber pull out experiments have been carried out with matrices made from these polymers (16). Although the spiro reduces the pressure, it made the fibers much more difficult to pull out by increasing the work of fracture, G_i from 230 Jm^{-2} to >400 Jm^{-2}. In order to measure the shrinkage pressure in this case, the fibers had to be coated with silicone release agent to reduce the strength of the bond between the fibers and the resin. The addition of 7.5 percent spiro was found to reduce the pressure from 23 MPa (epoxy cured at 130°C) to 7 MPa (copolymer, cured at 130°C). The spiro increased μ from 2.4 to 6.4. These high values were due to the extremely large "ploughing" effect. Polymer adhered very well to the fibers, and these adhering pieces of polymer remained on the fibers during the whole pull out process. The spiro not only decreased the shrinkage pressure, it also increased the adhesion between fibers and matrix. Even when silicone resin was used to reduce the adhesion, the fiber was not entirely free of polymer after being pulled out.

DISCUSSION

Data obtained from single fiber pull out experiments can be very useful by indicating the adequacy of bonding and by providing insight into processes taking place at the heart of the composite.

Thus, in the case of the glass reinforced polyester resins, it is clear that the interface could be improved. Fibers pull out cleanly; the work of fracture of the interface is much less than that of the resin, and the shear stress at the instant of interface failure is somewhat less than the shear strength of the resin estimated from the compressive strength.

The glass fiber interface with epoxy resins is somewhat more successful. However, the onset of slip will be delayed in a glass fiber reinforced epoxy, since the frictional shears are greater than the shear failure stress of the interface. These high frictional shears are due to the interface failure not being complete; pieces of resin remain adhered to the fibers, and plough through the matrix during pull out, generating stresses which are quite close to the matrix shear strength. The use of the spiro increases the strength of the interface and much polymer remains adhered making pull out extremely difficult.

In the case of the carbon fibers, the higher modulus of the fibers prevents continuous interface

failure, so that the work of fracture of the interface cannot be measured, at least with epoxy matrices. Lower friction coefficients with carbon promote relatively easy pull out, once the interface has failed.

The shrinkage pressures measured in these experiments provide useful data on the residual stresses inside composites. These are evidently quite high, i.e., about 20 MPa, and the epoxy and polyester resins, when fully cured, give similar values. The pressure can be reduced by the use of expanding (spiro orthocarbonate) monomers.

Reducing shrinkage pressures does provide a means for improving the toughness of carbon fiber pultrusions (15) and laminates. However, this approach is hampered by the improved adhesion that takes place when the spiros are used. Clearly, more detailed analysis of the implications of such factors as the work of fracture of the interface is required. The work of fracture may have to be reduced to promote fiber pull out; but at the same time, high tensile and shear strengths are required to retain off-axis, shear, and compression properties of composites. To achieve this, fiber surface coatings with unusual properties may be required.

CONCLUSIONS

Proper control of the embedding process and set-up used for pull out promote the evaluation of important interface or interphase, constants, i.e., the work of fracture, the shear strength, the coefficient of friction, and the normal pressure. The interface between the fibers and the polymer is generally much weaker than the polymer itself, both from the point of view of shear strength and work of fracture. Normal pressures at the interface depend more on the state of cure than on the actual polymer used. Coefficients of interfacial friction are also very dependent on the state of cure.

ACKNOWLEDGMENT

The authors are grateful to IMRI (DSS contract No. 09SD31155-1-5001) and to NSERC for financial support for this work.

REFERENCES

1. L. T. Drzal, *SAMPE J.*, **19**, 7 (1983).
2. B. W. Erickson and E. Pluedemann, "Composite Materials," Vol. 6, Ch. 1, Academic Press, New York (1964).
3. M. R. Piggott, *Polym. Compos.*, **3**, 179 (1982).
4. A. Sanadi and M. R. Piggott, *J. Mater. Sci.*, **20**, 421 (1985).
5. A. R. Sanadi and M. R. Piggott, *J. Mater. Sci.*, **20**, 431 (1985). (1985).
6. A. Kelly, "Strong Solids," p. 203, Clarendon Press, Oxford (1973).
7. M. R. Piggott, Proc. ICF5, p. 465, (1982).
8. M. R. Piggott, *J. Mater. Sci.*, **13**, 1709 (1978).
9. P. S. Chua and M. R. Piggott, *Compos. Sci. Technol.*, **22**, 33 (1985).
10. A. G. Metcalf and K. G. Schmitz, *ASTM, Proc.*, **64**, 1075 (1974).
11. J. W. Hitchon and D. C. Phillips, *AERE R* 9131 (1978).
12. P. S. Chua and M. R. Piggott, *Compos. Sci. Technol.*, **22**, 105 (1985).
13. P. S. Chua and M. R. Piggott, *Compos. Sci. Technol.*, **22**, 185 (1985).
14. L. S. Penn and S. M. Lee, *Fiber Sci. Technol.*, **17**, 91 (1982).
15. J. T. Lim, M. R. Piggott, and W. J. Bailey, *SAMPE Quarterly*, **15**, 25 (1984).
16. P. S. Chua and M. R. Piggott, *Compos. Sci. Technol.*, **22**, 245 (1985).

PANEL DISCUSSION

S. V. Hoa: I guess it would be very difficult to handle one single fiber. Would you tell us how you test one fiber alone and what scatter of data you get?

M. R. Piggott: Yes, it is very difficult, and I could not do it myself at this stage in life. It is a very delicate operation; my students with good eyesight can tease one fiber from a tow or roving. They then mount it on a special assembly, the most important part of which is a paper clip attached to a magnet which clamps itself to a steel bar, but which can be maneuvered by sliding up, down, and sideways on the bar. The paper clip can have up to three fibers attached to it, and each fiber is stuck to a piece of masking tape at the far end. This arrangement makes it possible to suspend the fibers so that they are almost perfectly vertical, yet their positions can be adjusted by moving the magnet. The rest of the specimen is built around that, as described in the paper. The operation is most impressive to watch, since the fibers, to most observers, are invisible.

L. A. Utracki: Mike, you showed the negative stresses or pressures around the polyester fibers when extrapolating to non-compressed situations. You have also been interested in the resins which showed expansion of volume during the curing. I presume that the negative stresses are due to volume shrinkage observed for common epoxy resins. Did you carry out the test using the spiro-type epoxies, and did you find positive pressures on the fibers in that case?

M. R. Piggott: You are correct, the volume shrinkage gives a compression which is a negative stress. This appears as a pressure exerted by the matrix on the fibers. The use of the spiro reduced this pressure to about one third of the value obtained when only the epoxy was used. The spiro also improved the adhesion between the fibers and the plastic to such an extent that we could only pull the fibers out when no external pressure was applied to the matrix. So for our experiments with glass, in which pressure was applied to the copolymer matrix, we had to coat the fibers with a silicone resin to reduce the adhesion and permit the fibers to be pulled out. With carbon we had no success when we applied pressure to the matrix. Adhesion appears to be better with carbon fibers than with glass. I believe that there is no significant covalent bonding between glass and the polymer; the pull out studies show that, with the polyester at least, the fibers came out with clean surfaces, and with both epoxy and polyester the interface appears to fracture more easily than the bulk polymer, and the shear strength of the interface seems to be less than the bulk polymer. With carbon fibers, on the other hand, it is thought that reactive groups, such as carbonyl, are present on the surface. We find that adhesion,

in the case of carbon fibers, is very good—perhaps too good to get optimum composite properties.

J. L. White: Do you think that this technique could be easily modified for thermoplastic composites?

M. R. Piggott: I have given some thought to this problem. Melting, and/or the application of pressure using powdered resins may be feasible. However, I haven't yet inspired a student to try it.

Note added in proof: Later work has led to a revision of the pressure and friction values. Pressures given here are one half those given in the original papers, and coefficients of friction are twice as great. The works of fracture have recently been interpreted on a different model, resulting in a downward revision of the values, to about 50–80 Jm^{-2} for epoxy, 60–190 Jm^{-2} for polyester, the higher values being for the high temperature cure. Silicone coated fibres gave works of fracture of about 30 Jm^{-2} in both cases.

Fracture of Mica-Reinforced Polypropylene: Mica Concentration Effect

T. VU-KHANH, B. SANSCHAGRIN, *and* B. FISA

Industrial Materials Research Institute
National Research Council of Canada
75, Boul. De Mortagne
Boucherville, Québec, Canada J4B 6Y4

Concepts of post-yield fracture mechanics were used to characterize the crack initiation and propagation resistances of mica-reinforced polypropylene containing different mica concentrations. Although mica addition leads to an apparently brittle composite, the crack initiation resistance is slightly increased with mica concentration up to 10 percent by weight; and significant improvement in crack propagation performance was found for polypropylene reinforced by up to 20 percent of mica in comparison to that of virgin polypropylene. The debonding of the interface between mica flakes and the matrix leads to a micro-ductility ahead of the crack tip in which the matrix is able to pull-out from mica particles and to stretch. This micro-ductility also prevents the brittle, unstable crack propagation, which is due to the coalescence of voids in pure polypropylene. Above 20 percent of mica, the reduction of the effective amount of the matrix material results in a substantial drop in the resistance to crack growth of mica-reinforced polypropylene.

INTRODUCTION

Fillers have been widely used in commercial production of polymers to improve physical properties for specific applications. The main effects of fillers on polymers are the increase of modulus and hardness, and the reduction of creep and distortion at elevated temperature (1). One of the recent additions to the family of fillers is ground and delaminated mica. This filler has been shown to be an attractive material since it combines interesting performance improvement with low cost. Addition of mica to plastics improves the chemical resistance and dimensional stability, and reduces the gas diffusivity of the resulting composites (2, 3). According to the theoretical calculations of platelet reinforced composites (4, 5), the modulus of polymers reinforced by mica is, in general, significantly increased as shown in the case of mica-reinforced polypropylene (6–12).

However the effects of mica on polymer strength remain unclear. Although theoretically mica should substantially increase the strength of plastics (4, 5, 13), Okuno and Woodhams (7) and Boaira and Chaffey (8) have noted a drop in strength for mica-reinforced polypropylene in the absence of a coupling agent due to poor bonding between mica and polymer. When a coupling agent is used, strength performance can be moderately improved. On the other hand, the impact resistance of polymers, as measured by Charpy or Izod tests, deteriorates when mica is added (6, 9, 12–14, 16). As pointed out by Friedrich and Karsch (15), when a thermoplastic polymer orientates or crystallizes with strain, it exhibits poor bonding with fillers. Consequently, it is able to separate and deform away from the filler surface (to stretch and to work harden). The matrix stretching generally requires a large amount of energy in a fracture process, whereas the energy required for the formation of voids and cracking of the interface between the polymer and the filler is considerably smaller. For these reasons the addition of fillers usually results in a more or less continuous and drastic reduction of the fracture properties. A better understanding of the fracture resistance of mica-filled polypropylene is thus needed for more confident use of this material.

In this study the fracture strength and mechanisms of a mica-reinforced homopolymer polypropylene were investigated. Fracture mechanics were used to characterize the material capacity to resist the crack growth. This type of study is important because failure processes are often associated with the propagation of cracks originating from flaws, and the fracture resistance of polymers is related to its crack extension resistance. In linear elastic fracture mechanics the material parameters which characterize the crack initiation are described by the

fracture toughness K_c or G_c (16–18). For a valid evaluation of these fracture toughness parameters, the theory envisages the dimensions of the specimen and the crack to be much larger than the size of the plastic zone around the crack tip. For ductile materials like plastics, a substantial amount of plasticity may occur before the crack starts to grow (19–21). This requires that the dimensions of the specimens used for the determination of G_c or K_c must be very large. However, injection molded products are relatively small compared to the size required, invalidating the use of linear elastic fracture mechanics. In the case of large-scale plasticity, post-yield fracture mechanics such as the path independent J-integral and the crack growth resistance R-curve method must be used as a quantitative characterization of fracture toughness. These concepts were employed to examine the fracture processes of mica-reinforced polypropylene. The fracture parameters in the elastic-plastic regime are also discussed.

EXPERIMENTAL

Materials

A phlogopite mica with a high aspect ratio, supplied by Marietta Resources International Ltd., Boucherville, Canada, was chosen for this study. This commercially available mica was an untreated Suzorite 200HK grade having a volume average flake diameter (22) of 149 μm and a shape factor ψ of 59.1, the latter parameter being closely related to the average aspect ratio (22).

The polymer was an injection grade polypropylene, Profax 6301 from Hercules Canada Ltd. The resin was in powder or "as polymerized" form, (with a melt index of 12 g/10 min. ASTM D1238) and an intrinsic viscosity of 1.7 (Decahydronaphthalene, 135°C).

Sample Preparation

Mica and polypropylene powders were dry blended in a Welex high intensity mixer (Model ESK-80) to obtain 1, 3, 5, 10, 20, 40 and 60 percent by weight of mica content. The dry blend was fed directly into an Engel reciprocating injection press (Model Es 150-70) having a clamping force of 70 tons.

The tensile-specimens (ASTM D638, type I) were molded using process conditions previously published (22). Samples for fracture tests (*Fig. 1*) were made by machining away sides of injection molded plates (initial dimensions 6 by 30 by 90 mm).

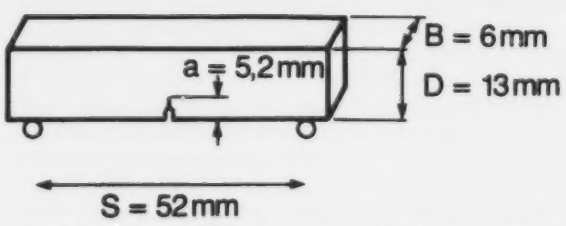

Fig. 1. Three-point-bend specimen used in fracture tests.

Testing Procedure

All tests were performed on a standard testing machine (Instron, Model 1125). The tensile tests were performed with a cross-head speed of 10 mm/min. The initial tangent modulus was determined from the slope of the load-deformation curves. The deformations were measured by a strain gage extensometer Instron, Model No. A325-24 2630-004, having a gage length of 1 inch. The yield strength was determined as the maximum load divided by the initial section of the specimen. An average value was determined from six samples.

The fracture toughness was measured, using the three-point-bend specimen, with a ratio of support span to specimen width, S/D, of 4 according to the recommendation of the ASTM standard test method, designation E-399.

The initial crack made in the three-point-bend specimen was 5.2 mm long, giving a ratio of initial crack length over specimen width (a/D) of 0.4. The initial crack was first made with a band saw to a depth of 3 mm and the final 2.2 mm was done by forcing a razor blade into the specimen in a special jig on a laboratory press. The notch made by the razor blade had a radius of less than 30 μm.

The cross-head speed in the three-point-bend fracture toughness tests was also 10 mm/min.

RESULTS AND DISCUSSION

Preliminary Results

Figures 2 to *4* show the effects of mica content on the Young modulus, the yield strength, and the yield and fracture elongations of mica-reinforced polypropylene. As pointed out in previously re-

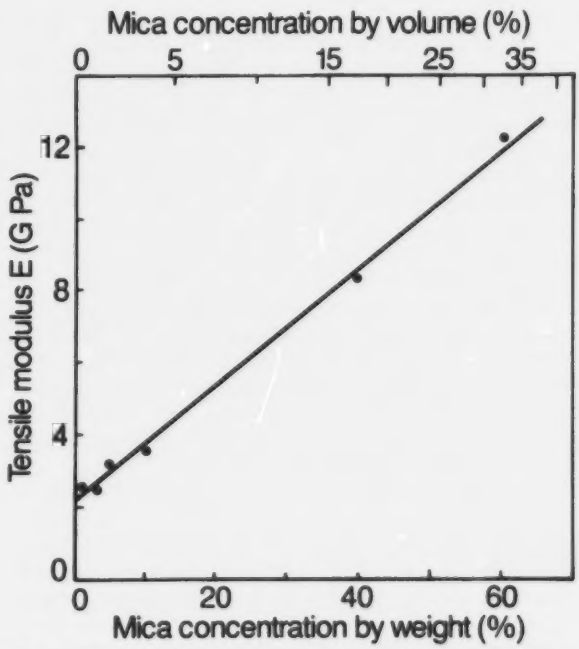

Fig. 2. Young modulus of mica-reinforced polypropylene as a function of mica concentration (with cross-head speed of 10 mm/min.).

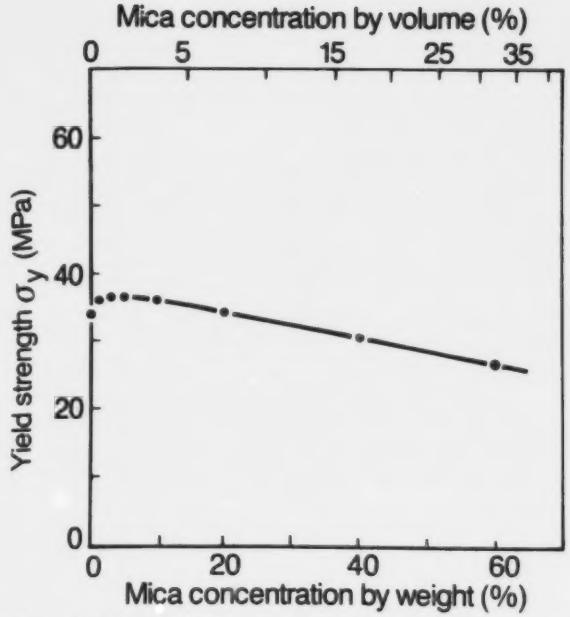

Fig. 3. Yield strength of mica-reinforced polypropylene as a function of mica concentration (with cross-head speed of 10 mm/min.).

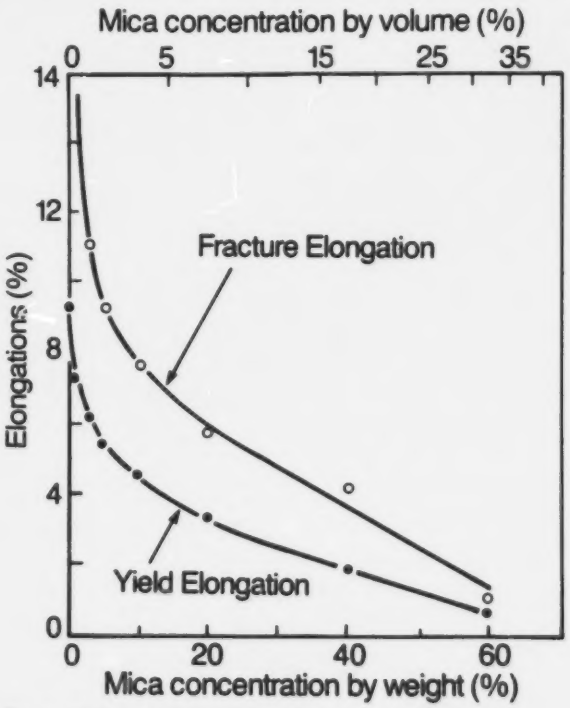

Fig. 4. Yield and fracture elongations of mica-reinforced polypropylene as a function of mica concentration (with cross-head speed of 10 mm/min.).

ported investigations, the Young modulus was found to increase strongly with mica content. The yield strength is slightly improved up to 10 percent; beyond 10 percent it decreases. However, the variation of the yield stress remains relatively small for all mica concentrations. This effect of mica on the yield strength of polypropylene is similar to its effect on low-density polyethylene (23).

In *Fig. 4* the yield and fracture elongations are plotted against mica content. Since it is very difficult to measure the true deformation at necking point, these elongations are considered to be the nominal deformations of the specimen gage length at yield and fracture. The nominal yield and fracture elongations are considerably reduced when mica is added (*Fig. 4*). These results suggest that mica addition would lead to a more or less continuous and drastic reduction of the fracture properties, resulting in a brittle product, as is the case in other filled polymers.

However, the load-displacement curves of the fracture toughness tests (*Fig. 5*) on three-point-bend specimens show a surprising effect. In the presence of a sharp notch, virgin polypropylene exhibits a purely brittle behavior. Fracture occurs at a constant deflection with the aid of the energy provided by the elastic strain energy stored in the sample. With the addition of mica, the fracture behavior of mica-reinforced polypropylene becomes more and more ductile. Up to 5 percent by weight of mica, the unstable fracture (at constant displacement) still occurs, but the amounts of plastic deformation and stable crack growth are increased with mica content. The plastic deformation accompanied by stable crack propagation is represented by the non-linear region of the load versus displacement curve. Since the area under these curves increases, the energy absorbed by the specimen to fracture increases with mica content—all the specimens tested having the same crack length and dimensions. Above 5 percent, no unstable fracture was observed at the cross-head speed of 10 mm/min. The crack grows with continuous supply of energy from the external load (with continuous

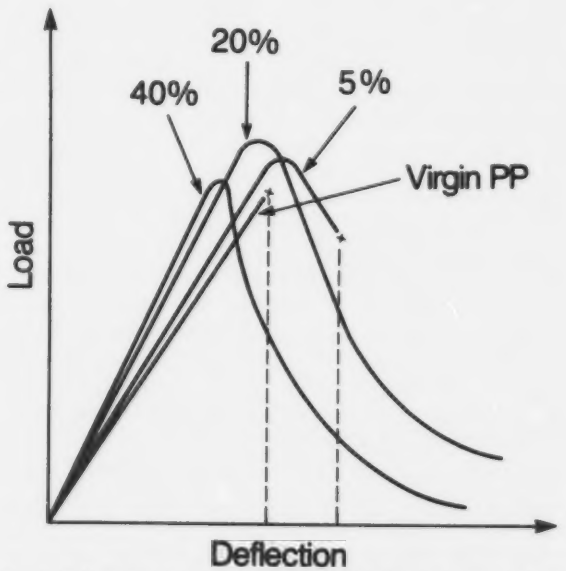

Fig. 5. Schematic drawing showing load-deflection curves of the three-point-bending fracture tests at different mica concentrations. X represents the point at unstable, brittle fracture.

increase in displacement until complete fracture). The amount of energy absorbed by the specimen to break, which is represented by the area under the load deflection curve, continues to augment up to 20 percent mica. Above 20 percent, the stable fracture still occurs, but the area under the load deflection curve decreases as the mica content is increased. This shows a diminution of the energy absorbed by the specimen.

The plane strain fracture toughness testing requires a small-scale yielding condition, that is, the crack length, specimen thickness and the specimen width must be much larger than the plastic zone size at the crack tip (r_p). Based on Irwin's approximation of the radius of the plane strain plastic zone size:

$$r_p = \frac{1}{6\pi} (K_{Ic}/\sigma_y)^2 \qquad [1]$$

where K_{Ic} is the material fracture toughness and σ_y is the yield stress. The criteria of validity of K_{Ic} value recommended in the standard procedure ASTM E-399 are:

$$\text{crack length } a > 2.5\ (K_{Ic}/\sigma_y)^2$$
$$\text{specimen thickness } B > 2.5\ (K_{Ic}/\sigma_y)^2.$$

It is also required that the ratio of the maximum load (*Pmax*) to the load obtained from a secant offset P_q (21) must be less or equal to 1.1. These conditions are not satisfied in these fracture tests, and the plane strain fracture toughness values determined from these curves become meaningless. In this case the standard procedure recommends the use of a dimensionless value, the specimen strength ratio, as a comparative measure of the toughness. The specimen strength ratio of three-point-bend specimens is given by (24):

$$Rsb = 6\ Pmax\ D/B(D - a)^2\ \sigma_y. \qquad [2]$$

It has also been shown that Rsb^2 is proportional to $K_{Ic}^2/\sigma_y^2 D$ (25) in the case of metals.

Figure 6 shows the variation of Rsb^2 with mica content. This result indicates qualitatively that the plane strain fracture toughness of polypropylene increases with mica addition up to 20 percent by weight and decreases above this concentration. However, the specimen strength ratio is only of comparative value, and its relation to the plane strain fracture toughness in the case of composite materials has not yet been demonstrated because of the complexity of the fracture mechanisms of these materials, (debonding between mica and matrix, formation of voids, matrix stretching, etc.). In order to confirm the effect of mica on crack initiation resistance of mica-reinforced polypropylene, other methods, taking into account the plasticity at the crack tip, must be used.

Crack Initiation Study

In large scale plasticity, it has been shown that the stress and strain fields at the crack tip can be described with the aid of a contour integral commonly known as *J*-integral originated by Rice (26). It is defined for two-dimensional problems and is given by:

$$J = \int_\Gamma W dy - T \frac{\delta u}{\partial x}\, ds \qquad [3]$$

where Γ is any contour surrounding the crack tip, T is the traction vector defined by the outward normal n along Γ (*Fig. 7*), $T_i = \sigma_{ij}\, n_j$, s is the arc length along Γ, u is the displacement vector, and W is the strain energy given by:

$$W = \int_0^{\epsilon_{ij}} \sigma_{ij}\, d\epsilon_{ij}. \qquad [4]$$

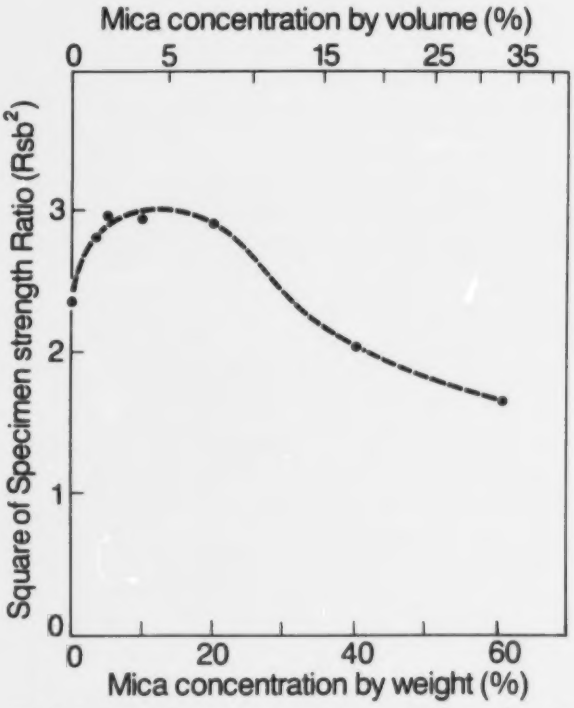

Fig. 6. Square of the specimen strength ratio (Rsb^2) as a function of mica concentration.

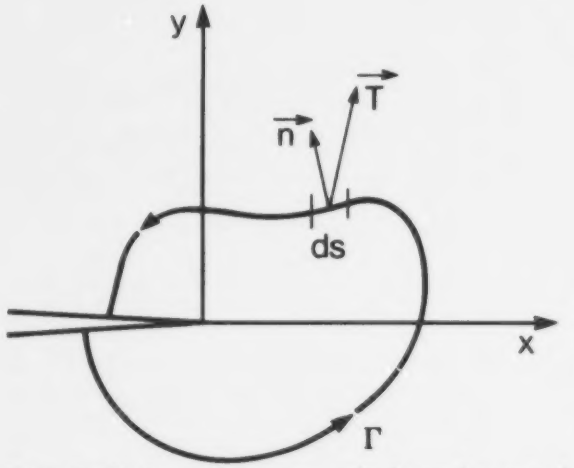

Fig. 7. Crack tip coordinate system and arbitrary line integral contour.

Hutchinson (27), and Rice and Rosengren (28) have shown that a singularity does exist at the crack tip in large scale plasticity, and the crack tip stress-strain singularity can be characterized by the *J*-integral parameter. It can, therefore, be used as a failure criterion for large scale yielding. *J* also represents the flow of energy into the crack tip region and is stated mathematically as:

$$J = \frac{dU}{da} \qquad [5]$$

where U is the potential energy and a is the crack length (27). For the pure elastic case (small scale yielding), the *J*-integral has been shown to be identical to the strain energy release rate G.

It is worth noting that as a fracture parameter, the *J*-integral has many limitations (29–31), and especially in the case of composite systems the deformation theory of plasticity is not applicable. In addition, there is formation of voids at the matrix-filler interface. This will result in a destruction of any characteristic crack tip singularity. However *J* can be considered as an alternative energy balance criterion of fracture since it represents the flow of energy into the crack tip region. Rice *et al.* (32) have introduced an approximate equation for the calculation of *J* in deeply notched, bend-type specimens.

$$J = \frac{2U}{B(D - a)} \qquad [6]$$

where U is measured from the area under the load versus load point deflection curve. This equation is the basis for the multiple specimen resistance (R) curve method for determining the fracture toughness first developed by Landes and Begley (33), which is now the ASTM recommended standard procedure (34). This method consists of loading several identical specimens having the same initial crack length, to different values of load point deflection and then unloading. These specimens will thus exhibit different amounts of crack growth. After unloading, the crack advance is marked by a penetrant ink and the specimen is broken open by impact at room temperature. The value of *J* at the point where the specimen is unloaded is determined from *Eq 6* for each specimen. This value of *J* is plotted as a function of crack advance (Δa). This gives the crack growth resistance curve, from which the fracture toughness at crack initiation J_{Ic} is determined at the intersection of the blunting line and the straight line fitted to the crack growth resistance curve as illustrated in *Fig. 8*.

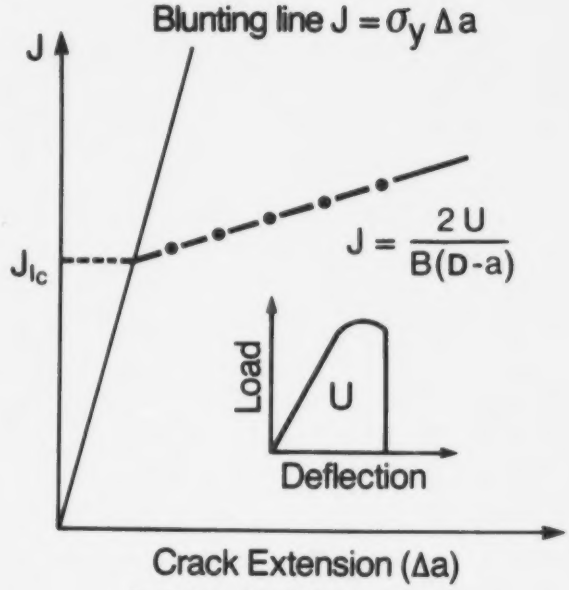

Fig. 8. Procedure for J_{Ic} measurement.

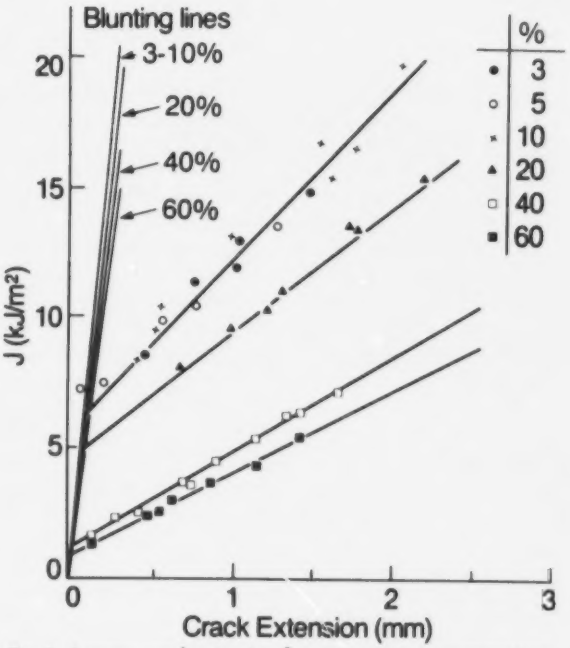

Fig. 9. J versus crack extension for various mica concentrations.

Figure 9 shows the *J* versus Δa curves for different mica contents. The blunting lines based on $J = 2\sigma_y \Delta a$ are also shown. It can be seen that the crack growth resistance is the same for 3, 5 and 10 percent by weight of mica when the crack advances. However, as pointed out previously, the amount of stable crack growth is lower with lower mica content. Above 10 percent, the crack growth resistance of mica-reinforced polypropylene decreases.

Figure 10 shows the fracture toughness at crack initiation for various mica concentrations. The J_{Ic} value increases at very low mica contents (<3 percent by weight), and attains a plateau region between 3 and 10 percent. Beyond 10 percent, J_{Ic} decreases slightly up to 20 percent and then drastically between 20 and 40 percent. This result confirms the measured value of specimen strength ratio shown above (*Fig. 6*), except for 20 percent by weight of mica content. The maximum specimen strength ratio was found for samples containing between 3 and 20 percent mica. On the other hand, the *J*-integral study shows that the plane strain

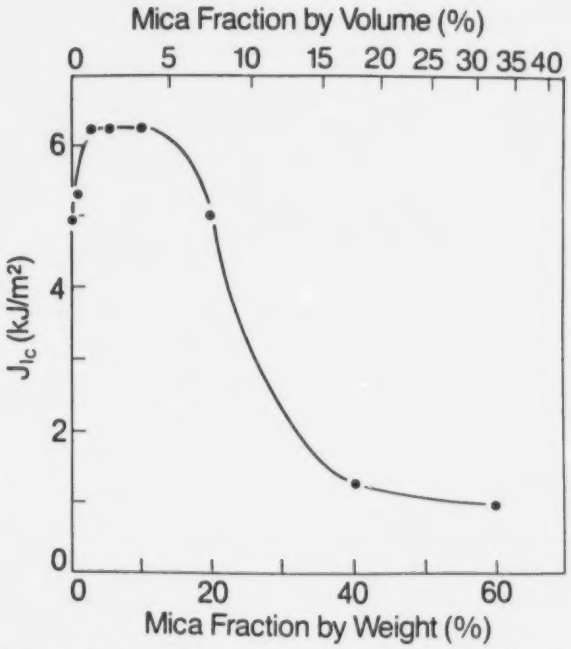

Fig. 10. Crack initiation resistance (J_k) as a function of mica concentration.

fracture toughness at crack initiation decreases above 10 percent. This suggests that at maximum load, there is probably a certain amount of stable crack growth which has already occurred, accompanied by an increase in the crack growth resistance. The maximum load may then not be an indication of the plane strain fracture toughness in this particular case. The effect of mica on the fracture toughness of mica-reinforced polypropylene is also rather surprising compared to the appearance of the load-deformation curves of fracture. These curves indicate a much more pronounced effect of plasticity when mica is added, resulting in higher energy required to break the specimen. It can be concluded from these results that addition of mica has a more pronounced effect on the crack propagation processes than on the crack initiation resistance.

The *J*-integral (R) curve method is not valid however, for crack growth study. In this method no crack growth is permitted because it necessarily involves unloading. This requires that the amounts of crack growth permitted in the multiple specimen resistance (R) curve method for determining J_{Ic} must be insignificant. The J_{Ic} fracture criterion refers to crack initiation rather than propagation.

Crack Propagation Study

Theoretically, in order that a crack can propagate, the energy available for crack propagation must be higher than or equal to the fracture energy of the material. The energy available for crack propagation or the strain energy release rate of a three-point-bend specimen can be calculated with the aid of the calibration factor used in the calculation of the stress intensity factor, as discussed in Ref. 35. The energy balance of a loaded specimen containing a crack shows that the strain energy release rate can be expressed as follows:

$$G = \frac{1}{2} P^2 \frac{dC}{dA} = \frac{1}{2} \frac{\Delta^2}{C^2} \frac{dC}{dA} \qquad [7]$$

where P is the applied load, C is the specimen compliance, Δ is the load point deflection and A is the crack area. C and dC/dA can be calculated numerically as shown in the Appendix. G can then be determined from *Eq 7*. *Figure 11* shows the variation of the dimensionless value of the strain energy release rate GD/E versus the crack length for different deformation levels in a three-point-bend specimen having a ratio of support span to specimen width of 4. The conditions for stable and unstable crack propagation are also illustrated in *Fig. 11* and have been thoroughly discussed in Ref. 35. For a material having a constant fracture energy during crack propagation, the crack can propagate in a stable or in an unstable manner depending on its initial length. For crack lengths shorter than $(a/D)_{lim.}$, the crack will propagate in an unstable manner since the energy release rate of the specimen increases for a constant deformation when the crack advances. For crack lengths $a/D \geq (a/D)_{lim.}$, this energy release rate decreases with crack growth, and the crack can propagate only if additional energy is provided, i.e., when the deformation is increased. In this case the crack propagation is stable.

Figure 11 shows that the value of $(a/D)_{lim.}$ is about 0.35. All the tested specimens were thus in a stable fracture condition with an initial crack length of 0.4. The fact that brittle fracture occurs in virgin polypropylene and at low mica content is probably due to the blunting effect in which the hydrostatic stress component reaches a critical value at a certain distance ahead of the crack tip. The blunting-induced unstable fracture is a phenomenon often

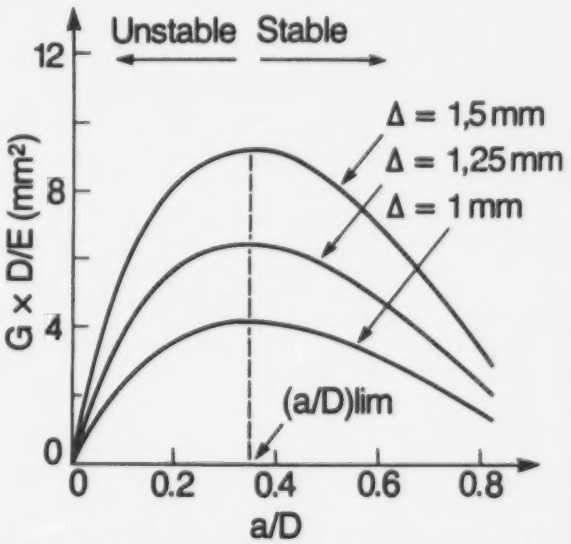

Fig. 11. Strain energy release rate in three-point-bend specimen versus crack length at different values of deflection.

observed in polymers, where a fracture nucleus forms ahead of the crack tip, as in the case of polycarbonate (36) and polyamide 11 (35, 37). For polypropylene, the fracture nucleus was believed to be related to the craze formation (38). This fracture mechanism will be discussed later. According to the shape of the available energy for the crack propagation curve for long cracks (*Fig. 11*), after instability the fracture energy should decrease considerably in order to satisfy the energy balance condition $G > Gc$. Thus the addition of mica improves the crack growth resistance of polypropylene in preventing brittle fracture, even though the crack growth resistance (J_{Ic}) at crack initiation is not significantly affected.

The fracture energy during crack propagation can be characterized by calculating the variation of the critical stress intensity factor during crack extension. This variation is also called the crack growth resistance curve or *R*-curve (39). It has been shown that there is a unique relationship between the amount of crack extension and the applied stress intensity factor for a given thickness. *R*-curve is often used to characterize the crack growth resistance of materials in which plastic deformation is large; and as the crack grows, the resistance to fracture increases due to the increased volume of plastically deformed material ahead of the crack tip. The *R*-curve is now an ASTM standard procedure (40) for Center-Cracked Tension panel (CCT), Compact Specimen (CS) and the Crack-Line-Wedge-Loaded specimen (CLWL). For three-point-bend specimens, the determination of the variation of the critical stress intensity factor with crack extension requires the determination of the specimen compliance versus the crack length. The compliance calculation and *R*-curve determination are given in the Appendix.

Figure 12 shows *R*-curves for various mica contents. The crack extension resistance, K_R, is plotted against the effective crack length determined by the secant method (see *Appendix*); the effective crack length being the physical crack size augmented for the effects of crack tip plastic deformation. The modulus used for the calculation of the effective crack length a_{eff} was the effective modulus determined from the initial slope of the load-displacement trace as discussed in Ref. 41. *Figure 12* shows that for up to 10 percent by weight of mica, the crack extension resistance (K_R) increases at a constant rate when the crack is growing, and that the amount of stable crack propagation before brittle fracture increases with mica content. At 10 percent no brittle fracture was observed; fracture was completely stable over the entire broken surface, and a plateau region was observed at maximum value of K_R. At 20 percent mica content K_R is less than that at 10 percent in the early stage of crack extension (*Fig. 13*) but attains a higher plateau region (at maximum K_R value). Above 20 percent of mica concentration, the fracture resistance is considerably reduced on the entire *R*-curve.

These results show that although mica addition leads to an apparently brittle composite by reducing

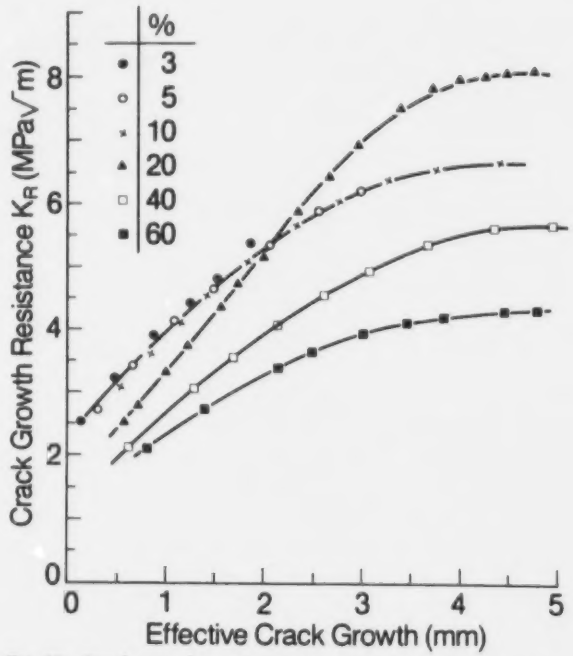

Fig. 12. Crack growth resistance (K_R) versus effective crack extension (Δa_{eff}) at various mica concentrations.

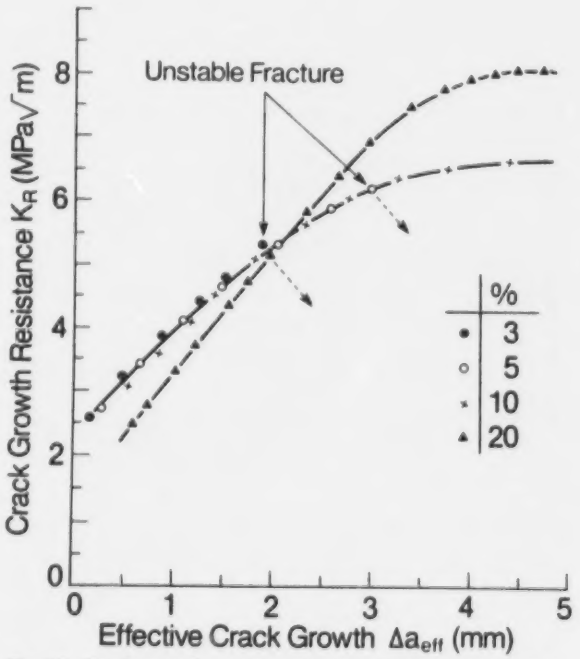

Fig. 13. Crack growth resistance (K_R) versus effective crack extension (Δa_{eff}) for 3, 5, 10 and 20 percent of mica.

both the yield strength and the fracture elongation of the material, in the presence of a defect (crack), the presence of mica can augment the ductility locally, resulting in a higher fracture energy (higher K_R value) during crack propagation of polypropylene reinforced by up to 20 percent of mica. The fracture energy at crack initiation, as shown in J_{Ic} measurement, is also slightly improved up to 10

percent by weight of mica content. At 20 percent, the fracture energy at crack initiation decreases slightly, but the maximum fracture energy attained in this case is much higher. *Figure 14* shows the maximum critical stress intensity factor reached during crack extension for various mica contents. This demonstrates the considerable enhancement of fracture resistance of polypropylene when it is reinforced by up to 20 percent of mica. Moreover, mica addition can prevent unstable crack propagation, which is the cause of most catastrophic failures. It is worth noting that this effect of mica on fracture resistance would be expected to be more important for materials which exhibit strong notch sensitivity, as in the case of polypropylene. This material is normally very ductile with a high capacity for stretching, but in the presence of a crack, the hydrostatic component of stress ahead of the crack tip leads to craze formation and, when the voids in the craze region coalesce, they cause catastrophic fracture. The effect of mica, in this case, is to permit the matrix to pull out and to stretch as illustrated in *Fig. 15*, giving a higher crack tip opening displacement (δ_c) and a higher crack growth resistance since these parameters have been shown to be directly related by:

$$K_c^2 = mE\epsilon_y\delta_c \qquad [8]$$

where m is a constant. This effect will be further demonstrated by microscopic examination of the fracture surfaces.

Fractographic Examination

Figure 16 shows the micrograph, as viewed by the scanning electron microscope, of the fracture surface of virgin polypropylene, and *Fig. 17* shows this surface in the region just ahead of the notch tip. In the blunting region there are circular marks of void formation and growth as shown at a higher magnification in *Fig. 18*. The size of circular marks seem to decrease when the distance from the notch tip increases. This is probably due to a higher

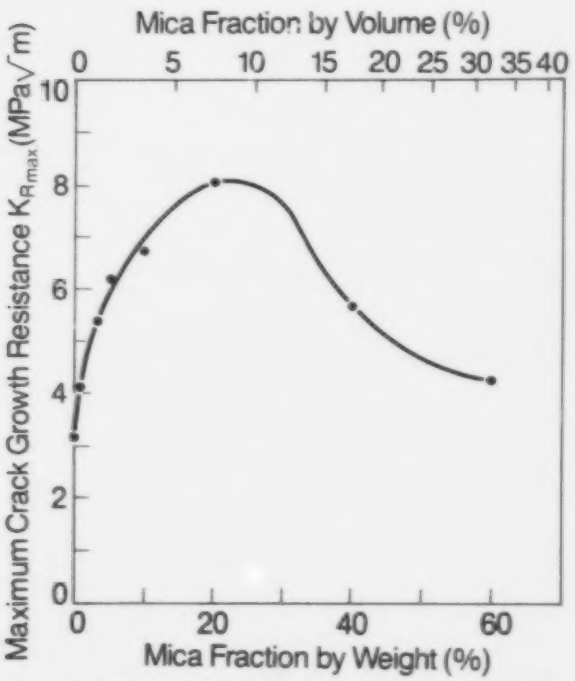

Fig. 14. Maximum crack growth resistance attained as a function of mica concentration.

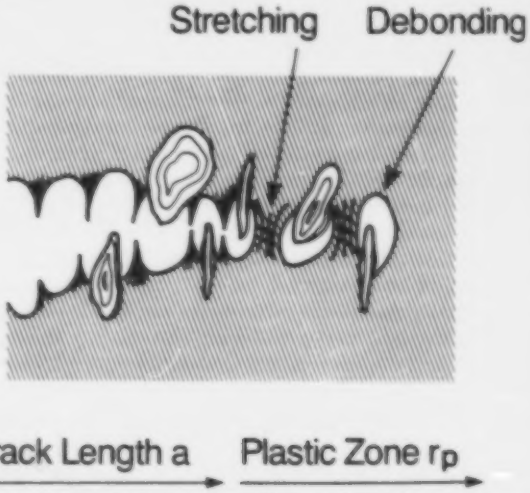

Fig. 15. Schematic drawing of pull-out and stretching processes of the matrix ahead of the crack tip.

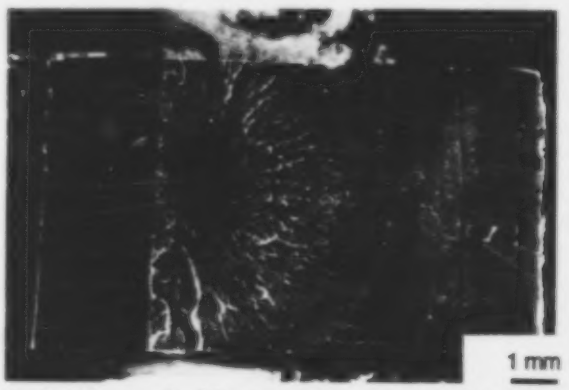

Fig. 16. Micrograph of fracture surface of virgin polypropylene as viewed by scanning electron microscope.

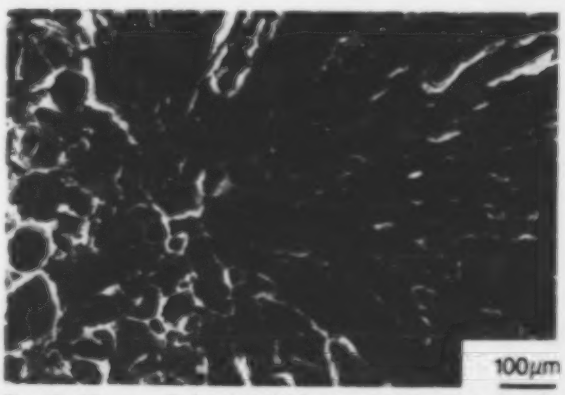

Fig. 17. Micrograph showing the fracture surface of virgin polypropylene in the region just ahead of the razor-notch tip.

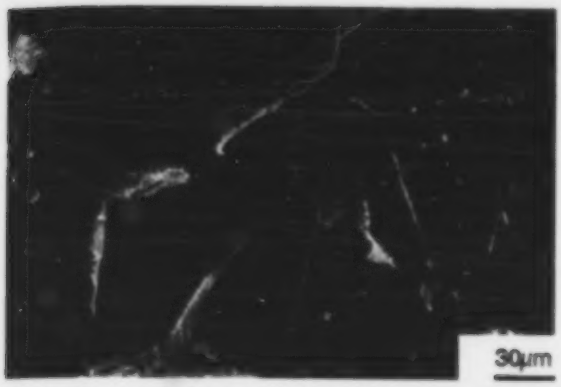

Fig. 18. Micrograph showing void formation and growth in the blunting region of virgin polypropylene.

density of void nucleation since the triaxiality of stress rises to a maximum at a certain distance from the notch tip. *Figure 17* indicates the region where a fracture nucleus is formed, leading to a brittle fracture. This fracture nucleus is probably associated with the coalescence of voids in the region of maximum hydrostatic component of stress, since in this region the density of voids and their growth rate would be expected to be the highest.

Figure 19 shows the fracture surface of polypropylene reinforced with 3, 5, 10, 20, and 60 percent by weight of mica. These fracture surfaces reveal a greater local ductility than that of pure polypropylene. The micro-drawing of the matrix is more pronounced when mica content is increased. Since the crack growth resistance of mica-reinforced polypropylene is improved with the addition of mica, at least up to 20 percent of mica concentration, the micro-drawing observed on the fracture surface should be the cause of the improved fracture resistance. The matrix drawing can also be attributed to the debonding between mica flakes and the matrix. It can be seen on these fracture surfaces that, in general, the matrix is pulled out from mica particles, and the stretching effect of the matrix is mainly around these mica flakes.

At low mica levels (*Figs. 19a–19c*), void formation can be seen in the matrix between the stretching

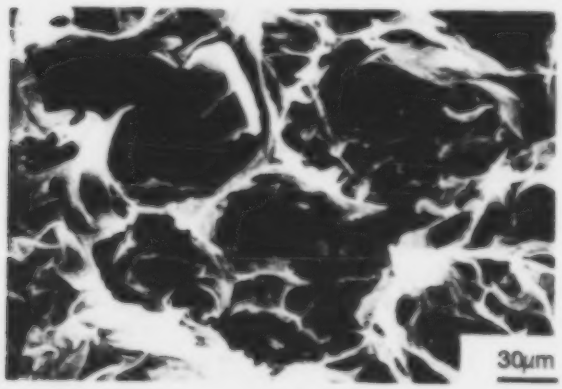

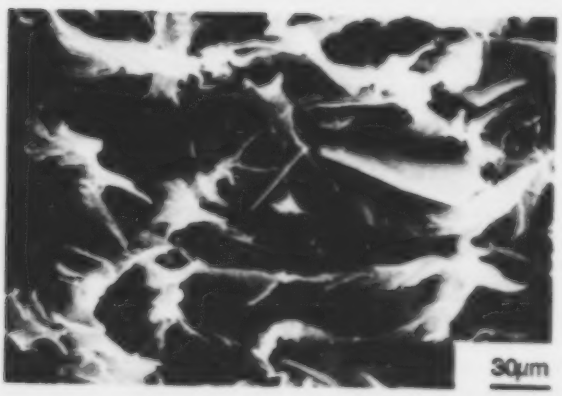

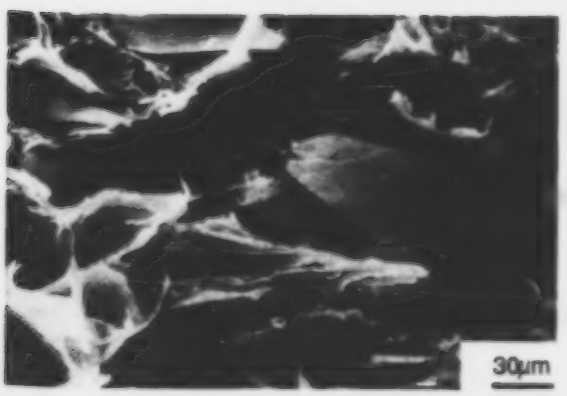

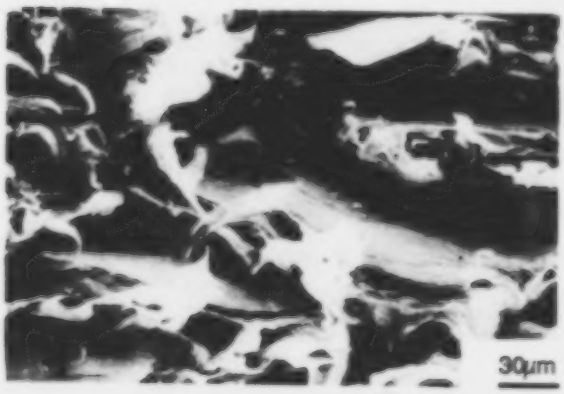

Fig. 19. Fracture surface of polypropylene reinforced by: 3 percent (a), 5 percent (b), 10 percent (c), 20 percent (d), and 60 percent (e) by weight of mica.

regions, and seems also to diminish as the mica content is increased. Since void coalescence is responsible for unstable, brittle fracture in virgin polypropylene, the void reduction is probably the cause of an increase in the amount of stable crack growth preceding unstable fracture when the mica fraction is increased. At 10 percent of mica the voiding effect seems to be at a minimum, and at 20 percent no void formation was observed on the fracture surface. This observation explains the disappearance of unstable fracture above 5 percent mica concentration.

At this stage it is not clear why the fracture energy at crack initiation and the crack growth resistance during stable crack propagation are identical for mica content of 3 to 10 percent, even though the stretching effect seems to increase and voiding seems to decrease. The only explanation proposed for the moment is that the debonding between the matrix and mica particles occurs probably very early with a very small interfacial fracture energy, and the matrix acts alone to bear the load and to resist the crack propagation. From the relationship $K_R^2 = m\epsilon_y E\delta_c$, the crack opening displacement δ_c should increase with mica content according to an observed increase of drawing. The local yield elongation remains constant; but since the effective section of the matrix decreases with higher mica content, E would decrease and K_R remain the same for mica content from 3 to 10 percent by weight.

Above 20 percent mica, the maximum drawing of the matrix is attained, but since the effective amount of the matrix material is small, as can be seen in *Fig. 19e* for the case of 60 percent of mica, the energy dissipated in plastic deformation of the matrix is reduced, resulting in a decrease of the fracture energy of the composite.

SUMMARY AND CONCLUSION

When polypropylene is reinforced by mica, the modulus is increased and the yield stress is slightly decreased. The yield and fracture elongations are also considerably reduced leading to an apparently brittle material. However in the presence of a defect, such as a crack, pure polypropylene breaks in a very brittle manner with low fracture energy due to the formation of voids in the crazed region ahead of the crack tip. This fracture behavior of polypropylene is much improved by the addition of up to 20 percent mica. In the presence of mica particles, the debonding between the matrix and mica flakes, which requires very little energy, causes a shear yielding deformation and a stretching effect of the matrix. This matrix drawing prevents the coalescence of voids, which normally occurs in the craze region of polypropylene and causes catastrophic failure.

Micro ductility induced by mica leads to a greater fracture energy at crack initiation for mica levels of up to 10 percent by weight. In this range, the amount of stable crack growth preceding the brittle fracture is also increased substantially, accompanied by a reduction of the voiding effect in the matrix. The unstable fracture, which is due to the blunting effect at the crack tip, was not observed at mica concentration of 10 percent and more. During the stable crack propagation, the crack growth resistance also increases strongly with crack extension, and attains a maximum plateau value in the case of complete stable fracture. In polypropylene containing more than 10 percent of mica by weight, the fracture energy at crack initiation decreased. The rate of decrease of J_{Ic} is greatest between 20 and 40 percent mica. At levels of 10 to 20 percent and above 40 percent, J_{Ic} decreases only moderately with the increasing mica content. J_{Ic} above 40 percent of mica is five times less than that observed below 20 percent mica loading.

At 20 percent of mica the crack growth resistance is reduced compared to that at lesser mica concentration in the early stage of crack extension. However, the resistance to crack propagation increased strongly during crack extension and attains a higher maximum value. At concentrations higher than 20 percent, the maximum crack extension resistance decreased with the increasing mica content, although the brittle (unstable) fracture was not observed. This was probably due to the reduction of the remaining matrix material resisting crack extension, even though maximum local deformation of the matrix was apparent.

Current work on this subject is focussed on the effect of other variables such as flake size, surface treatment, and flake orientation on the fracture behavior of mica-reinforced polypropylenes.

ACKNOWLEDGMENT

The authors would like to express their thanks to Mr. J. Dufour and to Mr. M. Thibodeau for their help in performing the experimental part of this investigation.

REFERENCES

1. M. O. W. Richardson, "Polymer Engineering Composites," Applied Science Publishers Ltd., London (1977).
2. R. T. Woodhams and M. Xanthos, "Handbook of Fillers and Reinforcements for Plastics," H. S. Katz, J. V. Milewski, Eds., p. 333, Van Nostrand Reinhold Co., New York (1978).
3. M. Xanthos, *Plast. Comp.*, **2**, 19 (1979).
4. G. E. Padawer and N. Beecher, *Polym. Eng. Sci.*, **10**, 185 (1970).
5. M. R. Piggott, *J. Mater. Sci.*, **8**, 1373 (1973).
6. J. Lusis, R. T. Woodhams, and M. Xanthos, *Polym. Eng. Sci.*, **13**, 139 (1973).
7. K. Okuno and R. T. Woodhams, *Polym. Eng. Sci.*, **15**, 308 (1975).
8. M. S. Boaira and C. E. Chaffey, *Polym. Eng. Sci.*, **17**, 715 (1977).
9. S. E. Tausz and C. E. Chaffey, *J. Appl. Polym. Sci.*, **27**, 4493 (1982).
10. J. P. Trotignon, B. Sanschagrin, and Piperaud, J. Verdu, *Polym. Compos.*, **3**, 230 (1982).
11. C. Busigin, G. M. Martinez, and R. T. Woodhams, *Polym. Eng. Sci.*, **23**, 766 (1983).
12. C. Busigin, R. Lahtinen, G. M. Martinez, G. Thomas, and R. T. Woodhams, *Polym. Eng. Sci.*, **24**, 169 (1984).
13. F. W. Maine and P. D. Shepherd, *Composites*, **5**, 193 (1974).
14. M. Fenton and G. Hawley, *Polym. Compos.*, **3**, 218 (1982).
15. K. Friedrich, U. A. Karsch, *J. Mater. Sci.*, **16**, 2167 (1981).
16. H. Liebowitz, Ed., "Fracture," Academic Press, New York (1968).

17. J. F. Knott, "Fundamentals of Fracture Mechanics," Butterworth, London (1973).
18. D. Francois, L. Joly, "La Rupture des Métaux," Masson et Cie, Paris (1972).
19. P. L. Fernando and J. G. Williams, *Polym. Eng. Sci.*, **20**, 215 (1980).
20. M. K. V. Chan and J. G. Williams, *Polym. Eng. Sci.*, **21**, 1919 (1981).
21. M. K. V. Chan and J. G. Williams, *Int. J. Fract.*, **145** (1983).
22. B. Sanschagrin, B. Fisa, and B. Favis, Technical Papers, 42nd Annual Technical Conference, Society of Plastic Engineers, 683, New York (April 30–May 3, 1984).
23. M. Arina, A. Honkanen, and V. Tammela, *Polym. Eng. Sci.*, **19**, 30 (1979).
24. E 399 Standard Test Method for Plane Strain Fracture Toughness of Metallic Material, Annual Book of ASTM Standards.
25. G. Succop, W. F. Brown Jr., ASTM STP632, 179 (1977).
26. J. R. Rice, *J. Appl. Mech., Trans. ASME*, 379, June (1968).
27. J. W. Hutchinson, *J. Mech. Phys. Sol.*, **16**, 13 (1968).
28. J. R. Rice and G. F. Rosengren, *J. Mech. Phys. Sol.*, **16**, 13 (1968).
29. J. A. Begley and J. D. Landes, ASTM STP514, part II, 1 (1972).
30. J. D. G. Sumpter, C. E. Turner, ASTM STP601, 3 (1976).
31. G. G. Chell, Ed., "Developments in Fracture Mechanics—2", Applied Science Publishers, London, U.K. (1981).
32. J. R. Rice, P. C. Paris, and J. G. Merkle, ASTM STP536, 231 (1973).
33. J. D. Landes and J. A. Begley, ASTM STP560, 170 (1974).
34. E 813 Standard Test Method for J_{Ic}, a Measure of Fracture Toughness, Annual Book of ASTM Standards.
35. T. Vu-Khanh and F. X. de Charentenay, *Polym. Eng. Sci.*, in press.
36. M. Kitagawa, *J. Mater. Sci.*, 17, 2514 (1982).
37. F. X. de Charentenay, J. J. Robin, and T. Vu-Khanh, 5th Int. Conf. on Deformation Yield and Fracture of Polymers, Cambridge, England, p. 33.1 (March 29–April 1, 1982).
38. M.Kitagawa and Yammaura, *J. Mater. Sci.*, **19**, 1863 (1984).
39. R. H. Heyer, ASTM STP527, 3 (1973).
40. E 561 Standard Practice for *R*-Curve Determination, Annual Book of ASTM Standards.
41. D. E. McCabe and J. D. Landes, ASTM STP668, 288 (1979).

NOMENCLATURE

a	crack length
A	crack surface area
Δa	crack extension
B	specimen thickness
C	specimen compliance
D	specimen width
E	Young modulus
$f(a/D)$	geometric correction factor for K determination
G	strain energy release rate
G_c	fracture energy
J	contour integral
J_{Ic}	critical J value at crack initiation (toughness parameter)
K	stress intensity factor
K_c	fracture toughness (critical stress intensity factor)
K_R	critical stress intensity factor during crack propagation
P	load
P_{max}	maximum load
Pa	load determined by the secant offset
R_{sb}	specimen strength ratio
S	specimen span
T	traction vector
u	displacement vector
W	strain energy
δ_r	crack opening displacement
ϵ	strain
σ	stress
Δ	load point deflection

APPENDIX

The stress intensity factor for a three-point-bend specimen is given (21) by:

$$K = (PS/BD^{3/2})\, f(a/D) \qquad [9]$$

where $f(a/D)$ is a calibration factor provided in Ref. 24. The strain energy release rate is expressed as (17)

$$G = \frac{K^2}{E} = \frac{1}{2} P^2 \frac{dC}{dA} = \frac{1}{2} - \frac{\Delta^2}{C^2} \frac{dC}{dA} \qquad [10]$$

Then, combining *Eq 9* and *Eq 10* dC/dA and C can be written as a function of a/D as follows:

$$\frac{dC}{dA} = \frac{dC}{d(a/D)BD} = \frac{S^2(f(a/D))^2}{EB^2D^3} \qquad [11]$$

$$C = C_0 + \frac{1}{EB} \frac{S^2}{D} \int_0^{a/D} (f(a/D))^2\, d(a/D) \qquad [12]$$

where C_0 is the specimen compliance for $a/D = 0$. By numerically calculating dC/dA and C, the available energy for crack extension, G, in a three-point-bend specimen can be obtained from *Eq 10* as a function of crack length a/D at different values of deformation Δ.

Knowing the relationship between the specimen compliance and the crack length, the effective crack length at any load level P can be determined as illustrated in *Fig. 20*.

PANEL DISCUSSION

L. A. Utracki: At 60 weight-percent of mica the flakes cannot be randomly oriented. We have shown that the maximum packing volume fraction of the freely rotating flakes is of the order of 4 percent and that for two dimensional arrays about 20 percent. This means that in composites contain-

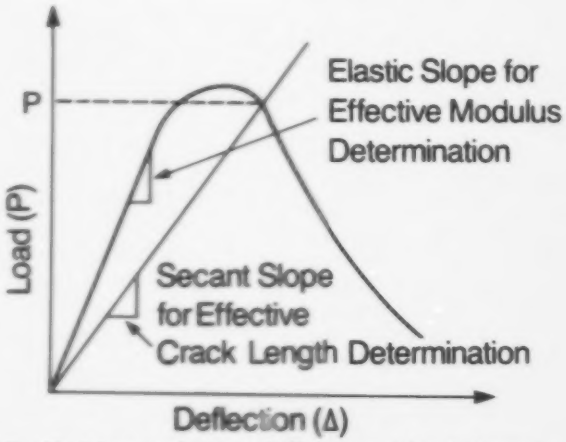

Fig. 20. Schematic drawing of effective crack length determination from the load-deflection curve.

ing more than about 10 weight-percent of mica, the flakes must be oriented parallel to each other. How is this phenomenon taken into account in your considerations?

T. Vu-Khanh: This is only the first part of a more general study on the fracture behavior of mica reinforced polypropylene. Experimentally we found that orientation of matrix plays a much more important role than that of mica flakes. Orientation of mica does not seem to have any significant effect on the fracture behavior of PP composites with mica.

J. L. White: What about the dispersion of the mica particles? If the orientation does not have any effect, what about the dispersion?

T. Vu-Khanh: These measurements represent an average response through the thickness of the injection molded specimens. Dispersion can have an effect on the resistance to fracture. We have also studied the effect of degradation of mica flakes during processing. Plotting the crack growth resistance as a function of crack growth time for degraded and non-degraded specimens, in the first case the curve starts higher and then falls below the dependence of non-degraded flakes. These results may be related to dispersion effects. If you look at the fractured surface, the main mechanism which governs the fracture resistance of the material is the stretching of the matrix resulting from debonding between flakes and polymer. If in some you have placed an aggregate of mica, the behavior should be similar to that of a system containing larger particles.

L. A. Utracki: I do not think that you answered Jim's question. In the case of aggregates you have a stack of dry mica particles with virtually zero cohesive force in between. It seems that on stretching they literally would disintegrate, accelerating the rate of crack growth. You do not have any debonding within the aggregate.

T. Vu-Khanh: Yes, but this plays exactly the same role. The debonding energy is very low compared to the stretching of the matrix. Even when you do not have any debonding the process is the same.

J. L. White: I bet you that if I went to your laboratory and put polypropylene and mica into a Banbury mixer for various mixing times and gave you the samples to test, you would find differences in the impact strength as a function of mixing time for the initial times, reaching a plateau level for longer mixing times when the filler is completely dispersed.

T. Vu-Khanh: There are also a number of points I would have to discuss before I could comment, for instance the mica degradation due to mixing, the type of impact test, etc. The test as described by ASTM is not directly related to the fracture energy of the material.

J. L. White: I used the impact test as an example. You can consider any crack propagation technique you want to answer my question. What I said about mica is true for any filler: glass fiber, C_aCO_3, talc....

G. L. Bata: There are two phenomena to consider: crack initiation and crack propagation.

J. L. White: Well, you can even argue that in addition there are three other factors: dispersion, loading, and filler-matrix interaction. But it is obvious from years of industrial experience that you must disperse your filler for it to reinforce the system.

T. Vu-Khanh: I can say simply that probably bad dispersion decreases the crack resistance of the material at the initiation period but increases the crack growth resistance during the propagation stage.

C. Dolce: You said that orientation is not important in the case of mica composites. Will that be true for short glass fibers?

T. Vu-Khanh: I do not think so. In the case of mica the mechanism of fracture almost entirely depends on stretching of the matrix. In the case of fibers, the debonding must have a significant influence. I did not measure the energy, but in this case it must be large.

C. Dolce: How did you measure the crack length at different points?

T. Vu-Khanh: The real crack length cannot be easily determined. That is why I calculated the effective crack length on the load-deflection plot by the compliance at each moment. The compliance is directly related to the effective crack length.

Use of Wood Fibers in Thermoplastic Composites II: Polyethylene

ALPHONS D. BESHAY

Science-Menoufia University Shebin El Koum, Egypt

and

BOHUSLAV V. KOKTA, *and* CLAUDE DANEAULT

Université du Québec à Trois-Rivières C.P. 500, Trois-Rivières, Québec, Canada G9A 5H7

Wood fibers of aspen in the form of chemithermomechanical pulp (CTMP) have been used as reinforcement in polyethylene (PE). The secant modulus, tensile strength, energy, and elongation at yield were measured. It was found that the mechanical properties of the composite were higher than those of PE by a factor of 2.6 for modulus, 2.3 for stress, and 2.1 for energy at yield. Compared to glass fiber composites, the CTMP composites showed higher elongation, about 100 percent higher energy, 106 percent higher stress, and 75 percent higher modulus. Note that the cost of treated wood fibers is several times lower than that of treated glass fibers.

INTRODUCTION

Reinforced thermoplastic polymer composites started to compete with metals in 1979 (1). Menges (2) reports that in the next ten years plastics composites will replace 65 percent of other materials in the world. Different inorganic fillers such as talc, mica, clay, fiberglass, etc. (3) are being incorporated into thermoplastics. Organic fillers have recently attracted great attention due to their lower price, low density, and renewable nature (4). The rising cost of resins and the need to economically enhance certain resin properties are incentives to extend and modify resins with fillers. The challenge is to find the right filler to do the right job.

McKenzie and Yuritta (5) reported improvement in tensile strength by using wood fibers as a filler for polyethylene (PE) and other polymers by lamination or impregnation. Sarma (6) has reported successful use up to 40 percent of hardwood or softwood sawdust as a filler for cation exchanger phenolformaldehyde sulfonic resin (6).

Seymour (7) reviewed use of cellulose fillers in polymer composites. He used wood flour as a reinforcement in different polymers including high density polyethylene. He considered the use of other cellulosic wastes as fillers such as ground wood waste, bark, nut shells, bagasse, corncube, bamboo, and cereal straws.

Gamova *et al.* (8) prepared composites from birchwood sawdust by means of thermomechanical copolymerization with styrene in the presence of 1 percent benzoyl peroxide. The resulting material exhibited low water absorption and a bonding strength of 30–45 MPa.

Belmares *et al.* (9) also found that there were large improvements in the tensile strength and modulus along with low elongation at break when the natural hard fibers were used in fillers.

Lawniczak (10) prepared composites from low density hardwood-polystyrene, called a "lignomer" by using an autoclave for bonding of styrene impregnated wood. He found improvement in bending and compressive strength and lower hygroscopicity.

Composites from the Grafted Pulp

Young and Nguyen (11) prepared composites from either mechanical or thermomechanical grafted pulps by the xanthation method using different vinyl monomers. He found an increase in the dry or wet strength after hot pressing.

Kokta *et al.* (12) prepared composites from aspen or birch chemithermomechanical pulps grafted with styrene by the xanthation method, and by mixing the grafted pulps with polystyrene. He found improvement in the composites' mechanical properties. The filler percentage varied from 10 to 40 percent and the improvement in the composites' mechanical properties was in the range of 40 percent compared to the original polystyrene.

Coran and Patel (13) prepared composites of 2-55 weight percent of cellulose fibers and grafted olefin polymers by using a bonding agent such as phenolformaldehyde resin, poly-isocyanate, etc.

The cellulosic fibers were rayon, cotton, hardwood, and kraft pulp. Some improvement of strength properties as well as swelling resistance was observed.

Goettler (14) grafted hardwood fibers with vinyl chloride in the presence of isocyanate as a bonding agent. He reported that the composites can be molded or extruded to produce useful articles, e.g., floor tile, tubing, etc.

Mansour *et al.* (15) prepared composites using both organic and inorganic fillers. They grafted bagasse and semi-chemical pulp of bagasse mixed with clay with methylmethacrylate using a sodium bisulfite system. The composites showed improvement in compression strength and water resistance.

Polyethylene Composites

Marchessault *et al.* (16) have shown that polyethylene could be directly polymerized on paper sheet, using the Ziegler-Natta polymerization technique. As a result, most of the paper sheet properties were improved.

Duchâteau (17) used wood fibers in amounts of 15 to 20 percent by weight and about 1 mm in length as a filler for polyethylene, polypropylene and polystyrene thermoplastic composites.

Nakajima (18) prepared composites from paper by impregnation with a resin consisting of 12 parts polyethylene, 28 parts polypropylene, and 60 parts waste paper. Sanyo-Kokusaka (19) prepared polyethylene composites by heating a mixture containing 83 percent wood pulp, 5 percent PE fibers, 10 percent resin, and 2 percent zinc stearate.

Michell et al (20–22) prepared composites from a laminate of paper and polyethylene (33 percent of LDPE). These composites have shown promising mechanical properties.

Composites Containing Coupling Agents

Morrell (23) reported that the use of coupling agents will facilitate the use of fillers. New materials with special properties like silanes, which are stable up to 400°C, are commercially available. Frequently, addition of a filler results in a loss of tensile strength. This is due to the resin having a higher elasticity than the filler. Bonding of the filler to the resin by means of a coupling agent helps to prevent the phase separation and results in stronger material.

Chun and Woodhams (24) have found that low molecular weight waxes prepared by maleation of thermally degraded polypropylene are effective substitutes for silane coupling agents in filled polypropylene resins. The addition of 1 to 5 percent maleated polypropylene has increased the tensile and flexural strengths of mica-filled polypropylene without significant loss in the modulus or fracture toughness.

The influence of maleated polypropylene wax coupling agents on the mechanical properties is similar to that of chlorinated paraffin waxes, but without the undesirable corrosiveness.

Gautts and Campbell (25) studied the effects of surface treatment of wood fibers incorporated into cement. The results of this investigation confirm that the mechanical performance of a wood fiber-reinforced cement composite can be altered by the use of coupling agents.

Hardwood Fibers—Thermoplastic Composites

The presented literature review shows that the use of hardwood fibers for thermoplastic reinforcement is extremely limited. The compatibility problem between hydrophilic fibers and hydrophobic thermoplastics may be further complicated by dimensional instability of resulting composites in humid conditions.

In addition, the poor interface contact between wood fibers and thermoplastic could contribute to phase separation under stress, especially at subzero temperatures, and lead to the deterioration of mechanical properties.

On the other hand, the short wood fibers could present considerable advantage in the reinforcement of thermoplastics if the above mentioned problems are overcome. Wood fibers have a relatively high aspect ratio and at the same time, their modulus is several times higher that that of most thermoplastics (13). Compared to inorganic fillers, they have the following advantages: lower cost, flexibility of wood fibers during processing; lower abrasion of equipment, absence of health problems; greater possibilities for surface modification, lower density, and the advantage of being a renewable abundant resource.

It seems logical to assume that the problem of compatibility of wood fibers with thermoplastics could be overcome by attaching a polymeric segment to the wood fibers having similar solubility parameters as the polymeric matrix used. In order to get strong attachment of polymers to cellulosics, grafting seems to be the ideal pathway. The present work deals with the use of grafted wood fibers for polyethylene reinforcement. Furthermore, the possibility of replacement of glass fibers by low cost hardwood aspen fibers in polyethylene composites is being examined.

EXPERIMENTAL

Materials

Linear low density polyethylene (LLDPE), Navopol LLGR-0534-A, was supplied by NOVACOR CHEMICALS LTD. Reported properties of LLDPE are as follows: melt index, 5 g/10 min; density, 934 kg/m^3.

The chemithermomechanical pulp of aspen or birch used in this work was prepared in a Sund Defibrator under the conditions listed in *Table 1*.

The thermomechanical pulp (TMP) used in this work, prepared from a wood mixture of 75 percent spruce and 25 percent balsam fir, was supplied by Abitibi-Paper Co. Mica-200-NP-Suzorite (200 mesh, coated) was supplied by Marietta Co., Montréal.

Glass fibers 731 BA 1/32 (0.8 mm, coated) were

Table 1. Conditions of the Preparation and Properties of Birch and Aspen Pulp

Cooking Conditions	Birch	Aspen	Properties	Birch	Aspen
Temperature Max. (°C)	126	126	Drainage index (CSF), ml	117	119
Retention time (min)	5	5	Brightness, Elrepho (%)	55.7	60.9
Pressure (psig)	20	20	Opacity, (%)	94.1	91.4
Na_2SO_3 (%/Dry wood)	5	5	Breaking length, km	4.22	4.46
NaOH (%/Dry wood)	5	5	Elongation (%)	1.79	1.79
pH	12.9	12.9	Tear index, $mN.m^2/g$	6.08	7.20
Consistence During Refining, (%)	21.8	23.9	Burst, index, $kPa.m^2/g$	1.88	2.59
Refining energy, MJ/kg	5.26	5.15	Yield (%)	90.0	92.0
Refiner output, kg/h	46.8	45.6	Kappa index No	128.0	121.7
			Lignin (%)	18.8	17.9

supplied by Fiber Glass of Canada via Mia Chemical, Montréal.

Coupling Agents:

i Vinyltri (2-Methoxy Ethoxy) Silane

$$CH_2 = CH - Si\ (0\ C_2H_4\ O\ CH_3)_3,$$

known as A-172,

ii Gamma-Methacryloxy-Propyltrimethoxy Silane

$$CH_2 = \underset{\displaystyle CH_3}{\overset{|}{C}} - \underset{\displaystyle O}{\overset{\|}{C}} - OCH_2 - CH_2 - CH_2 - Si\ (OCH_3)_3,$$

known as A-174,

iii Gamma-Amino Propyl Triethoxy Silane

$$H_2N - C_3H_6 - Si\ (O\ CH_2 - CH_3)_3,$$

known as A-1100,

were supplied by Union Carbide Company, Montréal.

All chemicals employed in this work were used as supplied by the manufacturers.

PREPARATION OF FIBER

Grafting

Grafting, which implies attachment of polymer branches to the wood fiber chain by a covalent linkage, has been successfully applied to different kinds of wood pulps using different vinylic monomers or their mixtures and redox systems of initiation with or without xanthation (26–30). In this work, the polymer loading of polyethylene (10 percent) was defined as follows: $(A\text{-}B)/B \times 100$ where A was the weight of the product after copolymerization and extraction, and B was the weight of fibers. Grafting procedures in conjunction with the application of grafted fibers in composites were recently published (12, 31).

Impregnation

Impregnation implies polymer deposition on fibers from polymer solution leading to physical bondage. The impregnation procedure used was as follows: 5 g of LLDPE was added to 200 ml of p-xylene and refluxed with stirring (at 100°C). 25 g of Untreated aspen (CTMP, 25 g 60 mesh size) was added to the solution and stirred under reflux for 2 hours. The mixture was left overnight in a mechanical shaker at 20°C. The impregnated pulp was filtered and dried for 12 hours at 105°C, then for 24 hours at 55°C, and ground to 60 mesh size before being mixed with LLDPE. The polymer loading was 20 percent.

Coupling Agent Treatment

The wood fibers were treated using silane coupling agents in dilute ethanol solution as follows: 0.8 g silane A-172 or A-174 was dissolved in 15 ml of ethanol (90 percent) and was added dropwise for 5 min to 20 g of aspen pulp (mesh 60), while stirring. After this addition continue stirring for ten min. The mixture was left at 105°C in the oven to dry for 2 hours before mixing with LLDPE.

Preparation of Composites

Mixing of polymer and fiber was performed with a roll mill, C. W. Brabender Laboratory Prep. Mill, No. 065. Usually 15 to 20 g of polymer was mixed with fibers at temperatures from 155 to 160°C, the resulting mixture collected and re-mixed 5–6 times, then allowed to cool down to room temperature and ground to mesh size 20.

The polymer-fiber mixture as prepared above was molded into the shoulder type test specimens, (6 to 24 at the same time), in a mold, which was covered by metal plates on both sides.

The weight of each specimen was 0.9 g when molded at a temperature of 155.5°C for 15 min at a pressure of 3.8 MPa. The starting temperature was 93.3°C and cooling time was 15 min.

The samples were taken out from the mold after a 15 min cooling period and then heat treated (annealed) at 105°C in the oven for 1–2 hours, and finally allowed to stand at least 3 to 4 hours in the testing room which was kept at 23°C and 50 percent relative humidity.

Mechanical Tests

Mechanical measurements were made on an Instron tester (Model 1131) at 23°C and 50 percent RH. The rate of elongation was 100 percent/min in all cases. All samples were 3.175 mm in width and 6.4 cm in length (1.7 cm between grips). The thickness of samples was usually 0.158 cm.

Dimensions of all samples were measured with a micrometer. All experimental data reported are averages of at least four measurements (12). Mechanical measurements of samples which have been

either pretreated in boiling water for 3 hours or tempered at −35°C in an Instron Environmental Chamber Systems (Model 3111), were made on an Instron tester (Model 4201). Samples pretreated in boiling water were tested at 23°C and 50 percent RH. The mechanical properties reported for this work are those measured at yield point. The secant modulus was evaluated from origin to yield point. The properties measured by an Instron 4201 were automatically calculated by an HP86B using the Instron 2412005 General Tensile Test Program. The chordal modulus was measured from 1 to 5 percent strain. Average coefficients of variation for mechanical properties were as follows: stress, 3.3 percent; strain, 4.9 percent; energy, 8.3 percent; and modulus, 2.3 percent.

RESULTS AND DISCUSSION

Composites of LLDPE Untreated Wood Fibers

In *Table 2* mechanical properties of LLDPE filled with CTMP (aspen or birch) as well as TMP (spruce and sapin) are shown. The results presented in this table show increases of stress and modulus for all wood fiber-filled composites, with the highest increases occurring with aspen hardwood fibers. The best performance of aspen fibers compared to either birch or spruce/fir fibers could be explained by internal structure as well as by their aspect ratio (13).

Nevertheless, in the categories of both elongation and energy at yield, the all-wood filled composites showed decreases compared to original LLDPE. These decreases may indicate poor interface contact between nontreated wood fibers and polyethylene.

Composites of LLDPE + Polyethylene Impregnated Wood Fibers

In order to improve interface contact between more hydrophilic wood fibers and the polymeric matrix formed by hydrophobic LLDPE, the wood fibers were coated by impregnation with LLDPE. *Table 3* presents the mechanical properties of the resulting composites.

It is clear that the impregnation leads to some positive effects on energy, stress, and elongation and to substantial negative effects on modulus, compared to original wood fibers. In general, the polymer deposition did not result in improvement since there was no chemical bonding between deposited polymer and wood fibers.

Composites of LLDPE + Silane Treated Wood Pulps

It is well-known that coupling agents can improve interface bonding between the filler and polymer matrix in cases of inorganic fillers such as glass fibers, mica, talc, etc. The silane coupling agent, recommended by Union Carbide Company for polyethylene, was applied in the case of our wood fibers.

The effects of fiber treatment by silanes A-172 and A-174 are presented in *Table 4*. In general, there was no substantial positive effect of wood fiber silane treatment on resulting composite properties compared to original wood fibers. It is possible that the vinyltri (2-methoxy) groups of silane A-172 or gamma-methacryloxypropyltrimethoxy groups of silane A-174 are not substantially more hydrophobic than the lignin groups already present on aspen wood pulp fibers.

Composites of LLDPE + Polyethylene Grafted Wood Fibers

The possibility of successful grafting of synthetic polymers on high lignin containing thermomechanical pulps has been recently shown by Kokta *et al* (29).

Paper sheets prepared from styrene grafted hardwood chemicothermomechanical pulp (34) have shown considerable improvement in mechanical properties such as wet breaking strength, dimensional stability, and breaking energy while retaining dry breaking strength similar to that of untreated pulps. The paper sheets mentioned above were composed of from 70 to 90 percent fibers and from 10 to 30 percent polymer. It was Gaylord (33) who, in 1972, patented the use of the grafted wood fibers

Table 2. Composites of Untreated Wood Pulps

Experiment	Energy (KJ) × 10^3				Elongation (%)				Stress (MPa)				Modulus (MPA)			
Fibers (wt %)	10	20	30	40	10	20	30	40	10	20	30	40	10	20	30	40
Aspen (CTMP) (Mesh 60)	1.5	15.4	8.4	8.3	14	10	7	5.8	12.6	15.2	18.4	27.1	90	152	262	467
Birch (CTMP)	9.6	10.9	5.0	2.7	16	10	9	6.7	22.5	22.6	18.8	17.1	148.5	226	208.8	255.2
TMP	1.4	6.2	4.3	1.8	10.4	10.3	10	6.7	19.3	18.1	17.4	13.1	189.5	175.7	174	195.5
LLDPE	20.4				34.6				14.8				43.5			

Table 3. Composites of Polymer Impregnated Pulps

LLPDE Impregnated Pulps (wt %)	Energy (KJ) × 10^3				Elongation (%)				Stress (MPa)				Modulus (MPa)			
	10	20	30	40	10	20	30	40	10	20	30	40	10	20	30	40
Aspen (Mesh 60)	16.9	13.9	12	11.1	19.6	16	15	15	34.0	22.2	18.4	16.1	122.4	138.8	122.7	107.3
Birch (Mesh 60)	15.7	13.3	11.2	10.8	19	14	13	11	23.7	21.4	22.8	12.4	112.6	152.8	175.4	117.7
LLDPE	20.4				34.6				14.8				43.5			

as a filler in thermoplastic composites. He has shown that softwood pulps grafted, using the ceric method of initiation, have mixed well with a thermoplastic polymer matrix.

The softwood as well as hardwood fibers grafted, using the xanthate-ferrous-hydrogen peroxide initiation, have been successfully applied as a reinforcer of polystyrene (12). The mechanical properties of polystyrene composites have increased in the order of 40 precent compared to the original polymer.

In the present work, aspen CTMP fibers grafted with polyethylene by radical initiation have been used as a reinforcer for LLDPE. The level of polymer addition used in this work was 10 percent.

Mechanical properties of LLDPE composites employing aspen CTMP grafted fibers, presented as a function of weight fraction of fibers as well as initiator concentration (used during aspen fiber grafting), are presented in *Table 5* and *Figs. 1–4*. It is obvious that all mechanical properties improve considerably when using grafted fibers. The fact that the best mechanical properties were obtained with the highest percentage of initiator suggests that aspen fibers, uniformly covered with either a shorter polymer chain or with larger number of chemical bonds between aspen and polyethylene, lead to better interface cohesion with LLDPE.

The improvement of energy by more than 100 percent (*Table 5* and *Fig. 1*) compared to energy loss of almost 40 percent when non-grafted aspen CTMP fibers were used (*Table 2*) strongly indicates dramatic improvement of interphase bonding in grafted aspen LLDPE composites. The increase of modulus by 160 percent (*Fig. 3*) is impressive but lower than the modulus increase when only untreated fibers were used (*Table 2*). Up to now we do not have an explanation for this fact. The improvement of stress (*Fig. 2*) by 133 percent can also be explained by better interface adhesion in the composite.

An even more interesting side effect of grafting is the improvement (or non-deterioration) of elongation of grafted aspen CTMP fibers (*Fig. 4*). The similar and even more dramatic improvement in elongation was also observed in the case of poly(methylmethacrylate)-grafted aspen fibers used in PMMA composites (35).

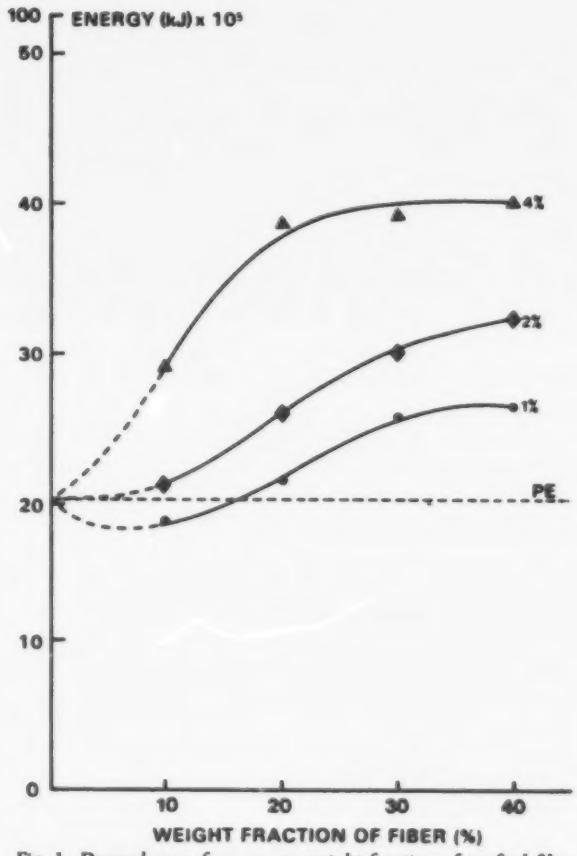

Fig. 1. Dependence of energy on weight fraction of grafted fiber at different concentration of initiator.

Table 4. Composites of Silane Treated Aspen Pulps

Aspen Mesh 60 (wt %)	Energy (KJ) x 10^5				Elongation (%)				Stress (MPa)				Modulus (MPa)			
	10	20	30	40	10	20	30	40	10	20	30	40	10	20	30	40
4% Silane A-172	12.3	13.3	11.8	9.64	24	21	19.4	12	15.6	17.7	18.4	19.7	65.0	84.3	95	164.2
4% Silane A-174	13.8	15.2	12.7	10.4	26	24.5	21	20	17.8	19.8	20.3	24.7	68.5	94.2	96.7	123.5
LLDPE	20.4				34.6				14.8				43.5			

Table 5. Composites of Grafted Aspen Fibers

Experimentally Grafted Aspen Pulps Initiator Concentration (wt %)	Energy (KJ) x 10^5				Elongation (%)				Stress (MPa)				Modulus (MPa)			
	10	20	30	40	10	20	30	40	10	20	30	40	10	20	30	40
1%	19.5	22.1	26.7	27.7	41.3	40.3	38.6	32.6	17.4	19.3	20.8	21.4	42.1	47.8	53.8	65.7
2%	22.1	27.4	31.7	34.3	40.0	38.9	35.8	31.5	18.7	21.4	22.2	22.7	46.8	54.9	62.0	72.2
4%	31.0	40.9	41.5	42.4	40.1	39.2	34.2	30.6	20.6	23.2	26.8	34.9	51.3	58.1	78.4	114.1
LLDPE	20.4				34.6				14.8				43.5			

* 10% of polyethylene addition.

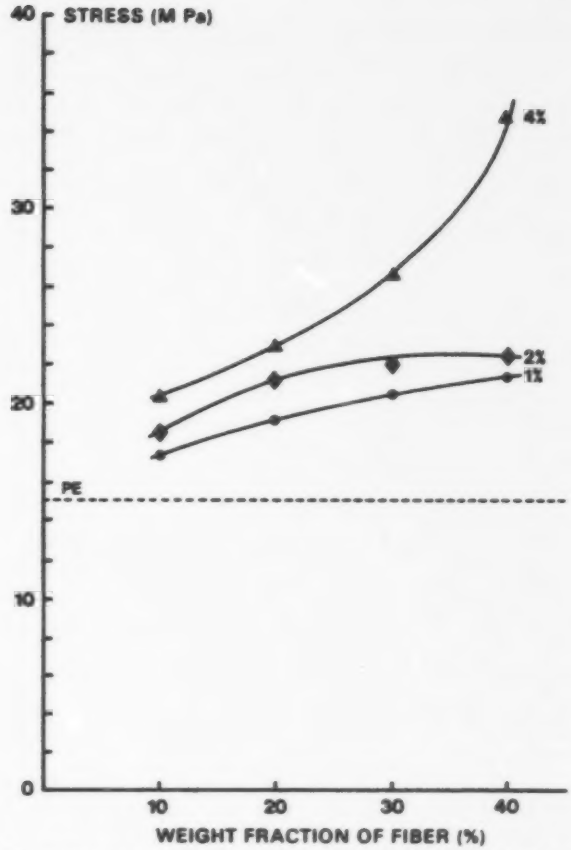

Fig. 2. Dependence of stress on weight fraction of grafted fibers at different concentration of initiator.

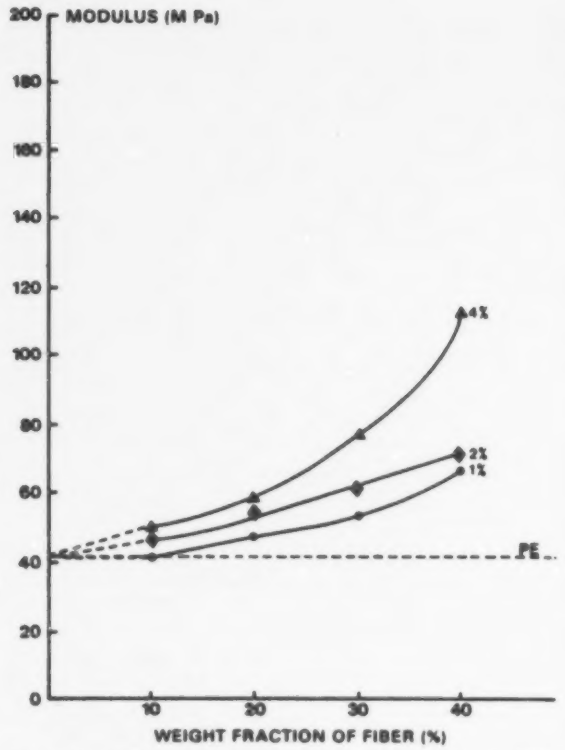

Fig. 3. Dependence of modulus on weight fraction of grafted fiber at different concentration of initiator.

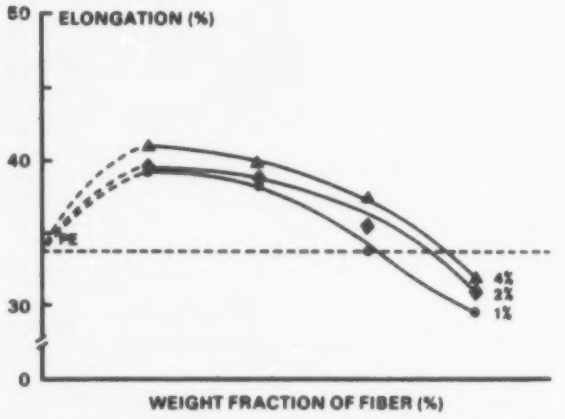

Fig. 4. Dependence of elongation on weight fraction of grafted fiber at different concentration of initiator.

Effect of Molding Temperature, Time and Pressure on LLDPE-Polyethylene Grafted Wood Fiber Composites

It is well recognized that operating conditions during composite formation can have a substantial effect on the resulting final properties (34). In order to find the optimum molding conditions in our laboratory setting, the effects of molding temperature (*Table 6*), and time and pressure (*Table 7*) were tested for grafted aspen fiber filled composites. These optimum conditions were found: temperature, 165.5°C; time of pressing, 10 min; and pressure, 3.3 to 3.8 MPa. Optical examination of composite samples indicated that the most uniform sample formation resulted under these optimum conditions.

Effect of Fiber Size of Grafted Aspen Pulps on Composite Properties

It has been shown that fiber length has an effect on grafted wood fiber thermoplastic composite properties (30–36). It was shown that the shortest fibers generally gave the best results.

In *Table 8* properties of the composite as a function of weight fraction of fibers as well as the fiber aspect ratio are presented. It is clear that in the case of grafted aspen fiber composites, the best properties for energy, stress, and elongation were for the "Mesh 60 mixture".

On the other hand, in the case of modulus the highest values were obtained for fibers of Mesh 60, with the values for the "Mesh 60 mix" being lower by about 30 percent.

More study will be needed to explain why the composites with grafted aspen fibers, having aspect ratio 46 (Mesh 20), do not have better properties than either "Mesh 60" or "Mesh 60 mix" with aspect ratio 13.9 or 11.9 respectively.

Table 6. Composites of Grafted Aspen Pulp Effect of Press Temperature

Experimentally Grafted Aspen Pulp (Wt %) (Mesh 60)	Energy (KJ) × 10^5				Elongation (%)				Stress (MPa)				Modulus (MPa)			
	10	20	30	40	10	20	30	40	10	20	30	40	10	20	30	40
171.1°C	29.6	37.3	38.2	38.5	33.5	36.5	28.7	27.6	20.25	22.4	27.6	30.27	60.19	61.32	58.7	109.5
165.5°C	31.0	40.9	41.5	42.4	40.1	39.2	34.2	30.6	20.55	23.16	26.78	34.82	51.29	59.06	78.39	11.41
154.4°C	28.8	34.9	37.2	38.0	32.1	30.4	29.6	26.5	19.7	22.5	25.6	27.4	61.3	74.1	86.4	96.3

Table 7. Composites of Grafted Aspen Pulp Effect of Time and Pressure

Experimentally Grafted Aspen Pulp (Wt %) (Mesh 60)	Energy (KJ) × 10^5				Elongation (%)				Stress (MPa)				Modulus (MPa)			
	10	20	30	40	10	20	30	40	10	20	30	40	10	20	30	40
B) Effect of Time																
5 minutes	26.5	34.6	35.8	32.7	34	32	28	24	19.6	20.0	25.1	25.4	57.6	62.5	89.6	105.8
15 minutes	30.80	39.7	40.2	41.5	40	38	32	20	20.4	23.0	26.4	29.9	51.0	60.5	82.1	99.6
20 minutes	27.6	30.6	35.20	27.7	39	31	31	29	18.6	20.4	26.2	28.4	47.7	65.8	84.5	101.9
10 minutes	31.0	40.9	41.5	42.4	40	39	34	30	20.6	23.1	26.8	34.9	51.6	59.2	78.4	114.1
C) Effect of Pressure																
20 arbitrary units	26.5	35.3	35.8	37.1	36	30	29	25	18.5	20.4	26.2	29.9	51.4	68.0	90.3	119.6
35 arbitrary units	—	—	41.5	—	—	—	34.2	—	—	—	26.8	—	—	—	78.4	—
40 arbitrary units	—	—	41.4	—	—	—	33.1	—	—	—	26.8	—	—	—	78.4	—
30 arbitrary units	31.0	40.9	41.5	42.4	40	39	34	30	20.6	23.2	26.8	34.9	51.3	59.7	78.4	114.1

Pressure (Arbitrary Units)	Pressure (MPa)
20	2.2
25	2.7
30	3.3
35	3.8
40	4.34

Table 8. Composites of Grafted Aspen Pulp Effect of the Mesh Size

Mesh Grafted Aspen Pulp (wt %)	Energy (KJ) × 10^5				Elongation (%)				Stress (MPa)				Modulus (MPa)			
	10	20	30	40	10	20	30	40	10	20	30	40	10	20	30	40
#1–40	24.6	30.8	35.9	32.5	29.2	27.4	27.8	24.4	19.45	24.03	26.46	31.59	66.66	87.58	95.08	129.74
#2–60 Mix.*	31.0	40.9	41.5	42.4	40.1	39.2	34.2	31	20.6	23.2	26.7	34.9	51.3	59.1	78.4	114.1
#3–20 Pure	25.5	32.1	31.0	31.1	29.2	27.5	26.0	24.9	24.1	26.85	29.77	30.00	82.5	92.6	114.5	120.50
#4–60 Pure	24.1	31.7	31.6	30.4	32	29.0	23.6	22.3	26.8	28.33	30.42	33.94	83.8	97.6	128.9	152.19
#5–80 Pure	26.3	32.7	34.3	33.8	33.2	30.1	28.9	25.4	20.2	22.6	28.6	29.27	60.8	75.1	99.0	115.2
LLDPE		37.1				34.6				14.8				43.5		

MESH	Average Fiber		
	Length (l) mm	Diameter (d) mm	Aspect (l/d)
20	1.107	0.024	46
40	0.46	0.027	17.7
**60	0.30	0.022	13.9
80	0.22	0.021	10.1
100	0.18	0.020	9.1
200	0.09	0.019	4.7

* "Mesh 60, Mix" is defined as the one containing the following fiber sizes: 60.8% of Mesh 80; 20.2% of Mesh 80; 15.5% of Mesh 100 and 3.5% of Mesh 200.
** For "Mesh 60 Mix" the average aspect ratio is about 11.9.

Composites of LLDPE with Grafted Aspen Pulp, Mica or Glass Fiber

Mechanical properties of composites of LLDPE and grafted aspen wood fibers prepared using the optimum molding conditions were compared to properties of LLDPE filled either with the manufacturer treated glass fibers or the manufacturer-treated mica.

Summary results presented in *Table 9*, and particularly results presented in *Figs. 5–8* show that the composites of grafted aspen wood fibers gave

Table 9. Composites of Grafted Aspen Pulp or Mica or Glass Fiber

Experiment Filler (wt %)	Energy (KJ) × 10^5				Elongation (%)				Stress (MPa)				Modulus (MPa)			
	10	20	30	40	10	20	30	40	10	20	30	40	10	20	30	40
*Grafted Aspen pulp "Mesh (60) Mix"	31.0	40.9	41.5	42.4	40.1	39.2	34.2	30.6	20.6	23.2	26.8	34.9	51.3	59.1	78.4	114.1
Mica (Suzorite-200-NP)	12.0	22.2	9.5	6.7	24	20	12	09	18.4	20.1	19.7	22.0	75.0	100.5	159.3	238.7
Glass Fiber (0.8 mm)	13.9	17.1	21.2	20.9	31	29	26	19	16.9	15.2	14.2	12.2	54.0	52.8	53.7	65.1

* 10% of polyethylene addition.

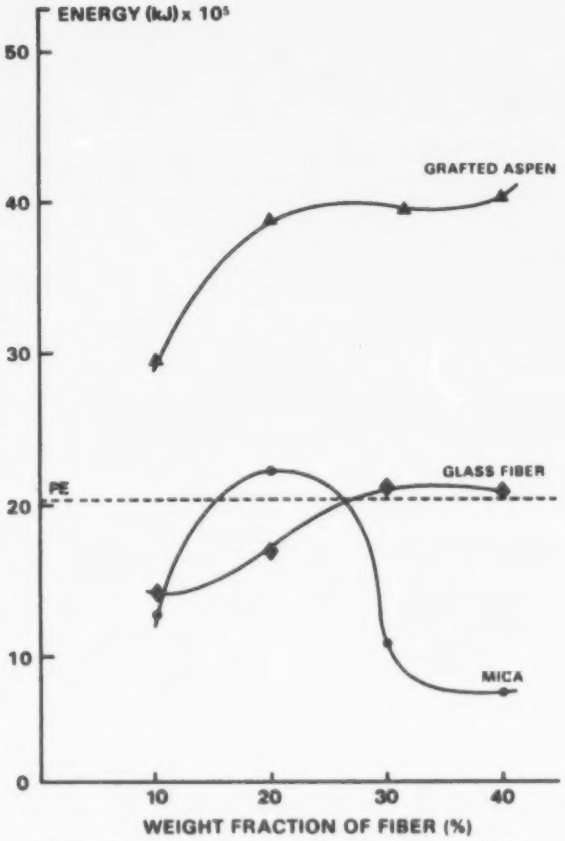

Fig. 5. Dependence of energy on weight fraction of filler.

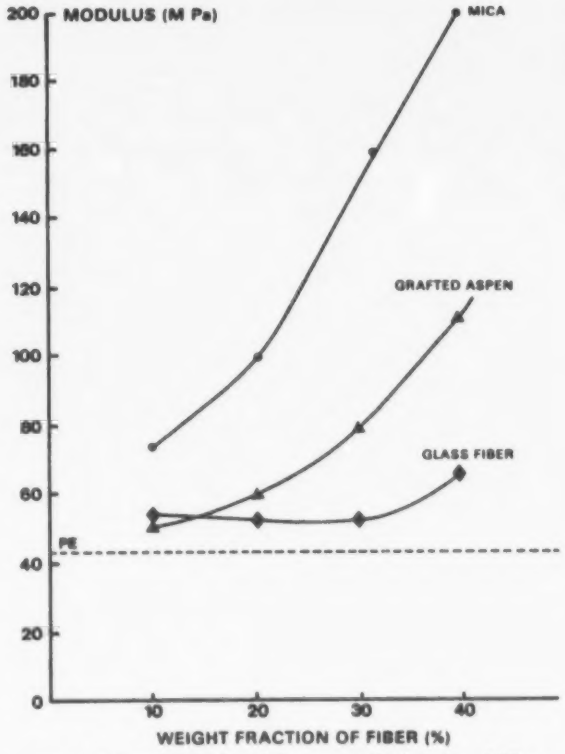

Fig. 6. Dependence of modulus on weight fraction of filler.

superior mechanical properties in the case of energy (*Fig. 5*), elongation (*Fig. 7*) and stress (*Fig. 8*). In the case where the modulus is the most important property (*Fig. 6*), only the mica-filled composites showed a higher value than grafted fiber-filled composites (238 MPA compared to 114 MPA), but this value was still far behind the one for aspen fiber composites (400 MPA +).

It is not without interest to mention the price of fillers used in this work. Grafted aspen CTMP wood fibers may cost from $250 to $350/ton. The price of treated mica is $700/ton and that of glass fibers is $2900/ton. The overall mechanical properties tested, as well as the price show good promise for using grafted wood fibers as a reinforcer in LLDPE composites. In addition, experience from our previous work (36) indicates that grafted sawdust could be used in place of grafted CTMP pulp and the price could drop to the $100/ton range.

Further research will explore the use of sawdust and will examine other composite properties, including evaluation at different temperature ranges and at extreme conditions. Preliminary results of that effort are presented in the two following paragraphs.

Effect of Boiling Water Pretreatment on LLDPE Composite Properties

Some initial results of research dealing with wood fiber composites' behavior after being exposed to adverse conditions are presented in *Table 10*. The mechanical properties of composites have been measured after boiling for 3 hours in water. It is very exciting to see that the strength of grafted aspen fiber composites remained virtually unaffected by boiling and the samples remained stronger than either LLDPE or mica or glass fiber

composites. In addition, some preliminary results showed that the wood fiber composites kept their strength and dimensional stability even after being submerged for 35 days in water at room temperature. Water absorption after a 35 day water treatment varied from 1.9 to 3.9 percent for 20 to 40 percent fiber content respectively.

The above mentioned results indicate that the incapsulation of wood fibers by polymers during grafting and subsequent compounding protects both from the properties as well as dimensional stability.

Effect of Sub-zero Temperature

Finally, some preliminary results dealing with composites behavior at −35°C is presented in *Table 11*. It seems that grafted aspen pulp composites do not lose their reinforcing properties even at −35°C and maintain their reinforcing advantage vis-a-vis glass fibers or mica.

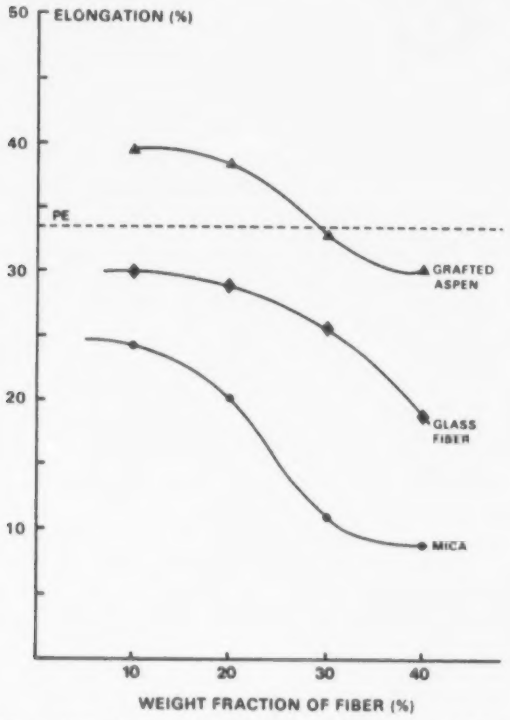

Fig. 7. Dependence of elongation on weight fraction of filler.

The authors are aware of the shortcomings of the work presented here and therefore these results should be treated as preliminary.

CONCLUSION

The objective of this work was to study the reinforcing effect of aspen pulp fibers in a polyethylene matrix. It was demonstrated that the grafted CTMP fibers improved the polyethylene properties as follows: modulus, + 160 percent; energy, more than 105 percent; stress, more than 130 percent. In addition, elongation at yield of grafted wood fiber composites did not significantly change compared to polyethylene.

Furthermore, grafted aspen fiber composites in

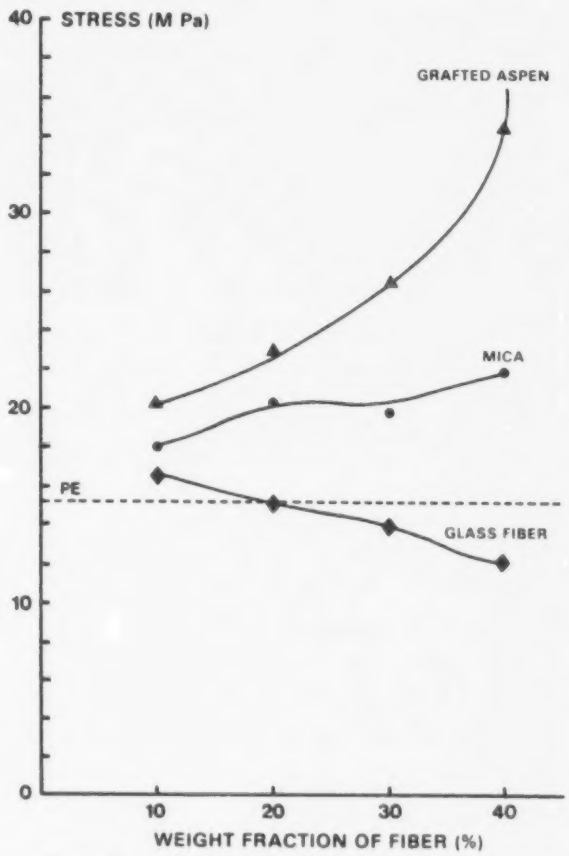

Fig. 8. Dependence of stress on weight fraction of filler.

Table 10. Composites of Grafted Aspen Pulp or Mica or Glass Fiber Effect of Boiling Water Pretreatment*

Experiment Filler (wt %)	Energy (KJ) × 10^6			Elongation (%)			Stress (MPa)			Modulus (MPa)		
	20	30	40	20	30	40	20	30	40	20	30	40
Grafted Aspen Pulp "Mesh 60 Mix"	40.1	41.7	45.0	23.5	21.2	19.1	22.9	25.5	30.5	282	341	429
Mica (Suzorite-200-NP)	10.8	—	—	9.5	—	—	16.8	—	—	232	—	—
Glass fiber (0.8 mm)	18.5	—	—	18.8	—	—	13.6	—	—	148	—	—
LLDPE		27			23.1			16.1			183	

* LLDPE and grafted aspen fibers (mica or glass fiber) composites, 3 hours boiling water pretreatment, followed 2 hours conditioning at 23°C and 50% RH before properties' evaluation. LLDPE also treated as above.

Table 11. Composites of Grafted Aspen Pulp or Mica or Glass Fiber Effect of Sub-zero Temperature*

Experiment Filler (Wt %)	Energy (KJ) x 10^6			Elongation (%)			Stress (MPa)			Modulus (MPa)		
	20	30	40	20	30	40	20	30	40	20	30	40
Grafted Aspen Pulp "Mesh 80 Mix"	41.9	44.3	28.6	10.0	15.8	9.0	37.1	40.0	45.3	383	513	655
Mica (Suzorite-200-NP)	11.3	—	—	6.5	—	—	26.3	—	—	330	—	—
Glass Fiber (6.6 mm)	21.1	—	—	12.3	—	—	24.9	—	—	345	—	—
LLDPE		32.5			19.2			24.9			290	

LLDPE and grafted aspen fibers (or mica or glass fiber) composites conditioned at −35°C for 15 minutes before properties' evaluation at −35°C.
LLDPE also treated as above.

general showed better mechanical properties than either mica or glass fiber-filled polyethylene. The cost of production of grafted aspen wood fibers ($250 to $350/ton) is considerably lower than the cost of mica ($700/ton) or glass fibers ($2900/ton).

ACKNOWLEDGMENTS

The authors acknowledge with thanks the financial support of the Natural Sciences and Engineering Research Council of Canada, the FCAC of the Province of Quebec, as well as the cooperation from Novacor Chemicals Ltd., Technical Centre, and NRCC's Industrial Materials Research Institute.

REFERENCES

1. R. Stedfeld, *Mater. Eng.*, **93**, 5 (1981).
2. G. Menges and J. Minte, Preprint, Composites '83 Symposium, 8200-8-1.41, 13, Industrial Materials Research Institute, NRCC, Boucherville (1983), pp. 33; paper No. 13.
3. J. E. Theberge and E. Hohn, *Polym. Plast. Technol. Eng.*, **16**, 41 (1981).
4. G. R. Lightsey, *Polym. Sci. Technol.*, **17**, 193 (1981).
5. A. W. McKenzie and F. P. Yuritta, *APPITA*, **32**, 460 (1979).
6. N. L. N. Sarma and P. Vasudevan, *Indian Chem. Manufacturer*, **18**, 10 (1980).
7. R. B. Seymour, *Popular Plastics*, **23**, 27 (1978).
8. I. A. Gamova, V. N. Vikhreva, and S. G. Mezhvuz, *Ser. Technol. Drev. Plit Plastikov*, **4**, 143 (1977).
9. H. Belmares, A. Barrera, G. Castillo, E. Verheugen, H. Monjaras, G. A. Patfoort, and E. N. Bucquoge, *Ind. Eng. Chem. Prod. Res. Dev.*, **20**, 555 (1981).
10. M. Lawniczak, *Holzforrsh, Holzverwert*, **33**, 71 (1981).
11. R. A. Young and C. Nguyen, *Svensk Paperstidning*, **14**, 414 (1979).
12. B. V. Kokta, R. Chen, C. Daneault, and J. L. Valade, *Polym. Compos.*, **4**, 229 (1983).
13. A. Y. Coran and R. Patel, *U.S. Pat.* 4,323,625, (1982).
14. L. A. Goettler, *U.S. Pat.* **4**, 376, 144, March 8, 1983.
15. O. Y. Mansour, A. Nagatty, A. D. Beshay, and H. Nosseir, *Cellulose Chem. Technol.*, in press (1984).
16. R. H. Marchessault, B. Fisa, and J. F. Revol, *ACS Symp. Ser.* **10**, 147 (1979).
17. H. Duchâteau, Société Industrielle et Commerciale de Transformation des Plastiques, *Fr. Pat.*, **2**, 471, 274, (1981).
18. Y. Nakajima, *Jap. Pat. Kokai*, **127**, 632 (1981).
19. Sanyo-Kokusaka Pulp Co. Ltd., *Jap. Pat Kokai*, **138**, 944 (1982).
20. A. J. Michell, J. E. Vaughan, and D. Willis, *J. Polym. Sci., Polym. Symp.*, **55**, 143 (1976).
21. A. J. Michell and D. Willis, *APPITA 31*, **5**, 347 (1978).
22. A. J. Michell, J. E. Vaughan, and D. Willis, *J. Appl. Polym. Sci.*, **22**, 2047 (1978).
23. S. H. Morrell, *Plastic and Rubber Processing and Applications*, **I**, 179 (1981).
24. I. Chun and R. T. Woodhams, Preprint, *Composites '83 Symposium*, 8200-8-1.41,3 Industrial Materials Research Institute, NRCC, Boucherville (1983); *Polym. Compos.*, **5**, 250 (1984).
25. R. S. P. Gautts and M. D. Campbell, *Composite*, **10**, 228 (1979).
26. B. V. Kokta and J. L. Valade, *TAPPI*, **55**, 366 (1972).
27. V. Hornof, B. V. Kokta, and J. L. Valade, *J. Appl. Polym. Sci.*, **20**, 1543 (1976).
28. V. Hornof, B. V. Kokta, and J. L. Valade, *J. Appl. Polym. Sci.*, **21**, 477 (1977).
29. B. V. Kokta, J. L. Valade, and C. Daneault, *Pulp and Paper Canada, Transactions*, TR59, (Sept. 1979).
30. B. V. Kokta, J. L. Valade, and C. Daneault, *Pulp and Paper Canada, Transactions*, TR5, (March 1981).
31. B. V. Kokta, L. Araneda, and C. Daneault, *Polym. Eng. Sci.*, **24**, 950 (1984).
32. B. V. Kokta and C. Daneault, TAPPI, *Proceedings 1983 Pulping Conference*, **2**, 429 (Oct. 1983).
33. N. G. Gaylord, *U.S. Patent*, **3**, 645, 939, (Feb. 29, 1972).
34. B. V. Kokta, C. Daneault, and J. L. Valade, *J. TAPPI Proceedings*, 1983 ISWP, **1**, 58 (May-June 1983).
35. B. V. Kokta, P. D. Kamdem, A. D. Beshay, and C. Daneault, *Proceedings of Papers, International Poplar Commission Symposium*, Ottawa, (Oct. 1–3, 1984), 15 pp., to be published 1985.
36. F. Dembélé, B. V. Kokta, A. D. Beshay and C. Daneault, *Proceedings of Papers, International Poplar Commisssion Symposium*, Ottawa, (Oct. 1–3, 1984), 25 pp., to be published 1985.

PANEL DISCUSSION

I. Pikulik: In the beginning you showed some information on paper made from grafted fibers, indicating enormous increases in wet strength—something in the order of thousands of percents! Under what conditions was this measured and what was the solid content in the paper at that time?

B. V. Kokta: This was the paper sheet which had grammage 50 g/m^2. The paper was pressed and heated. We compared that with pressed and heated ordinary paper. You could not achieve this increase in wet strength by using less expensive wet strength agents. However, we did not see potential for this kind of work for paper, since almost anything you do with paper has to increase the performance possibly without increasing the price. This is obviously impossible to do via grafting. This is why we re-directed our effort toward preparation of inexpensive fillers for plastics composites.

W. E. Baker: What was the starting elongation for polyethylene samples? Another question: You used molded plaques; does the polymer remain white after the molding?

B. V. Kokta: The starting elongation at yield was about 30 percent. We did not use bleached pulp, so the natural color of the fiber is slightly brown. The composites, as you can see, are brown. However, if started with bleached fibers they would have been whiter.

J. L. White: Doesn't the Monsanto Co. manufacture cellulosic fibers grafted and coated with isoprene? These are recommended as reinforcements in rubbers.

B. V. Kokta: I am not familiar with this product. I know that there are cellulosic fibers on the market used in combination with phenol-formaldehyde plastics, but I do not recall who manufactures them.

G. Benson: How would you mold these materials?

B. V. Kokta: You can mold these as you would any thermoplastic composite. We compounded the grafted fibers with polymers and then we compression molded the ASTM dog-bone specimens. You could extrude, injection mold, etc., as you would do with any fiber-filled thermoplastic system. Recently, we conducted the tests at low temperatures and after boiling water treatment. Composites were dimensionally stable after 3 to 4 days water exposure and they showed dimensional stability even after 35 days' immersion in water at room temperature. Furthermore, the wood-polyethylene composites also showed excellent mechanical properties, compared to glass fiber-filled composites, both at subzero temperatures and after 35 days aging at 105°C.

J. L. White: Since these fibers are more flexible they will not be damaged in shear flow as carbon or glass fibers are. They will go through mixing and subsequent molding processes with very little dimensional changes.

Modification of the Dynamic Damping Behavior of Epoxy/Glass Fiber Composites Via Fiber Coating with Functional Latices

B. SCHLUND* *and* M. LAMBLA

Ecole d'Application des Hauts Polymères
4, rue Boussingault, 67100-Strasbourg, France

A series of functionalized latices were synthesized using: n-butyl acrylate (BuA), butyl methacrylate (BuMA), and glycidyl methacrylate (GMA). The particle microstructure was controlled by a sequential addition of monomers. The glass fibers were commercially roll-coated using a mixture of these latices and amino-silane. The specimens were filament wound, compression molded, and cured. The effects of the morphology and reactivity of the latices were analyzed in dynamic as well as flexural modes. The uniformity of the coating as well as the nature of the latex are responsible for the mechanical behavior of the composites.

INTRODUCTION

At the present time the main research efforts on composite materials concentrate on the interface between filler and matrix. Indeed, it appears that a simple physical bonding is not enough to provide durability of mechanical properties of composites either in a humid environment or in cyclic dynamic tests. Only a permanent chemical bond can provide these functions. For this reason, composites with interfaces made up of reactive constituents have been being developed since 1960, and some manufacturers are using coupling agents to eliminate harmful effects of water. It has been found that the structure and nature of these coupling agents play an important role in the final mechanical characteristics of composites.

Recently Pfeiffer and Nielsen showed that placement of a thick, homogeneous elastomeric interlayer on a glass fiber provides a significant improvement in the mechanical properties of epoxy composites (1–3). The effects depend on the interlayer thickness acting as an energy absorber (4). The idea of a complex "sandwich" structure which possesses both specific viscoelastic properties as well as the moisture resistant ones, was proposed by Plueddemann (3). He suggested that the interface would be made of:

— a very thin layer of a modified silane to assure the chemical adhesion between the glass and the organic matrix;
— a thick polymer layer which, according to its nature and thickness, will provide the required modification of the mechanical properties.

In essence, the treatment involved silane-coating of glass fibers followed by deposition of a polymer prior to incorporation of such a complex structure into a matrix resin (3, 5).

In this paper, we discuss the way we coated the glass fibers, using an industrial roll-coating method with both amino-silane and reactive core-shell latices. In order to provide reactivity of the latex particles, with both the amino-silane coated fibers and the epoxy matrix, the epoxy groups were incorporated mainly into the shell of particles. At the same time, to control the viscoelastic properties of the interphase layer, different types of core material were selected and used.

In the following pages the synthesis and properties of the latices will be discussed, as well as the methods used for preparation of filament-wound composites and their behavior in dynamic and static tests.

EXPERIMENTAL

Synthesis and Characterization of the Interphase

Synthesis

Different types of latex were obtained by emulsion polymerization of the three following monomers:

* Present address: National Research Council of Canada, Industrial Materials Research Institute, 75, Blvd. de Mortagne, Boucherville, P. Q., Canada J4B 6Y4.

(1) n-butyl acrylate: (BuA) $CH_2{=}CH{-}C(=O){-}O{-}C_4H_9$

$T_g = -55°C$

(2) butyl methacrylate: (BuMA) $CH_2{=}C(CH_3){-}C(=O){-}O{-}C_4H_9$

$T_g = +21°C$

(3) glycidyl methacrylate: (GMA) $CH_2{=}C(CH_3){-}C(=O){-}O{-}CH_2{-}CH(O){-}CH_2$

$T_g = +45°C$

The monomers (1) and (2) were used in various proportions to obtain different glass transition temperatures, T_g. The Fox equation (6) allowed prediction of T_g of copolymers as a function of composition. The third monomer (GMA) provides the reactivity of the particles.

The polymerization was carried out by a stage-feed method. To modify the microstructure, the order of monomer addition and composition of the feed were varied. Consequently the mechanical properties of the coalesced latex films were changed (7–11).

We elected to vary the latex structural characteristics according to three parameters:

—the weight fraction of the functional agent (5 or 10 per cent of GMA). This influenced the chemical reactivity;

—the weight fraction of monomers (1) and (2). This influenced T_g. Two glass transition temperatures were selected: −20°C and +10°C;

—the order of monomer addition to change the particle microstructure. Three different structures were selected:

(i) homogeneous reactive particles, (ii) reactive core-shell particles with a thick reactive shell, and (iii) with a thin very reactive shell (see *Table 1*).

Nomenclature

The code name of the latices as used in the paper provides the three parameters:

$$A(X; Y).$$

The letter "*A*" specifies the copoly :erization conditions.

—*R* (reactive latex): particles with a "core-shell" structure; the GMA is inside the thick shell.

—*RR* (reactive reference latex): homogeneous distribution of GMA throughout the whole particle.

—*TRn* (very reactive latex): particles with a "core-shell" structure. The shell is very thin, containing high concentration of GMA. The GMA is introduced alone after "n" hours of BuA and BuMA polymerization.

The letters "*X*" and "*Y*" correspond respectively to the weight fraction of GMA and T_g. This same code will be used for composites as well.

Characterization of the Interphase

The latex films were dried at room temperature on silane-coated glass plates. Properties of the films were studied after three weeks aging. This period was sufficient to complete the coalescence. The tensile properties were measured according to ASTM 882-67. Dynamic mechanical analysis was performed in a Rheometrics mechanical spectrometer (RMS 605). The storage modulus G', the loss modulus G'', and the tan δ were measured as functions of temperature. From these curves T_g's were determined. This method was especially useful for heterogeneous particles, for which use of differential scanning calorimetry is rather difficult. Due to the potential reactivity of these materials, we studied the dynamic mechanical behavior before and after curing (2 hours at 180°C).

Table 1. General characteristics of reactive latices

T_g (°C)	Code	Composition (wt%) BuA (1)	BuMA (2)	GMA (3)	Schematic Representation
	R (5; +10)	11.4	83.6	5	reactive shell (5%)
+10	RR (10; +10)	12.5	77.5	10	reactive homogeneous particle (10%)
	R (10; + 10)	12.5	77.5	10	reactive shell (10%)
	R (5; −20)	47.1	47.9	5	reactive shell (5%)
−20	RR (10; −20)	48.2	41.8	10	reactive homogeneous particle (10%)
	R (10; −20)	48.2	41.8	10	reactive thick shell (10%)
	TR6 (10; −20)	48.2	41.8	10	reactive thin shell (10%)

In *Fig. 1* the dependence of tan δ on temperature for the four latices listed in *Table 1* is shown. The upper (solid line) and lower (broken line) curves represent the not-cured and cured sample behavior, respectively. It should be noted that with the exception of the homogeneous sample *RR*(10;−20) the remaining ones show two transitions, associated with the core-shell structure. Curing can either shift the transition to a higher temperature (without affecting the position of the transition peak of the core material) or in cases where the crosslinking density is very high (*Fig. 1c*), it hides the core structure performance (12).

The results of stress-strain tests (*Fig. 2*) also reveal the differences between the films: homogeneous reactive particles (curve A), classical core-shell reactive particles (curve B), and highly reactive particles (curve C). All these products show a classical S-shape behavior. It is important to note that TR6(10;−20) (curve C) had the highest elongation (about 1000 percent) and the highest initial modulus. This is an unusual combination of properties. In the same figure the result of thermal hardening on TR6 is also shown; curve C′ indicates a sharp decrease of elongation at break.

Preparation of Composites

Making of Coated Glass Fibers

A fifty-hole drawplate was used. The draw-ratio for the molten glass was adjusted to give fibers with a diameter of about 15 μm. The coating took place before the fibers were bonded together. The coating bath contained a mixture of: γ-amino-propyltriethoxy-silane, 0.45 percent in weight; latex containing 33 percent of dried materials, 7.55 percent, and water. The very reactive latex TR6(10;−20) was prepared without the amino-silane since its reactivity would cause latex coagulation. The fibers were wet on a single rotating role partially immersed in the coating solution. Then the fibers were wound on a winding tube and dried for 5 hours at 110°C.

Preparation of the Matrix Material

The epoxy resin was made from bisphenol and epichlorohydrin by Ciba-Geigy (CY205). To this commercial product the hardeners 1.4 butanediol, diglycidyl ether (DY026), and di[p-aminophenyl-methane] (HT972) were added. The viscosity of this material at 40°C was about 0.5 Pa; potlife was 5½ hours. The T_g of the cured matrix material as measured by a differential calorimetry spectrometer (DSC) was 130°C.

Filament Winding and Curing

The filamentary winding installation is presented in *Fig. 3*. The coated glass fibers were passed through a bath containing the epoxy matrix material described in "Preparation of the Matrix Material." The impregnated filaments were wound on a rotat-

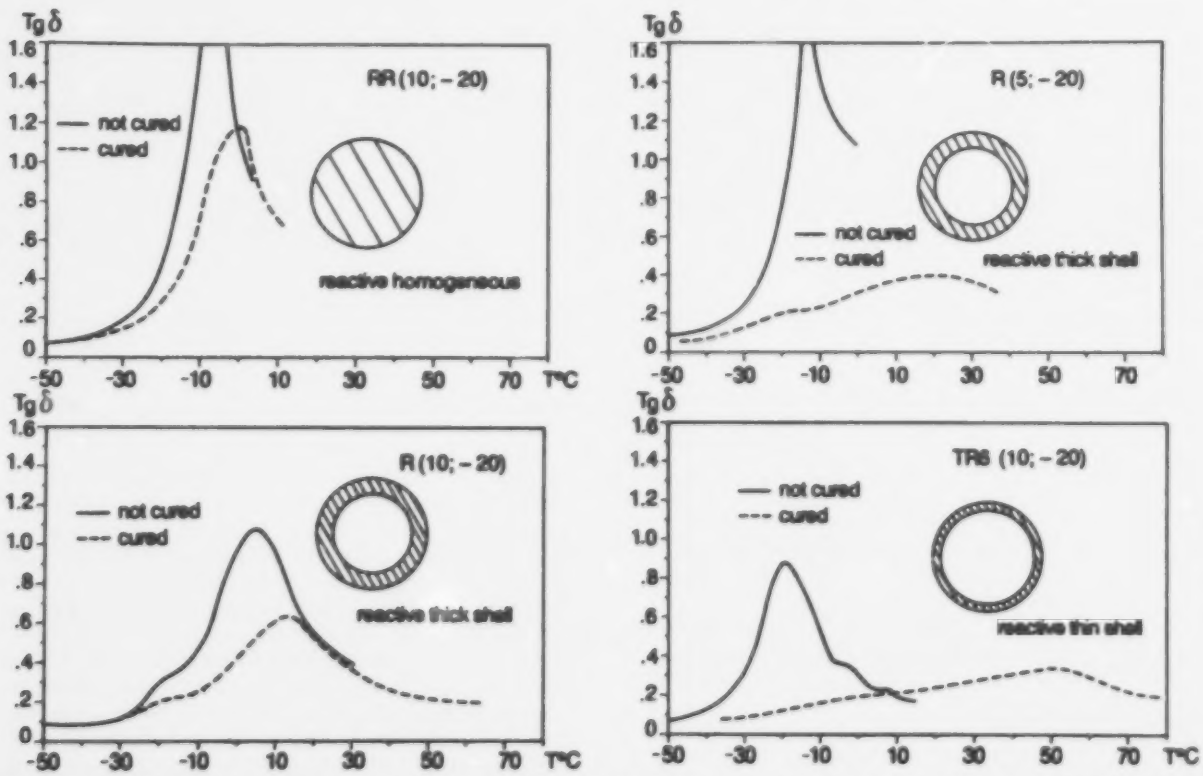

Fig. 1. The loss tangent versus temperature for the latex samples: (a) RR(10;−20), (b) R(5;−20), (c) R(10;−20), and (d) TR6(10;−20); the results before (solid line) and after (broken line) curing are shown.

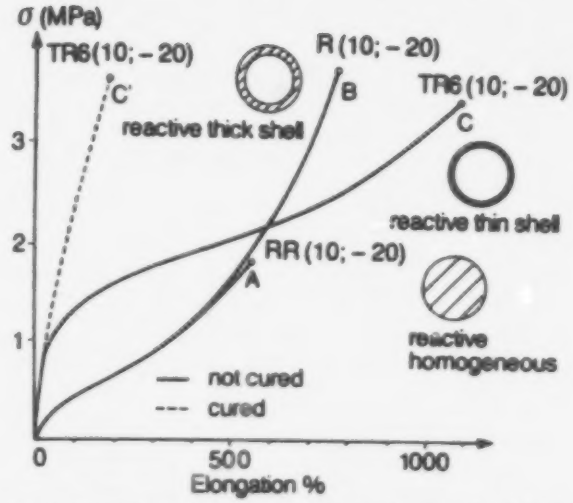

Fig. 2. Stress-strain behavior in elongation for coagulated latex films, for uncured samples: (A) RR(10;−20), (B) R(10;−20), and (C) TR6(10;−20); curve (C') corresponds to performance of TR6 after curing.

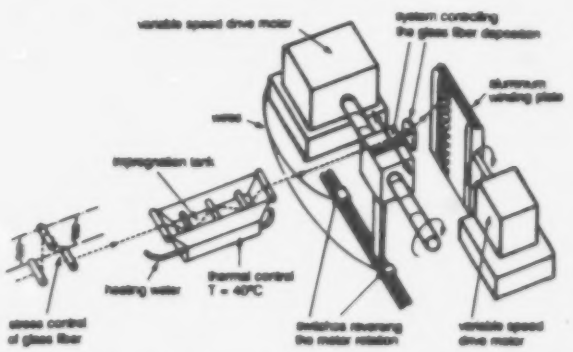

Fig. 3. Schematic representation of the filament winding system.

ing plate. A thermal regulation system heated the resin at 40°C in the impregnating tank. Two variable speed motors were used. The first controlled the winding speed, and the other the precise deposition of the fibers on the winding plate. The speeds were adjusted in such a way as to obtain close fiber-to-fiber contact. After winding, the aluminum plate on which the fibers were wound was clamped between two flat metal plates and placed in the oven. The final thickness of the composite was controlled by the shape of the winding plate, and as a result an amount of material deposited on it. The 24 hour curing was carried out at temperatures between 85 and 145°C.

Physical Properties of the Composites

Scanning Electron Microscopy (SEM)

The coated fibers as described in "Making of Coated Glass Fibers" as well as the composites were observed under SEM (Cambridge 604). We sought to observe the "quality" of the coating and the interfacial region for samples fractured in a transversal mode. Typical results are presented in *Fig. 4*.

Mechanical Spectrometer

To measure the mechanical properties of the composite, samples are sawed into rectangular sections: 2 by 6 by L (mm ± 0.05) with the fiber axis parallel to the length of the specimens. For RMS tests L = 60 mm was used, for the bending test L = 17 mm.

The bars were studied in RMS 605 using a dynamic torsional mode at frequency ω = 1 Hz and strain γ = 0.3 percent. To examine the effectiveness and the lifetime of the coating, the samples were tested before and after boiling for 24 hours in distilled water. Examples of the results are shown in *Fig. 5* (general behavior) and *Fig. 6* (the effect of the boiling water).

Bending Tests

The short beam bending test was carried out according to the European norm 01261005 (11, 13, 14). An Instron mechanical tester (model 8000) was used with hydraulic controls. Selecting the support span to sample thickness ratio (five in our case), the sample could be fractured by a successive delamination of the fiber layers.

Bending modulus, maximum strength and maximum deflection at break were measured. In addition the dynamic fatigue test under constant load was performed at a frequency of 10 Hz (11, 13, 14). Here the maximum deformation as a function of number of cycles was recorded.

RESULTS AND DISCUSSION

The results for the five selected composites $R(5;-20)$, $R(10;-20)$, $R(5;+10)$, $R(10;+10)$, $TR6(10;-20)$ will be discussed. For comparison purposes an industrial reference coating (a mixture of polyurethane and amino-silane coded PU) was examined. This coating is known to be easy to use with epoxy resins, and since the epoxy can diffuse into it, the mechanical properties are improved.

The "quality" of coatings is the most important parameter defining the mechanical behavior of composites. For this reason the SEM data will be discussed first.

SEM Data

The morphology of the coating layer and the fracture behavior of composites are of interest.

Fiber Observation

In *Fig. 4* two characteristic examples of the latex deposition are presented. In *Fig. 4a* [$R(10;-20)$] the coating is thick and regular, with inter-filament bonding. In *Fig. 4b* [$TR6(10;-20)$], the situation is different; the coating is deposited discontinuously on the glass fibers.

By detailed analysis of the coating under different SEM magnification the following elements were used to determine the "quality" of coating: (i) quantity of polymer, (ii) the continuity of the deposited

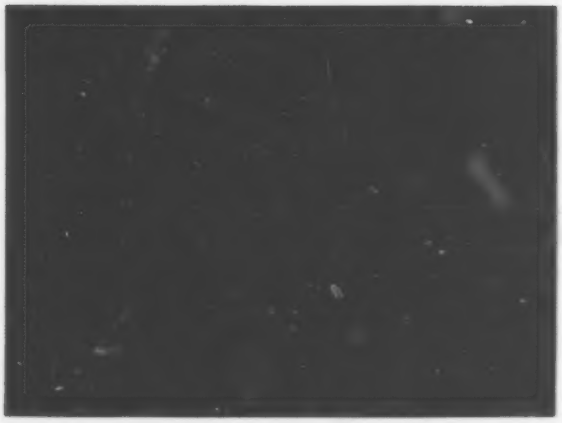

layer, and (iii) the regularity of the thickness layer. The combination of these three elements allowed classification of the coatings into three categories:

1. **continuous and regular coating,** with either the thick coatings of 0.6 weight percent of polymer on the fibers; *R*(10;−20), *R*(5;−20) and *R*(10;+10), or the thin coating with 0.4 weight percent of polymer on the fibers; PU
2. **partial coating,** where the coating is thick (0.6 weight percent deposited); R(5;+10)
3. **highly irregular coating,** the coating with TR6 (10;−20) was heterogeneous since it was impossible to add the amino-silane coupling agent to the coating bath (see Experimental).

Surface Fracture Observation

According to the fiber state after the rupture, the products were divided into three categories:

1. a composite group in which the fibers are covered with the coating material: *R*(5;−20); *R*(10;−20); *R*(5;+10) and *R*(10;+10). In *Fig. 4c*, the *R*(10;+10) composite is shown, and good adhesion to the fibers is to be noted. The separation of phases appears between the epoxy resin and the thick layer of the coating material.
2. Another group where the fibers are very clean and smooth as for the PU reference composite;
3. the last intermediate group; here the fibers are half-coated: TR6(10;−20).

The Effect of Boiling Water Treatment

An examination before and after the hot water treatment (24 hours at 100°C) reveals that in the absence of amino-silane, big cavities around the fibers are formed. This is illustrated in *Fig. 4d*. When the coupling agent is present, the coating remains on the fiber (*Fig. 4c*). Plueddemann (15) explained this behavior by the shrinkage of the rubber phase which was not chemically bonded to the glass fiber.

Thermomechanical Behavior

Samples Before Boiling Water Treatment

The dynamic mechanical properties are presented in *Fig. 5*, where the dynamic shear modulus G' of the composite (curve A), and its tan δ (curve B), are shown as well as the tan δ of the crosslinked coating (curve C), as functions of the temperature. The peak corresponding to the T_g of the core polymer particle is also visible in the composite spectrum in spite of its very small concentration.

Thick, continuous elastomer interlayer

For the $T_g = -20$°C interphases *Figs. 5b* and *5c*, a well-defined tan δ peak at low temperature is

Fig. 4. Scanning electron micrographs of the glass fibers coated with: (a) R(10;−20), (b) TR6(10;−20), (c) R(10;+10), and (d) TR6(10;−20). Figure (a) and (b) show quality of the coated fibers not compressed into a composite. Figure (c) and (d) show fractured composites respectively before and after a boiling water treatment (24 hours).

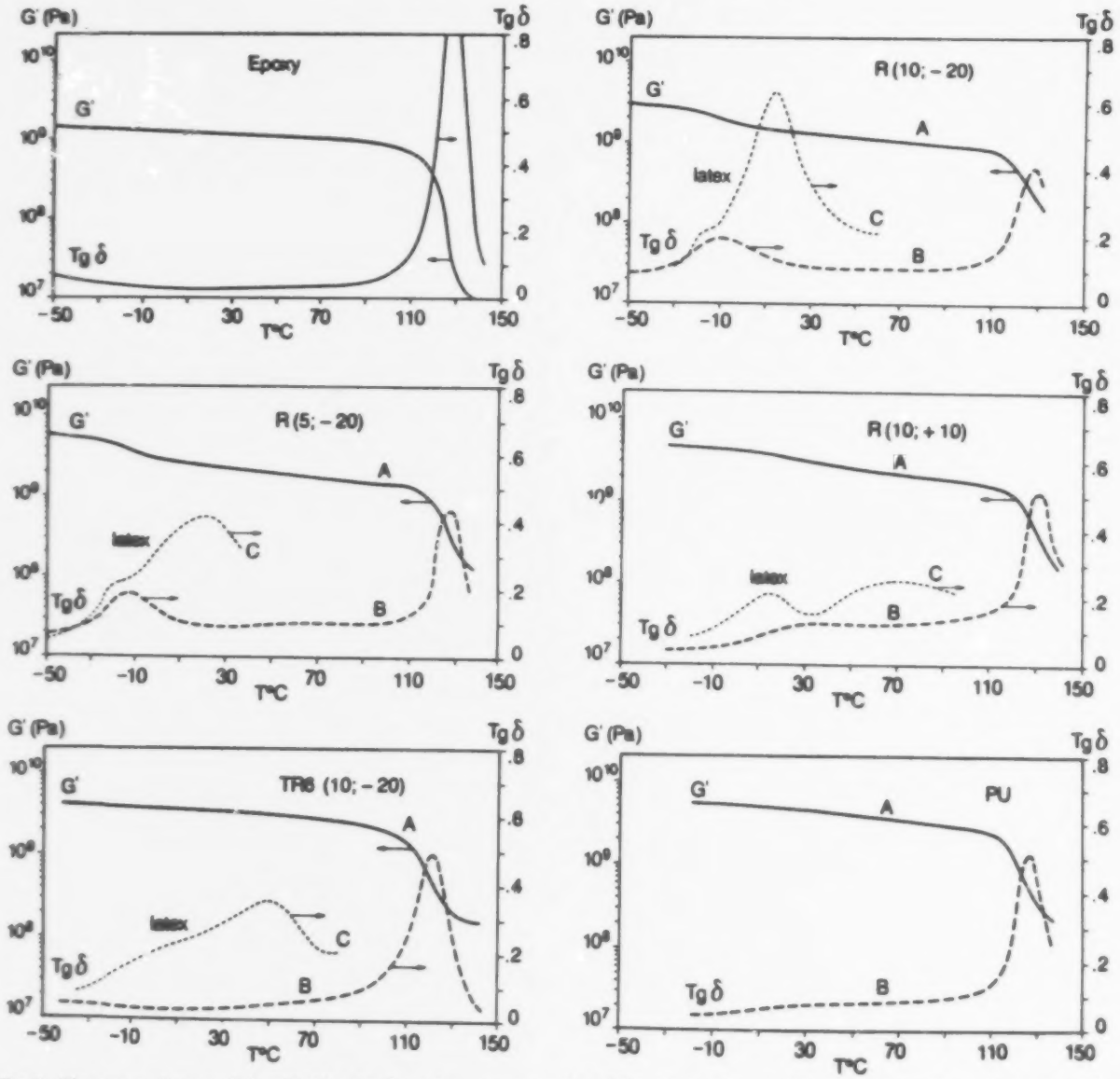

Fig. 5. The storage shear modulus, G', (line A), for: (a) pure epoxy resin and (b)–(f) cured composites versus temperature. Loss tangent for (a) pure epoxy resin and (b)–(f) cured composites, and for cured latexes (curves b–f), line C, versus temperature.

observed. Its value corresponds to the maximum of T_g of the latex particle core. Similarly, an increase in tan δ for the $T_g = +10°C$ interphase is observed. The increase in tan δ values starts approximately at T_g of the latex particle core and, as shown in *Fig. 5d*, reaches a plateau level before the T_g peak of T_g epoxy resin. One can explain this behavior by a partial penetration of the epoxy into the coating layer, hardening the elastomeric particles. This is confirmed by SEM.

The G' of the composites is strongly affected by the characteristics of the coating layer, in particular, when this layer is uniformly deposited on the fiber surface. In fact G' is determined by the longitudinal movements of glass fibers within the epoxy matrix. This interdependence between moduli of the coating layer and the composite is also observed plotting G' as a function of the fiber volume fraction. Similarly to Broutman (4), it was found (16) that for the $T_g = -20°C$ interphase, the modulus decreases significantly with the fiber content. However, for the $T_g = +10°C$ interphase G' was found to increase with the fiber concentration.

Thin and continuous coating: PU

The capacity of the epoxy resin to diffuse into the thin coating layer of PU eventually allows a direct chemical bonding between the amino-silane coupling agent and epoxy (17, 18). This behavior is shown in *Fig. 5f*. The slowly increasing tan δ can be explained by a deep and progressive diffusion of the resin into the coating layer. At the same time the G' of the composite is heightened since the

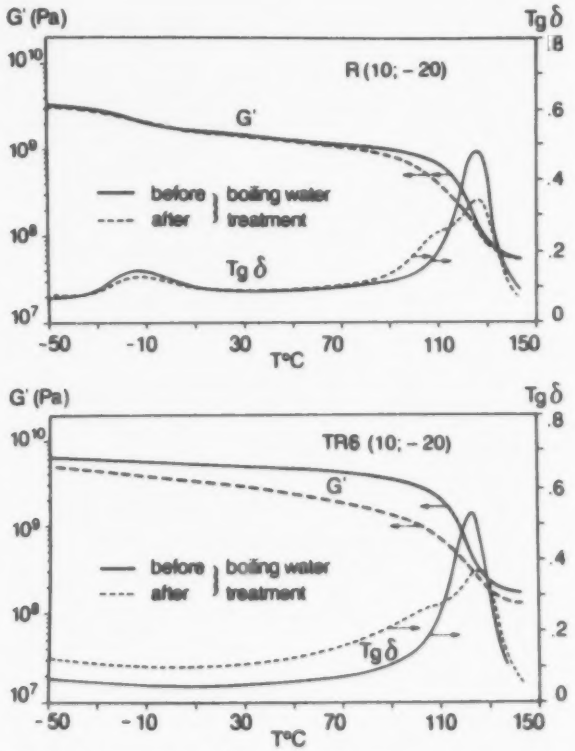

Fig. 6. The storage modulus and loss tangent versus temperature for cured composites containing: (a) amino-silane with R(10;−20), and (b) TR6(10;−20). Behavior before (solid line) and after (broken line) the boiling water treatment is illustrated.

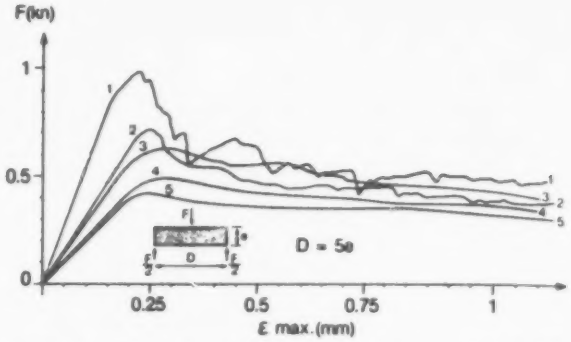

Fig. 7. Stress-strain dependence in bending curves: (1) PU with 84 weight-percent of glass fibers, (2) R(10;+10) with 80 weight-percent, (3) R(5;+10) 76 weight-percent, (4) R(10;−20) with 77 weight-percent, (5) R(5;−20) with 73 weight-percent. Note: the abrupt decrease of stress beyond the yield point following the nature of the latex interlayer.

Table 2. Dynamic shear storage modulus, G', at 20°C for 55% fiber volume composites

Sample	Dry modulus G' (Pa) × 10 T = 20°C	ΔG'(a) (%) T = 20°C
Pure epoxy resin	1.0	—
R(5;−20)*	1.6	7
R (10;−20)*	1.5	0
R (5;+10)*	3.2	6.5
R (10;+10)*	2.3	6.6
TR6 (10;−20)	4.1	50
PU*	4.1	13

(a): $\Delta G' = \frac{(G'\ 20°C)\text{ before boiling water treatment} - (G'\ 20°C)\text{ after boiling water treatment}}{(G'\ 20°C)\text{ before boiling water treatment}}$

*: coating with amino-silane.

interface is stiffened, allowing an efficient transfer of the load from resin to fibers.

Partial coating: R(5;+10)

In this case the interlayer does not entirely play its damping role. Effectively, the direct contact regions between epoxy resin and the glass fiber prevent the relative fiber-matrix movement. The mechanical properties of such composites show a maximum on the bending stress-strain curve (*Fig. 7*) caused by the direct contact regions. Only after the contacts are broken can the coating play its role.

Heterogeneous coating: TR6(10;−20)

It is impossible to talk about coating in this case. Here the latex is deposited in scattered aggregates of different size. Almost up to the T_g of the matrix, tan δ is very low indicating that the damping capacity is non-existent (*Fig. 5e*). Here epoxy resin-glass fiber contacts are so large as to hide completely the effect of the coating material. At the same time G' is one of the best among the studied products. This may suggest that interaction between glass and epoxy are strong even without the coupling agent. The boiling water test results demonstrate that the nature of the bonding is essentially physical or cohesive. The summary of the results is given in *Table 2* where the values of storage modulus, G', at 20°C for 55 volume percent of fiber are listed. It can be seen that if the coating is continuous, G' is directly dependent on T_g of the interphase. These results are in accord with Pfeiffer (1) and Broutman (4) data.

Sample After Boiling Water Treatment

In *Fig. 6* the storage modulus and tan δ are presented for the samples R(10;−20) containing a coupling agent, and for TR6(10;−20) without a coupling agent, respectively. In both cases, the performance before and after boiling water treatment, was examined. An example of the mechanical results (G' and $\Delta G'$ at $T = 20°C$) is presented in *Table 2*. It can be seen that initially G' of TR6(10;−20) was higher, but after boiling a significant drop is observed. At the same time, water treatment uniformly up to the T_g region increases the value of tan δ. By contrast, the mechanical properties of R(10;−20) were mainly unaffected by the very severe exposure to boiling water. The results indicate that the chemical bonding between the glass and the coating layer is not the only important parameter to provide a good resistance to boiling water.

Two other elements were important: 1. the continuity of the deposited layer on the glass, and 2. the chemical nature of the coat. Frequently, as illustrated in *Fig. 6*, one has to balance between the

superior water resistance and the mechanical properties: the $R(10;-20)$ does lower the value of the initial modulus in respect to TR6.

Effects of the Weight Fraction of GMA

Changing the GMA content from 5 to 10 weight percent does not appreciably change the mechanical properties. The reason for this is that the surface reactivity of both latex particles is similar, which is caused by the high value of the GMA copolymerization constant (19). In fact, the GMA influences the particle polarity and thus the quantity of the coating layer as far as both homogeneity and regularity are concerned. The boiling water treatment proves that the best coating to resist this abuse is obtained with the higher GMA content (see *Table 2*), generating a larger number of chemical bonds across the interface.

Bending Tests

Figure 8 shows different stress-strain behavior for five composite samples. Once more, the strong influence of the nature and "quality" of the interlayer on mechanical properties is clearly visible. The interlaminar ruptures are more brutal for the higher values of interlayer T_g (*Fig. 7*). For the coatings with $T_g = -20°C$ the interphase undergoes a plastical deformation, i.e., an interphase deformation without delamination. In *Fig. 8a* this behavior is schematically presented. For coating with $T_g = 10°C$, (e.g., $R(10;+10)$) the deformation occurs by partial delamination presented schematically in *Fig. 8b*. Finally, for PU coating, the deformation causes severe delamination with brittle interlayer fracture (*Fig. 8c*). In the case of a partial coating (TR6) the deformation causes even more severe delamination than that observed for PU, eventually leading to fracturing of the specimen across the glass fibers.

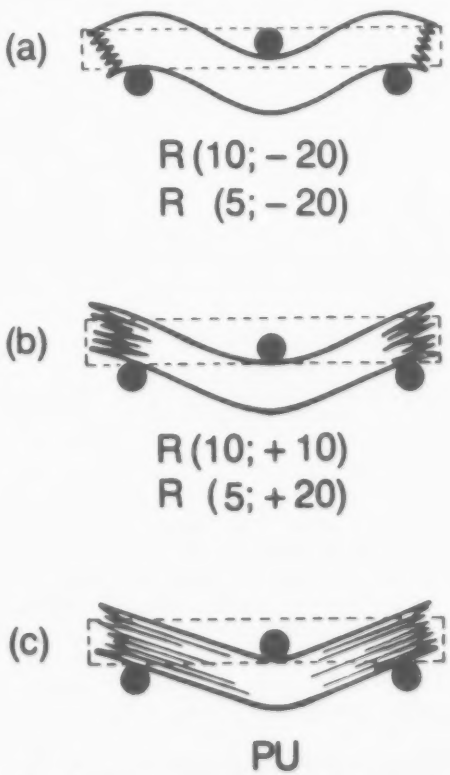

Fig. 8. The schematic representation of the deformation effect: (a) ductile deformation (after the test the samples recovered their initial shape), (b) semi-brittle deformation via the partial delamination mechanism (nearly complete recovery, rupture of the ends visible), and (c) brittle deformation with the total delamination (severely damaged sample, no recovery, smaller thickness).

CONCLUSIONS

1. It was demonstrated that it is possible to coat glass fibers with a thick interlayer of a coupling agent and reactive latex, using a single step, on-line industrial process.
2. It was shown that by changing the chemical nature of the monomer and especially the sequence of polymerization in the "stage-polymerization" process, it is possible to optimize the latex properties from the point of view of the reactivity and mechanical properties.
3. It was found that amino-silane plays an important role in the treatment, chemically bonding on the one hand to the glass fiber, on the other to the latex interlayer. Its role is dramatically evident in the boiling water test.
4. As shown by the mechanical tests, it is important that the fibers be completely covered with the coating layer. When the coating is not perfect the interface cannot fulfill its role and the mechanical properties become similar to those observed for glass/epoxy composites. By contrast, when the coating is uniform, the composites' behavior depends strongly on the nature of the interlayer as well as on its microstructure.
5. The latex having $T_g = -20°C$ was found to improve the low-temperature mechanical properties, increasing the value of tan δ and maximum deformation.

ACKNOWLEDGMENT

This work was carried out at the "Ecole d'Application des Hauts Polymères de Strasbourg." Financial help from the French national society SNEAP is gratefully acknowledged. We would also like to thank L. A. Utracki for his help in preparation of this paper and for the invitation to present it at the NRCC/IMRI symposium "Composites—'84."

REFERENCES

1. D. G. Pfeiffer and L. E. Nielsen, *J. Appl. Polym. Sci.*, **23**, 2253 (1979).
2. D. G. Pfeiffer and L. E. Nielsen, *J. Appl. Polym. Sci.*, **24**, 1451 (1979).
3. E. P. Plueddemann, Reinforced Plastics—Composites Institute, 29th Annual Technical Conference, The Society of the Plastics Industry Inc., 1974.
4. J. Broutman, *Polym. Eng. Sci.*, **14**, 581 (1974).
5. R. K. Iller, *J. Colloid Interf. Sci.*, **21**, 569 (1966).
6. T. Fox, *Bull. Am. Phys. Soc.*, **1**, 123 (1956).
7. H. Kenneth, *J. Coating Technol.*, **51**, 29 (1979).
8. M. R. Granio and D. J. Williams, *J. Polym. Sci.*, **8**, 2617 (1970).

9. K. Chujo, Y. Harada, S. Tokuharada and K. Tanaka, *J. Polym. Sci., Part C*, **27** (1969).
10. J. L. Gardon, *J. Polym. Sci.*, **12**, 2133 (1974).
11. M. J. Own, S. Morris, *Plast. Polym.*, August (1972).
12. B. Schlund and M. Lambla, *Die Ang. Makrom Chem.*,—*Appl Macrom. Chem. Phys.*, in press.
13. P. Yeung and L. J. Broutman, *Polym. Eng. Sci.*, **18**, 2 (1978).
14. S. Zweben, M. W. Wardle, *Polym. Compos.*, **2**, 2 (1981).
15. E. P. Plueddemann, "Composite Materials," p. 213, Academic Press, New York (1974).
16. B. Schlund, Thèse de docteur ingénieur, EAHP—Université Louis Pasteur, Strasbourg, France (1984).
17. H. Ishida and J. L. Koenig, *J. Colloid Interf. Sci.*, **64**, 3 (1978).
18. M. E. Schrader and A. Block, *J. Polym. Sci., Part C*, No. 34, 281 (1971).
19. B. Schlund, M. Lambla, Symposium on "Emulsion Copolymerization and Copolymers—Reactivity and Microstructure of Latex Particles," Lyon, France (March 1984).

PANEL DISCUSSION

L. A. Utracki: Bruno, it is not clear to me how and why many different coatings are on your glass fibers. Under normal industrial treatment the glass fiber manufacturer invariably deposits some coupling agent, usually silane. This is done with kissing rolls and it results in a very uneven, spotty coating. In your treatment do you start with these fibers or with neat ones? You use an impregnating tank with the latex and amino-silane. Is this on top of, or instead of, the silane treatment?

B. Schlund: The industrial treatment consists of coating glass fibers with functionalized small molecules such as amino-silanes. The coating layer is so thin that it has to be analyzed rather by FTIR than SEM. The quality of the coating depends on the technique of deposition. In our treatment, the latex is added to the amino-silane. This treatment is similar to industrial deposition of polyurethane (PU), on glass fiber. In that case PU is emulsified with a large addition of sodium lauryl sulfate, then amino-silane is added and the mixture is deposited in a single step on glass fiber. Our treatment is analogous, except that we do not need to add emulsifier to the latex. In the case of TR-6, amino-silane was found to coagulate the latex and for this reason it had to be eliminated from the coating formula.

M. Dumoulin: Does the boiling water treatment correspond to real end-use conditions to which the material will be submitted, or did you use it only to characterize the coatings?

B. Schlund: The boiling water treatment is used to provide information on the nature of the cohesion between the glass and organic phase. The work of Ishida and Koenig [*Polym. Eng. Sci.*, **18**, 2 (1978)] has shown that bonding between silane and glass is reversible. The boiling water test is conducted on the glass fiber-epoxy composite, by placing it in boiling water for 24 hours. We observed that in the absence of silane in the coating bath, or in the case where the coating was not uniform, the mechanical properties were severely affected by boiling water. On the other hand, in the presence of amino-silane *and* a continuous hermetic layer of latex around the fiber, the water treatment had a very slight effect on the mechanical behavior of composites.

L. Z. Pillon: What, in your opinion, is the mechanism, or the nature, of the glass fiber, amino-silane, and latex bonding? Do you think that chemical bonds across the interface are involved, or that only physical interactions are involved?

B. Schlund: We feel that chemical bondings are involved. The reaction occurs in two steps. First, during the drying of glass fiber (after coating with amino-silane/latex mixture) a chemical reaction between glass and amino-silane takes place. The reaction between the amino and epoxy groups, (i.e., between the bonded to glass amino-silane and latex particle) is possible but probably not complete at this stage due to the low temperature of drying. This is further illustrated in *Fig.* "A" where the two types of amino-silane bonding are shown. The molecule in the center forms a layer on the glass surface, without reacting with latex particles.

L. A. Utracki: You mentioned that the polyurethane (PU) treatment is commercially used. The sample with PU which you tested indicated a poor brittle coating. However, PU can be formulated to produce any toughness/flexibility one may want. My question is: what is the technical and economic benefit for going into latex coating versus that with reformulated, if need be, polyurethane?

B. Schlund: We used the best commercial PU available on the market; we do not know the PU formulation, as this is confidential. In principle PU can be reformulated, but on drying from aqueous medium, the hydrolysis of isocyanate groups has to take place resulting in a decrease of mechanical properties of the coated layer. One of the objectives of our work was to improve the low temperature impact properties of the continuous fiber composites.

We proved that the reactive latices can be directly used in a commercial application, and that the coating enhances the impact performance. The advantages of the proposed latex treatment are: (i) flexibility in designing the latex to specific performance, (ii) the latex is already in the form of sub-micron (0.2 to 0.3 μm diameter) particles, well-stabilized in the aqueous medium to which only amino-silane needs to be added, and (iii) the functionality of the latex can be adjusted to become reactive with different types of matrix polymers.

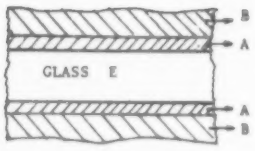

Zone A : Amino-silane layer bonding to glass and the latex layer B.

Zone B : Reactive latex layer

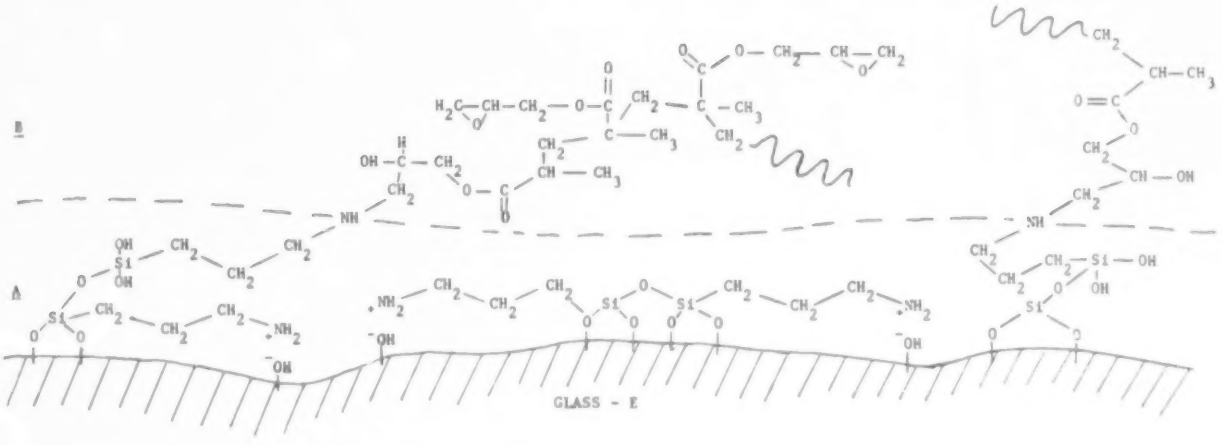

Figure A

Some Properties of Polypropylene Filled with Metal Fibers

T. KATSURA* *and* M. R. KAMAL

Department of Chemical Engineering McGill University 3480 University Street Montreal, Quebec, Canada H3A 2A7

L. A. UTRACKI

Industrial Materials Research Institute National Research Council of Canada 75, Boul. De Mortagne Boucherville, Quebec, Canada J4B 6Y4

Polypropylene/steel fiber composites were prepared and tested for mechanical, electrical, and permeability performance. To enhance adhesion of polypropylene to steel fibers, two kinds of coupling agents, maleated polypropylene wax and maleated polypropylene, were used. It was found that maleated polypropylene wax was more effective. However, as indicated by permeability measurements and scanning electron microscopy (SEM), adhesion was rather poor. Oxygen and water vapor permeabilities of the polypropylene/steel fiber composites increased with the steel fiber concentration. The lack of adhesion at the fiber-polymer interface created diffusive paths for the gas to penetrate the composite. Addition of polyamide to polypropylene caused a decrease in the permeability of the system, due to a reduction of the permeability of the matrix. The polypropylene/steel fiber composites become conductive at a volume loading of about 10 percent. At this concentration the volume resistivity of the composite is 10.8 ohm cm.

INTRODUCTION

In recent years, demand for electromagnetic interference (EMI) shielding of housings for electronic equipment has grown substantially. This has led to many efforts to produce polymeric materials with enhanced electrical conductivity. The most direct technique involves surface treatment of molded plastic structures, by vacuum plating with metals or coating with electrically conductive paint (1). However, vacuum plating is rather expensive, while coating is of limited value due to abrasion problems.

Another approach is to use polymer composites filled with electrically conductive fillers. Carbon black has been used to produce conductive rubbers. Such an approach was also used to produce EMI shielding plastics composites. However, at the required loading, such composites tend to be brittle. Other additives used to provide electrical conductivity include metallic fillers. Gurland (2) has shown that spherical or irregularly shaped metal particles can be loaded into the polymer to produce electrically conductive composites. However, here again high loadings are required.

Bigg and Bradbury (3–5) have studied the properties of electrically conductive polymer composites filled with short metallic fibers. They reported on electrical, thermal, and mechanical properties of aluminium fiber/polypropylene composites. Composites prepared with as little as 7.7 volume percent aluminium fibers, having an aspect ratio $p = 24$, exhibited resistivities below 200 ohm cm. At this low filler loading, the mechanical properties were similar to those obtained for composites containing comparable amounts of milled glass fibers.

The high aspect ratio metallic fibers are effective to produce electrically conductive composites at low concentration. Tolokan (6) demonstrated that stainless steel fibers with high aspect ratio were particularly advantageous. At a concentration of 5 percent by weight (or 1% by volume), 7 micron stainless steel fibers with $p = 1080$ provided 40 dB of EMI shielding in the 0.1 to 1000 MHz range. However, these fibers are quite expensive.

Recently, short metallic fibers obtained by the vibrational cutting method, have been introduced commercially. Due to the simplicity of production, the fibers are quite inexpensive. Nakagawa *et al* (7) studied the performance of such short metallic fibers in ABS/aluminum fiber and ABS/brass fiber composites. They reported that an increase of the

* On leave from: Corporate Research and Development, Toyo Seikan Group, 22-4 Okazawa-cho, Hodogaya-ku, Yokohama, Japan 240.

filler content causes an increase in the elastic modulus, while the tensile strength and the maximum elongation at break decrease. Microscopic observations of the tensile fractured surfaces indicate that adhesion between the resin and fibers is poor.

The following discussion reports on the preliminary results of a study initiated to investigate the mechanical, electrical, and permeability properties of polypropylene composites filled with short steel fibers, cut by the vibrational method. Polypropylene was selected since it is used extensively for packaging as well as for housing of electronic equipment. Since adhesion between polypropylene and metallic fibers was expected to be an important factor in determining mechanical properties, two kinds of coupling agent were used: maleated polypropylene wax (MPPW) and maleated polypropylene (MPP). MPPW is easy to apply, due to its low molecular weight, whereas MPP has strong bonding to metals.

Another purpose of this study is to evaluate the feasibility of using the polypropylene/steel fiber composites as food packaging materials. Thermal conductivity is important for these applications, due to sterilization or reheating requirements. It is expected that the steel fibers should lead to an increase in the thermal conductivity of the composites. The gas barrier properties are also important, to protect the contents. Polyamide was added to some of the formulations to evaluate its effect on some of the above properties.

EXPERIMENTAL

Materials

Hercules Pro-Fax 6501 polypropylene (PP) was used as a base material. To reduce the oxygen permeability of the matrix resin, some samples were prepared by blending DuPont de Nemours Zytel 211 polyamide-6, PA-6, with PP. The two coupling agents used in the study were: MPP, (Admer Q-3000 from Mitsui Petrochem. Co.) and MPPW (Epolene E-43 from Eastman Chemical Products Inc.). The properties of these resins are listed in *Table 1*.

The short steel fibers used in the present study were produced by Aisin Seiki of Japan, by means of the vibrational cutting method. These fibers were 3.0 mm long and 60 μm in effective diameter. Thus, the aspect ratio of these fibers was 50. The cross-section of the fibers was not circular, but rather triangular.

Preparation of Composites

The compositions of samples based on PP are given in *Table 2*. Samples based on PP/PA-6 blends are listed in *Table 3*.

In order to optimize the amount of the coupling agent, the series OP and OW were first prepared and tested. The appropriate amount of MPP or MPPW powder was dry-mixed with the steel fibers, prior to addition of these to PP melt. A Brabender two-roll mill, Model PM2000 was used, at 205°C and a rotational speed of 12/17 rpm. Initially, the resin was melted, then steel fibers with or without

Table 2. Composition of Polypropylene Composites

Material Code	Steel Fiber Content, $\bar{V}_f$ (Volume %)	MPP Wax Content (Weight % relative to the steel fiber mass)	MPP Content (Weight % relative to the steel fiber mass)
P-3	3	—	—
P-5	5	—	—
P-10	10	—	—
P-12	12	—	—
P-15	15	—	—
P-20	20	—	—
Q-3	3	5	—
Q-5	5	5	—
Q-10	10	5	—
Q-12	12	5	—
Q-15	15	5	—
Q-20	20	5	—
R-3	3	—	5
R-5	5	—	5
R-10	10	—	5
R-12	12	—	5
R-15	15	—	5
R-20	20	—	5
OP-1	15	—	1
OP-3	15	—	3
OP-4	15	—	4
OP-5	15	—	5
OP-10	15	—	10
OW-1	15	1	—
OW-3	15	3	—
OW-4	15	4	—
OW-5	15	5	—
OW-10	15	10	—

Table 1. Properties of Materials Used in the Study

Material Properties	Polypropylene	Polyamide-6	Maleated Polypropylene	Maleated Polypropylene Wax
Code	PP	PA-6	MPP	MPPW
Type	Pro-Fax 6501	Zytel 211	Admer Q-3000	Epolene E-43
Manufacturer	Herculus	DuPont de Nemours	Mitsui Petrochemical	Eastman Chemical
Molecular Weight, M_w	404,000	—	—	4500
Molecular Weight Distribution, M_w/M_n	5.5	—	—	—
Density at 25°C (K_g/m^3)	904	1130	—	934
Melt Index (dg/min)	4.0	—	180	—
Melting Point (°C)	167	228	154, 161	157
Zero-shear Viscosity (Pa·s)	2×10^4 (180°C)	—	—	0.37 (190°C)
Acid Number	—	—	—	45

Table 3. Composition of Composites Based on Polypropylene/Polyamide-6 Blends

Material Code	PP/PA-6 Composition Ratios (Weight)	Steel Fiber Content (Volume %)	MPP Wax Content (Weight % relative to the steel fiber mass)
N-10	90/10	—	—
N-20	80/20	—	—
N-30	70/30	—	—
N-40	60/40	—	—
NF-10-5	90/10	5	5
NF-20-5	80/20	5	5
NF-30-5	70/30	5	5
NF-40-5	60/40	5	5
NF-10-15	90/10	15	5
NF-20-15	80/20	15	5
NF-30-15	70/30	15	5
NF-40-15	60/40	15	5

coating agent were added. The total compounding time was held at 10 min.

To prepare the compositions listed in *Table 3*, the appropriate binary blends of PP/PA-6 were prepared in a C.W. Brabender single screw extruder, Model 2523, at 30 rpm. The temperatures for the barrel were set at 220/230/245°C, and for the die at 240°C. To prevent PA-6 oxidation, a C.W. Brabender roller type small batch mixer, Model 230V8, was used (instead of a two-roll mill, as for the PP composites). The samples were compounded for 8 min. at 245°C and 30 rpm.

Preparation of Moldings and Sheets

Moldings and sheets were prepared by compression molding. The molding temperature of the platens was 180°C for the PP-composites and 235°C for the PP/PA-6 ones. The samples for tensile and electrical resistivity tests were prepared using a brass mold and two flat and smooth brass plates covered with aluminum foils. During the compression and cooling stages, a force of 25 tons was applied. The moldings and sheets were cooled by circulating water, maintaining a cooling rate of 10 to 15°C per minute. For comparison, PP sheets were prepared from the virgin powder and from roll-milled material as well.

Electrical Resistivity

The electrical resistance across the ends of the test samples (13 mm width by 30 mm length by 2 mm thickness) was measured using an ohmmeter and converted into electrical volume resistivity. Each freshly cut end of the test sample was coated with electro-conductive paint.

Tensile Tests

Tensile tests were carried out according to the standard ASTM D-638 method. The test samples conformed to the dimensions of Type I (thickness = 2.0 mm) under the same ASTM designation. Nine tensile test samples were molded from each composite by compression molding, and the edges were polished to remove defects. The samples were conditioned at 25°C and 50 percent RH for 48 hours prior to testing. The tensile strength, elongations, and moduli of all the samples were determined using the Instron Tensile Tester Model 1123, at a strain rate of 50.0 mm/min. and at 25°C.

Impact Tests

Rheometrics High-Rate Impact Tester Model RIT-8000 was employed. This is a controlled-velocity device, in which a hemispherical probe impacts the unnotched sample and drives through it at a preselected speed. The force-deflection curve is displayed on the built-in computer monitor. The data points on the curves are selected by the operator, and a hard copy of the data and a plot are obtained. The impact speed employed was held at 19.05 m/min. The sheets of composites for the impact tests were prepared to have uniform thickness of 1.5 mm.

Oxygen Permeability

The method was based on ASTM standard D3985-81. The device employed was Ox-Tran 100 Twin Model manufactured by Modern Controls Inc. The test sheets were laminated between two aluminum foil masks to reduce the area of exposure from 100 cm^2 to 5 cm^2. The measurements were conducted at 25°C and 0 percent RH.

Water Vapor Permeability

The method was based on ASTM F 372-73. The Permatran W, manufactured by Modern Controls Inc., was used. The test sheets were laminated between two aluminum foil masks leaving the exposure area of 5 cm^2. All measurements were performed at 37.8°C (100°F) and 100 percent RH.

Scanning Electron Microscopy (SEM)

Sheets of the composites were fractured at liquid nitrogen temperature. The fractured surfaces were observed under SEM-JEOL Model JSM-35CF.

RESULTS AND DISCUSSION

Electrical Resistivities

The electrical volume resistivities of PP-composites are shown in *Fig. 1*. The polypropylene/steel fiber composites without a coupling agent became conductive (resistivity R = 2000 ohm cm), at a volume loading of 5 percent. At this loading, the resistivities of the composites containing MPP wax and MPP were respectively 10^{15} and $10^{5.5}$ ohm cm. At the volume loading of 10 percent, the resistivities of all three types of composites were about 10 ohm cm. At 20 percent loading, the volume resistivities of the composites without the coupling agent fell to 0.7, and for those containing MPP wax and MPP to 2.3 and 9.8 ohm cm, respectively. The differences between the conductivities of these three series of composites seem to be related to the condition of the matrix-steel fiber interface.

Figure 2 presents the Electron Spectroscopy for

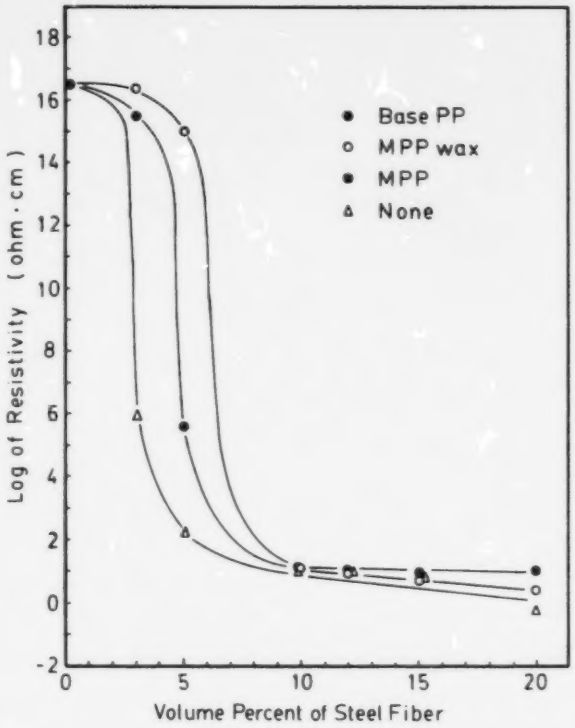

Fig. 1. Electrical resistivity as a function of steel fiber concentration.

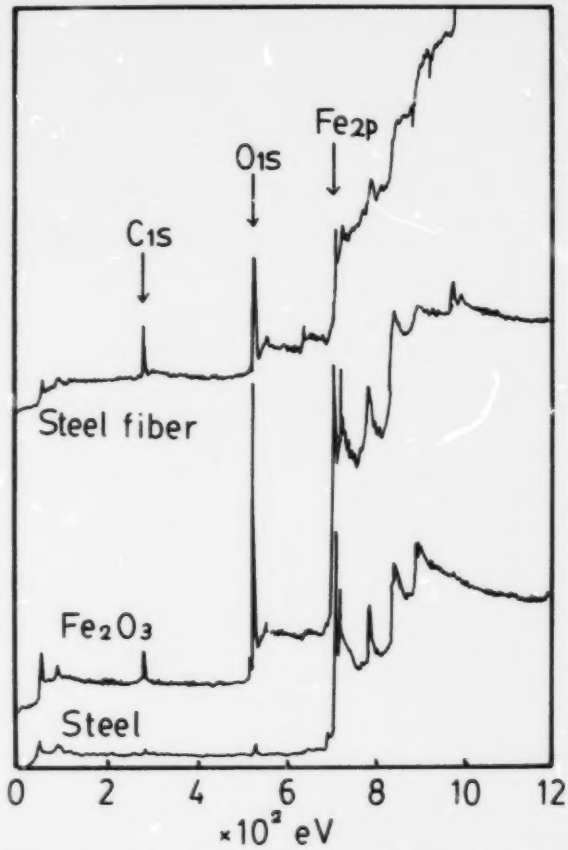

Fig. 2. ESCA wide band spectra of surface of steel fiber, Fe_2O_3 and steel.

Chemical Analysis (ESCA) wide band spectra of the steel fiber, oxidized steel (Fe_2O_3), and steel. As indicated by the spectrum, the surface of the steel fiber is oxidized. Generally, oxidation of steel surfaces generates two layers: the outer of FeO(OH) and the inner of Fe_3O_4. According to the quantitative analysis of the narrow band spectrum (not shown), the total thickness of the FeO(OH)/Fe_3O_4 layers on the surface of the steel fibers was estimated as 2.35 to 3.45 nm. MPP wax and MPP are known to have good adhesion to metals and oxides. Therefore, the layers of these coupling agents should form on the surface, thus hindering direct contact between the steel fibers.

Tensile Properties

Initially, to optimize the amounts of the two coupling agents, the series OP (containing MPP) and OW (containing MPPW) were tested (*Table 2*). As shown in *Fig. 3*, incorporation of MPP wax into the polypropylene/steel fiber composites increased the maximum tensile strength, reaching an optimal value at about 5 percent by weight relative to the steel fiber. Addition of MPP w as also found to be effective, but here improvement was small. On the basis of these results, 5 weight percent of coupling agents was selected for use in PP and PP/PA-6 composites. As indicated in *Tables* 2 and 3, samples without the coupling agents were also prepared.

The tensile properties of the three series of PP-composites (without coupling agent-series P, with 5 weight percent of MPPW-series Q, and with 5 weight percent of MPP-series R) are summarized in

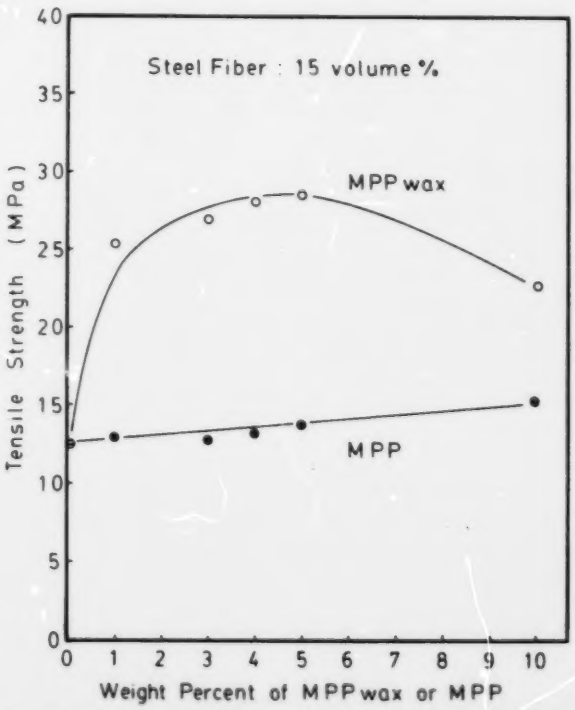

Fig. 3. Tensile strength of polypropylene/steel fiber composites as a function of MPPW and MPP concentration.

Table 4 and shown in *Figs. 4–6*. The data are averages of at least six measurements. All samples, including pure PP, showed a brittle behavior. No yield region was observed, and the maximum elongation at break was $\epsilon \leq 5.1$ percent. As shown in *Fig. 4*, MPPW is a more efficient binder than MPP. This conclusion is confirmed by the maximum stress at break, σ_c, data presented in *Fig. 5*. Only in series Q, the tensile strength of composites up to $\bar{V}_f \doteq 15$ volume percent of steel fibers was not appreciably reduced; MPP was effective only for concentrations up to 5 volume percent. The strength of composites without a coupling agent fell to about one-half of the matrix value upon addition of only 3 volume percent of steel fibers. It should be noted that, at 10 volume percent of loading where all three types of composites showed approximately the same resistivity, $R \doteq 10$ ohm cm, only in series Q the respectable value of σ_c was preserved.

Bigg (4) has shown that specially modified polypropylene, which reacts chemically with the silane surface treatment on glass fibers, is also effective in wetting the surface of aluminum fibers. Although MPP is known to bond strongly to metal surfaces, poor tensile strength has been obtained in this work for the composites containing MPP at a concentration of 5 percent by weight relative to the steel fiber mass. As demonstrated in *Fig. 3*, higher concentrations of MPP are required.

The theory of Kelly and Tyson (8) predicts the following relations between the tensile strength and composition:

$$\sigma_c = \bar{V}_f(1 - l_c/2l)\sigma_f + (1 - \bar{V}_f)\sigma_m \text{ (for } l \geq l_c) \quad (1)$$

$$\sigma_c = \bar{V}_f \tau_m l/d + (1 - \bar{V}_f)\sigma_m \text{ (for } l \leq l_c) \quad (2)$$

where $\bar{V}_f$ is the volume fraction of fibers; σ_f and σ_m are the tensile strengths of the fiber and matrix, respectively; l and d are the length and diameter of the fiber, respectively; τ_m is the shear strength of the matrix; and l_c is a critical fiber length given by

Table 4. Tensile Properties of Polypropylene/Steel Fiber Composites at 25°C and Strain Rate of 50 m…/min.

Additive	Material Code	Tensile Strength (MPa)	Elongation at Break (%)	Tensile Modulus (MPa)
None	PP (Compressed Powder)	29.2	2.0	854
	PP (Roll-milled Sheet)	31.5	5.1	864
	P-3	15.3	1.7	914
	P-5	14.2	1.3	1167
	P-10	13.2	1.3	1312
	P-12	12.4	1.4	1316
	P-15	12.5	1.3	1499
	P-20	11.2	1.3	1576
MPPW	Q-3	32.5	3.5	986
	Q-5	32.0	2.5	1196
	Q-10	29.4	2.1	1345
	Q-12	27.3	1.9	1364
	Q-15	28.1	2.0	1582
	Q-20	19.5	1.5	1585
MPP	R-3	31.5	2.3	1000
	R-5	28.3	1.2	1125
	R-10	16.1	1.5	1334
	R-12	14.7	1.2	1327
	R-15	13.5	1.4	1476
	R-20	12.1	1.4	1558

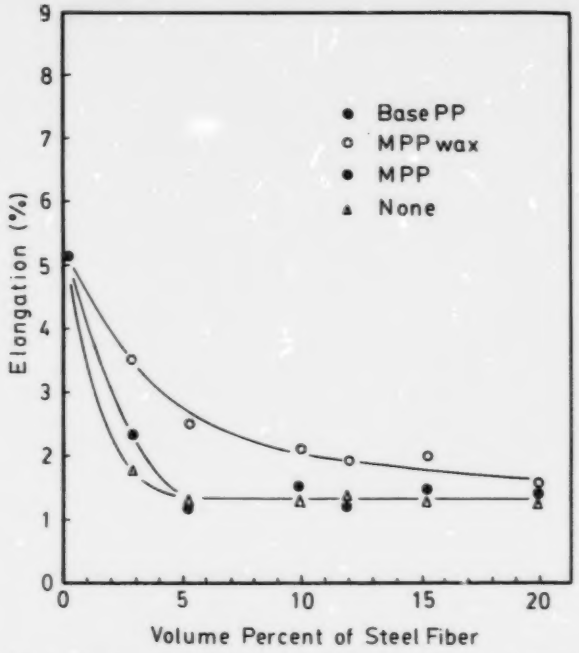

Fig. 4. Maximum elongation at break of polypropylene/steel fiber composites as a function of steel fiber concentration.

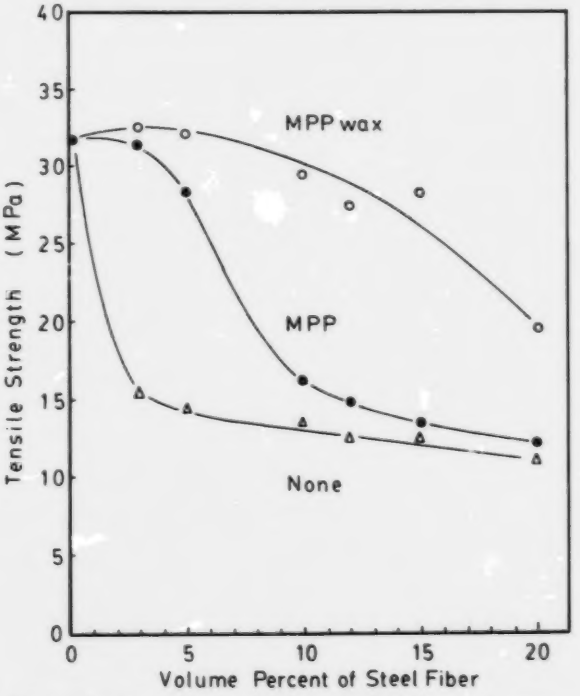

Fig. 5. Tensile strength of polypropylene/steel fiber composites as a function of steel fiber concentration.

$$l_c = d\sigma_f/2\tau_m. \quad (3)$$

The Kelly-Tyson theory is based on the idea of stress transfer along the length of the fiber. For long fibers (*Eq 1*), the strength of the fiber (σ_f) becomes increasingly important, whereas for short

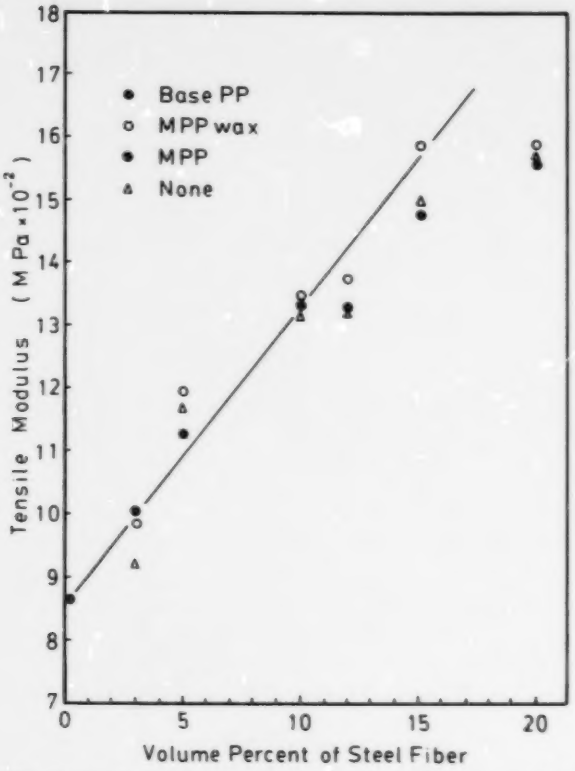

Fig. 6. Tensile modulus of polypropylene/steel fiber composite as a function of steel fiber concentration.

fibers (*Eq 2*), the strength of the fiber does not enter into the equation. Here the fibers act to redistribute the stress within the matrix rather than to transfer it to the fiber. Both *Eq 1* and 2 predict that, at low fiber concentration, σ_c should increase with $\bar{V}_f$.

Patel and Bogue (9) applied the Kelly-Tyson model to short glass fiber-filled amorphous polystyrene. They assumed the shear strength of the matrix to be $\tau_m = \sigma_m/2$, and they used glass fibers with fiber diameter $d = 12$ μm and aspect ratio $p = 34$. Substituting these values into *Eq 2* resulted in

$$\sigma_c = 16\bar{V}_f\sigma_m + \sigma_m \qquad (4)$$

which qualitatively agreed with their experimental data.

Unfortunately, the Kelly-Tyson model cannot be applied to our composites containing a crystalline polypropylene matrix. The mechanism of stress transfer at the polypropylene steel fiber interface is different from the model of the Kelly-Tyson theory. In order to obtain qualitative agreement, we would have to assume $\tau_m \leqslant \sigma_m/50$.

In *Fig. 6* the initial tensile moduli of the three series of composites are shown. All three series of composites appear to follow the same pattern of modulus rise with fiber concentration.

For low loadings, the tensile modulus of the composites (E_c) may be expressed as follows:

$$E_c = E_m (1 + B\,\bar{V}_f) \qquad (5)$$

where E_m is the tensile modulus of the matrix, and B is a constant (9). For spheres, $B = 2.5$ was given by Smallwood (10) and Guth (11). For rigid rods, Goddard (12) calculated:

$$B = 2p^2/9ln(p) \qquad (6)$$

where p is the aspect ratio. From *Eq 6* for steel fibers, with $p = 50$ as used in the present study, $B = 142$. On the other hand, from the slope of the line in *Fig. 6*, $B = 5.7$. The steel fibers, even though they are shaped like rods, effectively behave as spheres with random fiber orientation. Similar behavior has been reported for short glass/fiber-filled polystyrene, where B takes on rod-like values only at increasing fiber orientation (9). It is worth noting that in series *Q* (with MPPW), only samples containing 20 volume percent of filler deviate from the linear dependence predicted by *Eq 5*.

Impact Properties

The present study has employed a high-speed linear-impact test. This method is useful for measurement of the impact properties of plastic sheets. There is no need to prepare notched samples, which frequently lead to stress localization at the notch, and subsequently cause fracture by crack propagation rather than by the crack initiation mechanism.

The results of impact tests are summarized in *Table 5* and *Fig. 7*. For composites, the values of ultimate force at break are lower than for PP. The composites containing MPPW have relatively higher values than the two other series. While the ultimate force at break has a tendency to increase with the steel fiber content, the ultimate deflection at break remains approximately constant, independent of the steel fiber content and addition of coupling agents. In *Fig. 7*, the ultimate absorbed impact energy is plotted as a function of the volume percent of steel fibers. Excepting the *Q*-series, the two others show embrittlement upon addition of the filler. This type of embrittlement has also been observed with polymers filled with short glass fibers (13). The premature crack initiation due to the stress intensities at the ends of the fibers generally reduces the impact strength.

At higher loadings, the impact strength increases with concentration, especially for the composites containing MPPW. This recovery in the impact strength at higher fiber concentrations has also been reported for chemically modified polypropylene/glass fiber systems (13).

Oxygen and Water Vapor Permeabilities

Polypropylene is known to have high oxygen and low water vapor permeability. This was confirmed by the measurements reported in *Table 6* and *Figs. 8* and 9. However, contrary to expectation both permeabilities show an increase with fiber content. The increases are particularly rapid for the P-series of samples without coupling agent.

Laird (14) reported that the rate of diffusion of water along the glass-resin interface was 450 times as high as that through the resin alone, and that the

Table 5. Impact Properties of Polypropylene/Steel Fiber Composites at Impact Speed of 19.05 m/min.

Additive	Material Code	Ultimate Force at Break (Kg)	Ultimate Deflection at Break (mm)	Ultimate Absorbed Energy (Kg·cm)	Modulus (Kg/mm)
None	PP (Compressed Powder)	88.1	5.5	16.6	21.7
	PP (Roll-milled)	25.4	4.7	5.5	9.4
	P-3	6.3	4.8	2.3	3.4
	P-5	5.5	4.8	2.5	3.5
	P-10	5.6	5.2	3.2	3.4
	P-15	8.2	5.1	4.4	6.2
	P-20	13.0	4.9	5.8	6.9
MPPW	Q-3	16.8	4.6	5.8	4.4
	Q-5	20.1	5.1	6.2	5.0
	Q-10	23.5	5.3	8.3	5.0
	Q-12	25.0	5.2	9.0	6.4
	Q-15	27.4	5.4	10.8	9.9
	Q-20	25.2	5.4	7.8	7.8
MPP	R-3	11.4	5.3	4.2	4.9
	R-5	11.0	4.5	3.9	3.9
	R-10	13.2	5.2	4.8	4.7
	R-12	12.5	4.8	6.0	5.3
	R-15	15.1	4.9	5.5	7.5
	R-20	13.5	5.0	6.7	5.2

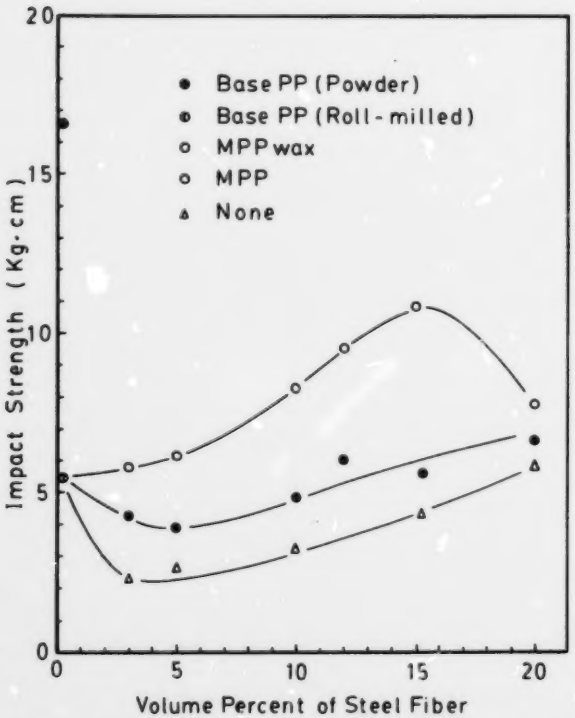

Fig. 7. Ultimate absorbed energy at break in impact force of polypropylene/steel fiber composites as a function of steel fiber concentration.

rate becomes considerably smaller when a coupling agent is used.

The permeability of multiphase systems is frequently expressed in terms of the Maxwell (the shape factor, $f = 2$) and Raleigh ($f = 1$) equations (15–17):

$$\tilde{P} = 1 + (f+1)(\tilde{P}_2 - 1)\bar{V}_f/[(\tilde{P}_2 + f) - (\tilde{P}_2 - 1)\bar{V}_f] \quad (7)$$

Table 6. Oxygen and Water Vapor Permeabilities of Polypropylene/Steel Fiber Composites

Material Code	Oxygen Permeability[1] Constants ($\times 10^{10}$)	Water Vapor Permeability[2] Constants ($\times 10^{11}$)
PP (Roll-milled)	991	5.69
P-3	—	16.3
P-5	4.46×10^5	19.3
P-10	—	169.4
Q-3	1067	6.39
Q-5	2109	7.44
Q-10	1.43×10^4	15.4
Q-12	—	21.2
Q-15	5.68×10^5	27.0
Q-20	3.83×10^6	112.3

(1) $cm^3 \cdot cm/cm^2 \cdot s$ Pa, 25°C, 0% R.H.
(2) $g \cdot cm/cm^2 \cdot s$, 37.8°C, 100° R.H.

where $\tilde{P} = P/P_1$ and $\tilde{P}_2 = P_2/P_1$ are the reduced permeabilities of the composite and dispersed phase respectively, and P_1 is the continuous phase permeability (*Fig. 9*).

It can be seen that, in order to predict the dependence reported in *Table 6*, one would have to assume negative values of P_2 (*Eq. 7*, as well as the Higuchi equation). The simple parallel or series models cannot represent the observed behavior. Clearly there is need for a new approach.

The observed increase of P and $\bar{V}_f$ can be understood by assuming that incorporation of each fiber into the system brings in a layer of high permeability. For permeability, as for conductivity, the fiber-fiber interactions are of great importance. The incremental increase of P can be written as:

$$dP = P(a + 2b\bar{V}_f)d\bar{V}_f \quad (8)$$

where a and $2b$ represent the relative "intrinsic" permeabilities of the incorporated fibers within the diluted and coupled interaction regions, respectively. Integration and rearrangement lead to:

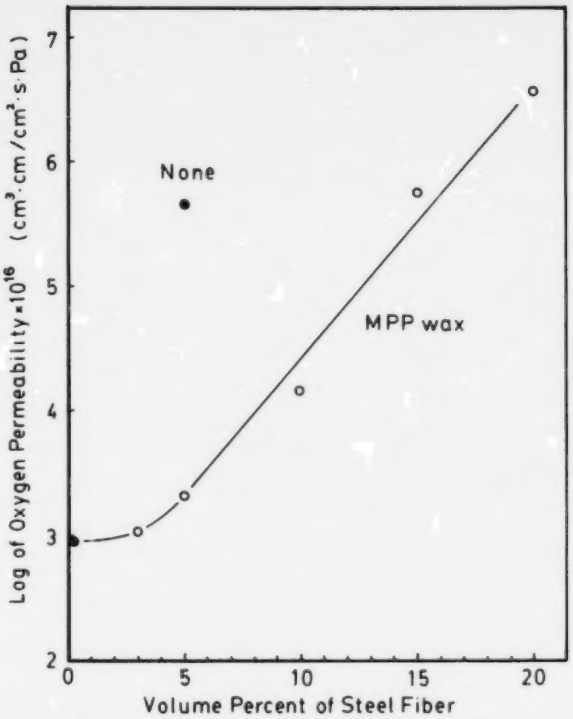

Fig. 8. Oxygen permeabilities of polypropylene/steel fiber composites as functions of steel fiber concentration.

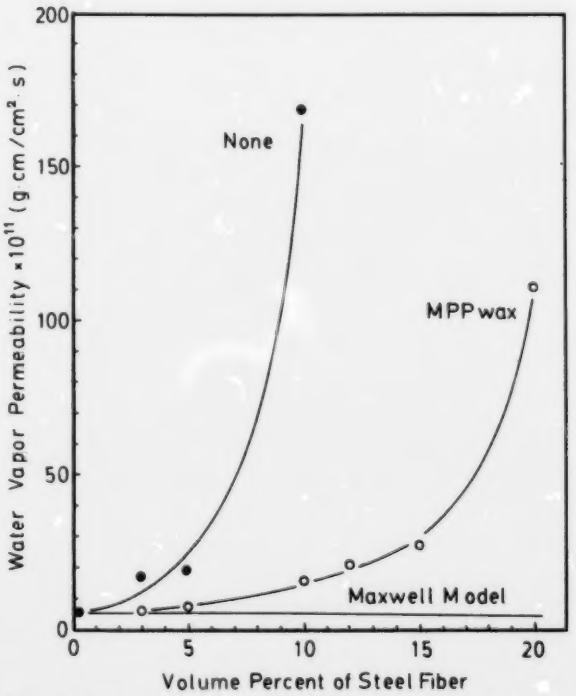

Fig. 9. Experimental and computed water vapor permeabilities of polypropylene/steel fiber composites as functions of steel fiber concentration.

$$Y = (ln\ \tilde{P})/\bar{V}_f = \tilde{P}_{2,0} + k\tilde{P}^2_{2,0}\bar{V}_f \qquad (9)$$

where $\tilde{P}_{2,0} = \lim_{\bar{V}_f \to 0} Y = a$, and $b = k\tilde{P}^2_{2,0}$, k being the interaction constant. To test this relation, the data for series Q (*Table 6*) were used. The results are shown in *Table 7*.

It can be seen that good correlation is obtained, and $\tilde{P}_{2,0}$ has a reasonable value. Since permeability of steel is practically zero, $\tilde{P}_{2,0} = 1$ to 2 indicates that, with each fiber, a highly permeable void-channel is being incorporated. It can be seen that this channel is relatively larger for H_2O than for O_2. This difference may be explained by the layer of MPPW, swollen during the pre-measurement conditioning of the samples at 100 percent RH. On the other hand, the total relative permeability, $\tilde{P}$, for O_2 is about 11-times higher than that for H_2O. This difference is due to the much higher energy of interaction between H_2O and the void channels than that for O_2.

The permeability of semi-crystalline polymers such as polyethylene, polypropylene and polyamide, decreases with an increase of the crystallinity (18). Michaels and Parker (19) have proposed that two impedance factors act to reduce the diffusion constants in semi-crystalline polymers below the values anticipated in completely amorphous polymers. Their expression is formulated as follows:

$$P = DS \qquad (10)$$

$$D = D_a/\tau\beta \qquad (11)$$

$$S = \bar{V}_a S_a \qquad (12)$$

where P is the permeability constant in the semi-crystalline polymer; D and D_a are the diffusion constants in the semi-crystalline polymer and the completely amorphous polymer, respectively; S and S_a are the solubility constants in the semi-crystalline polymer and in the completely amorphous polymer, respectively; and $\bar{V}_a$ is the volume fraction of amorphous material. τ is a geometric impedance factor accounting for the reduction in diffusion constant due to the necessity of molecules to bypass crystallites and move through the amorphous regions of non-uniform cross-sectional area. This quantity is commonly called the tortuosity factor. β is a chain immobilization factor, which takes into account the reduction in amorphous chain segment mobility due to proximity of the crystallites. β is also regarded as a gas-molecular-size-dependent geometric impedance term (20).

The geometric impedance factor τ increases with the increase of crystallinity in slowly cooled polyethylene samples (16, 19). However, Michaels *et al* (20) have observed that in polyethylene, τ decreases on annealing at elevated temperatures, de-

Table 7. Parameters of Equation 9 Computed for Oxygen and Water Vapor Permeabilities of Samples Q

Parameter	Permeability of O_2	Permeability of H_2O
least square correlation coefficient, r^2	0.927	0.955
$a = \tilde{P}_{2,0}$	1.064	1.881
$b = k\tilde{P}^2_{2,0}$	231.2	66.6
k	204.2	18.8

spite an increase in crystallinity. Similar results have been obtained for polypropylene (21) and cold-rolled polyethylene (22). On annealing of semi-crystalline polymers, there is a reduction of volume due to the increase of density. Crystallization can be considered to be associated with the formation of thick lamellas with a high concentration of intralamellar imperfections. The presence of intralamellar defects or voids within the lamellar bounderies has been postulated to account for the increase in the values of permeability.

The polypropylene/steel fiber samples were slowly cooled from the melt. The isotactic polypropylene crystallizes in the form of high density monoclinic crystals. At the same time, the volume change of the steel fibers is very small. This suggests that formation of voids at the polypropylene-steel fiber interface is to be expected. In particular, this should occur in the case of weak bonding between polypropylene and steel fibers.

It is known that the blending of polyamide into polyethylene reduces the oxygen permeability (23). The effects of blending of polyamide-6 into polypropylene and polypropylene/steel fiber composites on the oxygen and water vapor permeabilities are shown in *Table 8* and *Figs. 10* and *11*. As expected, incorporation of polyamide-6 reduces oxygen permeability of the matrix. The experimental data of polypropylene/polyamide-6 blends show lower values than those predicted from *Eq 7* (24–26). Similar results have been obtained for polypropylene/polyamide blends (23).

The oxygen permeabilities of composites filled with 5 and 15 volume percent steel fibers also decrease with an increase in the concentration of polyamide-6, although in the latter case, the decrease is less pronounced at the higher PA-6 levels.

The increase of water vapor permeabilities in the composites filled with 5 volume percent of steel fibers is similar to that of the unfilled PP/PA-6 blends. However, the composite filled with 15 volume percent steel fibers shows quite high values of water vapor permeability. This suggests that the polyamide-fiber wetting is poor. Thus, a substantial number of continuous diffusive pathways exist in the composite filled with 15 volume percent of steel fibers.

Table 8. Oxygen and Water Vapor Permeabilities of Polypropylene/Polyamide-6 Blends and Polypropylene/Polyamide-6/Steel Fiber Composites

Material Code	Oxygen Permeability[1] Constants (× 10^{10})	Water Vapor Permeability[2] Constants (× 10^{11})
N-0 (PP)	991	5.69
N-10	741	5.90
N-20	576	6.83
N-30	374	8.95
N-40	253	10.2
NF-10-5	1611	6.77
NF-20-5	1212	7.96
NF-30-5	903	10.0
NF-40-5	778	14.2
NF-10-5	2.4×10^5	55.7
NF-20-15	9.5×10^4	87.8
NF-30-15	6.2×10^4	157.0
NF-40-15	6.3×10^4	188.9

(1) $cm^3 \cdot cm/cm^2 \cdot s \cdot Pa$, 25°C, 0% R.H.
(2) $g \cdot cm/cm^2 \cdot s$, 37.8°C, 100° R.H.

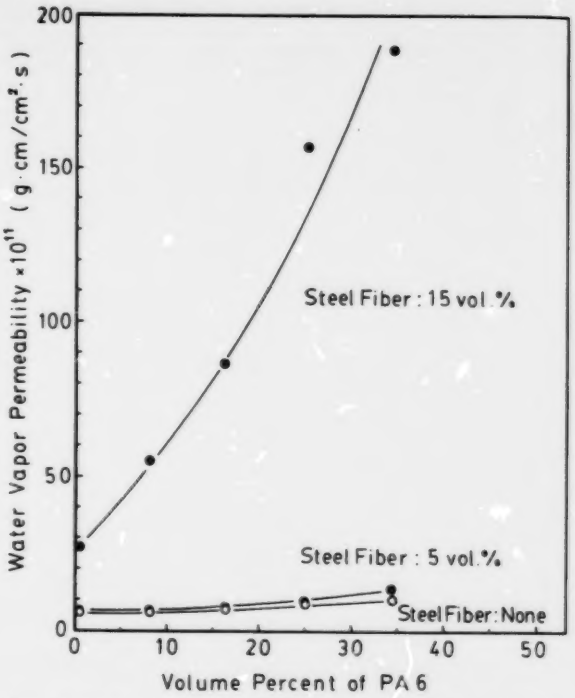

Fig. 10. Water vapor permeabilities of polypropylene/polyamide-6 blends and polypropylene/polyamide-6/steel fiber composites as functions of polyamide-6 concentration.

It is interesting to analyze these data, using the proposed *Eq 9*. Such an analysis suggests that addition of PA-6 causes a change in the mechanism of oxygen permeability. Thus, $\tilde{P}_{2,0}$ increases, whereas k decreases with PA-6 content. This most likely is related to spherical void formation between the PP and PA-6 domains. On increasing the PA-6 content, the steel fibers are more likely to be incorporated into the PA-6 domains, which causes a reduction of connectivity. In the case of water vapor permeability, $\tilde{P}_{2,0}$ remains virtually constant, and k seems to increase slightly with PA-6 content. Enhancement of water vapor permeability through the voids adjacent to the PA-6 phase is to be expected.

SEM Observations

The experimental data regarding oxygen and water vapor permeabilities suggest the existence of voids at the matrix-steel fiber and PP/PA-6 interfaces. In order to examine the fiber wettability, the fractured samples were observed under SEM. Selected micrographs are shown in *Figs. 12* to *22*. In *Figs. 14, 15, 20* and *21*, 'A' denotes the photomicrographs and 'B' the corresponding Fe maps, which indicate the locations of the fibers.

There was no visible void at the polypropylene-steel fiber interface of the Q-3 sample (steel fiber = 3 volume-percent, addition of MPPW) shown in *Fig. 12*. On the other hand, voids were detected at

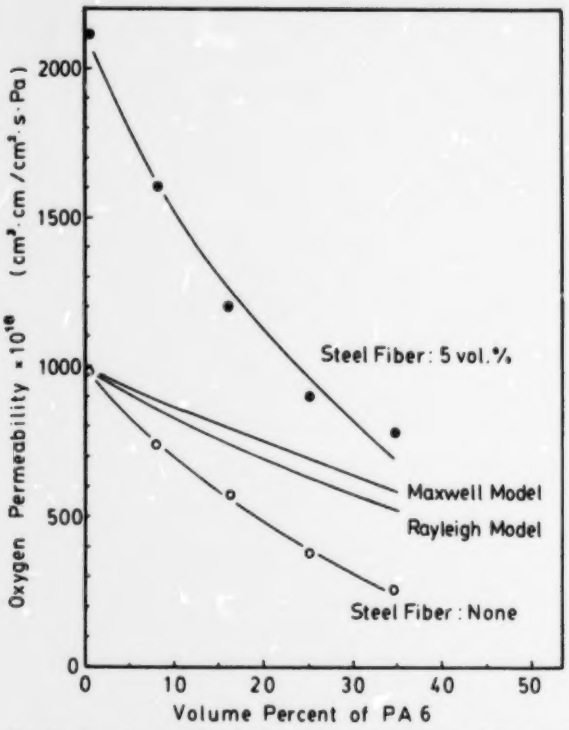

Fig. 11. Experimental and computed oxygen permeabilities of polypropylene/polyamide-6 blends and polypropylene/polyamide-6/steel fiber composites as functions of polyamide-6 concentration.

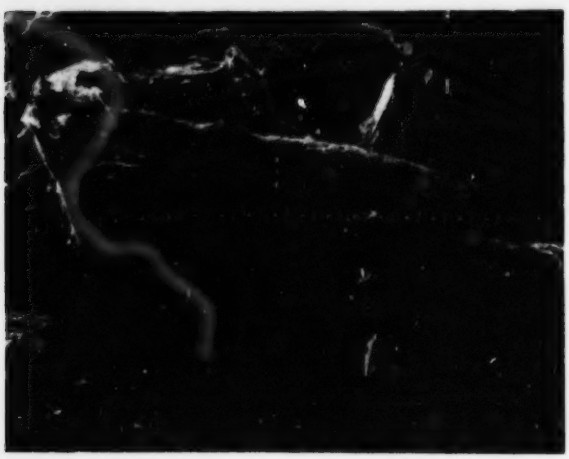

Fig. 12. Scanning Electron Micrograph of a fractured surface of polypropylene/steel fiber composite Q-3 (steel fiber: 3 vol %, with MPPW).

the polypropylene-steel fiber interface of the P-3 sample (steel fiber = 3 volume percent, no coupling agent, see *Fig. 13*). In *Fig. 14*, it was observed that in sample Q-3, the bonding between polypropylene and MPPW-treated steel fiber was good. Although polypropylene appeared to adhere to the steel fiber in the P-3 sample, in the absence of a coupling agent (*Fig. 15*), voids were observed at the polypropylene matrix-steel fiber interface.

Comparing the micrographs in *Fig. 16* for the Q-

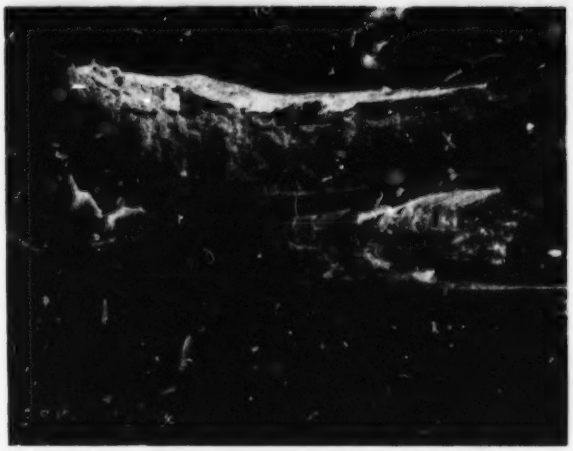

Fig. 13. Scanning Electron Micrograph of a fractured surface of polypropylene/steel fiber composite P-3 (steel fiber: 3 vol %, without a coupling agent).

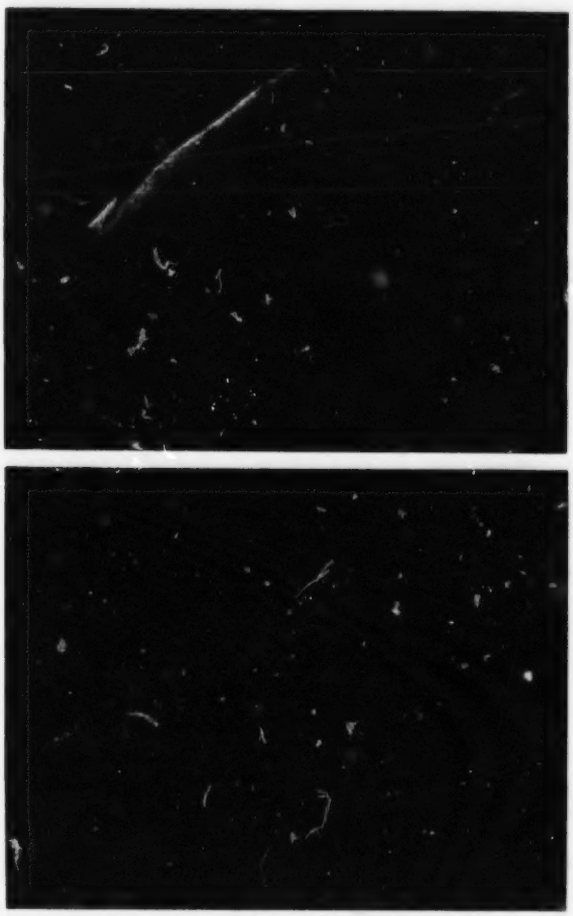

Fig. 14. Scanning Electron Micrograph of a fractured surface of polypropylene/steel fiber composite Q-3 (steel fiber: 3 vol %, with MPPW).

5 sample (steel fiber = 5 volume-percent, addition of MPPW) and in *Fig. 17* for the P-5 sample (steel fiber = 5 volume-percent, no coupling agent), it is clear that MPPW is an effective binder. In *Figs. 18*

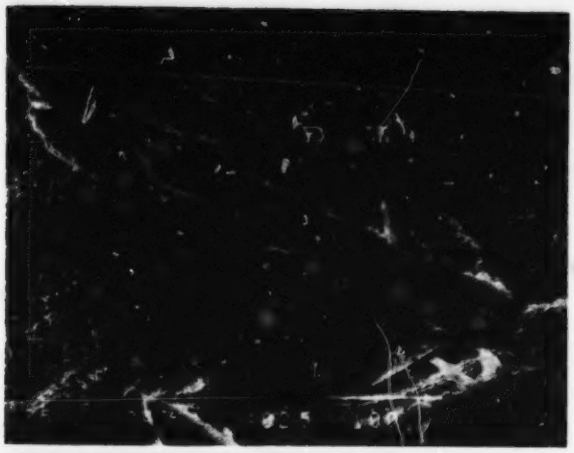

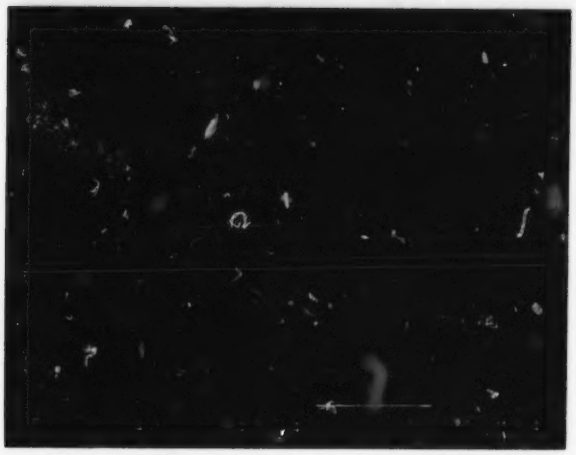

Fig. 15. Scanning Electron Micrograph of a fractured surface of polypropylene/steel fiber composite P-3 (steel fiber: 3 vol %, without a coupling agent).

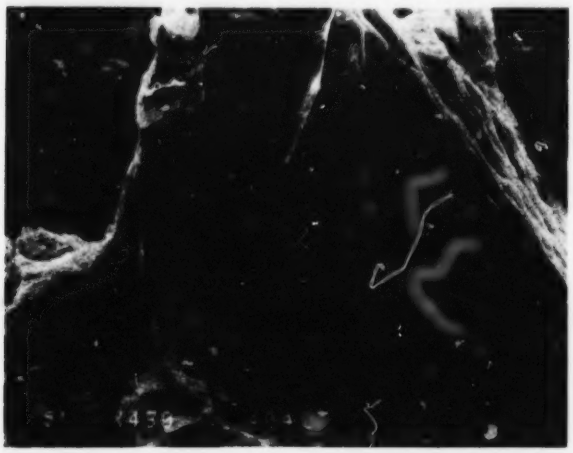

Fig. 16. Scanning Electron Micrograph of a fractured surface of polypropylene/steel fiber composite Q-5 (steel fiber: 5 vol %, with MPPW).

and 20, the SEM micrographs of the highly loaded Q-15 sample (steel fiber = 15 volume-percent, addition of MPPW) are presented. Here again voids were detected at the boundaries between the ma-

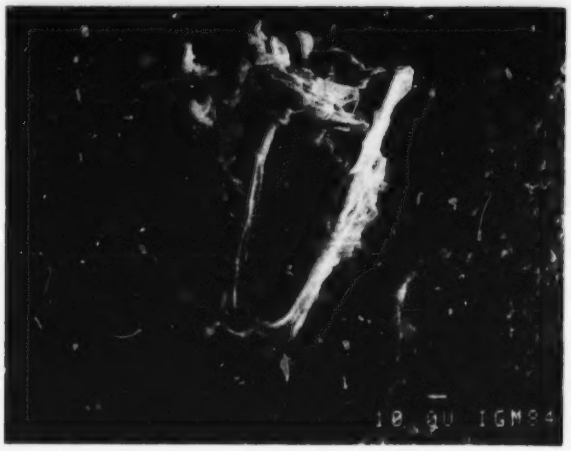

Fig. 17. Scanning Electron Micrograph of a fractured surface of polypropylene/steel fiber composite P-5 (steel fiber: 5 vol %, without a coupling agent).

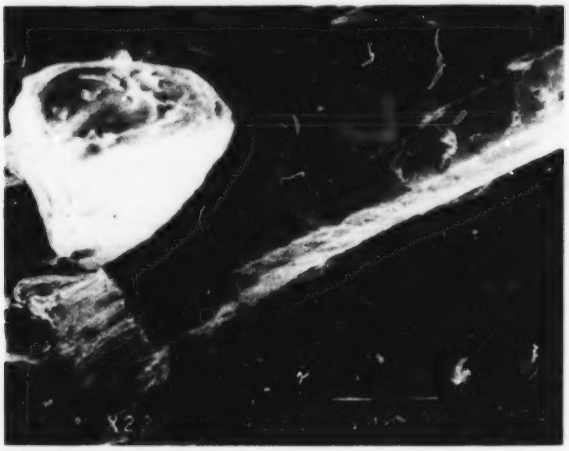

Fig. 18. Scanning Electron Micrograph of a fractured surface of polypropylene/steel fiber composite Q-15 (steel fiber: 15 vol %, with MPPW).

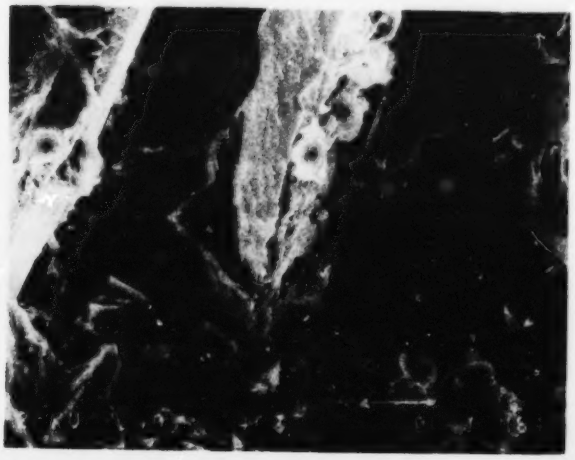

Fig. 19. Scanning Electron Micrograph of a fractured surface of polypropylene/steel fiber composite P-5 (steel fiber: 5 vol %, without a coupling agent).

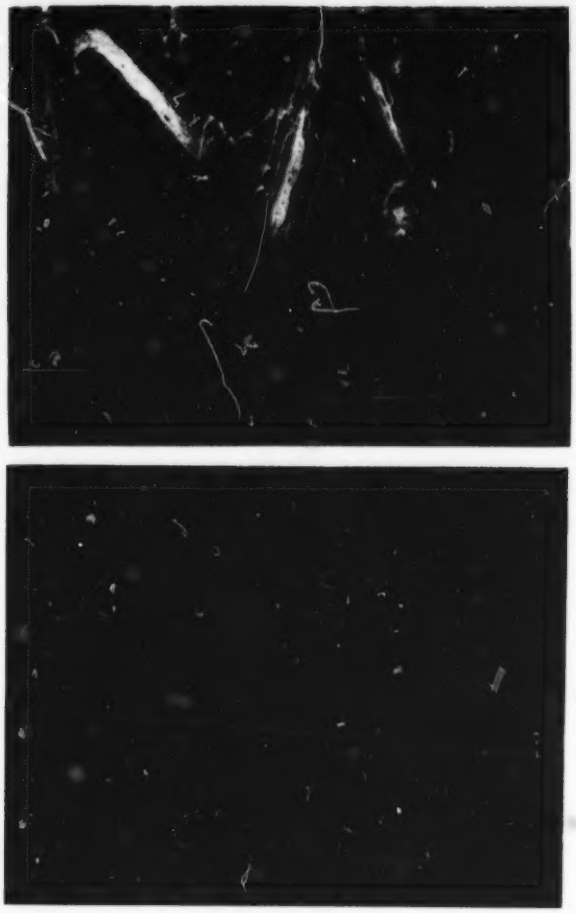

Fig. 20. Scanning Electron Micrograph of a fractured surface of polypropylene/steel fiber composite Q-15 (steel fiber: 15 vol %, with MPPW).

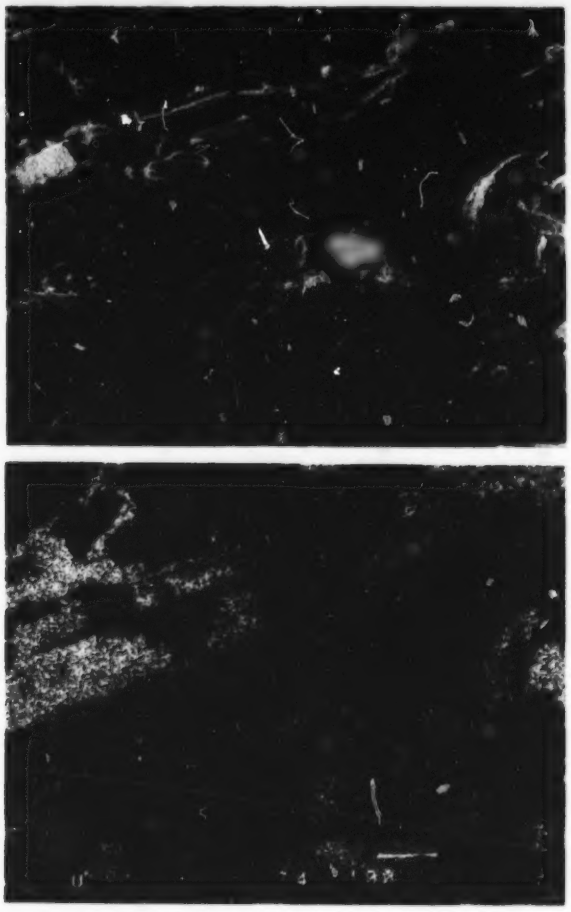

Fig. 21. Scanning Electron Micrograph of a fractured surface of polypropylene/steel fiber composite P-15 (steel fiber: 15 vol %, without a coupling agent).

trix and the fibers. In the present study, MPPW was dry-blended with the steel fibers prior to roll-milling. Therefore, it is probable that the fibers were not uniformly coated. Some voids could be produced at the weakly bonded matrix-steel fiber interface by shrinkage during crystallization. The connectivity of steel fibers increases in the highly loaded composites, and the opportunities for formation of continuous diffusive pathways augment. The rapid increase of oxygen and water vapor permeabilities at high loading, even in the presence of MPPW, seems to be caused by the formation of these continuous diffusive pathways. *Figures 19* and *21* show the micrographs of P-15 samples (steel fiber = 15 volume-percent, no coupling agent). The fractured surfaces of P-15 samples are very rough, and many voids are noted at the matrix-steel fiber interface as well as in the matrix itself. The fractured matrix surfaces also indicate the brittle nature of polypropylene fracture at liquid-nitrogen temperature. The reason that the *P*-series of composites have higher oxygen and water vapor permeabilities than the *Q*-series seems to be the consequence of the formation of a porous structure in the *P*-series especially at high loading.

The SEM micrographs in *Fig. 22* show the fractured surface of NF-40-15 sample (matrix: polypropylene/polyamide-6 = 60/40 in weight, steel fiber = 15 volume-percent). Polyamide-6 is randomly dispersed in the form of spheres in the polypropylene phase. There are also voids at the matrix-steel fiber interface. MPPW seems to be ineffective for this matrix.

CONCLUSION

The results reported here suggest that MPPW is an effective coupling agent for polypropylene/steel fiber composites. When the MPP concentration is 5 weight-percent, based on the content of steel fibers, it was found to be ineffective as a binder. Higher concentration of MPP would be reqired to improve polypropylene/steel fiber bonding.

The polypropylene/steel fiber composites become conductive at a volume loading of 8 to 10 percent, and, at this steel fiber volume fraction, the volume resistivity of the composites is approximately 10 ohm cm. The volume resistivity falls to a level of 1 to 2 ohm cm at volume loading at 20 percent.

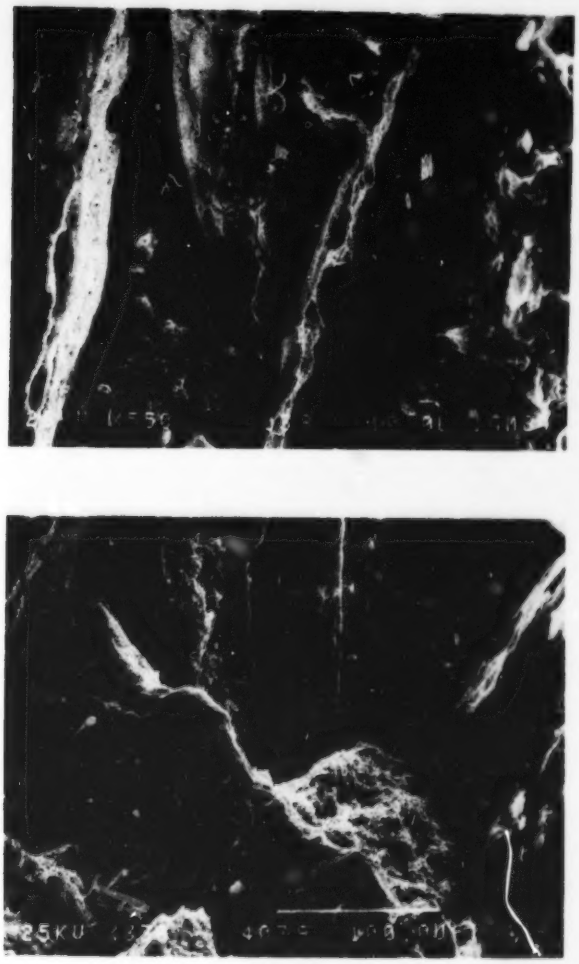

Fig. 22. Scanning Electron Micrograph of a fractured surface of polypropylene/polyamide-6/steel fiber composite NF-40-15 (polypropylene/polyamide-6 = 60/40 in weight, steel fiber: 15 vol %, with MPPW).

The deterioration in tensile and impact properties has often been observed in the case of short fiber-filled polymer composites. However, the above results show that the deterioration of tensile and impact properties of the composites containing MPPW as a coupling agent is minor at the 10 percent volume loading needed to initiate electrical conductivity.

The oxygen and water vapor permeabilities of the polypropylene/steel fiber composites increase with the steel fiber concentration. The increase of permeabilities of the composites containing MPPW as a coupling agent is smaller than that of the composites containing no coupling agent. The difference in the permeability behavior of these two series is related to the amount of voids at the matrix-steel fiber interface. SEM observations confirm that the rapid increase of permeabilities at high steel fiber loadings is caused by formation of the continuous pathways along the matrix-steel fiber interface. Addition of polyamide-6 into the composites reduced the oxygen permeability and, at 5 volume percent of steel fibers did not adversely affect the water vapor permeability.

ACKNOWLEDGMENTS

The authors would like to express their gratitude to the following NRCC/IMRI personnel: M. Thibodeau for the SEM studies, Messrs. F. Hamel, Y. Simard, and P. Sammut for aiding in the preparation of composites and measurement of permeabilities and tensile properties. Financial support of Toyo Seikan Kaisha, Ltd., The National Science and Engineering Research Council of Canada, and the Ministère de l'Éducation, Gouvernement du Québec are also gratefully acknowledged.

REFERENCES

1. P. J. LeBlanc and D. L. Reinhard. *Electronic Packaging and Production*, 95 (Feb. 1975).
2. J. Gurland, *Trans. Met. Soc. AIME*, **236**, 642 (1966).
3. D. M. Bigg, *Polym. Eng. Sci.*, **17**, 842 (1977).
4. D. M. Bigg, *Composites*, **10**, 95 (1979).
5. D. M. Bigg and E. J. Bradbury, *Polym. Sci. Technol.*, **15**, 23 (1981).
6. R. P. Tolokan, *Technical Papers*, Annual Technical Conference, Society of Plastic Engineers, **30**, 699 (1984).
7. T. Nakagawa, A. Yanagisawa, and H. Koyama, *Polym. Preprints, Japan*, **32**, 3033 (1983).
8. A. Kelly and W. R. Tyson, *J. Mech. Phys. Solid*, **13**, 329 (1963).
9. P. D. Patel and D. C. Bogue, *Polym. Eng. Sci.*, **21**, 449 (1981).
10. H. Smallwood, *J. Appl. Phys.*, **15**, 758 (1944).
11. E. Guth, *J. Appl. Phys.*, **16**, 29 (1945).
12. J. D. Goddard, *Polym. Eng. Sci.*, **19**, 125 (1979).
13. F. Ramsteiner and R. Theyson, *Composites*, **10**, 111 (1979).
14. J. A. Laird, NASA, Doc. N63-20121, 64 (1963).
15. J. C. Maxwell, "Electricity and Magnetism," 3rd ed., Vol. 1, Dover, New York (1904).
16. A. S. Michaels and H. J. Bixler, *J. Polym. Sci.*, **L**, 413 (1961).
17. R. M. Barrer, J. A. Barrie, and M. G. Rogers, *J. Polym. Sci.*, Part A1, 2565 (1963).
18. S. W. Lasoski and W. H. Cobbs, Jr., *J. Polym. Sci.*, **36**, 21 (1959).
19. A. S. Michaels and R. B. Parker, Jr., *J. Polym. Sci.*, **41**, 53 (1959).
20. A. S. Michaels, H. J. Bixler, and H. L. Fein, *J. Appl. Phys.*, **35**, 3165 (1964).
21. W. Vieth and W. F. Wuerth, *J. Appl. Polym. Sci.*, **13**, 685 (1969).
22. T. Katsura, *Kobunshi Ronbunshu*, **37**, 581 (1980).
23. M. R. Kamal, I. A. Jinnah, and L. A. Utracki, NRCC/IMRI Symposium "Polyblends-'84," Boucherville, Quebec, Canada, Apr. 17, 1984; *Polym. Eng. Sci.*, **24**, 1337 (1984).
24. W. I. Higuchi and T. Higuchi, *J. Am. Pharm. Assoc., Sci. Ed.*, **49**, 598 (1960).
25. C. A. Peterson, *J. Appl. Polym. Sci.*, **12**, 2649 (1968).
26. J. M. Charrier, *Polym. Eng. Sci.*, **15**, 731 (1975).

PANEL DISCUSSION

G. Benson: What type of steel fibers did you use?

T. Katsura: These were short steel fibers with an aspect ratio of 50 prepared by a vibrational cutting method out of mild steel. As shown in SEM, the surface was slightly oxidized with a layer of oxide about 3 nm thick.

G. Benson: Have you done any long term testing for corrosion?

T. Katsura: Not yet.

M. Kortschot: When you added maleated polypropylene or maleated propylene wax it required greater concentration of steel fibers to induce electrical conductivity. I assume that this is so because fibers become encapsulated. Did these coated fiber composites show a normal resistance or a tumbling effect?

T. Katsura: To measure the resistivity, we used compression molded samples with cut away sides pointed with an electrically conducting point. We used an ohmmeter and constant low voltage across. As I mentioned, the layers of the MPP or MPPW should form on the surface of steel fibers. Thus they hinder direct contact between the steel fibers. And the electrical resistivities of those composites seem to be larger than those of the composites without a coupling agent.

H. P. Schreiber: This was a very lovely paper. When you are making Raleigh or Maxwell calculations of the theoretical variation of permeability with fiber content you have to take into account inherent properties of the matrix of the polypropylene. We are doing rather similar work using glass beads as fillers in polypropylene. We found that upon increasing the volume loading, the matrix crystallinity increases. The permeability of the composite is sensitive to the amorphous content, so the baseline is shifting as the calculation involve higher and higher volume loading.

T. Katsura: The effect of crystallinity is minor for our case. As I showed in *Figs. 8* and *9*, the permeability *increases* with loading. Your argument would be valid if the observed permeability was significantly lower than predicted by either the Raleigh or Maxwell equations. We found that these dependencies cannot be used—they would require a negative value of permeability for steel fibers. This was the reason for proposing the new predictive relations which assume high permeability in the areas around the fibers and permit the estimation of the extent of this layer and its connectivity.

H. P. Schreiber: The enhancement of crystallinity caused a relative decrease of permeability by 10 to 15 percent. With glass beads we also found effects similar to yours, i.e., the permeation coefficient goes up with the concentration of uncoated, untreated glass beads. However, through plasma coating we even managed to get a reversed behavior.

J. L. White: Did you consider using the electrical conductivity to measure the fiber orientation? Electrical conductivity is a second order tensor analogous to polarizability. Just as you can measure birefringence to determine the molecular orientation, you should be able to use anisotropic measurements of electrical conductivity to measure the second moments of the orientation distribution of the fibers and then calculate the orientation factors.

T. Katsura: I believe that the fiber orientation in our composites is random, but maybe we should repeat the measurements in all three directions.

Note added in proofs: The second part of this work on: "Electrical and Thermal Properties of Propylene Filled with Steel Fibers", by T. Katsura, M. R. Kamal and L. A. Utracki will be published in Adv. Polym. Technol., 6, (1986).

Electromagnetic Interference Shielding with Nickel-Coated Mica Composites

M. T. KORTSCHOT *and* R. T. WOODHAMS

Department of Chemical Engineering and Applied Chemistry University of Toronto 200 College Street Toronto, Ontario, Canada, M5S 1A4

The topic of electromagnetic interference (EMI) has been reviewed briefly to outline the need for conductive composite materials. The characteristics of a conductive filler which lead to high efficiency at small filler concentrations were examined qualitatively. One of these characteristics, aspect ratio, was examined in detail by using nickel-coated micas as a means of molding composites containing ultra-thin layers of nickel. Using this technique, as little as 1.5 volume percent nickel can provide adequate shielding for 90 percent of current commercial applications.

INTRODUCTION

Electromagnetic interference (EMI) can be defined as spurious voltages and currents induced in electronic circuitry by external sources. In recent years the EMI problem, or electronic pollution as it is sometimes referred to, has received increasing attention. A story in the *Toronto Sun* in August, 1983 reported that Air Canada does not allow the use of personal computers on its flights for fear that radiated electromagnetic waves will interfere with the onboard navigational computers. The Canadian Department of Communications has even issued a warning for pilots using hand held calculators in the cockpit (1).

EMI can originate from a wide variety of sources: electronic circuitry, radios, radar, power lines, electric motors, and fluorescent lighting all contribute to electronic pollution. A common example of the effect of this radiated energy is the "ghost" on a television set.

Faced with increasing amounts of EMI caused in part by the proliferation of electronic devices, government agencies have responded with stringent regulations. For example, FCC Docket #20780 applies to all computing devices in the U.S.A. A computing device is an electronic device with a clock frequency of >10 kHz (2). As of October 1, 1983, all manufacturers of such devices must meet minimum standards for maximum permissible EMI emission.

The protection of electronic circuitry falls into two categories. Conducted EMI, which travels along power leads and data buses, can be attenuated with suitable filters, or compensated for through the use of less sensitive circuitry. Radiated EMI (transmitted through the air) can be stopped with a shielded enclosure, which also blocks EMI radiation from the electronics within the shield.

It is the latter topic, shielding, which is of increasing concern to plastics molders and compounders. The following sections deal with the basics of EMI shielding and the steps required to render polymers useful in this rapidly expanding field.

EMI SHIELDING

An electromagnetic shield is a conductive material which attenuates (through reflection and absorption) radiated electromagnetic energy. Shielding effectiveness (S.E.), is a number which quantifies the amount of attenuation typical of a particular material. It is defined as the ratio of incident to transmitted power and is usually expressed in decibels (dB):

$$\text{S.E.} = 10 \times \log(\text{Pin}/\text{Pout})\text{dB}.$$

Thus 30 dB corresponds to a 99.9 percent reduction in signal power across the shield. Shielding effectiveness can be expressed as the sum of three components (in dB) (see *Fig. 1*):

$$\text{S.E.} = R + A + B$$

R—reflected energy
A—absorbed energy
B—internal multiple reflected energy.

No ASTM standards exist for testing shielding effectiveness, although Committee D9 has completed Emergency Standard ES-7-83 which is currently being approved. ASTM described two practical means of measuring shielding in the laboratory.

The simplest and oldest technique is the shielded box (*Fig. 2*). A measurement of power received with the sample port open is compared with a measurement taken with a sample material inserted in the

port. This is repeated at several frequencies (or swept continuously over the range) to generate a shielding effectiveness spectrum for the material. This technique is recommended for the modeling of near field shielding situations. The shielded box suffers from resonance problems, however, and can produce erroneous results at lower frequencies.

An extension of the shielded box is the shielded room, where the sample separates much larger enclosures. This eliminates some of the resonance problems associated with the smaller box, but is prohibitively expensive to set up and is unlikely to be recommended by ASTM.

To eliminate all resonance problems, a transmission line method may be employed. For this technique, a signal from a coaxial cable is passed through a washer-shaped sample. The impedance of the cable can be adjusted to simulate free space measurements and thus the transmission line is useful for testing far field shielding, (i.e., simulating the protection of equipment from external radiation).

Figure 3 is an illustration of the output from the shielded room facility which was used in the current study.

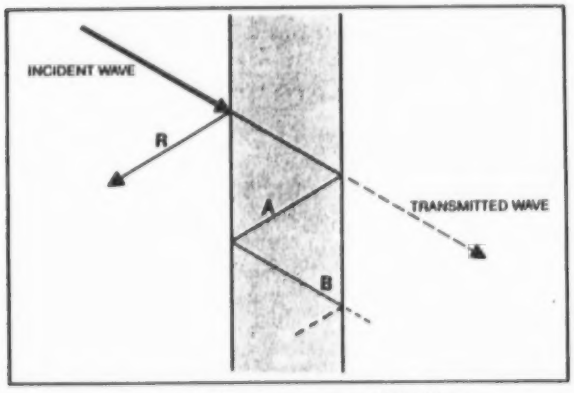

Fig. 1. The three components of shielding.

SHIELDING WITH PLASTICS

In the past, metal housings provided more than adequate shielding for most electronic devices; however, the trend towards non-conductive plastic housings is at odds with the goal of increased shielding effectiveness. Three solutions are available to the plastics molder who requires a conductive part: conductive coatings, conductive fillers, or inherently conductive polymers.

The first approach used by molders was to apply conductive coatings to the molded part. A variety of such techniques are currently in use: conductive paints (3), vacuum metallizing (4), chemical deposition (5), and zinc arc spraying (6) account for most of the market today. Each process has its own advantages which are discussed in the cited references and are summarized by Storms (3). In gen-

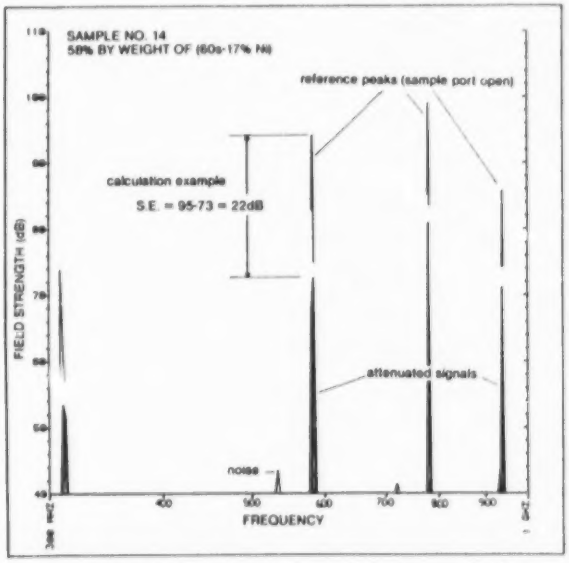

Fig. 3. Typical plotter output from shielded room facility.

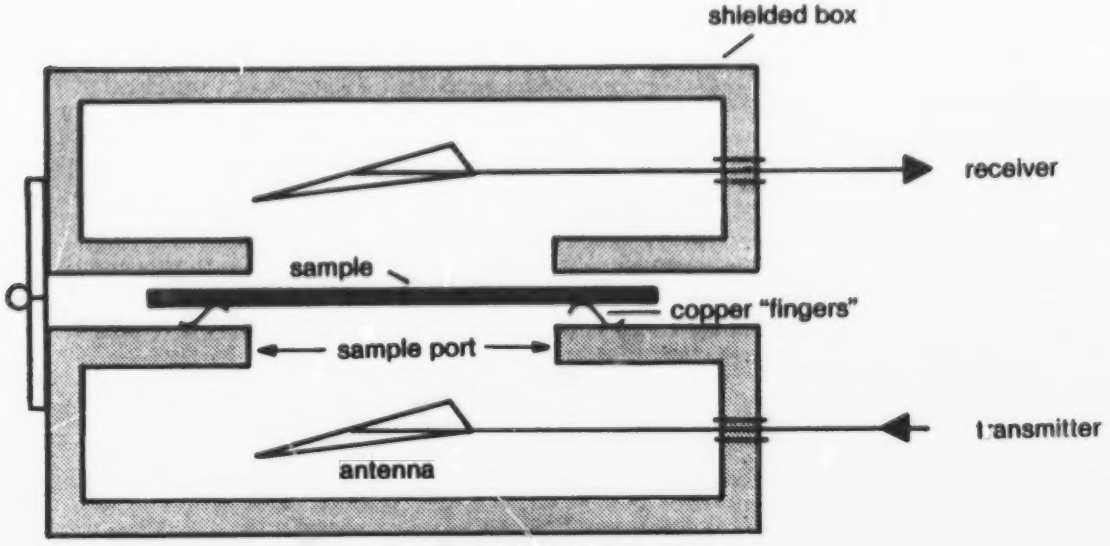

Fig. 2. Shielded box apparatus.

eral, a coating provides a high degree of conductivity (hence good shielding effectiveness), but can involve a labor intensive and time-consuming application procedure.

A second alternative is to incorporate a conductive filler into the plastic resin. Suitable filler materials in use today include steel wires, aluminum flakes, carbon black, metal powders, and metal coated glass fibers, flakes and spheres. Both thermal and electrical conductivities are dramatically increased through the use of metallic or metallized fillers.

A third approach is the use of inherently conductive polymers such as modified poly(p-phenylene sulfide) (7). These polymers are presently experimental, and it is estimated that it will be five to ten years before they become commercially available (8).

It should be apparent from *Table 1* that conductive composites offer some very distinct advantages. Even though spraying operations will soon be automated through robot technology, the capital cost of spraying equipment may be difficult to justify for some applications. The use of conductive fillers requires no equipment modification and provides added benefits such as reduced cycle time and increased thermal conductivity.

A major disadvantage of conductive fillers is the relatively large concentration required to achieve effective shielding. It is the objective of this work to define the conditions needed to increase the efficiencies of conductive fillers so that less material is required.

For many applications, the filled polymer system is preferred, and a recent survey indicates that the U.S. market for EMI fillers may reach $40 million in sales by 1987. (The total market for shielding polymers will be about $300 million.) (9)

CONDUCTIVITY

The concept of conductivity in polymeric materials predates the notion of shielding with polymers by many years. Work on the conductivity of a non-conductive matrix loaded with conductive particles dates back to 1955, and Gurland published his pioneering work on Bakelite-silver composites in 1966 (10).

While it is accepted that conductivity and shielding effectiveness are related, it is impossible for a truly universal one-to-one function to exist. Shielding effectiveness depends not only upon conductivity, but upon the reflection and absorption coefficients for a given filler, and the size, shape, and distribution of the spaces between filler particles. *Figure 4*, which is sometimes quoted in the literature, must therefore be applied with caution, although it is relatively accurate for most conductive composites. In general, a bulk resistivity of less than one ohm-cm would provide about 40 dB of shielding; this would suffice for 95 percent of current commercial applications.

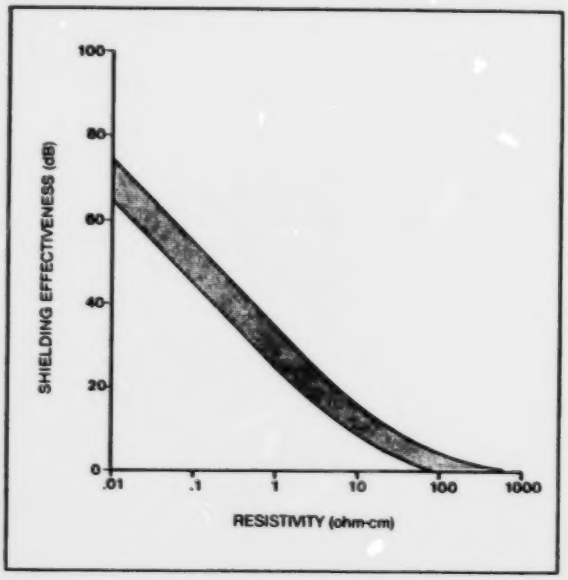

Fig. 4. Shielding effectiveness versus volume resistivity. This curve is not necessarily accurate for all materials.

Table 1. Relative Merits of the Alternatives for Shielding with Plastics*

Technique		Advantages	Disadvantages
Conductive Coating	—paint —arc/flame spray —vacuum metallization —chemical deposition —sputtering	—excellent conductivity, hence good shielding effectiveness —inexpensive, effective use of metal —does not alter mechanical properties —does not affect aesthetics if coating is applied to part interior	—extra processing step —a chip or scratch will cause an EMI "leak" —adhesion and corrosion must be controlled —high capital cost; will involve robot technology —coating thickness hard to control especially when coating complex parts
Conductive Fillers	—carbon black —carbon fibers —aluminum flakes —metallized glass —stainless steel fibers	—economic, one stage processing —little modification to existing machinery —reduced cycle times —increased thermal conductivity —surface damage does not affect integrity of shield	—large loadings required to provide adequate conductivity —fillers often degrade mechanical properties —color limited to silver, brown or black unless painted
Inherently Conductive Polymers	—doped —non-doped	—conductive without modification	—experimental —highly unstable —expensive

*References: Smoluk (24), Wehrenberg (25).

There are two possible electron paths in a filled plastic. The simplest path would be formed by a closed network of touching filler particles. This is the case for relatively high conductivity samples, and is the mechanism of conduction postulated by numerous authors (11, 12). The conductivity of such a composite is proportional to the number of conduction paths.

The existence of a continuous path is not always evident from photographic sections (13). For some polymers, complete filler wetting is expected, particularly in the case of surface treated fillers. The filler particles become encased in a thin film of polymer, effectively insulated from each other. Such a system can still be conductive, and the mechanism of conduction is known as tunneling. Tunneling involves the penetration of an electron through a potential barrier (as opposed to climbing over it), and is explained in quantum mechanical terms (14, 15). The conductivity of this type of composite is a function of the average width of the gap between particles.

The concentration of the conductive particles is the overriding factor determining the composite conductivity, shielding effectiveness, and cost. *Figure 5* illustrates the shape of a resistivity versus concentration curve for virtually any conductive filler.

Up to a critical concentration, the resistivity of the composite is roughly the same as that of the bulk resin. At the critical concentration, or "break point", the percolation threshold is reached as network formation commences, and the resistivity decreases greatly. A few weight percent beyond the break point will invariably produce a composite which has useful conductivity. An "efficient" EMI additive may be defined as one which has a very small critical concentration.

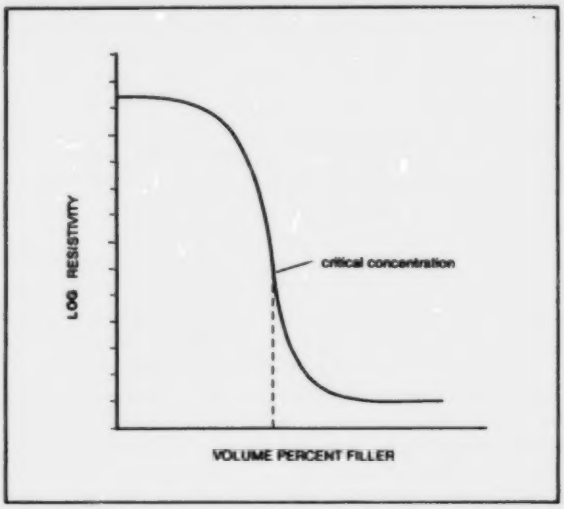

Fig. 5. Universal shape of the resistivity versus loading function for filled polymers.

FILLER EFFICIENCY

What characteristics of a conductive filler determine its efficiency or critical concentration? This question should be of the utmost importance to any producer of these additives. The answer has never been presented as a complete theory, and the rest of this paper will be devoted to a preliminary answer of this fundamental question.

The most obvious property of a filler affecting its critical composition is its density. Since the critical composition is a volume percentage for particles of a given shape, a filler of lower density will have a lower critical composition in terms of its mass percentage. Aluminum and coated microballoons are attractive materials from this point of view.

The rest of the filler efficiency variables are based loosely on the theory of packing, which was established in the 1930's (16, 17). Until now, workers have been interested in obtaining the maximum packing of filler particles so that resin demand could be minimized (18, 19). For an efficient EMI filler, however, the dry packing fraction should be minimized. The particles should form a close packed array at a low concentration. There are a number of ways to ensure that a filler will pack in a loose fashion.

The most inefficient packing (in traditional theory) occurs for narrow size distributions or single sized particles. In this case there are no smaller particles to fill the voids in the framework of contacting large particles. For an EMI filler, monosize particles are preferred. For example, a set of uniform spheres pack randomly to 62.5 percent of their theoretical density, and this is a maximum limit to the volume percentage of conductive spheres required to impart conductivity. If a wide size distribution is used, this upper limit may be as high as 80 percent.

The most important characteristic of any filler, in terms of both packing density and EMI efficiency, is its geometry or aspect ratio. The aspect ratio of a particle is defined loosely as the ratio of the longest to the shortest dimension: for short fibers it is length over diameter, and for flakes it is mean diameter over thickness. Milewski has measured the packing fraction of fibers of various aspect ratios and the relationship is illustrated in *Fig. 11* (19). Spheres, having aspect ratios of one, pack to 62.5 percent theoretical density; fibers with aspect ratios of 100, pack to about 5 percent theoretical density. Thus, if a conductive fiber with an aspect ratio of 100 could be distributed randomly inside a polymer matrix, 5 percent by volume would be the maximum concentration needed to impart conductivity. This is a significant improvement over the 62.5% upper limit for spheres.

Figure 6 is a computer simulation of the effect of aspect ratio on network formation. It is obvious from this illustration and the preceding discussion, that a very high aspect ratio filler is favored for increased conductivity and effective EMI shielding. However, in utilizing this type of flake or fiber it is essential the particles do not break down during processing.

There are two current methods for building du-

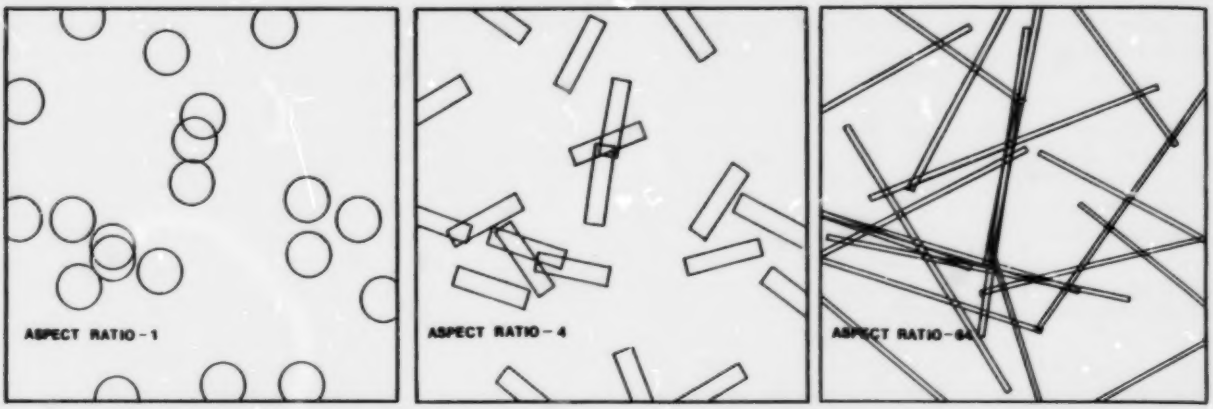

Fig. 6. The effect of aspect ratio on network formation. Each frame contains 20 area percent filler. The filler particles in each frame have the same randomly assigned positions and orientations. [After Davenport (22)].

rable high aspect ratio (HAR) particulate fillers for EMI shielding. One technique is to use a tough and strong material such as stainless steel. Bekaert currently produces 316L SS fibers with very high aspect ratios. One or two volume percent is sufficient to reach the percolation threshold, and this seems quite reasonable in the light of Milewski's theoretical predictions. Using this low concentration of stainless steel does not significantly alter the mechanical properties or appearance of the base resin.

The second method of incorporating HAR particles into a molded composite is to support a thin layer of metal on an inorganic filler. In this work, a thin nickel coating was deposited onto mica flakes. The nickel coating may be produced with an arbitrarily large aspect ratio (subject to the limits of uniform deposition), but it is supported and preserved during processing by the durable mica substrate. Since the aspect ratio of the nickel can be very large, perhaps one or two thousand, only very small quantities of nickel are required to impart conductivity to the resin composite. The economics of using metallized fillers are determined by the balance between coating costs and the reduction in the quantity of metal needed to impart conductivity or shielding.

NICKEL-COATED MICAS

Experimental

Using an electroless deposition process (21), 60-S Suzorite mica from Marrietta Resources International (Canada) Ltd. was coated with various thicknesses of nickel. The coated mica was tumble blended with powdered polyethylene (LLDPE) and injection molded in a small plunger machine. The molded impact bar was sectioned and tested for resistivity. The tensile bar was used in a specially designed template to measure its EMI attenuation.

Results and Discussion

Figures 7 through *10* are micrographs of the polished sections of the coated mica flakes. The coatings were polycrystalline, of uniform thickness, and continuous for nickel concentrations greater than 20 percent. At 17 percent nickel by weight, discontinuities in the coating were observed and this noticably decreased the conductivity of composites

Fig. 7. Cross-section of 60-S mica coated with 20 percent nickel. The aspect ratio of the nickel layer is between 1000 and 2000 (400×).

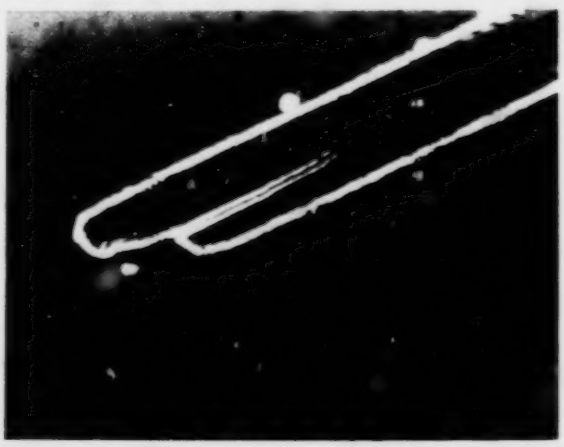

Fig. 8. Cross section of 60-S mica coated with 43 percent nickel showing excellent nickel penetration between mica layers (2000×).

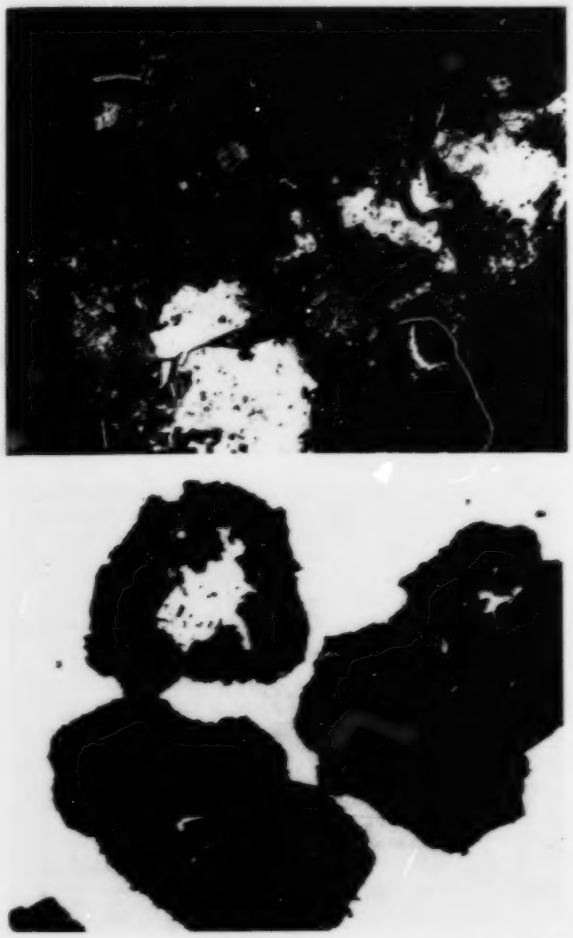

Fig. 9. Identical shots of three 60-S mica flakes coated with 17 percent nickel. The patchiness of the nickel coating is clearly visible. a) reflected light, b) transmitted light (10×).

molded with these imperfectly encapsulated mica flakes.

Figure 10 compares the nickel-coated mica composites with other types of conducting fillers. The performance of the mica flakes coated with 43 percent nickel was almost identical to that of commercial aluminum flakes. This is expected since the aspect ratio of the coated mica is quite similar to that of the aluminum flakes, both being about 20 to 50. The copper powder, which is a chunky low aspect ratio filler, was much less effective for imparting conductivity.

When the volume percentage of the nickel content alone is considered, the plot of nickel concentration versus resistivity is shifted far to the left indicating very high efficiency. Since the nickel coating has an effective aspect ratio near 500, only 3.0 percent by volume is sufficient to provide shielding for roughly 95 percent of all commercial applications.

The analysis of a nickel-coated mica composite on the basis of its nickel content, without consideration for the amount of mica required to support the nickel, is justified economically. The cost of replacing resin with mica is negligible, and therefore it is the nickel content (including the cost of deposition), which determines the price of the final composite. The viability of coated mica in the commercial marketplace is demonstrated by the existence of several other coated products (including microspheres, fiberglass, and carbon). In addition, nickel-coated mica is being commercialized in Japan where waste effluents from a nickel electroplating facility are being used as a cheap source of nickel.

Figure 11 illustrates the effect of nickel aspect ratio on the conductivity of a composite containing 10 weight percent nickel. As the total volume percentage of filler increased, the constant quantity of

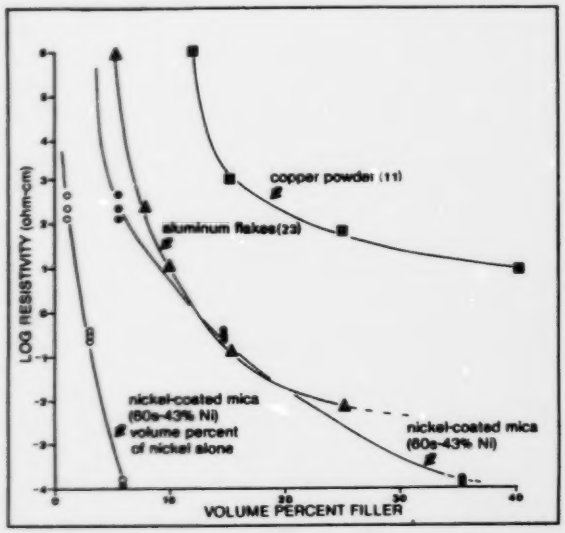
LOG RESISTIVITY (ohm-cm)
copper powder (11)
aluminum flakes(23)
nickel-coated mica (60s-43% Ni) volume percent of nickel alone
nickel-coated mica (60s-43% Ni)
VOLUME PERCENT FILLER

Fig. 10. Plot of resistivity versus volume percent filler. The aluminum and mica flakes compare quite closely because they have similar aspect ratios. If the nickel is considered independently, as if the mica were not present, it is evident that very little nickel is required to impart conductivity.

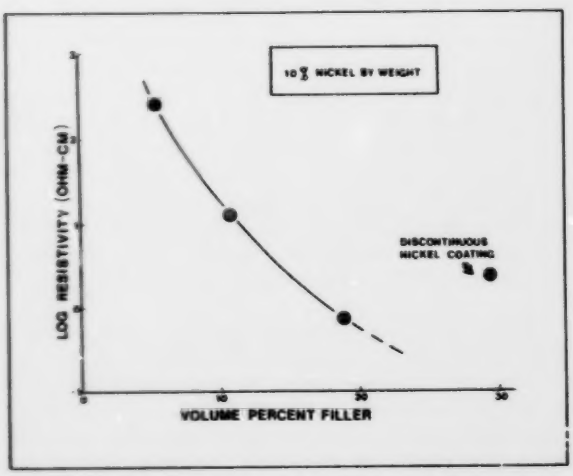

Fig. 11. The concentration of nickel in the composite was held at 10% by weight, and the amount of mica over which this nickel was spread was varied. A greater volume percent filler represents a higher nickel aspect ratio.

nickel was spread thinner and thinner resulting in greater aspect ratios and correspondingly lower resistivities. The point off the curve represents the mica coated with 17 percent nickel which had a patchy, discontinuous coating (*Fig.* 9). The effective aspect ratio of the coating was reduced and the conductivity was diminished accordingly.

The composite containing 18 volume percent filler was the most efficient produced in this study. This composite was filled with 60S flakes that were coated with 22 weight percent nickel; thus the nickel occupied about 1.5 percent of the total composite volume. With this small quantity of nickel, the resistivity of the composite has been lowered to less than one ohm-cm, rendering the composite adequate for the majority of current applications.

Figure 12 is a plot of critical composition versus aspect ratio for a variety of fillers. This illustrates that Milewski's theory of maximum packing fractions can be used to predict the critical concentration for conductivity. *Figure 12* is based on a graph published by Davenport of MBAssociates (22), to which has been added the results for a variety of other fillers including nickel-coated micas. The flake products conform well to Milewski's packing curve even though this curve was developed exclusively for fibers. A similar packing curve for flakes does not yet exist. It is evident that the ultra-thin nickel coatings are a very promising means of producing conductive composites with a minimum metal content.

Figure 13 is a shielding effectiveness scan produced by a shielded room system. The nickel-coated mica composite, which contained 10 weight percent of nickel, compares favorably with commercial conductive fillers. Unfortunately, the shielded room facility suffered from limited accuracy and did not conform to proposed ASTM standards. The results from this facility serve only to illustrate that significant EMI shielding is possible using nickel-coated mica composites.

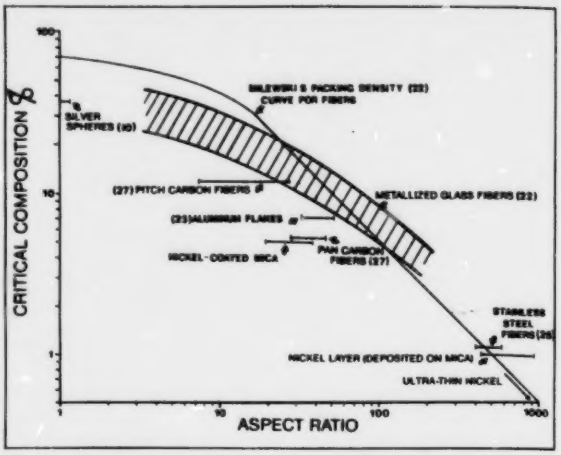

Fig. 12. Critical composition versus aspect ratio. The nickel coated micas, aluminum flakes, and stainless steel fibers fit very well on the plot developed by Davenport (22). The relationship between aspect ratio, packing efficiency, and critical composition is well defined.

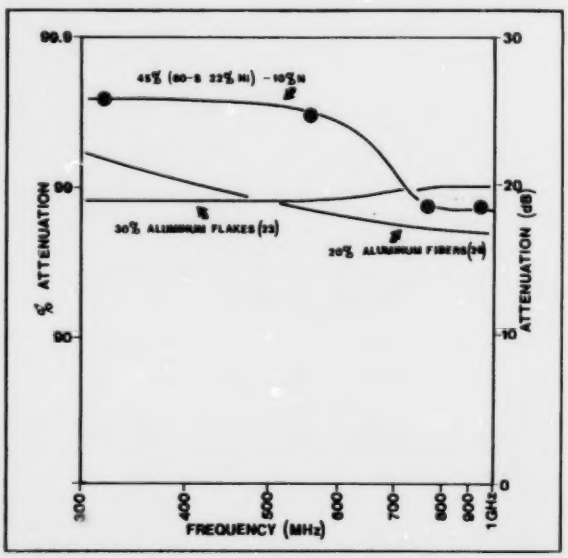

Fig. 13. The shielding spectrum of a 10 percent nickel composite is compared with those of two commercial fillers.

CONCLUSIONS

The critical composition of any conductive filler depends on a number of properties such as density, size distribution, and particle aspect ratio. The quantitative dependence of the critical composition on these properties is parallel to the dependence of packing fraction on the same properties. By analyzing the work which has previously been done in the field of particle packing, it should be possible to gain further insight into factors which influence the conductivity of composites used for EMI shielding.

It is evident from the current work that a filler's aspect ratio is particularly influential in determining its critical composition. Nickel-coated mica provides one solution to the problem of producing a very high aspect ratio metallic layer that will survive the rigors of injection molding. Using this technique, 1.5 volume percent nickel can provide sufficient conductivity and shielding effectiveness for 90 percent of current commercial applications. If thinner uniform coatings could be produced, it seems likely that the amount of metal needed to impart conductivity could be further reduced to less than one volume percent.

ACKNOWLEDGMENTS

The authors would like to thank the National Sciences and Engineering Research Council for their support of this work.

REFERENCES

1. C. T. Ristorcelli, *IEEE Trans. Electromagnetic Compatibility*, 42 (Feb. 1976).
2. S. R. Levy, *Metal Finishing*, 21 (July 1983).
3. C. D. Storms, *Metal Finishing*, 47 (Feb. 1983).
4. Walter J. Miller, *Metal Finishing*, 31 (March 1983).
5. J. E. McCaskie, *et al.*, *Modern Plastics*, 66 (March 1983).
6. M. L. Thorpe, *Plastics Engineering*, 23 (April 1982).

7. G. B. Street and T. C. Clark, *IBM. J. Res. Dev.*, **25**, 51 (1981).
8. "Conductive Plastics", *Chemical Week*, 38 (July 20, 1983).
9. P. J. Moody, "Plastics EMI Shielding: Materials, Equipment, Markets", Executive Report, Business Communications Co., Inc., Stamford, Connecticut, 1982.
10. J. Gurland, *Trans. Met. Soc. AIME.*, **236**, 642 (1936).
11. R. Mukhopadhyay, *et al.*, *J. Appl. Polym. Sci.*, **20**, 2575 (1976).
12. K. Miyasaka, *et al.*, *J. Mater. Sci.*, **17**, 1610 (1982).
13. W. F. Verhelst, *et al.*, *Rubber. Chem. Technol.*, **50**, 735 (1977).
14. A. P. French, *et al.*, "An Introduction to Quantum Physics", W. W. Norton. New York (1978).
15. R. D. Sherman, L. M. Middleman and S. M. Jacobs, *Polym. Eng. Sci.*, **23**, 36 (1983).
16. A. E. R. Westman and H. R. Hugill, *J. Am. Ceram. Soc.*, **13**, 767 (1930).
17. H. E. White and S. F. Walton, *J. Am. Ceram. Soc.*, **20**, 155 (1936).
18. J. V. Milewski, *Composites*, 258 (Nov. 1973).
19. J. V. Milewski, SPi, Reinf. Plas./Comp. Inst., 29th An. Tech. Conf. 10-B, pg. 1 (1974).
20. G. P. Bierwagen and T. E. Saunders, *Powder Technol.*, **10**, 111 (1974).
21. M. T. Kortschot, B. A. Sc. Thesis, U. of Toronto, 1984.
22. D. E. Davenport, *Polym. News*, **8**, 134 (1982).
23. Transmet Corporation, Transmet Flake Modified Conductive Plastics Solve Design Problems!, Sales Brochure, Feb. 1983.
24. G. Smoluk, *Mod. Plast.*, 48 (Sept. 1982).
25. R. H. Wehrenberg II, *Mech. Eng.*, 38 (March 1982).
26. D. M. Bigg, and D. E. Stutz, *Ind. Res. Dev.*, 103 (July 1979).
27. N. E. Fowler, *Plast. Eng.*, 29 (June 1981).

PANEL DISCUSSION

W. C. Faessler: How exactly did you get this nickel coating on the mica flakes?

M. Kortschot: A chemical, or electroless deposition procedure was used. Pretreated mica flakes were suspended in a solution of a nickel salt with strong agitation. To this suspension a reducing agent was added and after a brief period of inactivity, the nickel plated rapidly onto the flakes.

R. E. Prud'Homme: What is the reason for using 60S-grade mica instead of some other grade? Is this mica treated or natural?

M. Kortschot: The mica was untreated. There is a good reason for using large flakes. The minimum coating thickness is limited by coating technology, and is on the order of a few μm at the present time. If the thinnest coating possible were applied to both a large and a small flake, the nickel layer on the large flake would have the greater aspect ratio, and would represent the more efficient nickel useage.

L. A. Utracki: During our "Polyblends-'83" meeting, Julio Ottino mentioned some industrial trials for generating very large, metal-like, electrical conductivity in non-conductive polymers with less than one percent of metal. The concept was simply to deposit a monolayer of silver on polymeric spheres and then form those spheres by fusion into final shape products—ribbons, cases, connectors, etc. It was found that this is a workable but so far uneconomical concept. On the other subject. There is extensive literature on the relation between the maximum packing volume fraction, ϕ, and the aspect ratio, p, for monodispersed flakes as well as for rods. As could be expected, for the same value of p, the ϕ for flakes is higher than that for fibers. So if you are interested in very low ϕ systems, you should use fibrous fillers.

M. Kortschot: The inherent advantage of flakes is that they impart conductivity in all directions in a plane, whereas a highly directional melt flow could result in unidirectional conductivity if fibers are used. In this study mica was selected as a model system because the concept of metallic aspect ratio could be well defined. The theoretical interpretation is more difficult if coated rods are used. It may well be however, that metal-coated rods such as fiberglass will prove to be more efficient.

M. R. Kamal: Did you look at the mechanical properties or the microstructure of these moldings and determine whether the application of the nickel layer interfered with the adhesion of the mica to the matrix?

M. Kortschot: No, I did not study any mechanical properties. Because of the rough, polycrystalline nickel surface, I would expect improved adhesion between the flakes and the matrix.

J. L. White: What would concern me in using transition metals for coatings is that they are known catalysts for oxidative degradation. If you have materials which are catalysts for degradation and you put them through mixers or twin-screw extruders and then mold the parts out of them you may be guaranteed that your part will not last very long due to mechanical failure.

M. Kortschot: It is certainly true that precautions against degradation may be necessary such as the use of metal deactivators.

J. L. White: I was thinking that you may want to put your nickel-coated mica inside a pocket of inert polymer.

M. Kortschot: If the flakes were coated with a polymeric material they would tend to be insulated from one another. This is undesirable because it would impede network formation and reduce conductivity.

U.S. Postal Service

STATEMENT OF OWNERSHIP, MANAGEMENT AND CIRCULATION

Required by 39 U.S.C. 3685)

1A. TITLE OF PUBLICATION	1B. PUBLICATION NO.	2. DATE OF FILING
POLYMER COMPOSITES		11/5/85
3. FREQUENCY OF ISSUE	**3A. NO. OF ISSUES PUBLISHED ANNUALLY**	**3B. ANNUAL SUBSCRIPTION PRICE**
QUARTERLY	4	$24.00 member $60.00 non-member

4. COMPLETE MAILING ADDRESS OF KNOWN OFFICE OF PUBLICATION *(Street, City, County, State and ZIP+4 Code) (Not printers)*

14 Fairfield Drive, Brookfield Center, CT 06805

5. COMPLETE MAILING ADDRESS OF THE HEADQUARTERS OF GENERAL BUSINESS OFFICES OF THE PUBLISHER *(Not printer)*

14 Fairfield Drive, Brookfield Center, CT 06805

6. FULL NAMES AND COMPLETE MAILING ADDRESS OF PUBLISHER, EDITOR, AND MANAGING EDITOR *(This item MUST NOT be blank)*

PUBLISHER *(Name and Complete Mailing Address)*

Robert D. Forger 14 Fairfield Drive, Brookfield Center, CT 06805

EDITOR *(Name and Complete Mailing Address)*

Dr. Roger S. Porter 14 Fairfield Drive, Brookfield Center, CT 06805

MANAGING EDITOR *(Name and Complete Mailing Address)*

7. OWNER *(If owned by a corporation, its name and address must be stated and also immediately thereunder the names and addresses of stockholders owning or holding 1 percent or more of total amount of stock. If not owned by a corporation, the names and addresses of the individual owners must be given. If owned by a partnership or other unincorporated firm, its name and address, as well as that of each individual must be given. If the publication is published by a nonprofit organization, its name and address must be stated.) (Item must be completed.)*

FULL NAME	COMPLETE MAILING ADDRESS
Society of Plastics Engineers, Inc.	14 Fairfield Drive Brookfield Center, CT 06805

8. KNOWN BONDHOLDERS, MORTGAGEES, AND OTHER SECURITY HOLDERS OWNING OR HOLDING 1 PERCENT OR MORE OF TOTAL AMOUNT OF BONDS, MORTGAGES OR OTHER SECURITIES *(If there are none, so state)*

FULL NAME	COMPLETE MAILING ADDRESS
None	

9. FOR COMPLETION BY NONPROFIT ORGANIZATIONS AUTHORIZED TO MAIL AT SPECIAL RATES *(Section 423.12 DMM only)*
The purpose, function, and nonprofit status of this organization and the exempt status for Federal income tax purposes *(Check one)*

☐ (1) HAS NOT CHANGED DURING PRECEDING 12 MONTHS

☐ (2) HAS CHANGED DURING PRECEDING 12 MONTHS

(If changed, publisher must submit explanation of change with this statement.)

10. EXTENT AND NATURE OF CIRCULATION *(See instructions on reverse side)*	AVERAGE NO. COPIES EACH ISSUE DURING PRECEDING 12 MONTHS	ACTUAL NO. COPIES OF SINGLE ISSUE PUBLISHED NEAREST TO FILING DATE
A. TOTAL NO. COPIES *(Net Press Run)*	725	750
B. PAID AND/OR REQUESTED CIRCULATION 1. Sales through dealers and carriers, street vendors and counter sales	---	---
2. Mail Subscription *(Paid and/or requested)*	498	491
C. TOTAL PAID AND/OR REQUESTED CIRCULATION *(Sum of 10B1 and 10B2)*	498	491
D. FREE DISTRIBUTION BY MAIL, CARRIER OR OTHER MEANS SAMPLES, COMPLIMENTARY, AND OTHER FREE COPIES	---	---
E. TOTAL DISTRIBUTION *(Sum of C and D)*	498	491
F. COPIES NOT DISTRIBUTED 1. Office use, left over, unaccounted, spoiled after printing	227	259
2. Return from News Agents	---	---
G. TOTAL *(Sum of E, F1 and 2–should equal net press run shown in A)*	725	750

11. I certify that the statements made by me above are correct and complete	SIGNATURE AND TITLE OF EDITOR, PUBLISHER, BUSINESS MANAGER, OR OWNER
	Circulation Manager

PS Form 3526, July 1984 *(See instruction on reverse)*

Subject Index

A

Aramid:epoxy interphase, characterization of, 195
Aramid fibers, unidirectional composites and, tensile strength of, 54

C

Calcium carbonate, filled polyethylene, flow patterns, 215
Capillary die, filled polyethylene, calcium carbonate and titanium dioxide, 215
Carbon:epoxy interphase, characterization of, 195
Carbon fibers
  glass fibers and, interface between thermosetting polymers, 242
  orientational behavior induced by, liquid crystal polymer, 181
Cellulose, reinforcement, nylon-reaction injection molded composites, 162
Chlorinated paraffins, structural changes, processing conditions of particulate filled polypropylene, 34
Colloidal dispersion, flow of suspensions, 209
Composite materials
  mechanics, properties of planar-random fiber composites, 133
  moisture diffusion in, stress dependence of the coefficient, 9
Composites: *see* specific type
Compounding, short fiber reinforced injection moldable thermoplastic composites and, 20
Compression molding, sheet molding compounds, 13
Conventional compressed fibers, tensile fatigue of glass fibers and composites, 168

D

Dispersive mixing, roll-mills, 222

E

Electromagnetic interference shielding, nickel-coated mica composites, 296
Epoxies
  glass fiber composites and, dynamic damping behavior of, modification via fiber coating with functional latices, 272
  high performance matrices, salicylic acid modification of, 47
  polyfunctional, graphite composites, 65, 72

F

Fiber: *see also* specific type of fiber
  process induced orientation, numerical simulation, 82
Foams, properties of, relations between mixing and, 115
Fracture mechanics
  analysis, polypropylene composites, 1
  glass-cloth-reinforced composites, 29

G

Glass-cloth-reinforced composites, fracture behavior of, 29
Glass fiber composites, epoxy and, dynamic damping behavior of, modification via fiber coating with functional latices, 272
Glass fibers
  carbon fibers and, interface between thermosetting polymers, 242
  content, injection molded polypropylene compound, 93
  mechanical degradation, during compounding with polypropylene, 232
  tensile fatigue of, conventional and surface compressed fibers with, 168
Glass poly(ethylene terephthalate) injection-molding compound, matrix phase microstructure, 87
Glass-reinforced composites, interfacial strength, 142
Graphite composites, formulations for, polyfunctional epoxies, 65, 72

I

Injection-molded composites, nylon-reaction, cellulose-reinforced, 162
Injection-molded poly(ethylene terephthalate) system, orientation of short glass fibers in, 41
Injection molding compound, glass poly(ethylene terephthalate), matric phase microstructure, 87

L

Latices, functional, fiber coating with, epoxy/glass fiber composites and, 272

M

Metal fibers, polypropylene filled with, properties of, 282
Mica, concentration effects, polypropylene, 249
Mica composites, nickel-coated, electromagnetic interference shielding, 296
Moisture, diffusion, stress effects, composite materials, 9

N

Nickel, mica composites coated with, electromagnetic interference shielding, 296
NMR: *see* Nuclear magnetic resonance
Nuclear magnetic resonance, solid state carbon-13, chemically modified surfaces and, 156
Nylon-reaction injection molded composites, cellulose-reinforced, 162

P

Planar-random fiber composites, properties, composite-material mechanics, 133
Polyester composites, microcellular, processing of, 175
Polyethylene
  calcium carbonate and titanium dioxide filled, flow patterns in, 215
  wood fibers, in thermoplastic composites II, 261
Poly(ethylene terephthalate)
  glass injection molding compound, matrix phase microstructure, 87
  injection molded system, orientation of short glass fibers, 41
Polymeric materials, thermal response, high temperatures, 110
Polymers
  filled
    interaction balances and properties of, 201
    mixing and properties of, 115
  liquid crystal, induced orientational behavior by carbon fibers, 181
  thermosetting, interface between glass and carbon fibers and, 242
Polypropylene
  composites, fracture mechanics analysis, 1
  compounding with, mechanical degradation of glass fibers during, 232
  filled with metal fibers, properties of, 282
  injection molded composites, glass fiber content and, 93
  mica-reinforced, fracture of, 249
  particulate filled, processing conditions of, chlorinated paraffins and, 34

R

Radiant heat flux apparatus, thermal response measurement, high temperatures, polymeric materials, 110
Roll-mills, dispersive mixing in, 222

S

Salicylic acid, high performance epoxy matrices, 47
Sheet molding compounds
  compression molding of, processing-property relations, 13
  kinematics of flow, 105
Short fiber composites, crack length estimation procedure, 185
Short glass fibers, direct determination of, injection molded poly(ethylene terephthalate) system, 41
Silane coupling agents, new potential of, 151
Solid state carbon-13 NMR: *see* Nuclear magnetic resonance
Solution-cast metal-filled composites, electrical resistivity of, 58

Stress dependence, coefficient of moisture diffusion, composite materials, 9
Surface compressed fibers, tensile fatigue of glass fibers and composites, 168
Suspensions, flow of, 209
Syntactic foam, three-phase microballoon composites, 100

T

Temperature, high, thermal response to polymeric materials, 110
Thermoelastic analysis, residual stresses, unidirectional, high-performance composites, 123
Thermoplastic composites, short fiber reinforced injection moldable, compounding effects, 20
Thermoplastic composites II, wood fibers and, polyethylene, 261
Titanium dioxide, filled polyethylene, flow patterns, 215

U

Unidirectional composites
aramid fibers and, tensile strength of, 54
high-performance, residual stresses, thermoelastic analysis, 123

W

Wood fibers, thermoplastic composites II and, polyethylene, 261

Author Index

Abbås, K. B., 162
Agarwal, B. D., 29, 185
Agrawal, D. C., 29
Andison, D., 242

Bacci, D.,
Banerji, K., 29
Barone, M. R., 105
Bert, C. W., 133
Beshay, A. D., 261
Bigg, D. M., 20
Bramuzzo, M, 1

Caulk, D. A., 105
Chua, P. S., 242
Chung, T. S., 181

Daly, J. H., 195
Daneault, C., 261

Enikolopian, N. S., 54

Fakirov, S., 41
Fakirova, C., 41
Fisa, B., 232, 249

Garton, A., 195
Gillespie, J. W., Jr., 82
Gilwee, W. J., 65, 72
Grigorian, G. A., 54
Gurion, Z., 181

Hagen, S. C., 110, 184
Han, C. D., 13
Henderson, J. B., 110, 184
Hing, K., 201
Hsieh, A. J.-Y., 168
Huang, Z.-H., 34

Ibrahim, A. M., 47
Ishida, H., 34

Kamal, M. R., 282
Katsura, T., 282
Kenig, S., 100
Kenney, M. E., 151
Kline, R. A., 133
Koenig, J. L., 142, 156
Kokta, B. V., 261
Kompaniets, L. V., 54
Kortschot, M. T., 296
Kourtides, D. A., 65, 72
Kumar, P., 185

Lambla, M., 272
Lee, B.-L., 115
Lhymn, C., 87
Li, C. G., 168

Ma, C.-Y., 215
Manas-Zloczower, I., 222
Mandell, J. F., 168
Marom, G., 9
McGarry, F. J., 168
Min, K., 215
Misra, A., 93

Nairn, J. A., 123
Narkis, M., 100
Neumann, S., 9
Nir, A., 222
Nir, Z., 65, 72

Oh, S. Y., 13

Parker, J. A., 65, 72
Patro, B. S., 185
Piggott, M. R., 242
Pipes, R. B., 82
Potapov, V. V., 54
Prut, E. V., 54

Ratier, I., 100
Richard, C., 201
Roberts, R. W., 58

Sanschagrin, B., 249
Savadori, A, 1
Schlund, B., 272
Schreiber, H. P., 201
Schultz, J. M., 87
Seferis, J. C., 47
Singh, R. R., 58
Sounik, D. F., 151
Stamatoff, J. B., 181
Suh, N. P., 175

Tadmor, Z., 222

Utracki, L. A., 282

Vanderschuren, J. A., 82
Van de Ven, T. G. M., 209
Vu-Khanh, T., 249

Weissert, F. C., 215
White, J. L., 215
Woodhams, R. T., 296

Xavier, S. F., 93

Youn, J. P., 175

Zadorecki, P., 162
Zaper, A. M., 156

Society of Plastics Engineers

Executive Office, 14 Fairfield Drive, Brookfield Center, CT 06805, U.S.A.
(203) 775-0471
Telex No. 643-712

MEMBERSHIP APPLICATION

I am applying for:

☐ Membership
☐ Reclassification (no charge)
☐ Reinstatement (initiation fee not required)

NAME: _____
First Middle Last

DATE OF BIRTH: _____
Month Day Year

ADDRESS:
Fill in both addresses and check your preferred mailing address.

☐ **COMPANY** (spell out name)

_____
_____
_____
City State (Prov.) Zip

POSITION: _____

☐ **HOME** _____

_____
City State (Prov.) Zip

Job Function
What is the *primary* end product manufactured or service performed at your company location?

Please Check your Primary job function (check one only).
____ 01 Production or Manufacturing Engineering
____ 02 Design or Design Engineering
____ 03 Purchasing
____ 04 Sales or Marketing
____ 05 Research or Development Engineering
____ 06 General or Corporate Management
____ 07 Other (Specify)

DIVISIONS
My free primary Division choice is _____
check (✓) others below as secondary Divisions (cost -$4 each).

____ 21 Color and Appearance
____ 22 Extrusion
____ 23 Injection Molding
____ 24 Electrical and Electronic
____ 25 Thermoforming
____ 26 Engineering Properties and Structure
____ 27 Vinyl Plastics
____ 28 Thermoset
____ 29 Thermoplastics Materials & Foams (Nonvinyl)
____ 30 Blow Molding
____ 31 Plastics in Automotive
____ 33 Plastics Analysis
____ 34 Decorating
____ 35 Moldmaking and Mold Design
____ 36 Medical Plastics
____ 37 Marketing (information)
____ 38 Polymer Modifiers & Additives (information)

Grade	Requirements
Senior Member	Minimum of twelve (12) experience credits and current continuous membership in the Society for a minimum of two (2) years.
Member	Minimum of six (6) experience credits.
Affiliate Member	Less than six (6) experience credits.
Student Member	Regularly enrolled FULL-TIME student in a course of study in plastics.

Check below the membership grade for which you believe details of your experience in plastics qualifies you (see grades above).

☐ Student Member ☐ Member
☐ Affiliate Member ☐ Senior Member

Statement of Fees *(U.S. FUNDS ONLY)*
MEMBERSHIP YEAR: 7/1 thru 6/30
$10.00 INITIATION FEE MUST BE ATTACHED IN ORDER TO PROCESS YOUR APPLICATION. INITIATION FEE IS SEPARATE FROM ANNUAL DUES.

- **SENIOR MEMBER, MEMBER, AFFILIATE**
  Annual Dues 7/1 - 6/30 $45.00
  If joining after 12/31 $22.50
  If joining after 4/1 $10.00 (initiation fee only)
- **STUDENT MEMBER**
  Annual Dues whenever joining $5.00 (no initiation fee/ not pro-rated)
- **REINSTATED MEMBER**
  Annual Dues whenever reinstated $45.00 (no initiation fee/ not pro-rated)

I wish to join the _____ Section.

REFERENCES The Bylaws require the names of three references who are familiar with your work. One of them should be a member of the Society. Assistance in providing member-references will be given on request. Signatures are not necessary.

1. (Member-Sponsor) _____
2. _____
3. _____

STATEMENT OF COLLEGE WORK

Years attended From	Years attended To	Institution	Major	Degree	Education Credits

RECORD OF QUALIFYING EXPERIENCE IN PLASTICS

DATES From Mo.	DATES From Yr.	DATES To Mo.	DATES To Yr.	Give your title, name and location of employer. List in chronological order. Describe duties fully and state any important engineering work you have done in each position. If space is not sufficient, use separate sheet.	Time in years (a)	% in plastics (b)	Qualifying experience (a x b)
					yrs./mo.		yrs./mo.

SUB-TOTAL

Total education and experience credits. ▶

CREDENTIALS COMMITTEE APPROVAL ONLY Approved Grade	
(S)	Date
(S)	Date

Office use only:	Division
ID#	Job Class
Grade	Date Elected
Section	

I certify that the statements made in this application are correct. I agree, if elected, to be governed by the Constitution and Bylaws of the Society and to promote the objectives of the Society.

_____
Signature in ink. Date

If applying for Member or Senior Member, please complete *in detail:*

STATEMENT OF COLLEGE WORK

Years attended		Institution	Major	Degree	Experience Credits (see notes below)
From	To				

RECORD OF QUALIFYING EXPERIENCE IN PLASTICS

DATES				Give your title, name and location of employer. List in chronological order. Describe duties fully and state any important engineering work you have done in each position. If space is not sufficient, use separate sheet.	Time in years (a)	% in plastics (b)	Qualifying experience (a × b)
From		To					
Mo.	Yr.	Mo.	Yr.				
					yrs./mo.		yrs./mo.
						SUB-TOTAL	
						Total education and experience credits. ▶	

Grade	Requirements
Senior Member	Minimum of twelve (12) experience credits and current continuous membership in the Society for a minimum of two (2) years.
Member	Minimum of six (6) experience credits.
Affiliate Member	Less than six (6) experience credits.
Student Member	Regularly enrolled FULL-TIME student in a course of study in plastics.

CREDENTIALS COMMITTEE APPROVAL ONLY		Approved Grade
(S)	Date	
(S)	Date	

Experience Credits
Grade of Membership . . .

Membership grades are based on experience credits which are earned as follows:

1. **Experience credits earned for education.**
   Maximum credits allowable for education shall be six (6). Use highest degree credits ONLY.

Doctorate in science or engineering	**6 credits**
Masters in science or engineering	**5 credits**
Bachelors in science or engineering	**4 credits**
Any degree other than above	**2 credits**
Associate or Adjunct in Plastics	**2 credits**
Associate or Adjunct (awarded by Community College or equivalent for two-year course of studies, without specializing in plastics).	**1 credit**

When filling in the "Statement of College Work" above, place the corresponding number of credits earned in the right-hand column.

2. **Experience credits** are determined by the proportion of time involved in actual technical and engineering duties in plastics for each position held. For instance, if only three of the five years you worked for the XYZ Co. comprised technical or engineering duties, then three (3) years (60% of 5 yrs.) would constitute the "Qualifying Experience" you would enter in years and months in the right-hand column under "Record of Qualifying Experience in Plastics."

   Please detail carefully the engineering skill required for each position to help the Credentials Committee judge experience as "qualifying."

When you have determined the number of credits which you believe you have earned, consult the following member grade requirements. Indicate on the reverse side the grade of membership for which you believe you are qualified.

INFORMATION FOR AUTHORS

Submission of original and review articles is encouraged. There is no limit on length. Three copies of the manuscript should be submitted, which should be typed, one side only, double space, with at least a 1-inch margin. Submission will be taken to imply that the paper has not been previously published, that it is not being considered elsewhere for publication, and that if accepted it will not be published elsewhere in the same form, in any language, without the consent of the editor or publisher. Authors must agree to transfer copyright to the publisher when an article is accepted for publication. Unless notified to the contrary by the authors, the publisher assumes that the act of submitting the article signifies the author's agreement to such copyright transfer to the publisher. The journal carries a voluntary page charge. Each manuscript should include:

A separate title page, headed by a concise, meaningful title (avoid abbreviations) for the paper. This page should provide:

- The name and affiliations of each contributing author at the time the paper was prepared.
- Indicate by asterisk any changes of address for each author since article preparation.
- Acknowledgment of any prior oral presentation and original source of the material.

A separate abstract page, consisting of a single paragraph of 100–200 words to include the title and the names and addresses of the authors. Define any abbreviations for substances or methods (such as ABS, SAXS, etc.).

A list of references, on a separate page at the end of the text, numbered in order of text citation. The references are to be abbreviated in the form used in Chemical Abstracts using the names of all authors preceded by initials; see Bibliographic Guide for Editors and Authors, American Chemical Society, Washington, D.C.

- Within the text, the reference citations are typed in parentheses in line with the main copy (no superscripts or subscripts), thus:

  According to Young, et al. (1) . . .

- In the list of references the general style is as follows:

  For periodicals:

  1. S. S. Young, J. L. White, E. S. Clark and Y. Oyanogi, Polym. Eng. Sci., 20, 798 (1980).

  The journal name and volume are to be underlined and the year is placed in parentheses. The issue number is given only when needed for identification. The article name is eliminated unless the reference is unclear without it.

  For books: The title to be spelled out in full.
  5. H.-G. Elias, "Macromolecules," Ch. 1, Vol. 2, Plenum Press, New York (1977). (Include the state when the city is not identifiable.)

A list of nomenclature, identifying symbols and abbreviations, commonly desirable at the end of the text. Footnotes are to be avoided.

Equations, numbered and typed in the appropriate place in the text. Where symbols cannot be typed, write them neatly in ink.

Tables, each typed on a separate page, with a heading, and numbered with arabic numerals that correspond to the order in which they are cited in the text. The tables should be inserted in the manuscript after the references and before the figures.

Figures, assembled at the end of the manuscript and preceded by a typed list of captions that explain them. Please also supply a set of original figures or sharp glossy photos thereof, on 8½ × 11 paper or attached to sheets of this size, one sheet for each figure. Each should be identified on the front edge or on the back (photographs) with the name of the first author and the figure number (e.g., Smith, Fig. 1). Originals are to be prepared with high contrast India ink and to bear uniformly stencilled notations. Line drawings and photos should be of a quality suitable for good photographic reproduction and retained legibility upon size reduction to one quarter. Manuscript transmittal letter should indicate if the figures need be returned.

Send manuscripts to:
Roger S. Porter, Editor
POLYMER COMPOSITES
% Polymer Science & Engineering
University of Massachusetts
Amherst, Massachusetts 01003

For information concerning publication dates, page charges and reprint orders contact:
Editorial Department
Society of Plastics Engineers
14 Fairfield Drive
Brookfield Center, Connecticut 06805